PHOTO-REACTIVITY OF BIFUNCTIONAL NAPHTHALENE COMPOUNDS TOWARD DNA

by

Qi Zhang

A Dissertation Submitted in

Partial Fulfillment of the

Requirements for the Degree of

Doctor of Philosophy

in Chemistry

at

The University of Wisconsin-Milwaukee

December 2022

ABSTRACT

PHOTO-REACTIVITY OF BIFUNCTIONAL NAPHTHALENE COMPOUNDS TOWARDS DNA

by

Qi Zhang

The University of Wisconsin-Milwaukee, 2022
Under the Supervision of Professor Xiaohua Peng

DNA interstrand cross-link (ICL) can covalently bind two DNA strands, preventing DNA strands separation, and therefore, blocking DNA transcription and replication, which are essential biological processes for cell division. Among different methods to induce DNA interstrand cross-linking, photoinduction is an important way to activate the cross-linking reactions due to its many characteristics, such as non-invasive, controllability, selectivity and biorthogonality. My research mainly focuses on developing novel binaphthalene compounds which can be activated by 350 nm UV light to produce DNA interstrand cross-linking via alkylation. We designed and synthesized a series of binaphthalene analogues with different substituents at the position-4' on the naphthalene rings (**1a-1e, 12a-12g, 22a,b, 23a-23d** and **24a-24d**) and/or various leaving groups, including triphenylphosphonium salts (**1a-1e**), amine functional groups (**12c-12e**), ether functional groups (**12b**, **22a**,**b**, **23a-23d**, and **24a-24d**), acetate (**12a)**, phenylthio group (**12f**), and phenylselenide (**12g**) (Scheme 1). The reactivity of these novel compounds towards DNA have been studied by DNA interstrand cross-linking assay. The efficiency and mechanism of DNA ICL formation have been investigated. Most of these

compounds showed higher DNA cross-linking yields than previously reported binaphthalene bononates. Both substituents (R) and leaving groups (L) affect their reactivity towards DNA ICL.

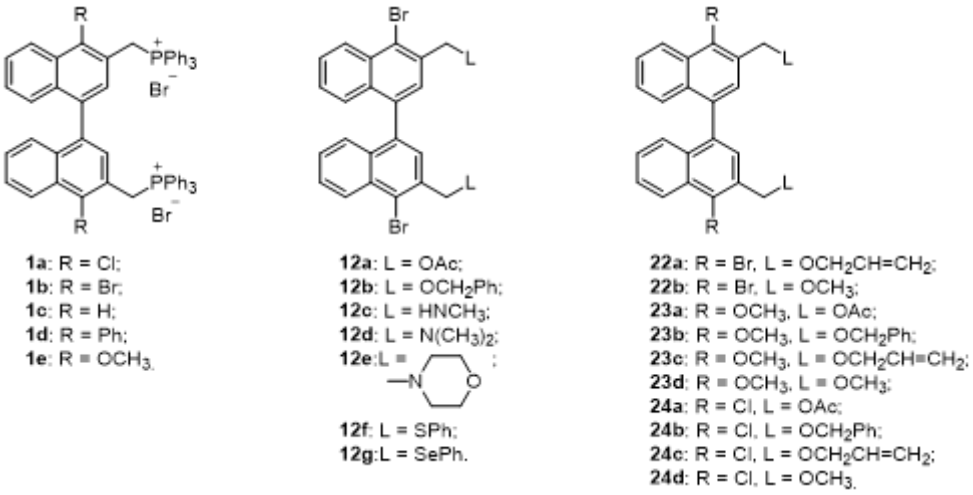

Scheme 1. The structure of binaphthalene analogues.

With triphenylphosphonium (TPP^+) salts as a leaving group, **1a-e** showed not only various efficiency of ICL formation but also different reaction rates due to different substituents at the position-4 of the naphthalene ring. The electron-withdrawing groups facilitate the ICL reaction, such as **1b** and **1d**, while the electron-donating groups slow down the cross-linking process, like **1e**. Although **1d** showed a fast ICL reaction rate possibly due to its strong UV absorption, its ICL formation efficiency was low because of the bulky size of the phenyl group that might prevent the DNA interstrand cross-linking. The study indicated that the electronic effect, steric effect and UV-absorption combine to influence the final ICL formation. In addition, the aromatic substituents influenced the reactivity of these compounds towards dG and dA. Compound **1b** showed the poorest photo-reactivity toward dA, while **1d** was the most reactive toward dA. The 2-naphthalenylmethyl cations photo-generated from **1a-e** can alkylate dC, dG and dA while DNA interstrand cross-linking reaction only occurred with dG-dC base pairs.

We also observed that different leaving groups greatly influence the DNA ICL formation and the photo-reactivity toward DNA. Bromo-substituted binaphthalene analogues **12a-j** with different leaving groups showed different cross-linking reaction rates and ICL formation efficiency. The photo-reactivity toward dA and dG was also affected by different leaving groups. For example, alkylation took place with dAs and dGs for **12a** and **12g** while other compounds (show compound number here) only alkylated dGs. In addition, DNA ICL formation mainly occurred at dG sites for all compounds while monoalkylation took place with dG or dG/dA, which depends on the leaving groups. For **22a**, **b**, **23a-d**, **24a-d**, different substituents and leaving groups combine to influence the DNA ICL formation.

The mechanism investigation of ICL formation indicated that all binaphthalene analogues generated naphthalenylmethyl free radicals (**6**) that were spontaneously transformed to the corresponding cations (**7)** directly producing DNA ICL products via alkylation (Scheme 2).

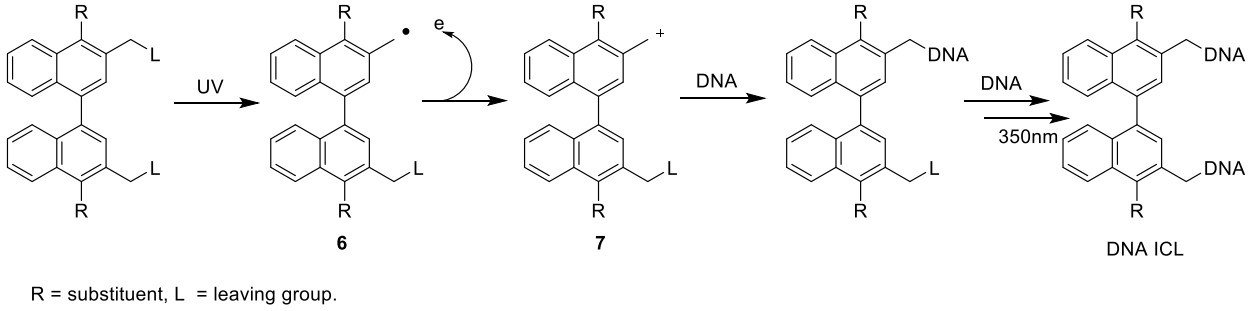

Scheme 2. Proposed mechanism for photo-induced ICL formation by binapthalene analogues.

Furthermore, we found that the DNA ICL formation of **12g** was greatly improved in the presence of hydrogen peroxide. It is likely that H_2O_2 can convert a poor leaving group (-SePh) to a better leaving group (-SeOPh) by oxidation, which promote photo-induced DNA ICL formation (Scheme 3). ICL Mechanism investigation suggested that both carbocations and free radicals

were involved in DNA cross-linking process induced by 350 nm irradiation in the presence of H_2O_2.

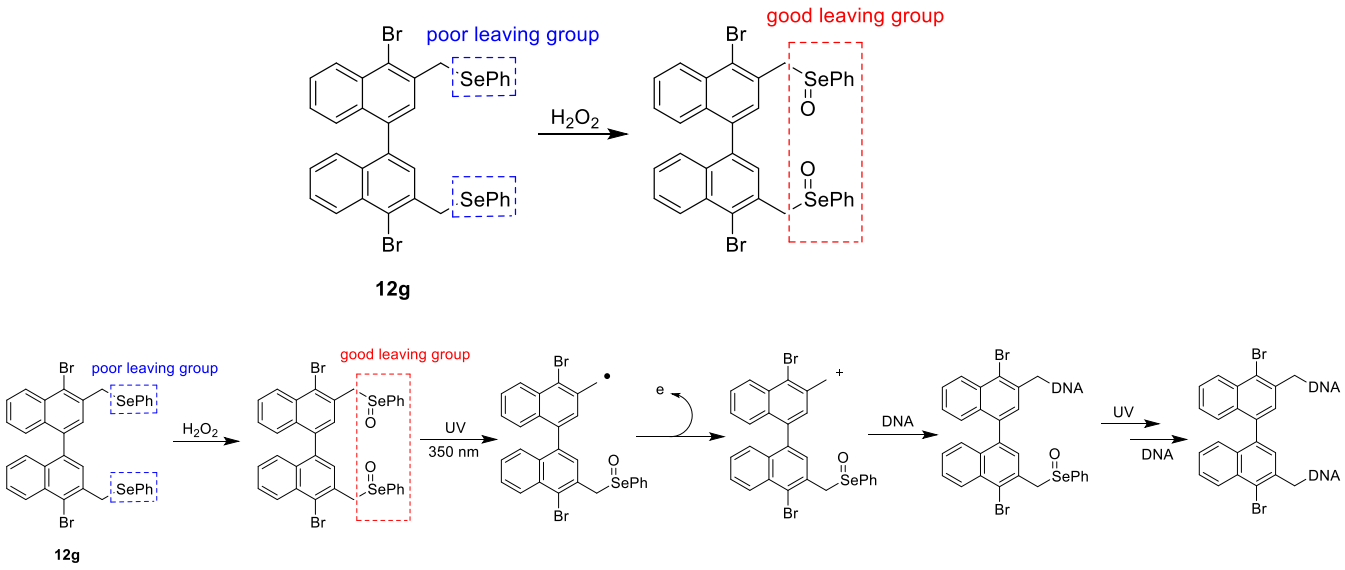

Scheme 3. Proposed mechanism for photo-induced ICL formation by **12g** in the presence of hydrogen peroxide.

Finally, we designed and synthesized three BINOL analogues **34**-**36** with different configurations (*R*-, *S*- and *Rac*-) to investigate the chirality effect on DNA ICL formation (Scheme 4). It was found that different organic solvents affected the DNA interstrand cross-linking efficiency. Compounds dissolved in acetonitrile (CH_3CN) can induce higher DNA ICL yields with less DNA damage than those dissolved in dimethylformamide (DMF) or dimethyl sulfoxide (DMSO). We further observed that the chirality of BINOL precursors didn't influence DNA ICL formation. For example, similar ICL yields were observed for **34a-c**. It is likely due to the small size of these molecules, different configurations do not affect their binding interaction with DNA double helixes.

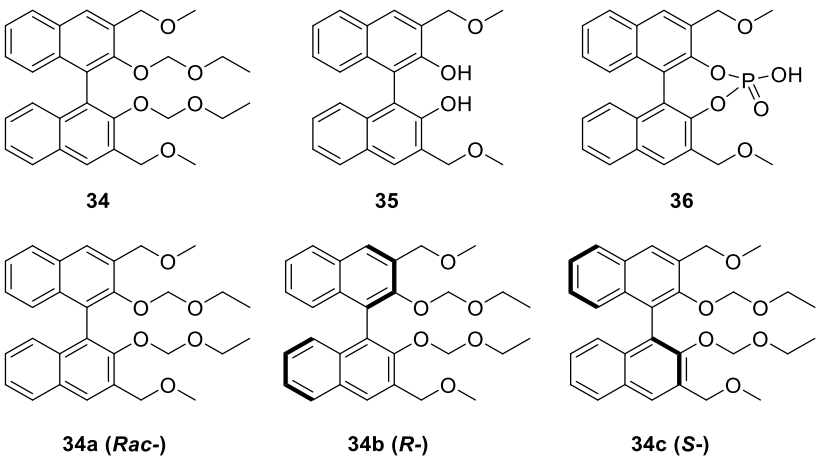

Scheme 4. BINOL derivatives **34**-**36** and different configurations of **34** (**a**-**c**).

TABLE OF CONTENTS

LIST OF FIGURES

LIST OF TABLES

LIST OF SCHEMES

LIST OF ABBREVIATIONS

AIBN	Azobis-(isobutyronitrile)
ATP	Adenosine Triphosphate
CNVK	3-Cyanovinycarbazole nucleoside
COSY	Correlation spectroscopy
CRBN	Cereblon
DCM	Dichloromethane
DMF	Dimethylformamide
DMSO	Dimethyl sulfoxide
DNA	Deoxyribonucleic acid
EDG	Electron-donating group
EDTA	Ethylenediaminetetraacetic acid
ESI	Electrospray
EWG	Electron-withdrawing group
HPLC	High-performance liquid chromatography
HRMS	High resolution mass spectrometry
HSQC	Heteronuclear single quantum coherence spectroscopy
ICL	Interstrand cross-link
LCMS	Liquid chromatography-mass spectrometry
NBS	N-bromosuccinimide
NMR	Nuclear magnetic resonance

ODNs	Oligonucleonides
PBS	Phosphate-buffered saline
PNK	Polynucleotide kinase
QM	Quinone methide
RNA	Ribonucleic acid
ROS	Reactive oxygen species
TEA	Triethylamine
TEMPO	4-Hydroxy-2,2,6,6-tetramethylpiperidin-1-oxyl
THF	Tetrahydrofuran
TLC	Thin layer chromatography
TMEDA	Tetramethylethylenediamine
TMS	Tetramethylsilane
TPP	Triphenylphosphonium
UV	Ultraviolet

ACKNOWLEDGEMENTS

First, I wish to acknowledge my advisor, Prof. Xiaohua Peng. She is an outstanding scholar and supervisor. I appreciate that she has given me a great help on my research and always provides many excellent advice on my projects. With her great guidance, I have learned a lot of research techniques and accumulated the skills for being thorough with my research. She always generously provided her profound knowledge and expertise to help me solve the problems in the research work. It is my great honor to have Dr. Peng as my supervisor.

I would like to appreciate Prof. James Cook, Prof. Mark Dietz, Prof. M. Mahmun Hossain and Prof. Arsenio Pacheco, who are my committee members. They gave me a lot of insightful comments and valuable advice for my research. I really appreciate their generosity in sharing their expertise.

Next, I would like to thank all group members in Prof. Peng's lab, including Dr. Zechao Lin, Dr. Heli Fan, Dr. Muhammad Asad Uz Zaman, Anahit Campbell, Nurul Islam Setu, Taufeeque Ali and Eron Saxon. It is my great pleasure to be a group member and work with them. I appreciate their kind assistance in my study and research work. In addition, I would like to thank all faculty members and staffs in the Department of Chemistry & Biochemistry at University of Wisconsin-Milwaukee.

Last but not least, I wish to thank my parents Liming Zhang and Cuiyang Meng, for their great encouragement and support in my life. I would like to thank all my friends who had helped me in my study and life.

Chapter 1 Introduction

1.1 DNA Structure, Function, and Reactivities

Deoxyribonucleic acid (DNA) is a polymer composed of two polynucleotide chains that coil around each other and form a double helix. In general, the two complementary strands of DNA double helix are in opposite directions to each other (antiparallel) (Figure 1-1). DNA carries genetic information, which is the key for the development of cell growth. DNA replication and transcription are biological processes to make copies of nucleic acids in the cell, which is essential in the life process. DNA replication is catalyzed by DNA polymerase that uses DNA as a template to make copies of DNA while the transcription process catalyzed by RNA polymerase and transcriptase that produces RNA with DNA as a template (Figure 1-2). As DNA is the repository of genetic information in each living cell, its integrity and stability are essential to maintain the high fidelity of DNA replication and transcription. However, DNA integrity is always under attack from the environment, such as chemical agents and photoirradiation, which cause DNA damages finally leading to mutation and possibly disease if not repaired. Thus, understanding the chemical and photochemical reactivity of DNA towards various reagents is essential to life.

The nucleotides on the DNA strands consist of three subunits: a nucleobase, a five-carbon sugar and a phosphate group. Different living systems have identical sugar phosphate backbone but differ from the base sequences. There are four nucleobases in DNA, including two purines [guanine (G) and adenine (A)] and two pyrimidines [cytosine (C) and thymine (T)]. Purines always pair with pyrimidines to form two Watson-Crick base pairs, i.e. G/C and A/T base pairs, which is critical to maintain high fidelity of DNA replication and transcription (Figure 1-1). This

complementary nature of the based-paired structure provides a redundant copy of the genetic information in each strand of DNA, making DNA well suited to the storage of genetic information.

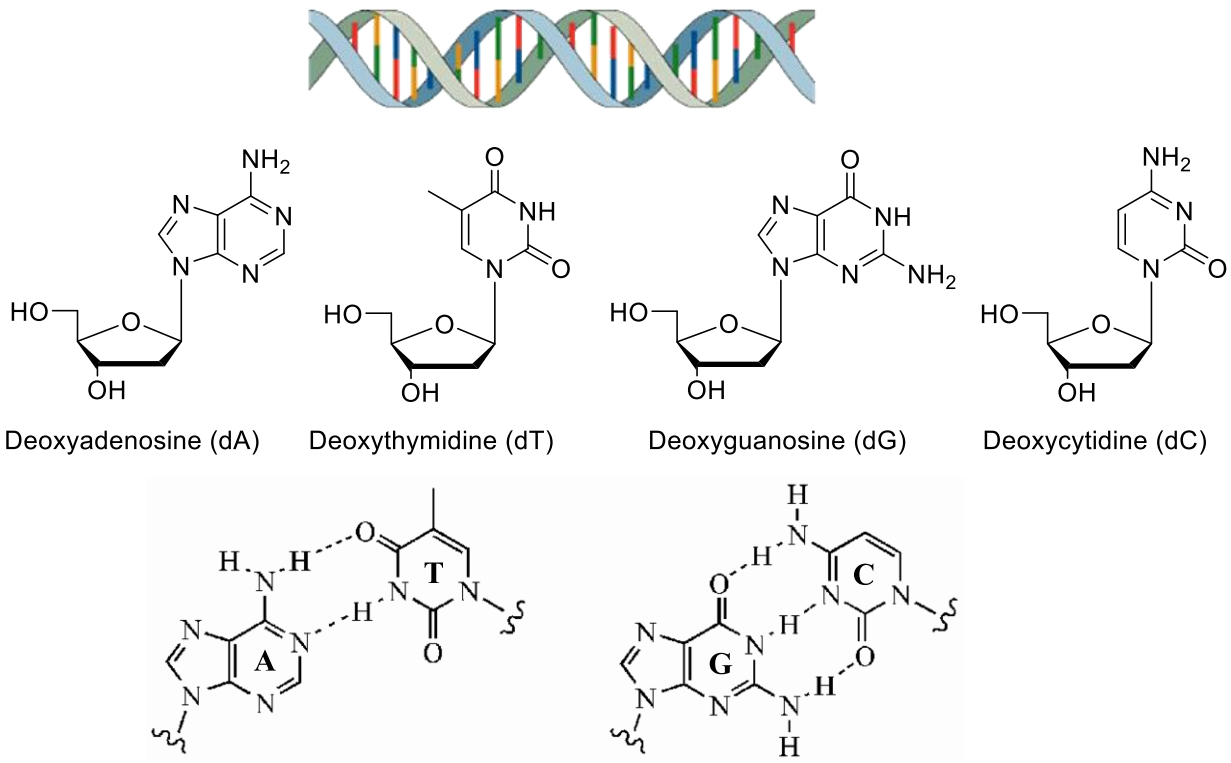

Figure 1-1. DNA double helix (top), structures of four DNA bases (dA, dT, dG, dC) (middle) and Watson-Crick base pairing (bottom).

As the source of genetic information, DNA is essential to build the cells and organisms. DNA damage is a serious threat to the genome integrity. It was reported that more than 10,000 DNA lesions were generated per day in each human cell.[4] There are two major sources of DNA damage, e.g. endogenous and exogenous damages.[5] Endogenous damage is naturally present within the cells, mainly arising from the hydrolytic and oxidative reactions with water and reactive oxygen species (ROS). Exogenous DNA damage is usually induced by external factors, such as ionizing radiation, ultraviolet (UV) irradiation, or chemical agents (alkylating and cross-linking agents).

Ionizing radiation including alpha, beta, gamma, neutrons and X-rays can damage DNA directly or indirectly, such as via formation of ·OH. UV light causes DNA damage via two pathways, either exciting substrates to induce photochemical alterations or affecting DNA by transferring energy from photosensitizers. Some chemicals can modify DNA by alkylation. Both DNA base moieties and the phosphate backbone can react with a variety of electrophiles, including alkyl halides, quinone methides (QMs) and carbocations.[6] The cross-linking of DNA occurs when the agents covalently bind with two nucleotides of DNA. The DNA cross-linking occurs either within the same strand (intrastrand cross-link) or between two complementary strands of DNA double helix to form DNA interstrand cross-link (ICL). DNA ICL are the source of the cytotoxicity of many antitumor and anticancer agents. My dissertation focuses on developing a series of crosslinking agents, which are activated upon UV irradiation and induce DNA ICL formation. The work describes the synthesis of these crosslinking agents, the mechanism investigation of DNA ICL formation, and determination of the reaction sites toward DNA. In addition, I studied the chirality effect of the substrates on DNA ICL formation.

1.2 Photoinduced DNA Interstrand Cross-Link Formation via Three Mechanisms

There are various methods to induce DNA interstrand cross-linking, such as photoinduction, activation by chemical agents or enzymes, via "click" chemistry, etc.[6] Among them, photoinduction is particularly important because of its non-invasive, selective, biorthogonal, and controllable characteristics. Photoactivation of DNA-modifying agents has attracted great attention for biological application. Three major mechanisms have been reported for photo-induced DNA ICL formation, including [2+2] cycloaddition, alkylation via quinone methide (QM) and alkylation via carbocation formation.[6] A wide variety of compounds have been developed to induce DNA ICL formation via photo-induced cycloaddition or QM formation. DNA ICL

formation via photo-induced carbocation generation were less explored. Until 2013 Li research group found that 5-(2'-Deoxyuridinyl) methyl radical was unlikely to undergo radical disproportionation reaction *in vivo*. Instead, the free radicals could undergo oxidation to form cation.[7] Then, Greenberg group verified that DNA ICL formation induced by phenyl selenide and aryl sulfide modified nucleotides were produced via photogenerated 5-(2'-deoxyuridinyl) methyl carbocation, not directly from 5-(2'-deoxyuridinyl) methyl radical.[8] Later on, Peng and co-worker discovered that several aryl boronates and bis(nitroimidazole) compounds induced DNA ICL formation via photogenerated carbocations.[9] Most recently, Peng group has developed various bifunctional aromatic compounds that can be activated upon UV irradiation to generate carbocations that directly produce DNA ICL formation.

1.2.1 Photo-induced DNA ICL formation via [2+2] Cycloaddition

Since the discovery of carvone transferred into carvone camphor upon the exposure of sunlight[10] has been confirmed, a flurry of research identified the photochemical [2+2] cycloaddition reaction between enones and alkenes. In photoinduced DNA ICL formation, [2+2] cycloaddition occurs between two photosensitive unsaturated molecules which are activated in the presence of UV light, producing a new cyclobutene product. It is a clean reaction and easily occurred with pyrimidine bases in DNA, such as TT dimer (Scheme 1-1)[6,7]. In 2013, Peng and co-worker developed a coumarin-modified nucleoside **Ia** that induces DNA ICL formation via a [2+2] cycloaddition reaction with dT or dC upon 350 nm irradiation. The fluorescence of coumarin in **Ia** is quenched after forming ICL products so that it will allow the detection of DNA ICL formation based on the fluorescence change (Scheme 1-2).[11] Later on, various coumarin analogues (**Ib-1**, **Ib-2**, and **Ib-3)** were designed and employed for efficient DNA ICL formation as well as ligation of ODNs (oligodeoxyribonucleotides) (Scheme 1-3).[12,13] The linker units (R_2 = OCH_2CH_2OH in **Ib-1**, R_2 =

OH in **Ib-2** or **Ib-3**) between the coumarin moieties and DNA sequences strongly affected the ligation efficiency and DNA ICL formation. Coumarin analogues with -OH linker unit (**Ib-2**and **Ib-3**) are more favorable for DNA photoligation than **Ib-1** with a linker of two-carbon chain. However, **Ib-1** was much efficient in producing DNA ICL formation than **Ib-2** and **Ib-3.** Almost quantitative DNA ICL formation was observed for **Ib-1**, which was more than twice higher than those produced by **Ib-2** and **Ib-3**. The DNA photoligation and ICL formation induced by coumarin moieties was reversible, which can be directly quantitated using fluorescence spectroscopy. Recently, Lee research group developed a coumarin nucleotide **Ic** that was capable of forming DNA ICL with dT and dC upon irradiation at 365 nm less than 5min (Scheme 1-3).[14]

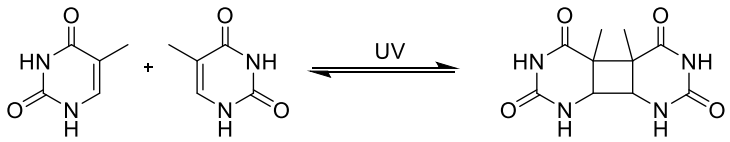

Scheme 1- 14. Formation of cyclobutane dimmer of dT upon photoirradiation.

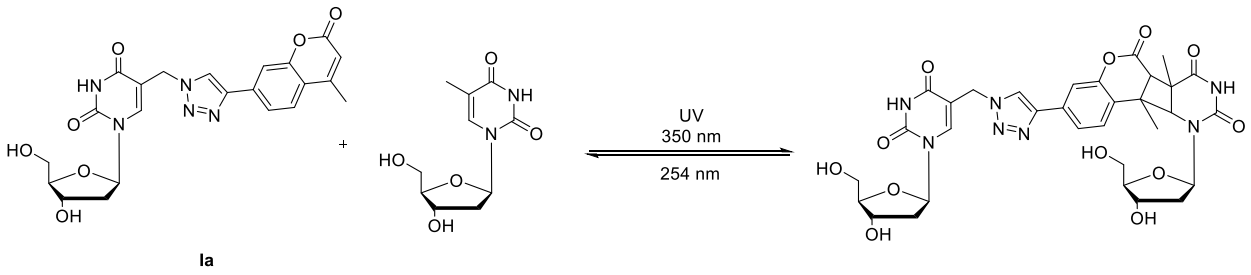

Scheme 1-15. Coumarin-modified nucleoside **Ia** and its [2+2] cycloaddition with thymidine.

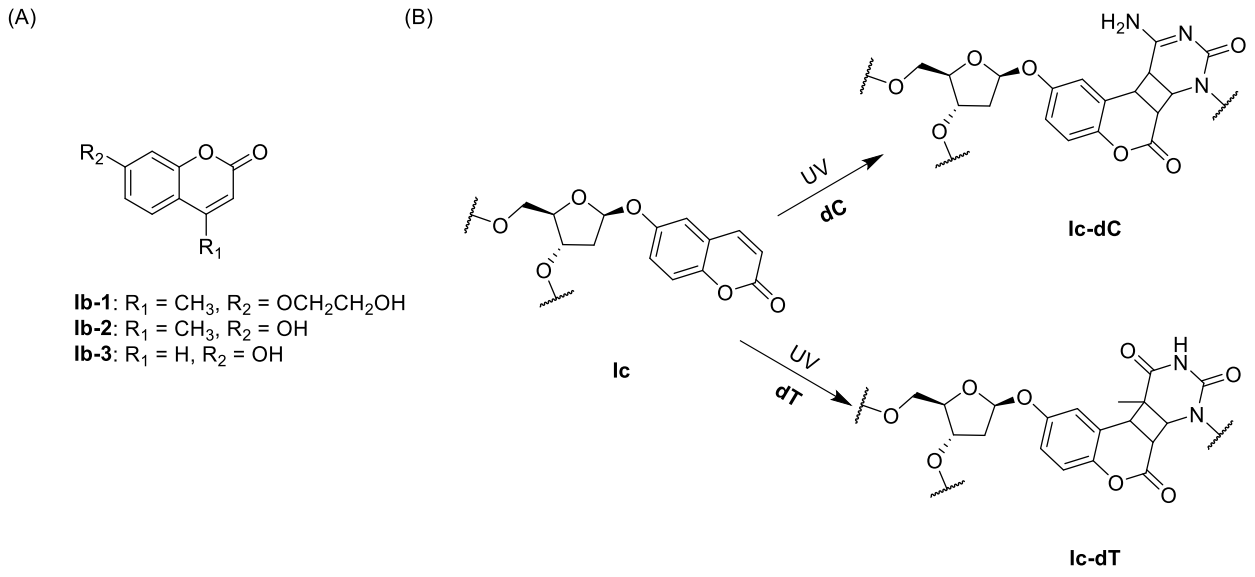

Scheme 1-16. (A) Coumarin analogues with a two-carbon linker unit (**Ib-1**) and with -OH linker unit (**Ib-2** and **1b-3**); (B) coumarin-modified nucleotide **Ic** and the cycloaddition reaction with dC or dT.

Except for coumarin moieties, *p*-stibazole,[15] and 3-cy-anovinycarbazole[16,17,18] were also reported to induce DNA ICL formation via [2+2] photocycloaddition. Asanuma research group found that *p*-stibazoles induced DNA ICL formation via [2+2] cycloaddition reaction upon 340 nm irradiation. The DNA cross-linking induced by *p*-stibazoles is ultrafast, which only took about 3 min (Scheme 1-4).[15] Dr. Fujimo, Dr. Yoshimura and other researchers reported that 3-Cyanovinycarbazole nucleoside (^{CNV}K) **Id** induced photo-reversible DNA ICL formation with pyrimidine bases via a [2+2] cycloaddition reaction at 366 nm for only 1s and the cross-linked ODNs **Id-dC** or **Id-dT** can be reverted to the original ODN **Id** by 312 nm irradiation for 60s (Scheme 1-5A).[16,17,18] In later research, they also found that the product **Id-dC** can be converted to cross-linked uracil **Id-dU** with 90℃ heating. Such DNA ICL reaction can be applied in photochemical RNA editing (Scheme 1-5B).

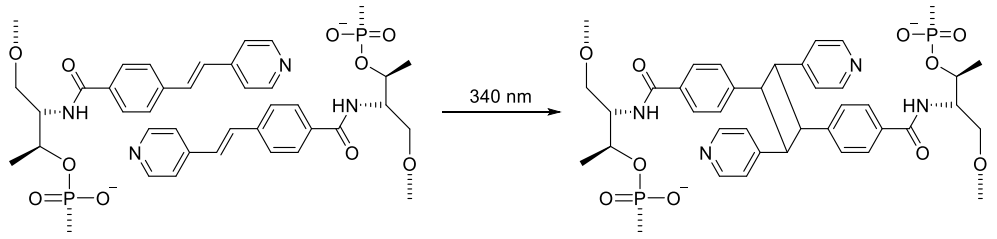

Scheme 1-17. [2+2] Photocycloaddition reaction between p-stilbazole moieties.

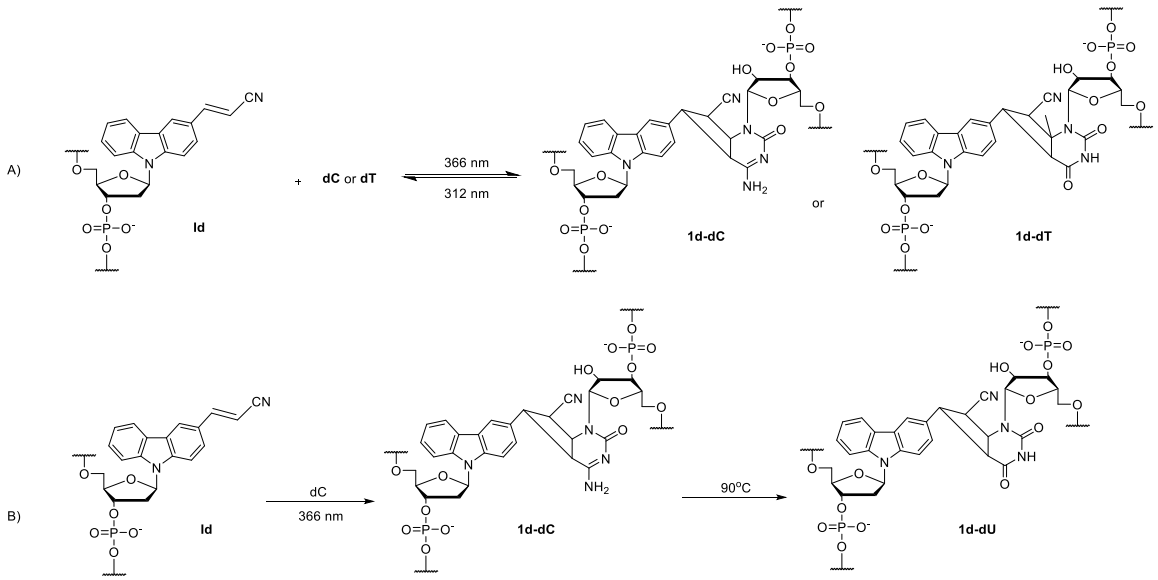

Scheme 1-18. A) Photoinduced [2+2] cycloaddition reaction with pyrimidine bases by **Id**; B) the conversion of ICL product **Id-dC** to **Id-dU** at 90°C.

1.2.2 DNA ICL Formation via Photo-Generated Quinone Methide

Quinone methide (QM) consists of a cyclohexadiene with an exocyclic methylidene and a carbonyl group. QMs are highly polarized, reactive, and readily accessible through reactions of photochemical excited states.[19,20] They are strong electrophiles that are highly reactive with nucleobases. The cyclic nitrogens, exocyclic amino groups and oxygens in the guanine, cytosine and adenosine are good nucleophiles that can react with QMs (Scheme 1-6).[21,22,23]

A variety of bifunctional aromatic compounds have been developed to induce DNA interstrand cross-linking via photo-generated QM formation, such as phenol, biphenol and BINOL analogues[6]. In 1998, Wan research group developed a clean and efficient photochemical reaction for the formation of (*o*-, *m*-, *p*-) QMs upon 254 nm UV irradiation with hydroxybenzyl alcohol. It was observed that the *o*-QMs can be formed readily, compared with other two forms.[24] Then, the research groups of Freccero and Kresge reported the generation of *o*-QMs upon photoirradiation and studied their thermal activation.[19,25] With the encouragement of the work in Freccero group, Zhou group developed phenol biquaternary ammonium salt **Ie** and biphenol biquaternary ammonium salt **If** as efficient photo-inducible DNA cross-linking agents in 2003 (Scheme 1-7).[26] Compounds **Ie** and **If** can be photo-activated upon >400 nm irradiation to generate QMs that directlyproduce efficient DNA interstrand cross-linking (Scheme 1-7A, Scheme 1-8A, 1-8B). Within 30 min irradiation, the biphenol compounds (**If**) produced highly efficient DNA ICL formation with a yield 100 times higher than that of the phenol analogues (**Ie**) with the same concentration (10 μM), indicating that the biphenol compounds were more potent DNA cross-linking agents. Freccero and co-workers have developed two photo-activatable BINOL derivatives **Ig-1** and **Ig-2** that can induce DNA ICL formation upon UV irradiation (Scheme 1-7B).[27] These BINOL derivatives can be activated by the wavelength longer than 360 nm to produce BINOL-QMs that cross-link DNA via alkylation (Scheme 1-8C). The BINOL derivative with biquaternary ammonium salts as leaving groups (**Ig-2**) induced highly efficient DNA ICL formation with 90% yield. However, the presence of the charged quaternary ammonium moieties prevented **Ig-2** from crossing biological membranes, limiting its *in vivo* applications. Therefore, to improve the cell permeability, BINOL-amino acid derivatives (BINOLAMs) **Ih-1**-**7** (Scheme 1-7C) were developed.[28]

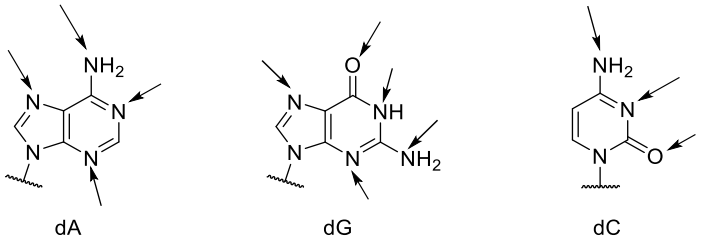

Scheme 1-19. Possible alkylation sites on dA, dG and dC.

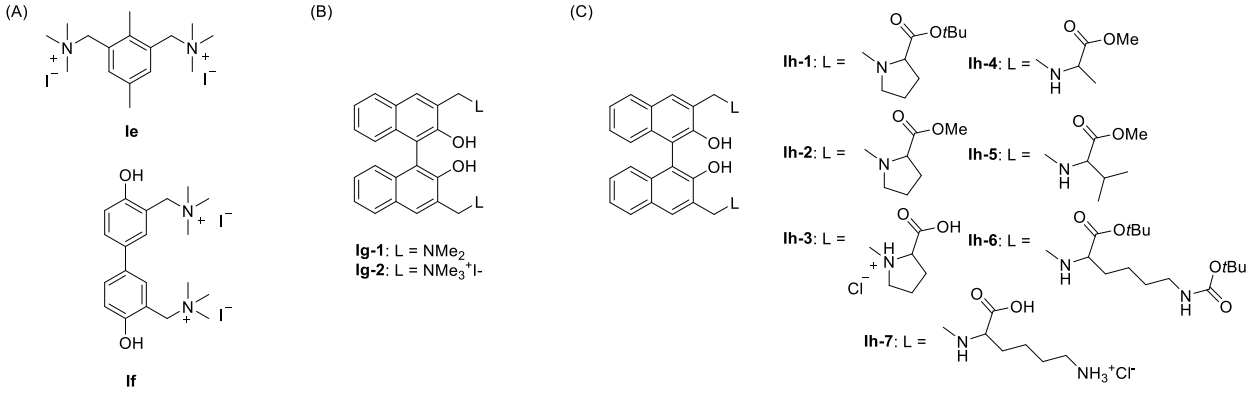

Scheme 1-20. (A) Phenol and biphenol biquaternary ammonium salts **Ie** and **If**; (B) BINOL derivatives (**Ig-1** and **Ig-2**); (C) BINOL-amino acid derivatives **Ih-1-7**.

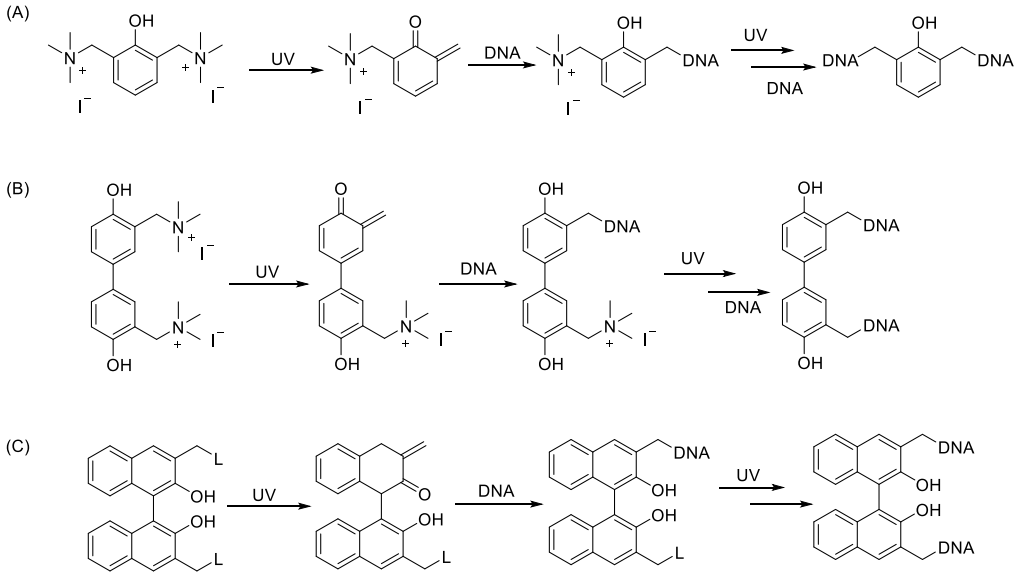

Scheme 1-21. Mechanism of photoinduced DNA ICL formation via QMs.

Later on, it was observed that both aromatic substituents and leaving groups (L) affect QM formation. Among various benzylic leaving groups (L = NR_2, OH, NMe_3I), the ammonium salts are more favorable for photo-induced DNA ICL formation because positively charged ammonium salts are not good nucleophiles therefore not competing with DNA to react with QMs. Highly efficient DNA ICL formation was observed with precursors containing the ammonium salts as leaving groups. It was also reported that the electron-donating groups (EDGs) greatly facilitate QM generation and regeneration while the electron-withdrawing groups (EWGs) slow down or suppress such process possibly due to the electron deficiency property of QMs.[29]

1.2.3 Photo-Induced Carbocation Formation

In addition to [2+2] cycloaddition and QM formation that are involved in photo-induced DNA interstrand cross-linking process, carbocation generation is another possible mechanism for photo-induced DNA ICL formation[6]. Photo-induced carbocation formation have not received much attention until the recent decade. In 2013, the research groups of Li and Greenberg have discovered that photo-irradiation of modified thymidines induced DNA interstrand cross-linking via carbocations, not free radicals although both intermediates were produced during the photo-activation process.[7, 30] In Li's work, the reactivity of 5-(2'-deoxyuridinyl) methyl radical **Ii** was re-examined by photolytic cleavage of the C-S bond in 5-(phenylthiomethyl)-2'-deoxyuridine (PhSmdU). The photoreaction of PhSmdU linked to thymine was processed upon 254 nm irradiation for 5 min in the presence or absence of O_2, and HPLC and MS data clearly indicated that 5-(2'-deoxyuridinyl) methyl radical can be oxidized to cation in aerobic atmosphere and reduced to anion in anaerobic condition (Scheme 1-9A).[7] Greenberg group provided the direct evidence of the existence of 5-(2'-deoxyuridinyl) methyl radical by using 4-hydroxy-2,2,6,6-

tetramethylpiperidin-1-oxyl (TEMPO) as radical trapper and the respective carbocation with methoxyamine as carbocation trapper (Scheme 1-9B).[30]

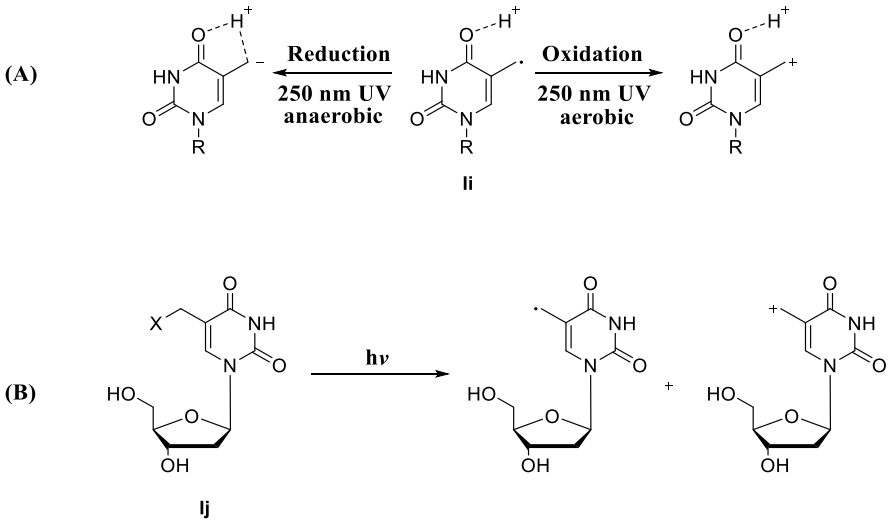

Scheme 1-22. (A) Redox of 5-(2'-Deoxyuridinyl) methyl radical **Ii**; (B)Reaction of modified thymine **Ij** upon irradiation.

Peng group later designed and synthesized various bifunctional aromatic compounds and studied their mechanism for inducing DNA ICL formation. These bifunctional aromatic compounds include a series of bisnaphthalene derivatives (Scheme 1-10),[9,31,32] bisnitroimidazole compounds (Scheme 1-11)[33] and benzene analogues (Scheme 1-12).[34,35,36,37] As naphthalene moiety can be activated with the visible light that has absorption wavelength larger than 350 nm and is compatible with living cells, it has the potential to be applied in biological systems without harm to DNA and proteins.[31,32] Peng and co-workers have developed a series of binaphthalene analogues that can be activated upon 350 nm irradiation to induce DNA cross-links via carbocation formation. Initially, two binaphthalene boronates **Ik-1** and **Ik-2** with bromine or trimethyl ammonium salts as leaving groups were synthesized and characterized. These compounds induced DNA ICL formation upon 350 nm irradiation with about 10% yields.[9] Due to the low ICL yields that prevent the detailed

mechanism investigation of these compounds, other analogues have been developed for further optimization, including 1,1'-binaphthalene analogues **Il**, **Im**, and **1a-1e**[31,32] Most of these new analogues greatly improved DNA cross-linking efficiency with ICL yields improved about 2-4 times. In addition to the binaphthalene compounds, several bifunctional phenyl derivatives **Io**, **Ip**, and **Iq** were reported to induce DNA ICL formation upon UV irradiation (Scheme 1-12). [34,35,36,37] Similar to the binaphthalene analogues, the photoreactivity of these bifunctional phenyl derivatives was influenced by the substituents on the aromatic rings as well as the leaving groups. Among various bisnitroimidazole compounds containing different leaving groups, **In-4** with nitrogen mustard showed the highest ICL yield due to that the released nitrogen mustard also cross-linked DNA.[34] In summary, a variety of parameters affect the photoreactivity of the aromatic compounds towards DNA, including the parent moiety, the aromatic substituents, the leaving groups, UV absorption, etc. .[32,34,37] Both the electronic effect and steric effect of the aromatic substituents and the leaving groups combine to influence the photo-induced DNA ICL formation.

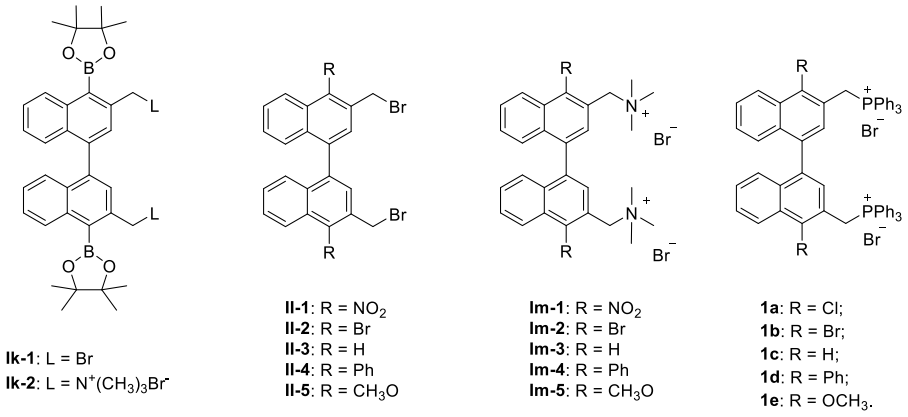

Scheme 1-23. Binaphthalene derivatives.

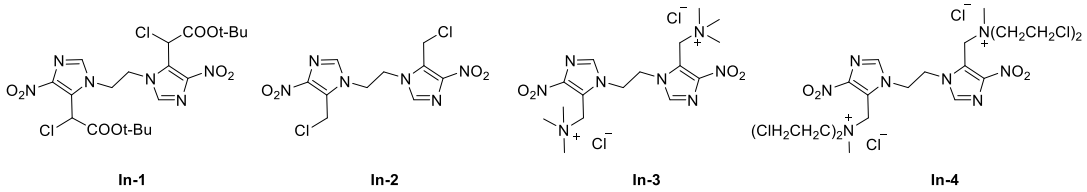

Scheme 1-24. Bisnitroimidazole compounds.

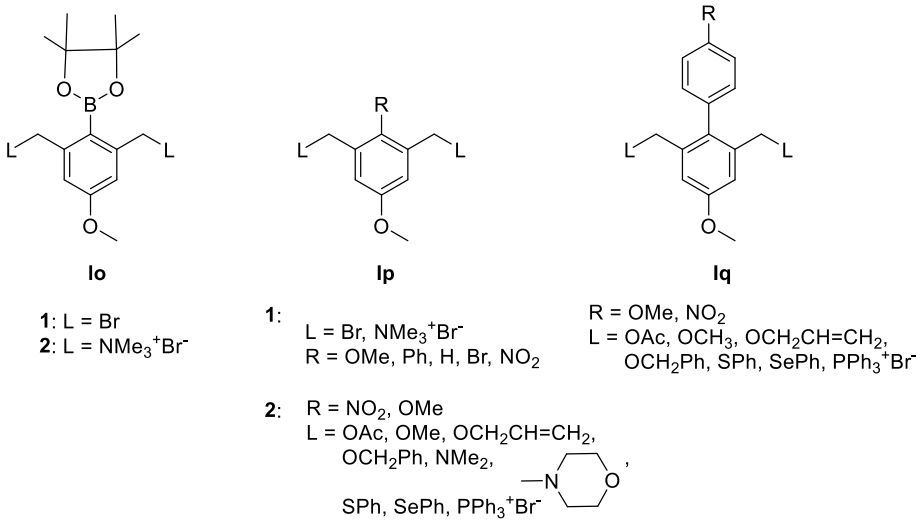

Scheme 1-25. Benzene compounds.

The detailed mechanism investigation suggested that both carboncations and free radicals are involved in the photo-induced DNA ICL formation by these bifunctional aromatic compounds while the carbocations directly alkylate DNA to form ICL products. Generally, there are two pathways to generate carbocation, either from direct heterolysis of C-L bond (L = leaving group) or homolysis of C-L bond to form free radicals that are oxidized to the cations. Most binaphthalene analogues undergo the homolysis of C-L bond upon photo irradiation to generate the free radicals **Ir** that are spontaneously converted to the corresponding carbocations **Is** (Scheme 1-13A). [9,31,32] Slightly different phenomena were observed for the phenyl boronates for which the pathways of the carbocation generation depend on the leaving groups of the substrates.[35] The phenyl boronate with bromo as leaving group produced benzyl cations **Iu** via the oxidation of free radicals **It** while the phenyl boronate with trimethyl ammonium salts as leaving group generated cations **Iu** via direct heterolysis of C-N bond (Figure Scheme 1-13B, 1-13C). Further study showed that the aromatic substituents also affect DNA ICL formation mechanism. For example, only carbocations are involved in photo-induced DNA ICL formation by compound **Iw** containing trimethyl ammonium

salts as leaving group and a nitro substituent at the position-2 while both pathways were observed for photo-induced carbocation generation by compound **Iv** with bromo substituent which depend on the concentrations of TEMPO (Figure 1-2).[34] The free radicals were involved in photo-induced DNA cross-linking process of **Iv** in the presence of low concentration of TEMPO (0-2.0 mM) as shown by the decreased ICL yield while increased ICL yield was observed when high concentration of TEMPO (> 2.0 mM TEMPO) was used suggesting that the pathways for the carbocation generation are more complex, both direct heterolysis of the C-N bond or the formation of free radical are possible. The high concentrations of TEMPO might suppress the formation of free radical and enable the alternate pathway in which the direct heterolysis of C-L bond produced carbocation. For bisnitroimidazole compounds, the carbocation was produced from the oxidation of free radical photo-generated by the homolysis of C-L bond (Scheme 1-13D)[33], which was similar to those of binaphthalenes and most benzene compounds.

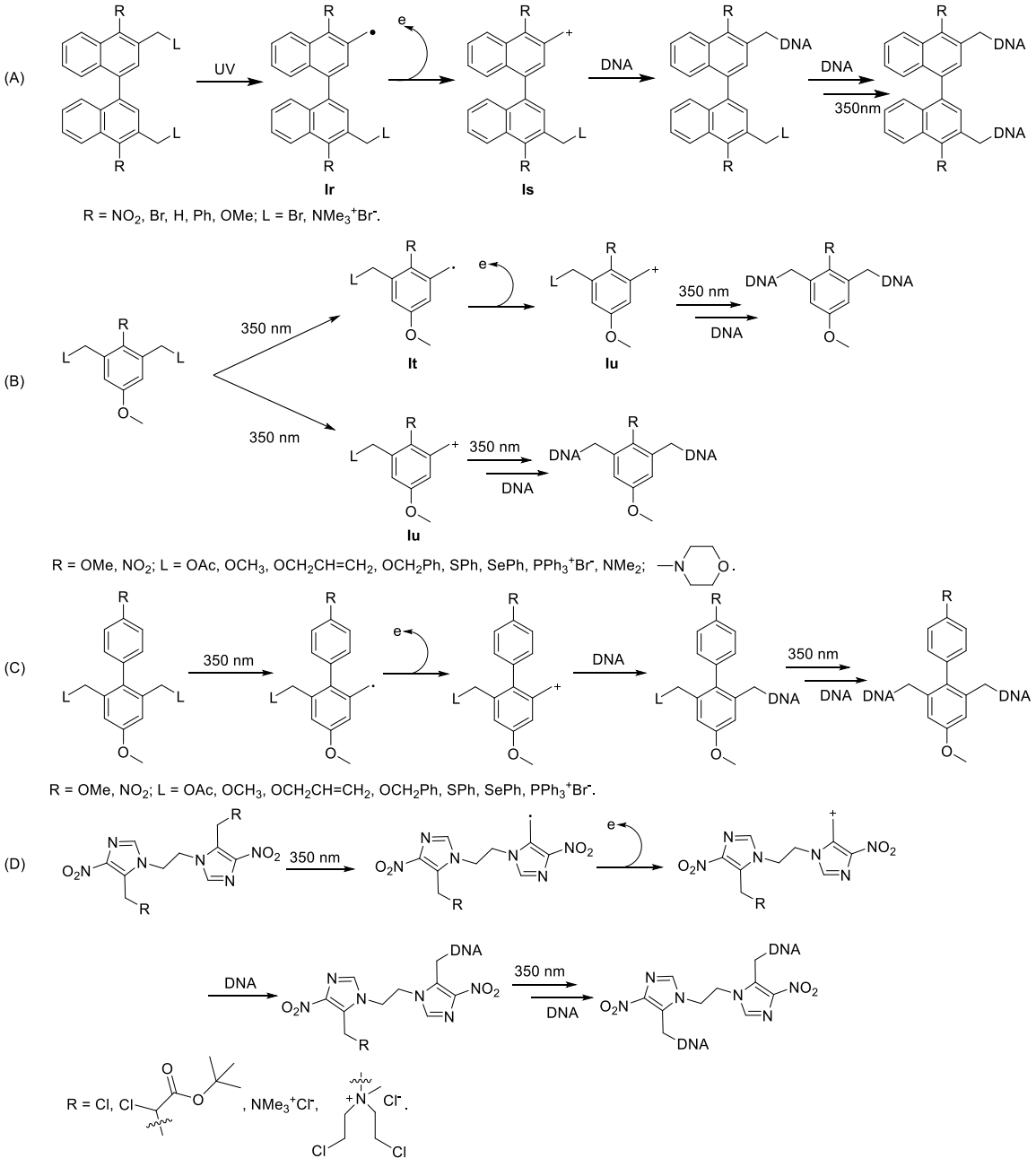

Scheme 1-26. Proposed mechanism of carbocation formation. (A) Binaphthalene analogues; (B), (C) benzene analogues; (D) bisnitroimidazole compounds.

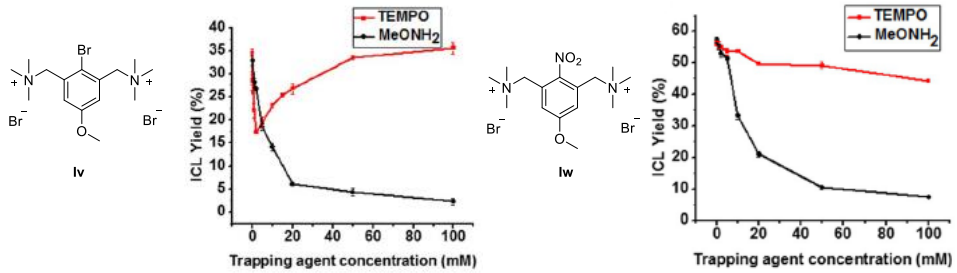

Figure 1-2. Carbocation and radical trapping with DNA ICL formation for phenyl trimethyl ammonium salts with bromo substituent (**Iv**) (left) or nitro substituent (**Iw**) (right).

1.3 References

[1] Watson, J. D.; Crick F.H. Molecular structure of Nucleic Acids; A structure for Deoxyribose Nucleic Acid. *Nature.* **1953**, 171, 737-738.

[2] Travers, A.; Muskhelishvili, G. DNA Structure and Function. *FEBS Journal.* **2015**, 282, 2279-2295.

[3] Rich, A.; Nordheim, A.; Wang, A. H. The Chemistry and Biology of Left-Handed Z-DNA. *Annual Review of Biochemistry.* **1984**, 53, 791-846.

[4] Carusillo, A.; Mussolino, C. DNA Damage: From Threat to Treatment. *Cells.* **2020**, 9, 1665-1685.

[5] Chatterjee, N.; Walker, G.C. Mechanisms of DNA Damage, Repair and Mutagenesis. *Environ. Mol. Mutagen.* **2017**, 58, 235-263.

[6] Fan, H.; Peng, X. Novel DNA Cross-Linking Reagents. *In Advances in Molecular Toxicology*; Fishbein, J. C.; Heilman, J. M., Eds.; Elsevier, 2016; Vol. *10*, pp 235−292.

[7] Goodsell, D.S. The Molecular Perspective: Ultraviolet Light and Pyrimidine Dimers. *The Oncologist*. **2001**, 6,298-299.

[7] Lin, G.; Li, L. Oxidation and reduction of the 5-(2′-deoxyuridinyl)methyl radical. *Angew. Chem., Int. Ed.* **2013**, 52, 5594−5598.

[8] Weng, L.; Horvat, S. M.; Schiesser, C. H.; Greenberg, M. M. Deconvoluting the reactivity of two intermediates formed from modified pyrimidines. *Org. Lett.* **2013**, 15, 3618−3621.

[9] Wang, Y. B.; Lin, Z. C.; Fan, H. L.; Peng, X. H. Photoinduced DNA Interstrand Cross-Link Formation by Naphthalene Boronates via a Carbocation. *Chem. - Eur*. J. **2016**, 22, 10382−10386.

[10] Ciamician, G.; Silber, P. Chemische Lichtwirkungen. *Berichte Der Deutschen Chemischen Gesellschaft.* **1908**, 41, 1928–1935.

[11] Haque, M. M.; Sun, H.; Liu, S.; Wang, Y.; Peng, X. Photoswitchable Formation of a DNA Interstrand Cross-Link by a Coumarin-Modified Nucleotide. *Angew. Chem. Int. Ed.* **2014**, 53, 7001–7005.

[12] Sun, H.; Fan, H.; Peng, X. Quantitative DNA Interstrand Cross-Link Formation by Coumarin and Thymine: Structure Determination, Sequence Effect, and Fluorescence Detection. *J. Org. Chem.* **2014**, 79, 11359–11369.

[13] Sun, H.; Fan, H.; Eom, H.; Peng, X. Coumarin-Induced DNA Ligation, Rearrangement to DNA Interstrand Cross-Links, and Photorelease of Coumarin Moiety. *ChemBioChem*. **2016**, 17, 2046–2053.

[14] Rozelle, A. L.; Kumar, R. N.; Lee, S. Photo-induced DNA Interstrand Cross-Links Formed by a Coumarin-modified Nucleoside. *Nucleoside, Nucleotides and Nucleic Acid.* **2019**, 38, 1-12.

[15] Kashida, H.; Doi, T.; Sakakibara, T.; Hayashi, T.; Asanuma, H. *p*-Stilbazole Moieties As Artificial Base Pairs for Photo-Cross-Linking of DNA Duplex. *J. Am. Chem. Soc.* **2013**, 135, 7960-7966.

[16] Yoshimura, Y.; Fujimoto, K. Ultrafast Reversible Photo-Cross-Linking Reaction: Toward in Situ DNA Manipulation. *Org. Lett.* **2008**, 10, 3227−3230.

[17] Fujimoto, K.; Konishi-Hiratsuka, K.; Sakamoto, T.; Yoshimura, Y. Site-Specific Cytosine to Uracil Transition by Using Reversible DNA Photo-Crossling. *ChemBioChem*. **2010**, 11, 1661−664.

[18] Fujimoto, K.; Konishi-Hiratsuka, K.; Sakamoto, T.; Yoshimura, Y. Site-Specific Photochemical RNA Editing. *Chem. Commun.* **2010**, 46, 7545-7547.

[19] Chiang, Y.; Kresge, A. J.; Zhu, Y. Flash Photolytic Generation of *ortho*-Quinone Methide in Aqueous Solution and Study of Its Chemistry in that Medium. *J. Am. Chem. Soc.* **2001**, 123, 8089-8094.

[20] Toteva, M. M.; Richard, J. P. The Generation and Reactions of Quinone Methides. *Advances in Physical Organic Chemistry.* **2011**, 45, 39-91.

[21] Rokita, S. E.; Yang, J.; Pande, P.; Greenberg, W. A. Quinone Methide Alkylation of Deoxycytidine. *J. Org. Chem.* **1997**, 62, 3010-3012.

[22] Pande, P.; Shearer, J.; Yang, J.; Greenberg, W.A.; Rokita, S. E. Alkylation of Nucleic Acids by a Model Quinone Methide. *J. Am. Chem. Soc.* **1999**, 121, 6773-6779.

[23] Cao, S.; Peng, X. Exploiting Endogenous Cellular Process to Generate Quinone Methides In Vivo. *Current Organic Chemistry*. **2014**, 18, 70-85.

[24] Brousmiche, D.; Wan, P. Photogeneration of an *o*-Quinone Methide from Pyridoxine (Vitamin B_6) in Aqueous Solution. *Chem. Commun.* **1998**, 491-492.

[25] Modica, E.; Zanaletti, R.; Freccero, M.; Mella, M. Alkylation of Amino Acids and Glutathione in Water by o-Quinone Methide. Reactivity and Selectivity. *J. Org. Chem.* **2001**, 66, 41-52.

[26] Wang, P.; Liu, R.; Wu, X.; Ma, H.; Cao, X.; Zhou, P.; Zhang, J.; Weng, X.; Zhang, X.; Qi, J.; Zhou, X.; Weng, L. A Potent, Water-Soluble and Photoinducible DNA Cross-Linking Agent. *J. Am. Chem. Soc.* **2003**, 125, 1116-1117.

[27] Richter, S. N.; Maggi, S.; Colloredo-Mels, S.; Palumbo, M.; Freccero, M. Binol Quinone Methides as Bisalkylating and DNA Cross-Linking Agents. *J. Am. Chem. Soc.* **2004**, 126, 13973-13979.

[28] Doria, F.; Richter, S. N.; Nadai, M.; Colloredo-Mels, S.; Mella, M.; Palumbo, M.; Freccero, M. BINOL-Amino Acid Conjugates as Triggerable Carriers of DNA-Targeted Potent Photocytotoxic Agents. *J. Med. Chem.* **2007**, 50, 6570-6579.

[29] Weinert, E. E.; Dondi, R.; Colloredo-Melz, S.; Frankenfield, K. N.; Mitchell, C. H.; Freccero, M.; Rokita, S. E. Substituents on Quinone Methides Strongly Modulate Formation and Stability of Their Nucleophilic Adducts. *J. Am. Chem. Soc.* **2006**, 128, 11940-11947.

[30] Weng, L.; Horvat, S. M.; Schiesser, C. H.; Greenberg, M. M. Deconvoluting the reactivity of two intermediates formed from modified pyrimidines. *Org. Lett.* **2013**, 15, 3618−3621.

[31] Lin, Z.; Fan, H.; Zhang, Q.; Peng, X. Design, Synthesis, and Characterization of Binaphthalene Precursors as Photoactivated DNA Interstrand Cross-Linkers. *J. Org. Chem.* **2018**, 83, 8815−8826.

[32] Zhang, Q.; Lin, Z.; Peng, X. Photoreactivity of Binaphthalene Triphenylphosphonium Salts: DNA Interstrand Cross-link Formation and Substituent Effects. *Chemical Research in Toxicology.* Accepted on March 14th, **2022**.

[33] Han, Y.; Chen, W.; Kuang, Y.; Sun, H.; Wang, Z.; Peng, X. UV-Induced DNA Interstrand Cross-Linking and Direct Strand Breaks from a New Type of Binitroimidazole Analogue. *Chem. Res. Toxicol.* **2015**, 28, 919−926.

[34] Fan, H.; Sun, H.; Peng, X. Substituents Have a Large Effect on Photochemical Generation of Benzyl Cations and DNA Cross-Linking. *Chem. - Eur. J.* **2018**, 24, 7671−7682.

[35] Wang, Y.; Liu, S.; Lin, Z.; Fan, Y.; Wang, Y.; Peng, X. Photochemical Generation of Benzyl Cations That Selectively Cross-Link Guanine and Cytosine in DNA. *Org. Lett.* **2016**, 18, 2544−2547.

[36] Fan, H.; Sun, H.; Zhang, Q.; Peng, X. Photoinduced DNA Interstrand Cross-Linking by 1,1′-Biphenyl Analogues: Substituents and Leaving Groups Combine to Determine the Efficiency of Cross-Linker. *Chem. - Eur. J.* **2021**, 27, 5215−5224.

[37] Fan, H.; Peng, X. Photoinduced DNA Interstrand Cross-Linking by Benzene Derivatives: Leaving Groups Determine the Efficiency of the Cross-Linker. *J. Org. Chem.* **2021**, 86, 493−506.

Chapter 2 Photoreactivity of Binaphthalene Triphenylphosphonium Salts: DNA Interstrand Cross-link Formation, Substituent Effects, and Mechanism Investigation

2.1. Introduction

Photo-activation of DNA-modifying agents has attracted great attention as photo-induction is noninvasive and biorthogonal with high spatio-temporal resolution and control. In addition, no additional chemicals are needed for photochemically activatable DNA-modifying agents, which can avoid the conditions that are not compatible with in vivo applications. Several research groups have developed a wide variety of photo-activatable precursors that induced DNA interstrand cross-linking upon photo-irradiation.[1] The photo-inducible DNA cross-linking agents have found wide applications, including DNA manipulation[2] and detection,[3] DNA computing,[4] constructing DNA-based reversible photoswitches, stabilizing DNA nanostructure,[5] as well as cancer treatment. It has been reported that photo-irradiation can generate different active species directly producing DNA ICL formation, including quinone methides (QMs),[6–11] aldehyde formation from a furan moiety,[12] or carbocations.[13–20] Among them, photo-induced DNA ICL formation via carbocations was less explored until 2013 when research groups of Li and Greenberg have discovered that photo-irradiation of modified thymidines induced DNA interstrand cross-linking via carbocations, not free radicals although both intermediates were produced during the photo-activation process.[13,14] Then, the Peng group has found that various bifunctional aromatic compounds can be activated by photo-irradiation to generate biscations that directly produce DNA ICL formation via alkylation, including a series of benzene analogues,[15,17,19,20] bisnitroimidazole compounds,[16] and bisnaphthalene derivatives.[18,21] Further study suggested that two pathways were involved for

carbocation formation, via either free radical oxidation or heterolytic cleavage of C−L bond (L: leaving group), which strongly depends on the substrates.[15] Among the photo-activatable bifunctional aromatic compounds, the naphthalene analogues are particularly attractive for biological applications as the naphthalene moiety has extended π-system leading to absorptions in the visible light spectrum. The naphthalene compounds can be potentially utilized in biological systems without harm to biological materials, such as DNA and proteins, as they can be activated by a light of wavelength longer than 350 nm that is compatible with living cells. Freccero and co-workers reported that several 2,2′-hydroxyl 1,1′-binaphthalene analogues induced DNA interstrand cross-linking via Binol−QM formation upon UV−vis photo-activation.[8,9] They also discovered that several Binol−amino acid conjugates can be activated by mild photoactivation to produce efficient DNA ICL formation with superior cytotoxicity.[22] Very recently, our group have demonstrated that binaphthalene boronates (A, Scheme 2-1) undergo photo-activation with 350 nm irradiation to produce naphthalenylmethyl radicals that are spontaneously transformed to the corresponding carbocations directly forming DNA ICL via alkylation. Further study suggested that substituents greatly affected the efficiency of DNA ICL formation.[21] We have also shown that the photo-reactivity of the bifunctional benzene derivatives toward DNA is correlated to their UV absorbance.[15] These results encouraged us to design, synthesize, and characterize five new potential photo-inducible DNA cross-linking agents, triphenylphosphonium (TPP^+) salts **1a**−**1e** (Scheme 2-1). We have chosen to investigate the photochemical reactivities of the TPP^+ salts **1a**−**1e** toward DNA for the reasons discussed below. The TPP^+ salts combine lipophilic and hydrophilic properties with superior water solubility and cell membrane permeability. TPP^+ moiety has been used for targeting mitochondria.[23,24] Other advantages of TPP^+ moiety include stability in biological systems and easy synthesis. The promising features of TPP^+ moiety provide

opportunities to expand the biological applications of the photo-inducible DNA cross-linking agents **1a**−**1e**. This work is part of a more comprehensive study aimed at utilizing the superior properties of the triphenylphosphonium salts **1a**−**1e** as precursors of naphthalenylmethyl cations. This study will focus on the photoactivities of **1a**−**1e** toward DNA upon 350 nm irradiation by investigating their DNA cross-linking capabilities, alkylation sites, and mechanism for DNA ICL formation.

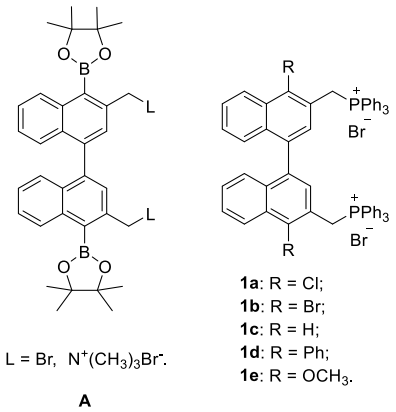

Scheme 2-9. Binaphthalene boronates **A** and triphenyl phosphonium salts **1a-1e.**

2.2. Binaphthalene Triphenylphosphonium Salts as Photo-Inducible DNA Cross-Linking Agents

2.2.1. Synthesis of Compounds 1a-1e.

We designed and synthesized five 1,1′-binaphthalene analogues **1a**−**1e** containing TPP^+ salt as leaving group and different aromatic substituents at position 4 (Scheme 2-2A). Compound **1a** was synthesized starting from 4-bromonaphthalene (**3b**) that was first converted to 4-chloronaphthalene (**3a**) by treatment with copper chloride (CuCl) in dimethylformamide (DMF) (Scheme 2-2A).[26] A lead-catalyzed coupling reaction of **3a** generated 4,4′-dichloro-1,1′-

binaphthalene (**4**) that was treated with N-bromosuccinimide (NBS) and azobis-(isobutyronitrile) (AIBN) to yield 4,4′-dichloro-1,1′-binaphthalene dibromide **2a**. Compound **2a** was transformed to TPP^+ salt **1a** by reacting with triphenylphosphine in toluene. The coupling reaction took place at the para position to bromo group, which was determined by ^1H correlation spectroscopy (COSY) and ^1H-^{13}C heteronuclear single quantum coherence spectroscopy (HSQC). The TPP^+ salts **1b**−**1e** were synthesized from the corresponding 4,4′-disubstituted 1,1′-binaphthalene dibromides **2b**−**2e** by nucleophilic substitution of the bromo group with triphenylphosphine (Scheme 2-2B). Compounds **2b**−**2e** were prepared as previously described.[21] The structures of new compounds were determined by NMR and HRMS.

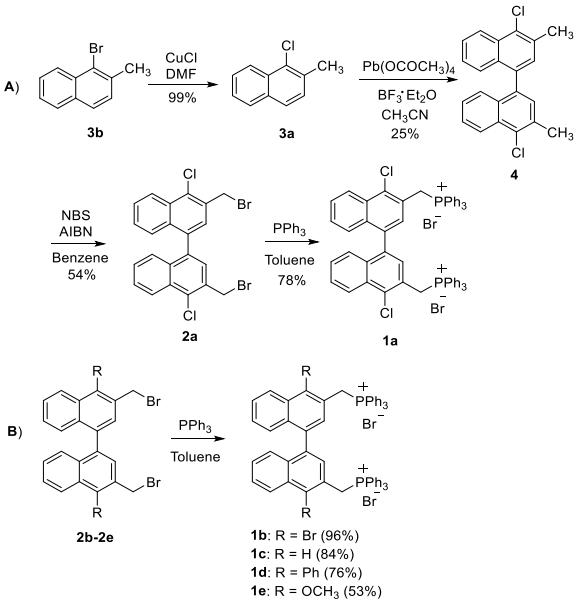

Scheme 2-10. Synthesis of 4,4'-bisubstituted 1,1'-binaphthalene triphenylphosphonium salts **1a**-**1e**.

2.2.2. DNA Duplex Preparation, including Synthesis, Purification and 5'-End ^{32}P-Labeling.

Duplex **5** (Figure 2-1) was applied in the photo-induced DNA interstrand cross-linking study with the binaphthalene analogues. The sequence of **5** is part of a p53 gene which plays a role in regulation or progression through the cell cycle and apoptosis. Its point mutations or deletions can cause a series of cancers. The single-strands ODN **5a** and **5b** were synthesized by solid-phase oligo synthesis method, with phosphoramidite approach and automated ABI 394 DNA/RNA synthesizer. The synthesis is a cyclical process that assembles a chain from 3'-end to 5'-end. Each cycle includes four steps, such as detritylation, coupling, oxidation and capping (Scheme 2-3). In detritylation step, 4,4'-dimethoxytrity group of **A** is removed to allow the subsequent phosphoramidite (Scheme 2-4) addition. Then activated **C** with the protection of diisopropylamino groups couples with **B** to form a P-O bond. Next, P (III) is oxidated to P (V) from **D** to **F**. To prevent further chain extension, the unreacted 5'-end hydroxyl groups are acetylated in the capping step (shown as **E**).

```
          6                   22    27
5'-dGCCTAGTTCTTTTAATTACTTGCAATGCAAGTAATTAAAGCTTGATCTG-3'   (5a)
3'-dCGGATCAAGAAAATTAATGAACGTTACGTTCATTAATTTCGAACTAGAC-5'   (5b)
```

Figure 2-1. DNA duplex **5**.

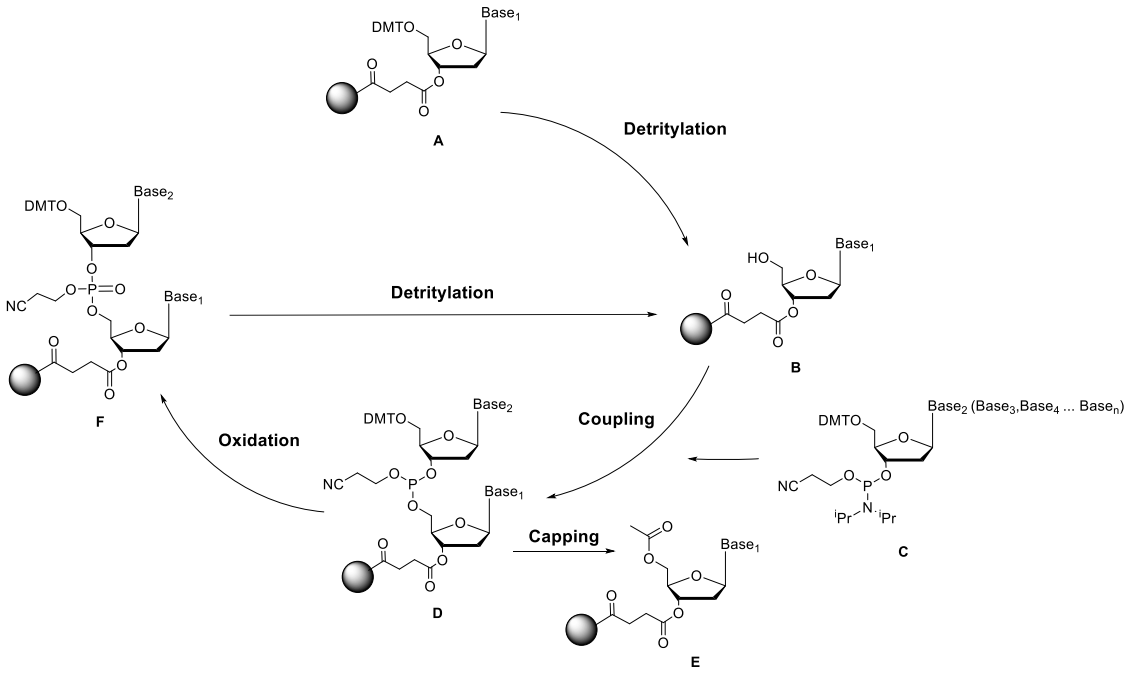

Scheme 2-11. Automated DNA synthesis cycle.

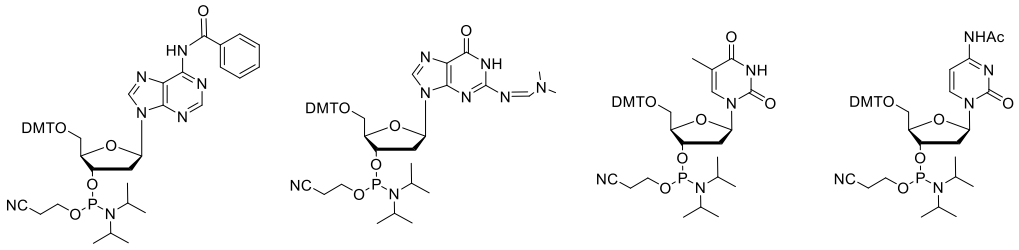

Scheme 2-12. The Structures of the phosphoramidites used for ODN synthesis.

After the synthesis is completed, the ODNs were deprotected and cleaved from the solid support using a mixture of 40% aqueous $MeNH_2$ and 28% aqueous NH_3 (1:1) via incubation at room temperature (rt) for 2 h. The protecting groups for the exocyclic primary amino groups of adenine, cytosine and guanine were removed so that proper hydrogen bonds between the complementary nucleobases will form (Scheme 2-5). Meanwhile, in this process, the ODN was cleaved from solid support to obtain the free 3'-OH via ester hydrolysis. The deprotected ODN strands were further purified with 20% Denaturing Polyacrylamide Gel Electrophoresis (PAGE).

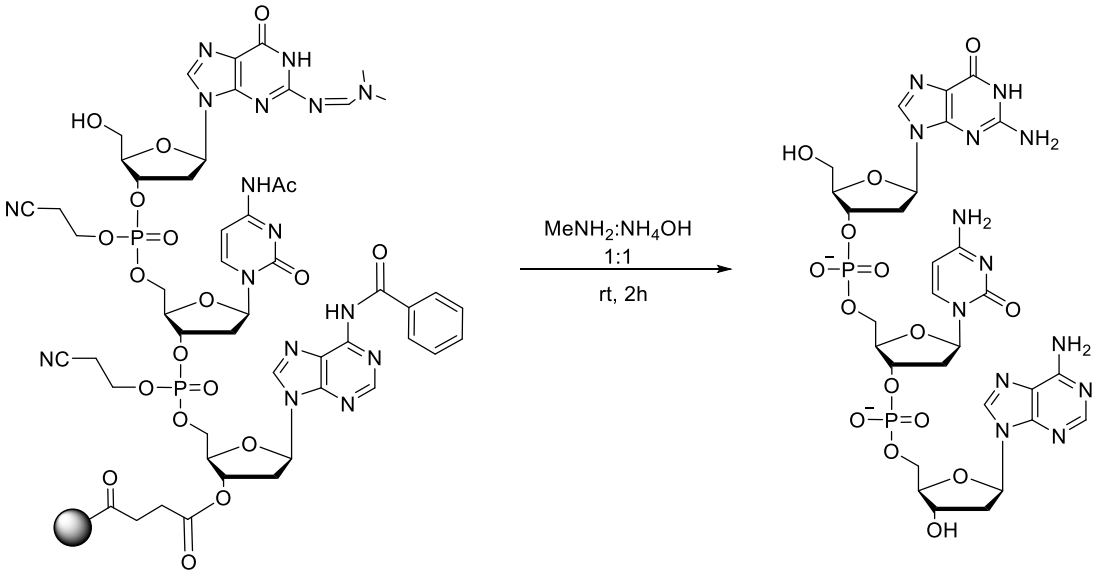

Scheme 2-13. Deprotection of nucleotides and cleavage of ODNs from solid support.

The ^{32}P-labelling of ODNs with polynucleotide kinase and [γ-^{32}P] ATP is an ultrasensitive method for detecting nucleic acid sequences. The ^{32}P-ATP can be incorporated into the 5'-end of an ODN via an enzymatic reaction catalyzed by T4 polynucleotide kinase (T4 PNK) (Scheme 2-6) which was first identified by Richardson, Novagrodsky, and Hurwitz in T-phage infected E. coli. T4 PNK catalyzes the transfer of the gamma phosphate of ATP to the 5' hydroxyl terminus of ODNs.[27-29] In this work, either ODN **5a** or **5b** was ^{32}P-labeled at the 5'-teminus.

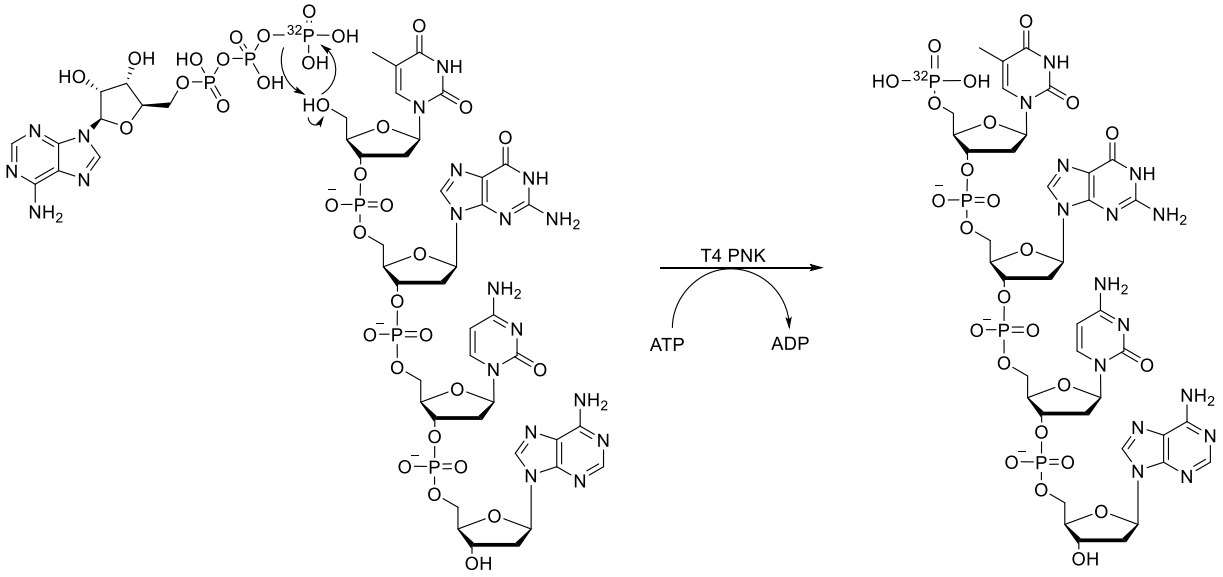

Scheme 2-14. 5'-end oligonucleotide labeling.

2.2.3. Photo-Induced DNA Interstrand Cross-Link Formation by 1a-1e.

The photo-reactivity of 4,4′-disubstituted 1,1′-binaphthalene TPP^+ salts **1a**−**1e** toward DNA was investigated with 49-mer DNA duplex (**5**) in a phosphate buffer. The reaction mixture was irradiated using an irradiator (Rayonet Model RPR-100) with 350 nm UV light. The DNA interstrand cross-linking yield was determined by denaturing PAGE with phosphorimager analysis (ImageQuant 5.2). The initial study indicated that DNA ICL products were not formed by **1a**− **1e** without UV irradiation, but efficient ICL formation was observed with 350 nm irradiation of **1a**−**1e** (Figure 2-2). To fully investigate the photo-reactivity of **1a**−**1e** toward DNA, we determined reaction time, rate constants, and efficiency for DNA interstrand cross-linking, and minimum concentration (C_{opt}) needed to reach the highest ICL yields for **1a**−**1e** (Table 2-1 and Figure 2-3, 2-4). The reactions of these binaphthalene compounds with DNA followed the first-order kinetics with respect to DNA. The aromatic substituents greatly affect the efficiency and reaction rates for photo-induced ICL formation by **1a**−**1e**. In general, the electron-withdrawing substituents (i.e., Cl, Br, and Ph) facilitate the ICL reaction, while a donating group (i.e., OMe) slows down the DNA

cross linking process. It is likely that withdrawing groups increase the electrophilicity of the photo-generated naphthalenylmethyl cation leading to a faster ICL reaction while the donating substituent decreases its electrophilicity, therefore causing a slower cross-linking reaction. In addition to the electronic properties of the aromatic substituents, UV absorption also affects photo-reactivity.[20] Thus, we investigated the effects of different substituents on the UV absorption of **1a**−**1e** to determine the correlation between the photo-reactivity of these compounds and their UV absorption. UV spectra of **1a**−**1e** were measured in methanol at 0.2 mM concentration (Figure 2-5) and the molar extinction coefficients were calculated based on the Beer−Lambert Law (Table 2-1). We observed that **1a**, **1b**, and **1d** showed a maximum UV absorption at longer wavelengths and larger extinction coefficients (ε) than **1c** and **1e**, which might be one of the factors that lead to the higher reactivity toward DNA. However, the order of the rate constants for **1a**−**1e** ($k_{1b} > k_{1a} > k_{1d} > k_{1c} > k_{1e}$) is slightly different from the order of the maximum UV absorption, i.e., $\varepsilon_{308(1b)} > \varepsilon_{308(1d)} > \varepsilon_{308(1a)} > \varepsilon_{308(1e)} > \varepsilon_{308(1c)}$. The small discrepancy between the order of UV absorption and that of the reaction rates for **1a**/**1d** and **1c**/**1e** might be caused by other factors that offset the effect of UV absorption on their photo-reactivity toward DNA. Although a phenyl group (**1d**) greatly improved the molar extinction coefficient at the maximum absorption wavelength that favors DNA cross-linking reaction, its bulky size may impede ICL reaction, resulting in a slower reaction rate for **1d** than **1a**. Similarly, a methoxy group in **1e** increased the molar extinction coefficient at the maximum absorption wavelength in comparison to the parent compound **1c**, while the reaction rate of **1e** is slightly slower than **1c**, which might be due to the electron-donating effect of the OMe group that decreases the electrophilicity of the naphthalenylmethyl cation photo-generated from **1e**. Collectively, these data demonstrated that there is a clear correlation between the photo-

reactivity of **1a**−**1e** and their UV absorption, while the electronic effect, steric effect, and UV absorption combine to influence the final ICL formation yield.

Having obtained the optimized reaction time for **1a**−**1e**, we studied the compound concentration effects on DNA ICL formation (Figure 2-4). Generally, the cross-linking yields increased with the increased concentrations of **1a**−**1e** until the yields reached the maximum. The maximum cross-linking yields reached at the C_{opt} of less than 0.4 mM for all compounds tested. For better comparison, we determined the ICL efficiency for all compounds at the same concentration (0.2 mM) as well as at the C_{opt} values for different compounds. The ICL efficiency is in the order of **1a** ≈ **1b** > **1e** > **1c** > **1d** at a 0.2 mM concentration (Figure 2-2, lanes 6−10), which is similar to those obtained at the optimized concentrations. Under both conditions, the highest ICL yields were observed with **1a** and **1b**, while the lowest ICL efficiency was observed for **1d** (Table 2-1). In comparison with the parent compound **1c**, the introduction of a Ph group slightly decreased the photo-induced DNA ICL formation while OMe substituent slightly increased ICL yield, and the halogen substituents greatly improved the ICL efficiency. It is likely that the bulky size of the phenyl group in **1d** prevents the efficient interaction between **1d** and alkylation sites in DNA, leading to a low ICL efficiency. This is consistent with the effect of the aromatic substituents on the ICL reaction rate. Significant amounts of DNA damage were observed with concentrations of **1a**−**1e** higher than the C_{opt}. Overall, this study indicated that different substituents on the binaphthalene TPP^+ salts not only significantly affect the reaction rate for DNA cross-linking but also influence the ICL efficiency.

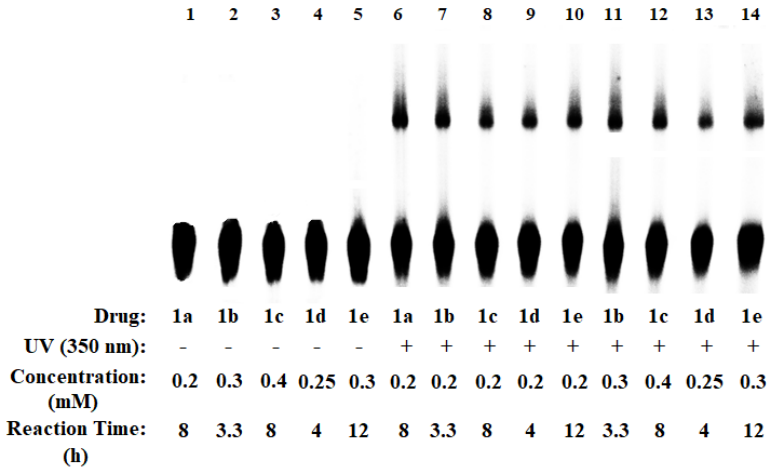

Figure 2-2. Photoinduced DNA interstrand cross-link formation by **1a-1e** upon 350 nm irradiation. Lanes 1-5: DNA with the drug (optimal concentration) without 350 nm irradiation; lanes 6-10: DNA with 0.2 mM **1a-1e** upon 350 nm irradiation: lane 6: **1a** (ICL yield, 26 ± 5 %); lane 7: **1b** (22 ± 4 %); lane 8: **1c** (16 ± 1 %); lane 9: **1d** (14 ± 1 %); lane 10: **1e** (21 ± 0.5%); lanes 11-14: DNA with **1a-1e** (optimal concentration) upon 350 nm irradiation: lane 11: **1b** (25 ± 4%); lane 12: **1c** (20 ± 1%); lane 13: **1d** (18 ± 1%); lane 14: **1e** (24 ± 1%). The DNA cross-linking yields were obtained with duplicate experiments and presented as average ± standard deviation.

Table 2-1. The optimal cross-linking reaction conditions, ICL yields, and UV absorption data for 1a-1e.[a]

Compound	Reaction Time (h)	Conc. (mM) [b]	ICL (%) [c]	λ_{max} (nm)	$\varepsilon_{\lambda max}/\varepsilon_{308}$ ($M^{-1}cm^{-1}$)	k (10^{-5} S^{-1})
1a (R=Cl)	8	0.2	30 ± 1	308	10775	1.35
1b (R=Br)	3.3	0.3	29 ± 1	308	13550	2.43
1c (R=H)	8	0.4	21± 1	299	8725/6125[d]	0.63
1d (R=Ph)	4	0.25	17 ± 1	305	13650/13350[d]	1.12
1e (R=OCH_3)	12	0.3	24 ± 1	300	10525/9775[d]	0.51

[a] DNA ICL reaction was carried out in a phosphate buffer (pH 8) with DNA duplex **5** upon irradiation of 350 nm light; [b] The minimum compound concentration required to achieve the highest DNA ICL yields; [c] The maximum DNA interstrand cross-linking yields observed for each compound under optimal conditions (the data are presented as average ± standard deviation from two individual experiments); [d] The molar extinction coefficients at 308 nm.

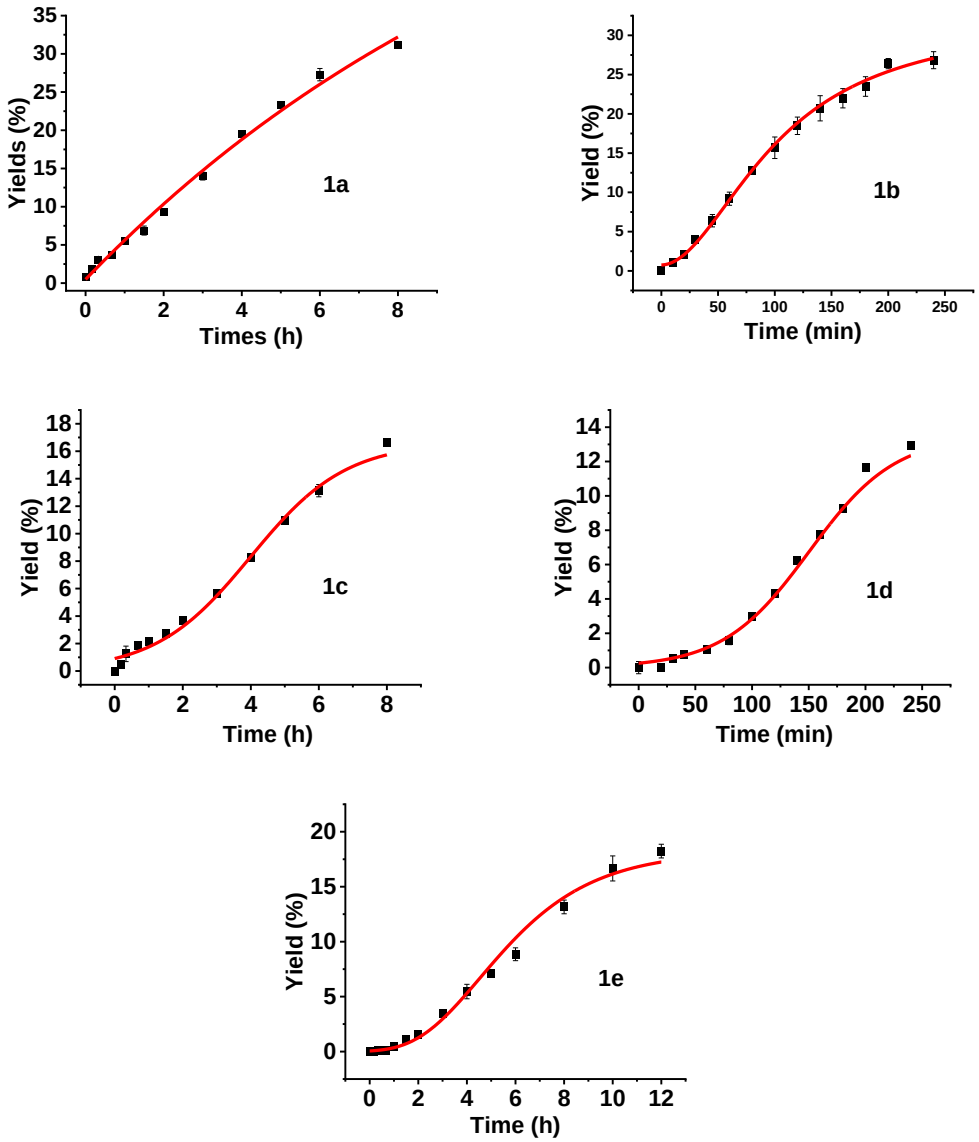

Figure 2-3. Time-dependence of DNA ICL formation of duplex 5 for **1a**-**1e** upon photo-irradiation. **1a** (500 μM) upon 350 nm irradiation at time points 0, 0.17 h, 0.33 h, 0.67 h, 1 h, 1.5 h, 2 h, 3 h, 4 h, 5 h, 6 h, 8 h; **1b** (300 μM) upon 350 nm irradiation at time points 0, 10 min, 20 min, 30 min, 45 min, 60 min, 80 min, 100 min, 120 min, 140 min, 160 min, 180 min, 200 min, 240 min; **1c** (300 μM) upon 350 nm irradiation at time points 0, 0.17 h, 0.33 h, 0.67 h, 1 h, 1.5 h, 2 h, 3 h, 4 h, 5 h, 6 h, 8 h; **1d** (300 μM) upon 350 nm irradiation at time points 0, 20 min, 30 min, 40 min, 60 min, 80 min, 100 min, 120 min, 140 min, 160 min, 180 min, 200 min, 240 min; **1e** (300 μM) upon 350 nm irradiation at time points 0, 0.17 h, 0.33 h, 0.67 h, 1 h, 1.5 h, 2 h, 3 h, 4 h, 5 h, 6 h, 8 h, 10 h, 12 h. Duplicates were done at each time point.

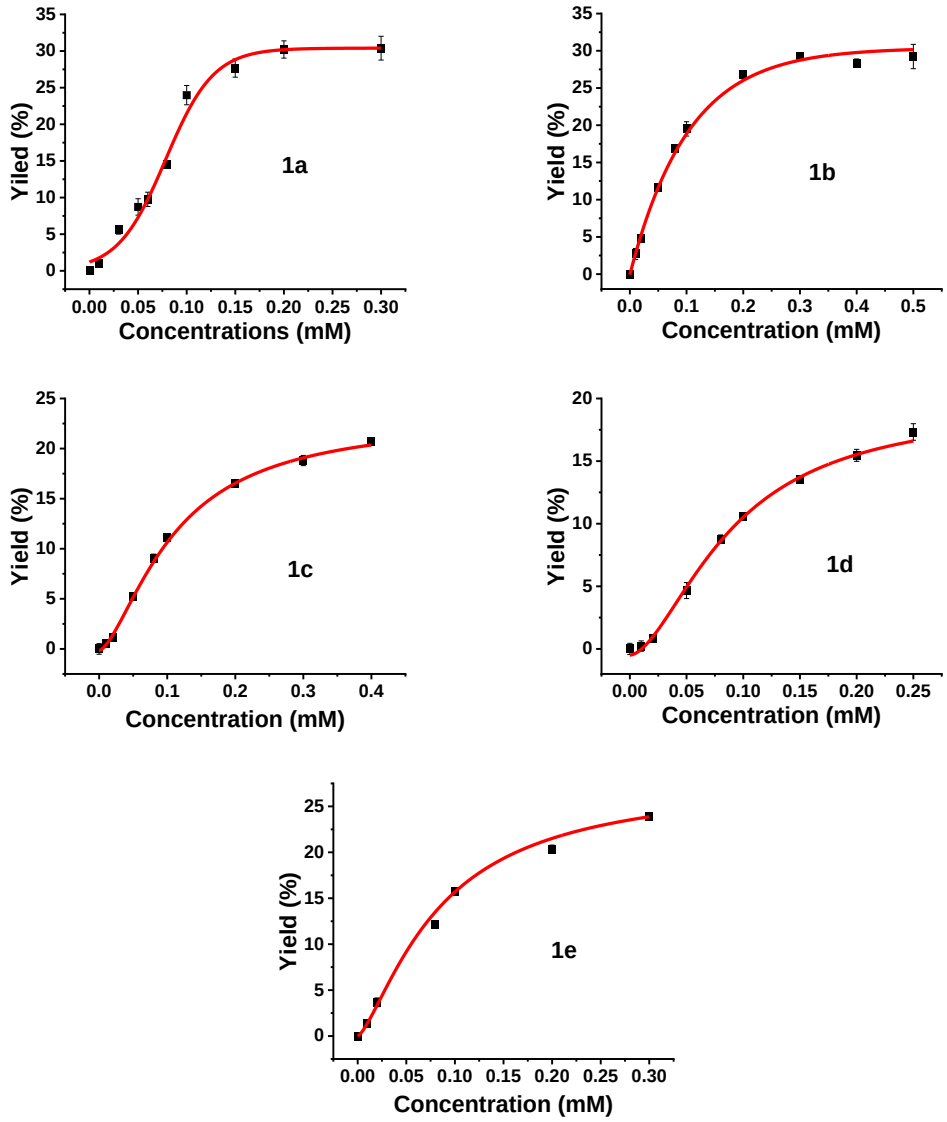

Figure 2-4. Concentration-dependence of DNA ICL formation of duplex **5** for **1a-1e** upon photo-irradiation. Phosphor image autoradiogram of 20% denaturing PAGE analysis of **1a-1e** under varying concentrations. **1a**: 0, 0.01 mM, 0.03 mM, 0.05 mM, 0.06 mM, 0.08 mM, 0.1 mM, 0.15 mM, 0.2 mM, 0.3 mM, reaction mixtures were photo-irradiated at 350 nm for 8 h; **1b**: 0, 0.01 mM, 0.02 mM, 0.05 mM, 0.08 mM, 0.1 mM, 0.2 mM, 0.3 mM, 0.4 mM, 0.5 mM, reaction mixtures were photo-irradiated at 350 nm for 200 min; **1c**: 0, 0.01 mM, 0.02 mM, 0.05 mM, 0.08 mM, 0.1 mM, 0.2 mM, 0.3 mM, 0.4 mM, reaction mixtures were photo-irradiated at 350 nm for 8 h; **1d**: 0, 0.01 mM, 0.02 mM, 0.05 mM, 0.08 mM, 0.1 mM, 0.15 mM, 0.2 mM, 0.25 mM, reaction mixtures were photo-irradiated at 350 nm for 4 h; **1e**: 0, 0.01 mM, 0.02 mM, 0.08 mM, 0.1 mM, 0.2 mM, 0.3 mM, reaction mixtures were photo-irradiated at 350 nm for 12 h.

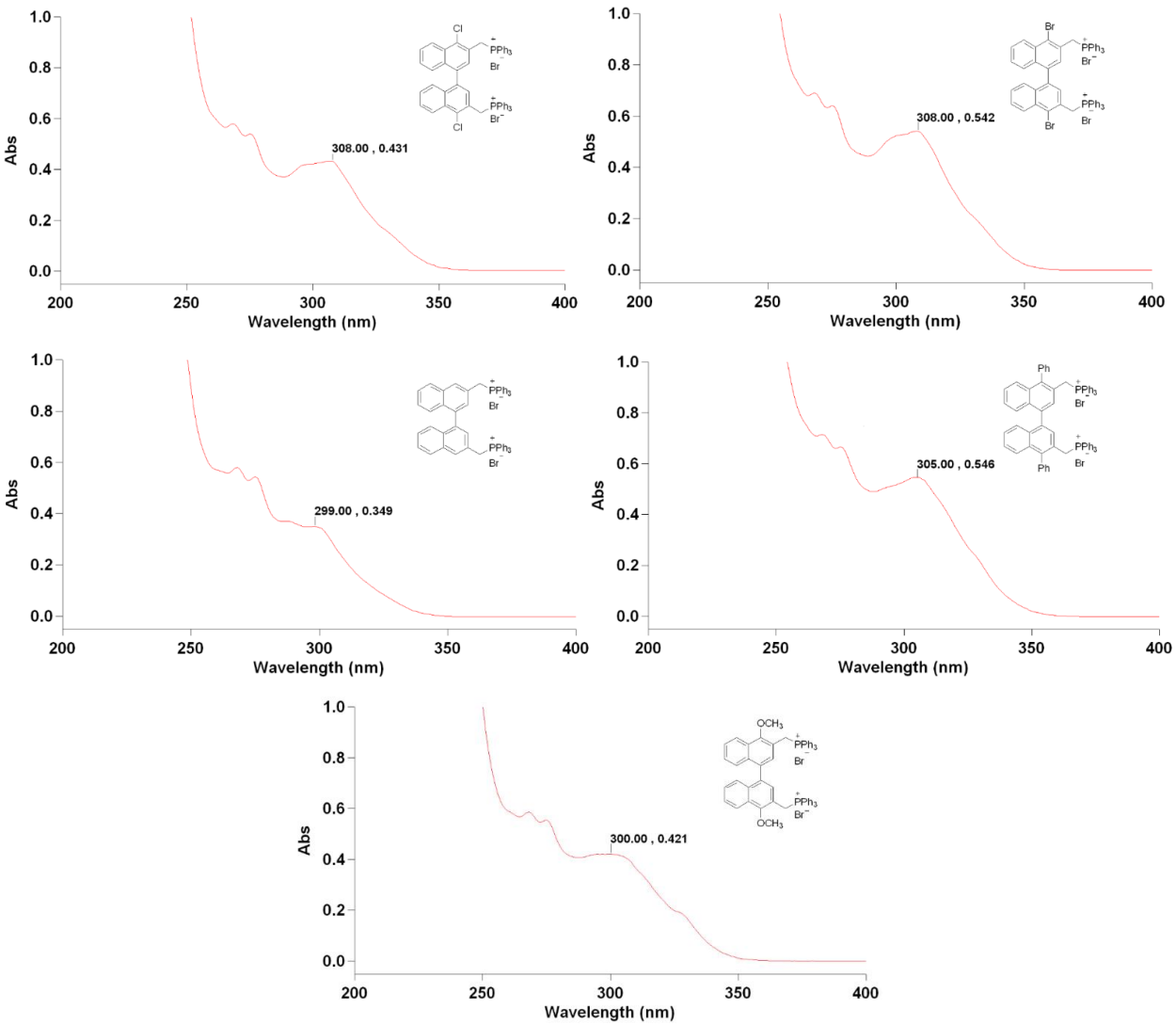

Figure 2-5. UV absorption spectra for **1a-1e**.

2.2.4. Mechanism of Photo-Induced DNA ICL Formation by 1a-1e.

It has been reported that photo-induced DNA interstrand cross-linking can be generated via [2 + 2] cycloaddition reaction or alkylation via photo-generated QM or carbocations.[1] Our previous work suggested that photo-irradiation of 1,1-binaphthalene analogues with bromine or ammonium salts as the leaving group generated the naphthalenylmethyl radicals that were spontaneously transformed to the naphthalenylmethyl cations directly producing DNA interstrand cross-linking via alkylation.[18,21] We have also observed that there were two pathways for benzylic carbocation

formation, either via oxidation of photo-generated benzyl radicals or heterolytic cleavage of C−L bonds, which is dependent on the aromatic substituents and the benzylic leaving groups.[15] To investigate the detailed mechanism for DNA ICL formation induced by **1a**−**1e**, we studied the effect of free radical trapping agents as well as cation trappers on DNA ICL formation of duplex **5** induced by **1a**−**1e**. As previously reported, methoxyamine was used as a carbocation trap and 2,2,6,6-tetramethylpiperidin-1-oxyl (TEMPO) was used as a radical trap. The two trapping agents were then tested separately as challengers for DNA ICL formation of DNA duplex **5** induced by **1a**−**1e** upon 350 nm irradiation. The influence of TEMPO and methoxyamine on DNA interstrand cross-linking induced by **1a-1e** is shown in Figure 2-6. The presence of TEMPO and methoxyamine greatly decreased ICL yields of **1a**−**1e**, which indicated that DNA ICL formation induced by **1a**−**1e** was inhibited by both methoxyamine and TEMPO. For example, the ICL yield of **1a** gradually decreased with increasing concentrations of TEMPO and methoxyamine and finally dropped from ~33 to <2% with 200 mM TEMPO or methoxyamine. The same phenomena were observed for **1b**−**1e**. The suppression of DNA ICL formation by TEMPO and methoxyamine suggested that both carbocations and free radicals were engaged in DNA ICL formation induced by **1a**−**1e**. Therefore, we conclude that the photo-irradiation of **1a**−**1e** produced the carbocation cross-linker **7** via the oxidation of free radical **6** not through the heterolysis of the C−L bond. To obtain direct evidence for carbocation and free radical formation, we carried out free radical and carbocation trapping reactions with the monomers. As **1a** showed the highest ICL yield and cross-link trapping efficiency, it was chosen as a representative for monomer trapping reaction. The trapping reactions were monitored by thin-layer chromatography, which showed that **1a** was consumed upon 350 nm irradiation for 3.5 days in the presence of 10.0 equiv. TEMPO or in the presence of 40 equiv methoxyamine upon 350 nm irradiation for 3 days. The LCMS-IT-TOF

analysis indicated that the mono-free-radical-trapping product **8a** was formed in the reaction of **1a** and TEMPO upon 350 nm irradiation while the cation-trapping product **9a** was detected with 350 nm irradiation of **1a** in the presence of methoxyamine (Scheme 2-8). Formation of **8a** and **9a** provided direct evidence for the proposed mechanism for photo-induced DNA interstrand cross-linking induced by **1a** (Scheme 2-7). The bisradical or biscation trapping products were not observed in the monomer trapping reactions, which suggested that the photo-activation of **1a** is a stepwise process with less efficiency for the activation of the second leaving group by UV light that is the rate-determining step for DNA ICL formation. We also observed that monomer reactions took much longer than DNA ICL formation induced by **1a** (3 days vs 8 h), which suggested that the binding interaction of **1a** with DNA speeds up the photo-activation process.

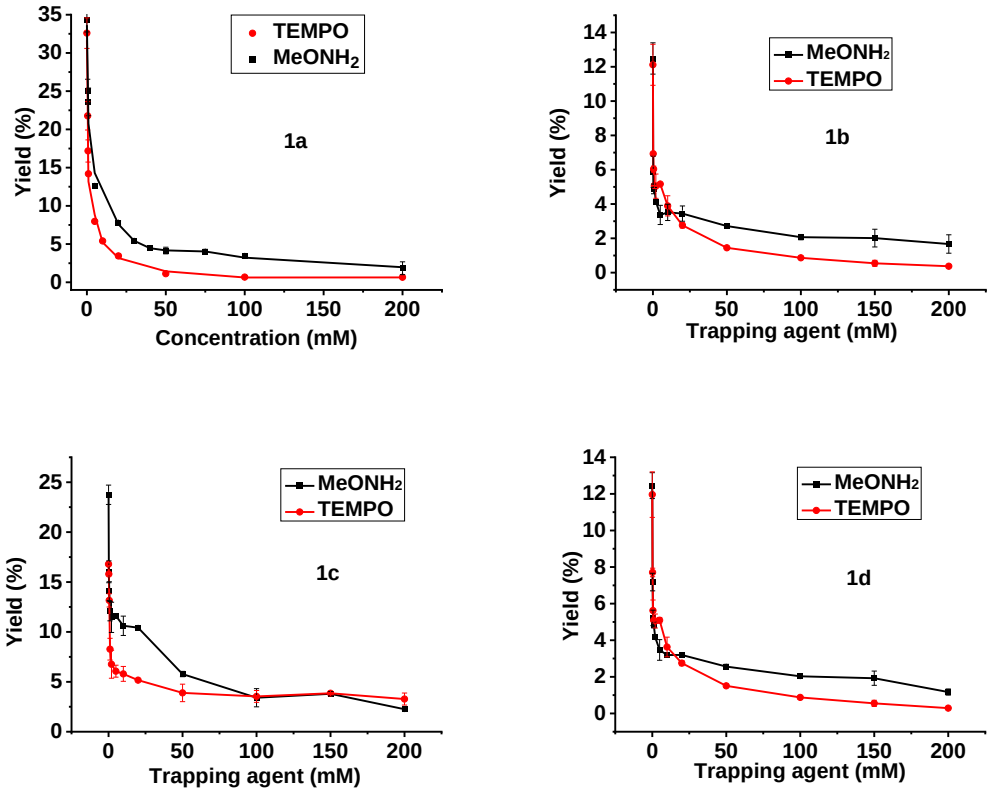

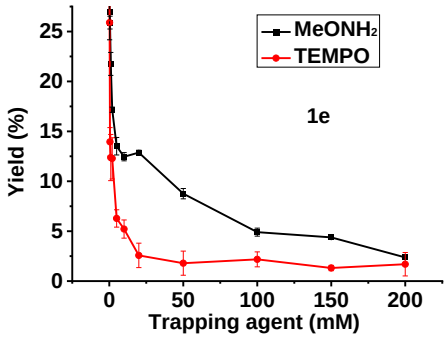

Figure 2-6. The effect of methoxyamine and TEMPO on DNA interstrand cross-linking induced by **1a-1e**.

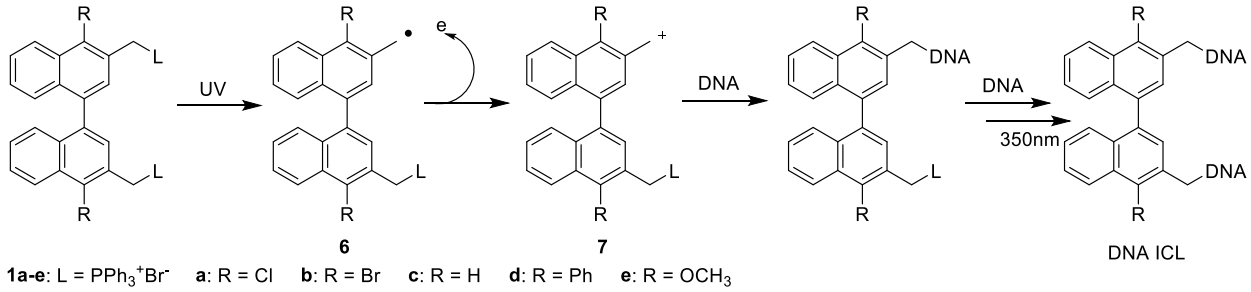

Scheme 2-15. Proposed mechanism for photo-induced ICL formation by **1a-1e**.

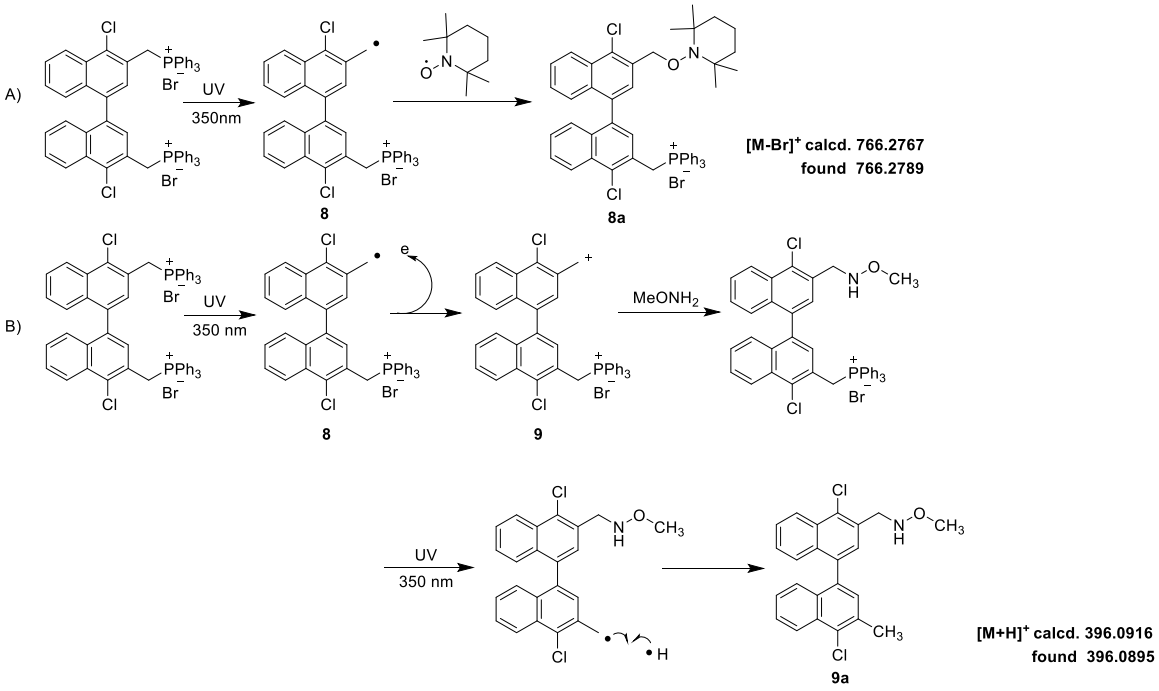

Scheme 2-16. (A) Formation of the free radical trapping product **8a** and (B) generation of the cation trapping product **9a** obtained with **1a** upon 350 nm irradiation.

2.2.5 Determination of DNA Interstrand Cross-Linking Sites of 1a-1e.

Since base modification greatly affects the stability of nucleotides, studying the heat stability of cross-linked DNAs under different conditions has been used to determine the alkylation sites on DNA strands. It has been well established that N7-alkylated purine nucleosides undergo deglycosylation upon heating under basic conditions at 90°C, causing cleavage of DNA strands.[30,31] Thus, we investigated the heat stability of DNA cross-linking products formed with **1a**−**1e**. Two methods were used to purify DNA ICL products used for heat stability study: precipitation or denaturing PAGE. The purified DNA ICL products and/or the mono-alkylated ODNs (ODN **5a′**) were then incubated in pH 7 phosphate buffer or 1.0 M piperidine at 90 °C for 30 min. We observed that purification methods did not affect the final results. The phosphor-image autoradiogram of 20% denaturing PAGE analysis of DNA cross-linking products formed by **1a** and **1d** is shown in Figure 2-7 and the data of **1b**-**1e** are displayed in Figure 2-8. DNA ICL products formed by **1a**−**1e** were stable upon heating in pH 7 phosphate buffer as no DNA cleavages were observed (Figure 2-7A, lanes 2 and 5; Figure 2-7B, lane 3). However, obvious cleavage bands were detected when cross-linked products were heated in 1.0 M piperidine for 30 min (Figure 2-7A, lane 2 vs 3, lane 5 vs 6; Figure 2-7B, lane 3 vs 4). For **1a**, the major cleavage sites were dGs, such as G22 and G27 (Figure 2-7A, lane 6 vs 7), indicating that the dGs were the prominent "labile alkylation sites". According to the Maxam and Gilbert reaction mechanism, N7-alkylated purine nucleosides undergo deglycosylation upon heating under basic conditions at 90 °C, leading to cleavage of DNA strands. Thus, we propose that N7-alkyl-G lesion is one of the possible alkylation adducts formed between DNA and **1a**−**1e**. A similar cleavage pattern was observed with single-

stranded ODN **5a′** isolated from ICL reaction mixture upon heating in 1.0 M piperidine, which suggested that apart from interstrand cross-linking, mono-alkylation or intrastrand cross-link reaction could occur at dG sites.

It is worth noting that some of them showed obvious cleavage bands at dAs in addition to dGs, such as **1c**, **1d**, and **1e** (Figure 2-8). However, their photo-reactivity toward dG and dA was slightly different. For better comparison, we determined the ratio of cleavages at dG_{27} + dG_{22} to those at dA_{25} + dA_{24} ($Cleav_{dG/dA}$). The $Cleav_{dG/dA}$ of ICL products induced by **1a**−**1e** is in the order of **1b** > **1a** > **1c** > **1e** > **1d**, which suggested that **1b** showed the poorest photo-reactivity toward dA, while **1d** was the most reactive toward dA (Table 2-2). These data indicated that aromatic substituents have an effect on the reactivity of the photo-generated 2-naphthalenylmethyl cations toward DNA.

Alkylation reactions occurred with pyrimidines cannot be detected by studying the heat stability of alkylated pyrimidines that are stable upon heating under basic conditions. To determine whether alkylation reaction could take place with pyrimidines, we did cross-linking assay with two different DNA duplexes **10** and **11**. Duplex **10** contains dTs/dCs in one strand and dAs/dGs in the other, while **11** is a 24-mer dAs/dTs self-complementary duplex. DNA ICL products were not detected with duplex **11** in the presence of **1a** upon 350 nm irradiation (Figure 2-9, lane 7), indicating that **1a** did not form cross-links between dA and dT sites neither between two dAs in complementary strands. However, the irradiation of **10** and **1a** with 350 nm light resulted in DNA ICL formation with about 8% yield (Figure 2-9, lane 2). Collectively, these results demonstrated that the DNA ICL reactions induced by **1a** took place between dC and dG. The slightly low ICL yield with duplex **10** was due to the short DNA sequences that contain less cross-linking sites. Although **1a** did not induce ICL formation with duplex **11**, we performed the heat stability study to determine whether monoalkylation took place with dAs. Duplexes **10** and **11** were irradiated

with **1a** with 350 nm light for 8 h, precipitated, and then heated in 1.0 M piperidine or phosphate buffer (pH 7) at 90 °C for 30 min. Cleavage bands were observed with dAs in **11**, which suggested that the 2-naphthalenylmethyl cation photo-generated from **1a** did alkylate dAs (Figure 2-9, lanes 9 and 10). It was also observed that cleavages only occurred at dG sites of duplex **10** but not at dAs, suggesting that **1a** is more reactive toward dGs than dAs upon photo-irradiation (Figure 2-9, lane 4).

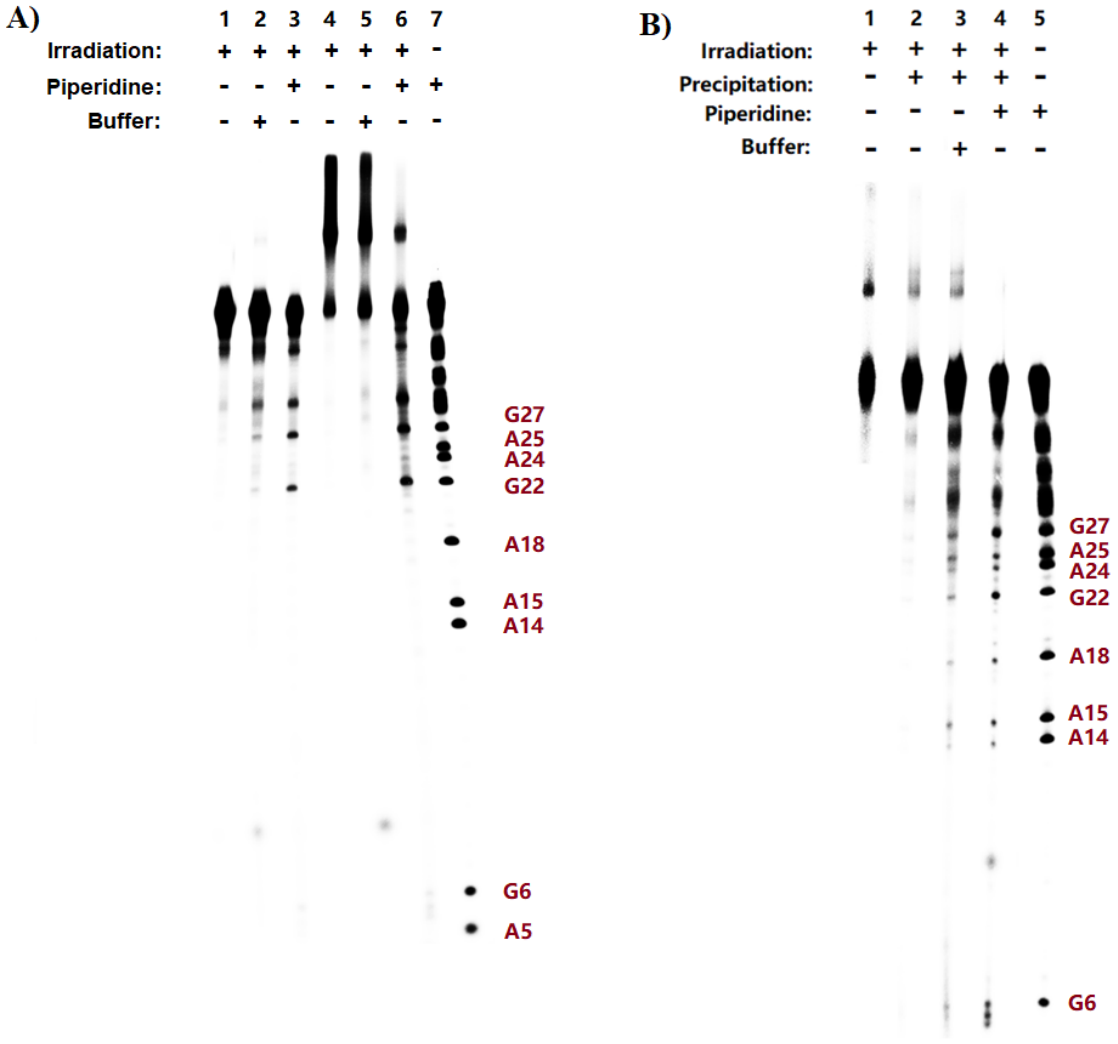

Figure 2-7. Determination of the cross-linking sites of **1a** and **1d** with DNA duplex **5**.A) Phosphorimage autoradiogram of 20% denaturing PAGE analysis of the DNA interstrand cross-linking products and single-stranded ODN **5a´** isolated from the ICL reaction induced by **1a**: lane 1, ODN **5a´** (control); lane 2, ODN **5a´** heated in phosphate buffer (pH 7, 90°C for 30 min); lane

3, ODN **5a´** heated in 1.0 M piperidine (90℃ for 30 min); lane 4, DNA interstrand cross-linking products (control); lane 5, DNA cross-linking products heated in phosphate buffer (pH 7, 90℃ for 30 min); lane 6, DNA cross-linking products heated in 1.0M piperidine (90℃ for 30 min); lane 7, G/A sequencing. B) Phosphorimage autoradiogram of 20% denaturing PAGE analysis of the DNA interstrand cross-linking products and single-stranded ODN **5a´** isolated from the ICL reaction induced by **1d**: lane 1, DNA ICL reaction mixture without precipitation; lane 2: DNA ICL reaction mixture after precipitation; lane 3: ICL products heated in phosphate buffer (pH = 7, 90 ℃ for 30 min); lane 4: DNA ICL product in 1.0 M piperidine at 90 ℃ for 30 min; lane 5: G/A sequencing.

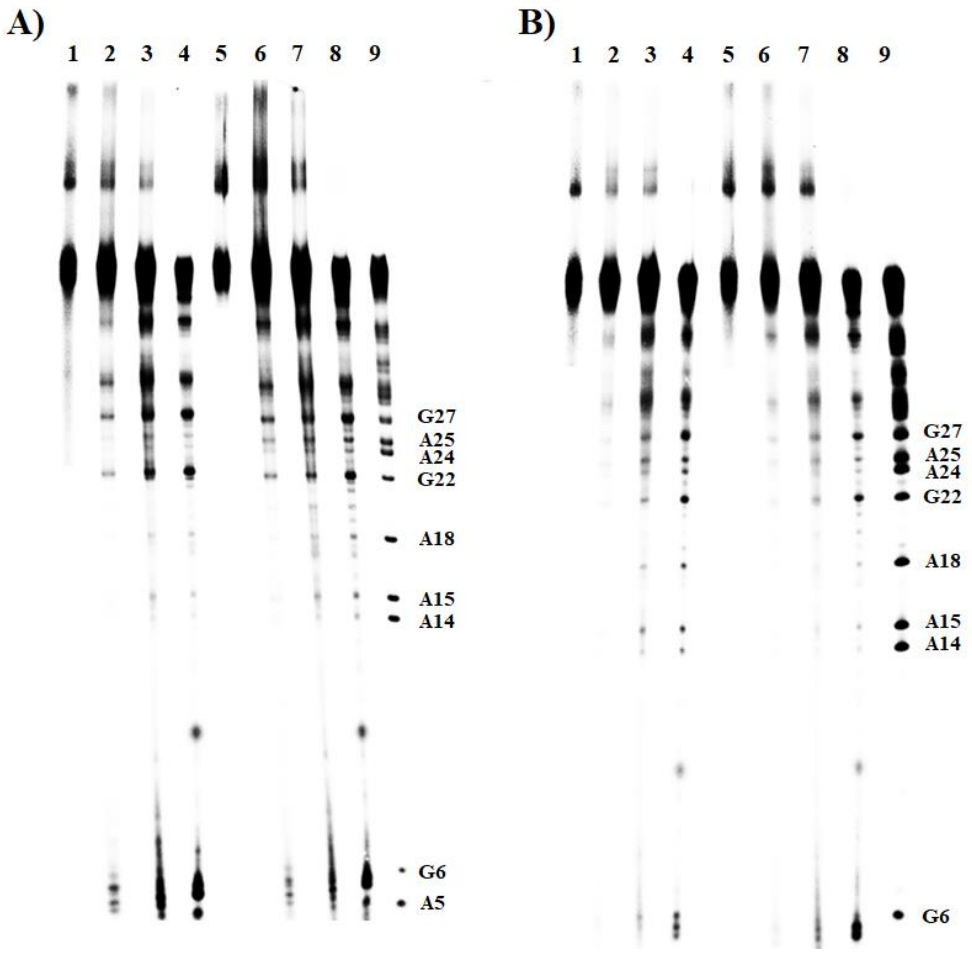

Figure 2-8. Determination of cross-linking sites of **1b**-**1e**. Phosphorimage autoradiogram of 20% denaturing PAGE analysis of the DNA ICL products. A) compounds **1b** and **1c** (lanes 1-4 for **1b** and lanes 5-8 for **1c**): lane 1, ICL product formed with **1b** without purification; lane 2: ICL product purified with precipitation (control); lane 3: purified ICL product heated in a phosphate buffer (pH = 7) at 90 ℃ for 30 min; lane 4: purified ICL product heated in 1.0 M piperidine at 90 ℃ for 30 min; lane 5: ICL product formed with **1c** without purification; lane 6: ICL products purified by precipitation (control); lane 7: purified ICL products heated in phosphate buffer (pH = 7) at 90 ℃ for 30 min; lane 8: purified ICL products heated in 1.0 M piperidine at 90 ℃ for 30 min; lane 9:

G + A sequencing. B) compounds **1d** and **1e** (lanes 1-4 for **1d** and lanes 5-8 for **1e**): lane 1: ICL product formed with **1d** without purification; lane 2: ICL product purified with precipitation (control**)**; lane 3, purified ICL products heated in a phosphate buffer (pH = 7) at 90 ℃ for 30 min; lane 4: purified ICL product heated in 1.0 M piperidine at 90 ℃ for 30 min; lane 5: ICL product formed with **1e** without purification; lane 6: ICL product purified with precipitation (control); lane 7: purified ICL products heated in a phosphate buffer (pH = 7) at 90 ℃ for 30 min; lane 8: purified ICL products heated in 1.0 M piperidine at 90 ℃ for 30 min; lane 9: G + A sequencing.

Table 2-2. The ratio of cleavages at dG27 and dG22 to those at dA25 and dA24 with **1a**-**1e**.[a]

Compound	**1a** (R = Cl)	**1b** (R = Br)	**1c** (R = H)	**1d** (R = Ph)	**1e** (R = OCH_3)
Cleav.[b] (dG/dA)	3.61	4.56	2.98	1.88	2.38

[a] The DNA ICL reaction was carried out in phosphate buffer (pH 8) with 50 nm **5** upon irradiation with 350 nm light. The DNA cross-linking products were purified and heated in 1.0 M piperidine at 90 ℃ for 30 min. The cleavage bands at dG_{27}/dG_{22} and dA_{25}/dA_{24} were quantified. [b] Ratio of cleavages at dG_{27}/dG_{22} to that at dA_{25}/dA_{24}.

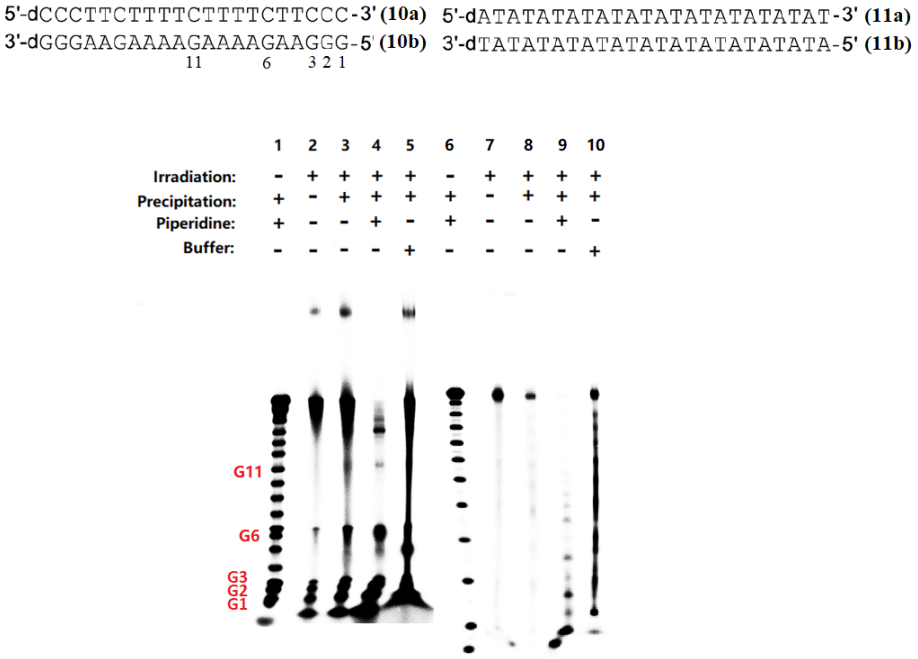

Figure 2-9. DNA sequence effects on ICL reactions induced by **1a** and determination of the alkylation sites of **1a** with DNA duplexes **10** and **11** [Phosphor-image autoradiogram of 20% denaturing PAGE analysis of the DNA cross-linking reaction mixture upon heating in a pH 7 phosphate buffer or 1.0 M piperidine. A mixture of **10** (10 μM) or **11** (10 μM) and **1a** (0.2 mM) in phosphate buffer (pH 8) was irradiated with 350 nm light for 8 h. Lane 1: G + A sequencing (DNA strand **10b** was ^{32}P-labelled**)**; Lanes 2-5: DNA duplex **10** was treated under different conditions;

Lane 6: G + A sequencing of DNA strand **11a**; Lanes 7-10: DNA duplex **11** was treated under different conditions. [DNA reaction mixtures obtained after photo irradiation was precipitated before heating in piperidine or buffer solution].

2.2.6 Conclusions

In conclusion, we have designed and synthesized five novel 1,1′-binaphthalene analogues **1a**−**1e** with TPP^+ salts as a leaving group and demonstrated their photo-inducible DNA cross-linking capability. All TPP^+ salts **1a**−**1e** can be activated upon 350 nm irradiation to produce the naphthalenylmethyl free radicals that are spontaneously transformed to the corresponding cations leading to DNA ICL formation. In comparison to the original 1,1-binaphthalene boronate esters A that showed low ICL yields (∼10%), **1a**−**1e** greatly improved DNA cross-linking efficiency with 2−4 times higher ICL yields. The aromatic substituents not only affect ICL efficiency but also influence the selectivity toward dG and dA. Groups with small size, such as halogens and methoxy group, favor ICL formation, while a bulky phenyl group prevents DNA interstrand cross-linking. The naphthalenylmethyl cations photo-generated from **1a**−**1e** can alkylate dC, dG, and dA while DNA interstrand cross-linking reaction only occurred with dG-dC base pairs.

2.3. Experimental Section

General Information. Chemicals and reagents were purchased commercially and used directly without additional purification. Thin-layer chromatography (TLC) was performed on precoated silica gel plates to monitor the reaction process with UV light. Oligonucleotides (ODNs) were synthesized by DNA/RNA ABI synthesizer (Model. 394 from AZCO® BioTech. Inc.) with standard automated DNA synthesis techniques, deprotected by using with a mixture of 40%

aqueous $MeNH_2$ and 28% aqueous NH_3 (1:1) at rt for 2 h, and further purified by 20% denaturing PAGE. ODNs were labelled with [γ-^{32}P] ATP following standard procedure.[25] [γ-^{32}P] labeled ODN strand was hybridized with complementary strand under 90℃ for 5 min and naturally cooled to rt to obtain radioactive DNA duplex. Radiolabeled ODNs were quantified with a Molecular Dynamics phosphorimager equipped with ImageQuant, version 5.2, software. ^{1}H, ^{13}C, COSY, and HSQC NMR spectra were collected on a Bruker DRX 300 or 500 MHz spectrophotometer with TMS as internal stander. High resolution mass spectrometry was carried out on a Shimadzu LCMS-IT-TOF mass spectrometer at the University of Wisconsin-Milwaukee Mass Spectrometry Lab.

Compound Synthesis and Characterization.

((4,4′-Dichloro-[1,1′-binaphthalene]-3,3′-diyl)bis(methylene))bis-(triphenylphosphonium) Bromide (1a). A solution of 2a (1.00 g, 1.96 mmol) and PPh_3 (1.08 g, 4.12 mmol) in toluene (50 mL) was heated to reflux under argon and stirred for 24 h. The reaction mixture was allowed to cool to rt, then filtered, and washed with Et_2O (3 × 50 mL) to afford the crude product that was purified through column chromatography (CH_2Cl_2/MeOH = 20/1), yielding **1a** (1.34g, 78% yield) as a white solid. Mp 212−214 °C; ^{1}H NMR (500 MHz, $CDCl_3$): δ = 8.13 (d, J = 8.57 Hz, 2H), 7.75−7.60 (m, 32H), 7.38 (s, 2H), 7.34 (t, J = 7.53 Hz, 2H), 7.08 (d, J = 8.35 Hz, 2H), 5.84 (t, J = 14.46 Hz, 2H), 5.32 (t, J = 14.40 Hz, 2H); ^{13}C NMR (125 MHz, $CDCl_3$): δ = 136.0, 135.9, 135.4, 135.4, 134.4, 134.3, 134.2, 133.8, 133.8, 132.7, 132.6, 131.2, 131.2, 130.7, 130.6, 130.5, 130.4, 130.4, 130.4, 130.2, 128.1, 128.0, 126.3, 125.0, 123.5, 123.4, 117.5, 116.8; HRMS (ESI): m/z [M − 2Br]$^{2+}$ calcd for $C_{58}H_{44}Cl_2P_2^{2+}$: 436.1142, found: 436.1112.

((4,4'-Dibromo-[1,1'-binaphthalene]-3,3'-diyl)bis(methylene))bis(triphenylphosphonium) Bromide (1b). A solution of **2b** (1.67 g, 2.80 mmol) and PPh_3 (2.57 g, 9.80 mmol) in toluene (70

mL) was heated to reflux under Argon and stirred for 24 h. The reaction mixture was cooled to rt, then filtered, washed with Et_2O (3 × 70 mL) to afford the crude product that was then purified through column chromatography (CH_2Cl_2/MeOH = 20/1) to give **1b** (96% yield) as a white solid. m.p. 224℃-226℃; 1H NMR (300 MHz, CD_3OD) δ = 8.25 (d, *J* = 8.57 Hz, 2 H), 7.88-7.84 (m, 6 H), 7.76-7.57 (m, 30 H), 7.41 (t, *J* = 7.60 Hz, 2 H), 7.04 (s, 2 H), 6.97 (d, *J* = 8.36 Hz, 2 H), 5.45-5.25 (m, 4 H); ^{13}C NMR (75 MHz, CD_3OD): δ = 136.9, 136.8, 135.4, 135.4, 134.2, 134.1, 134.1, 134.0, 134.0, 132.7, 132.7, 132.3, 132.2, 130.3, 130.3, 130.2, 130.1, 130.0, 129.5, 128.5, 128.3, 127.8, 125.8, 117.6, 116.4; HRMS (ESI): *m/z* $[M-2Br]^{2+}$ calcd for $C_{58}H_{44}Br_2P_2^{2+}$: 480.0637, found: 480.0589.

([1,1'-Binaphthalene]-3,3'-diylbis(methylene))bis(triphenylphosphonium) Bromide (1c). A solution of **2c** (115 mg, 0.26 mmol) and PPh_3 (205 mg, 0.78 mmol) in toluene (10 mL) was heated to reflux under argon and stirred for 24 h. The reaction mixture was cooled to rt, then filtered, washed with Et_2O (3 × 10 mL) to afford the crude product that was purified through column chromatography (CH_2Cl_2/MeOH = 20/1) to give **1c** (84% yield) as white solid. m.p. 231℃-233℃; 1H NMR (300 MHz, CD_3OD): δ = 7.86 (m, H), 7.74 (m, 30 H), 7.52 (t, *J* = 7.44 Hz, 2 H), 7.32 (t, *J* = 7.44 Hz, 2 H), 6.98 (d, *J* = 8.34 Hz, 2 H), 6.91 (s, 2 H), 5.20 (m, 4 H); ^{13}C NMR (75 MHz, DMSO): δ = 137.7, 135.5, 134.6, 134.5, 133.1, 133.0, 131.5, 130.8, 130.7, 130.5, 130.3, 128.4, 127.7, 127.4, 125.9, 125.5, 125.4, 118.8, 117.6, 117.6; HRMS (ESI): *m/z* $[M-2Br]^{2+}$ calcd for $C_{58}H_{46}P_2^{2+}$: 402.1532, found: 402.1475.

((4,4'-Dphenyl-[1,1'-binaphthalene]-3,3'-diyl)bis(methylene))bis(triphenylphosphonium) Bromide (1d). A solution of **2d** (194 mg, 0.33 mmol) and PPh_3 (258 mg, 0.98 mmol) in toluene

(10 mL) was heated to reflux under argon and stirred for 24 h. The reaction mixture was cooled to rt, then filtered, washed with Et_2O (3 × 10 mL) to afford the crude product that was purified through column chromatography (CH_2Cl_2/MeOH = 20/1) to give **1d** (76% yield) as a white solid. m.p. 231℃-233℃; 1H NMR (300 MHz, CD_3OD): *d* = 7.87 (brs, 6 H), 7.64 (brs, 12 H), 7.54 (brs, 4 H), 7.45 (brs, 5 H), 7.35 (brs, 15 H), 7.11 (brs, 2 H), 7.06 (brs, 2 H), 6.93 (brs, 2 H), 6.54 (brs, 2 H), 4.98 (brs, 4 H); ^{13}C NMR (75 MHz, DMSO): δ = 141.6, 141.5, 137.4, 136.6, 135.7, 134.3, 134.2, 132.8, 131.9, 130.9, 130.7, 130.3, 130.3, 129.6, 129.5, 129.4, 128.8, 127.8, 127.7, 127.1, 126.2, 123.7, 123.6, 118.3, 117.2; HRMS (ESI): *m/z* $[M\text{-}2Br]^{2+}$ calcd for $C_{70}H_{54}P_2^{2+}$: 478.1845, found: 478.1793.

((4,4'-Dimethoxy-[1,1'-binaphthalene]-3,3'-diyl)bis(methylene))bis(triphenylphosphonium) Bromide (1e). A solution of **2e** (500 mg, 1.00 mmol) and PPh_3 (577 mg, 2.20 mmol) in toluene (20 mL) was heated to reflux under argon and stirred for 24 h. The reaction mixture was cooled to rt, then filtered, washed with Et_2O (3 × 20 mL) to afford the crude product that was purified through column chromatography (CH_2Cl_2/MeOH = 20/1) to yield **1e** (319 mg, 53% yield) as a white solid. m.p. 180℃-182℃; ^1H NMR (300 MHz, CD_3OD): *d* = 8.02 (d, *J* = 8.7 Hz, 2 H), 7.84-7.62 (m, 32 H), 7.34 (t, *J* = 7.2 Hz, 2 H), 6.91 (d, *J* = 8.4 Hz, 2 H), 6.78 (s, 2 H), 5.21-4.96 (m, 4 H), 3.95 (s, 6 H); ^{13}C NMR (75 MHz, CD_3OD): δ = 135.1, 135.0, 135.0, 134.3, 134.2, 134.1, 134.0, 134.0, 133.9, 133.8, 133.1, 133.0, 130.3, 130.3, 130.2, 130.1, 130.0, 130.0, 129.8, 129.6, 129.6, 127.6, 127.5, 127.2, 126.6, 126.3, 122.3, 118.6, 118.6, 117.5, 117.4, 116.0, 115.8; HRMS (ESI): *m/z* $[M\text{-}2Br]^{2+}$ calcd for $C_{60}H_{50}O_2P_2^{2+}$: 432.1638, found: 432.1593.

1-Chloro-2-methylnaphthalene (3a). To a solution of 1-bromo-2-methylnaphthalene (**3b**) (10.87 g, 0.492 mol) in DMF (200 mL), copper chloride (9.75 g, 0.984 mol) was added. The reaction

mixture was stirred at 153 ℃ overnight and cooled to rt, then filtered by vacuum. Hexane (200 mL) was added in the filtrate, and the mixture was washed with water, then brine, dried over anhydrous Na_2SO_4, and concentrated under reduced pressure. The resulting residue was purified via column chromatography (Hexane) to yield **3a** (8.67 g, 99%) as a colorless oil. ^{1}H NMR (500 MHz, $CDCl_3$): δ ppm 8.35 (d, *J* = 8.56 Hz, 1H), 7.85 (d, *J* = 8.15 Hz, 1H), 7.71 (d, *J* = 8.34 Hz, 1H), 7.64-7.60 (m, 1H), 7.54-7.51 (m, 1H), 7.38 (d, *J* = 8.35 Hz, 1H), 2.64 (s, 3H); ^{13}C NMR (125 MHz, $CDCl_3$): δ 20.9, 124.2, 125.7, 126.5, 127.0, 128.0, 128.7, 130.7, 131.2, 133.1, 133.5. The NMR spectra were in agreement with those reported. [31]

4,4'-Dichloro-3,3'-dimethyl-1,1'-binaphthalene (4) To a solution of 1-chloro-2-methylnaphthalene (**3a**) (3.4 g, 19.25 mmol) and lead tetraacetate (8.54 g, 19.25 mmol) in acetonitrile (25 mL), boron trifluoride diethyl etherate (6 mL) was added at 0 ℃. The reaction mixture was stirred at rt for overnight, poured into water (75 mL), and extracted with DCM (3 × 75 mL). The organic layer was combined, dried over Na_2SO_4, filtered, and concentrated to afford the crude product that was passed through a short column of basic alumina, eluted with hexane to remove the Pb and color impurity, then further purified through column chromatography (Hexane) to yield **4** (0.85g, 25.1%) as a white solid. m.p. 127℃-129℃; ^{1}H NMR (500 MHz, $CDCl_3$): δ = 8.44 (d, *J* = 8.55 Hz, 2 H), 7.61-7.58 (m, 2 H), 7.39 (s, 2 H), 7.37-7.30 (m, 4 H), 2.68 (s, 6 H); ^{13}C NMR (500 MHz, $CDCl_3$): δ = 20.9, 124.4, 125.9, 126.8, 127.1, 130.7, 130.7, 131.1, 132.4, 133.0, 136.3 (Note: Due to the difficulty of ionization for this type of compound, HRMS was not obtained. However, the final product **1a** made from **4** was characterized by NMR and HRMS).

3,3'-Bis(bromomethyl)-4,4'-dichloro-1,1'-binaphthalene (2a). A mixture of **4** (180 mg, 0.51 mmol), NBS (228 mg, 1.28 mmol), and AIBN (8.8 mg, 0.05 mmol) in benzene (10 mL) was heated

to reflux, stirred for 6 h, then cooled to rt and concentrated, then CH_2Cl_2 (10 mL) was added. The mixture was washed with water, brine, dried over anhydrous sodium sulfate, and concentrated under reduced pressure, then purified through column chromatography (Hexane/CH_2Cl_2 = 50/1) to give **2a** (140 mg, 54%) as a white solid: m.p. 138℃-140℃; ^{1}H NMR (500 MHz, $CDCl_3$) δ = 8.49 (d, *J* = 8.52 Hz, 2 H), 7.67-7.64 (m, 2 H), 7.56 (s, 2 H), 7.43-7.36 (m, 4 H), 4.92-4.87 (m, 4 H); ^{13}C NMR (500 MHz, $CDCl_3$): δ = 31.2, 125.3, 126.8, 127.6, 127.7, 129.4, 131.2, 132.1, 132.3, 133.5, 136.7 (Note: Due to the difficulty of ionization for this type of compound, HRMS was not obtained. However, the final product **1a** made from **2a** was characterized by NMR and HRMS).

Free-Radical-Trapping Reaction with Monomers. Compound **1a** (200 mg, 0.23 mmol, 1 equiv) and TEMPO (360 mg, 10.0 equiv) were dissolved in CH_3CN and H_2O (1/1) (2 mL), which was irradiated with 350 nm light for 3.5 days. The reaction mixture was concentrated and then extracted with CH_2Cl_2 (3 × 5 mL). The organic phase was combined, washed with water and brine, dried over anhydrous Na_2SO_4, and concentrated under reduced pressure to obtain the crude product, which was further purified by column chromatography (hexane/EtOAc = 20/1) and analyzed by the liquid chromatography−mass spectrometry ion-trap time of flight (LCMS-IT-TOF).

Carbocation Trapping Reaction with Monomers. To a solution of $MeONH_2$·HCl (0.768 g, 9.2 mmol, 40 equiv) in DMF (2 mL), trimethylamine (1.4 mL, 10.12 mmol, 44 equiv) was added, which was stirred at rt for 30 min, and then **1a** (200 mg, 0.23 mmol, 1equiv) in DMF (2 mL) was added. The reaction mixture was stirred at rt for 20 min, irradiated with 350 nm light until the starting material was consumed (~3 days), then quenched by water (4 mL), and extracted with ethyl acetate (3 × 4 mL). The organic phases were combined, washed with brine, dried over anhydrous Na_2SO_4, and concentrated under reduced pressure to obtain the crude product, which

was further purified by column chromatography (hexane/EtOAc = 20/1) and analyzed by LCMS-IT-TOF.

DNA ICL Formation. In a potassium phosphate buffer (pH 8, 100 mM), the ^{32}P-labeled ODN (0.5 μM) was hybridized with the complementary strand (1.5 equiv) by heating at 90 °C for 5 min and cooling to rt naturally. Then, 100 mM potassium phosphate buffer (pH 8, 2 μL), 1 M NaCl (2 μL), and certain concentrations of **1a**−**1e** in CH_3CN (6 μL) were added to the ^{32}P-labeled ODN duplex (2 μL, 0.5 μM). Autoclaved water was added to give a final volume of 20 μL (final concentration range: 0.01−0.5 mM). The reaction mixture was irradiated with 350 nm light, then quenched with an equal volume of 90% formamide loading buffer, and subjected to 20% denaturing PAGE.

Carbocation Trapping Assay of DNA ICL Formation. A solution of $MeONH_2$·HCl (2 M) was titrated with NaOH (5 M) to pH 7.0, which was diluted to the desired concentration (5/2 to 4000/2 mM). The resulting $MeONH_2$·HCl solution (2 μL) with desired concentration was added to a mixture containing 2 μL of ^{32}P-labeled ODN duplex (0.5 μM), 2 μL of NaCl (1 M), and 2 μL of pH 8 potassium phosphate (100 mM). Then, 6 μL of **1a**−**1e** in CH_3CN with optimal concentrations and 6 μL of autoclaved distilled water were added to give a total volume of 20 μL (final $MeONH_2$ concentration: 0.25−200 mM). After irradiation with 350 nm light for the desired time, the reaction mixture was quenched with 20 μL of 90% formamide loading buffer, then subjected to 20% denaturing PAGE.

Free-Radical-Trapping Assay of DNA ICL Formation. A solution of TEMPO in CH_3CN (10/3 to 4000/3 mM, 3 μL) was added to a reaction mixture containing 2 μL of ^{32}P-labeled ODN duplex (0.5 μM), 2 μL of NaCl (1 M), 2 μL of pH 8 potassium phosphate (100 mM), 3 μL of **1a**−**1e** in CH_3CN with optimal concentrations, and 8 μL of autoclaved distilled water to give a total volume

of 20 μL (final TEMPO concentration: 0.5−200 mM). The reaction mixture was irradiated with 350 nm light for the desired time, quenched with 20 μL of 90% formamide loading buffer, and subjected to 20% denaturing PAGE.

Heat Stability Study of the Isolated DNA Cross-Linking Products Formed with 1a for the Determination of Alkylation Sites. A solution containing 0.5 μM ^{32}P-labeled ODN duplex **5** (60 μL), 1 M NaCl (12 μL), 100 mM pH 8 potassium phosphate (12 μL), and 2/3 mM 1a in CH_3CN (36 μL) was irradiated at 350 nm for 6 h. The alkylated ODNs were purified by 20% denaturing PAGE following standard procedures. The gel band containing cross-linked products or single-stranded ODNs was cut, crushed, extracted with a mixture of NaCl (200 mM) and EDTA (20 mM) (2.0 mL), and further purified on a C18 column (1 cc, 100 mg) eluting with H_2O (3 × 1.0 mL), followed by MeOH/H_2O (3/2, 1.0 mL). The isolated ICL products and single-stranded ODNs were lyophilized by a Centrivap concentrator of LABCONCO. The isolated ICL products were dissolved in 45 μL of autoclaved distilled H_2O and aliquoted into three parts (20, 20, and 5 μL). One portion (20 μL) of the isolated ODNs was incubated with 10 M piperidine (10 μL) and autoclaved distilled water (70 μL) at 90 °C for 30 min. The second portion (20 μL) was added to 1.0 M NaCl (10 μL),10 mM pH 7 potassium phosphate buffer (10 μL), and 60 μL of autoclaved distilled water and incubated at 90 °C for 30 min. The third portion (5 μL) was used as a control sample. Single-stranded ODNs were studied in the same way. Solvent of all samples was removed by vacuum, dissoved in the mixture of 90% formamide loading buffer and H_2O (1:1), and subjected to 20% denaturing PAGE analysis.

Determination of Alkylation Sites by Studying the Heat Stability of DNA ICL Products Formed with 1b−1e. A solution containing 60 μL of ^{32}P-labeled ODN duplex **5** (0.5 μM), 12 μL of NaCl (1 M), 12 μL of pH 8 potassium phosphate (100 mM), and 36 μL of **1b**−**1e** in CH_3CN

(optimal concentrations) was irradiated with 350 nm light for 6 h. Then, the reaction mixture (120 μL) was coprecipitated with 40 μL of calf thymus DNA (25 μg/mL) in the presence of 20 μL of NaOAc (3 M) and 540 μL of ethanol at −80 °C for 30 min and centrifuged at 15000 rpm for 5 min by Eppendorf centrifuge. The supernatant was removed. The pellet was dissolved in 60 μL of autoclaved distilled water, precipitated with 10 μL of NaOAc (3 M) and 240 μL of ethanol at −80 °C for 30 min again, and centrifuged for 5 min at 15000 rpm. After removal of the supernatant, the pellet was lyophilized, dissolved in 45 μL of autoclaved distilled water, and aliquoted to three parts. One portion (20 μL) of the precipitated ODN adducts was incubated with 10 M piperidine (10 μL) and autoclaved distilled water (70 μL) at 90 °C for 30 min. The second portion (20 μL) was added to 1.0 M NaCl (10 μL), 10 mM pH 7 potassium phosphate buffer (10 μL), and 60 μL of autoclaved distilled water and incubated at 90 °C for 30 min. The third portion (5 μL) was used as a control sample. Finally, all three samples were dissolved in the mixture of 90% formamide loading buffer and H_2O (1:1) and subjected to 20% denaturing PAGE analysis.

2.4. References

(1) Fan, H.; Peng, X. Novel DNA Cross-Linking Reagents. *In Advances in Molecular Toxicology*; Fishbein, J. C.; Heilman, J. M., Eds.; Elsevier, 2016; Vol. *10*, pp 235−292.

(2) Yoshimura, Y.; Fujimoto, K. Ultrafast reversible photo-cross-linking reaction: toward in situ DNA manipulation. *Org. Lett.* **2008**, 10, 3227−3230.

(3) Ogasawara, S.; Fujimoto, K. SNP genotyping by using photochemical ligation. *Angew. Chem., Int. Ed.* **2006**, 45, 4512−4515.

(4) Ogasawara, S.; Ami, T.; Fujimoto, K. Autonomous DNA computing machine based on photochemical gate transition. *J. Am. Chem. Soc.* **2008**, 130, 10050−10051.

(5) Tagawa, M.; Shohda, K.; Fujimoto, K.; Sugawara, T.; Suyama, A. Heat-resistant DNA tile arrays constructed by template-directed photoligation through 5-carboxyvinyl-2′-deoxyuridine. *Nucleic Acids Res.* **2007**, 35, No. e140.

(6) Freccero, M. Quinone Methides as Alkylating and Cross-Linking Agents. *Mini-Rev. Org. Chem.* **2004**, 1, 403−415.

(7) Percivalle, C.; Doria, F.; Freccero, M. Quinone Methides as DNA Alkylating Agents: An Overview on Efficient Activation Protocols for Enhanced Target Selectivity. *Curr. Org. Chem.* **2014**, 18, 19−43.

(8) Richter, S. N.; Maggi, S.; Mels, S. C.; Palumbo, M.; Freccero, M. Binol quinone methides as bisalkylating and DNA cross-linking agents. *J. Am. Chem. Soc.* **2004**, 126, 13973−13979.

(9) Verga, D.; Nadai, M.; Doria, F.; Percivalle, C.; Di Antonio, M.; Palumbo, M.; Richter, S. N.; Freccero, M. Photogeneration and reactivity of naphthoquinone methides as purine selective DNA alkylating agents. *J. Am. Chem. Soc.* **2010**, 132, 14625−14637.

(10) Wang, P.; Liu, R.; Wu, X.; Ma, H.; Cao, X.; Zhou, P.; Zhang, J.; Weng, X.; Zhang, X. L.; Qi, J.; Zhou, X.; Weng, L. A potent, water-soluble and photoinducible DNA cross-linking agent. *J. Am. Chem. Soc.* **2003**, 125, 1116−1117.

(11) Chatterjee, M.; Rokita, S. E. The Role of a Quinone Methide in the Sequence Specific Alkylation of DNA. *J. Am. Chem. Soc.* **1994**, 116, 1690−1697.

(12) Op de Beeck, M.; Madder, A. Sequence Specific DNA Cross-Linking Triggered by Visible Light. *J. Am. Chem. Soc.* **2012**, 134, 10737−10740.

(13) Weng, L.; Horvat, S. M.; Schiesser, C. H.; Greenberg, M. M. Deconvoluting the reactivity of two intermediates formed from modified pyrimidines. *Org. Lett.* **2013**, 15, 3618−3621.

(14) Lin, G.; Li, L. Oxidation and reduction of the 5-(2′-deoxyuridinyl)methyl radical. *Angew. Chem., Int. Ed.* **2013**, 52, 5594−5598.

(15) Fan, H.; Sun, H.; Peng, X. Substituents Have a Large Effect on Photochemical Generation of Benzyl Cations and DNA Cross-Linking. *Chem. - Eur. J.* **2018**, 24, 7671−7682.

(16) Han, Y.; Chen, W.; Kuang, Y.; Sun, H.; Wang, Z.; Peng, X. UV-Induced DNA Interstrand Cross-Linking and Direct Strand Breaks from a New Type of Binitroimidazole Analogue. *Chem. Res. Toxicol.* **2015**, 28, 919−926.

(17) Wang, Y.; Liu, S.; Lin, Z.; Fan, Y.; Wang, Y.; Peng, X. Photochemical Generation of Benzyl Cations That Selectively Cross-Link Guanine and Cytosine in DNA. *Org. Lett.* **2016**, 18, 2544−2547.

(18) Wang, Y. B.; Lin, Z. C.; Fan, H. L.; Peng, X. H. Photoinduced DNA Interstrand Cross-Link Formation by Naphthalene Boronates via a Carbocation. *Chem. - Eur. J.* **2016**, 22, 10382−10386.

(19) Fan, H.; Sun, H.; Zhang, Q.; Peng, X. Photoinduced DNA Interstrand Cross-Linking by 1,1′-Biphenyl Analogues: Substituents and Leaving Groups Combine to Determine the Efficiency of Cross-Linker. *Chem. - Eur. J.* **2021**, 27, 5215−5224.

(20) Fan, H.; Peng, X. Photoinduced DNA Interstrand Cross-Linking by Benzene Derivatives: Leaving Groups Determine the Efficiency of the Cross-Linker. *J. Org. Chem.* **2021**, 86, 493−506.

(21) Lin, Z.; Fan, H.; Zhang, Q.; Peng, X. Design, Synthesis, and Characterization of Binaphthalene Precursors as Photoactivated DNA Interstrand Cross-Linkers. *J. Org. Chem.* **2018**, 83, 8815−8826.

(22) Doria, F.; Richter, S. N.; Nadai, M.; Colloredo-Mels, S.; Mella, M.; Palumbo, M.; Freccero, M. BINOL-amino acid conjugates as triggerable carriers of DNA-targeted potent photocytotoxic agents. *J. Med. Chem.* **2007**, 50, 6570−6579.

(23) Zielonka, J.; Joseph, J.; Sikora, A.; Hardy, M.; Ouari, O.; Vasquez-Vivar, J.; Cheng, G.; Lopez, M.; Kalyanaraman, B. Mitochondria-Targeted Triphenylphosphonium-Based Compounds: Syntheses, Mechanisms of Action, and Therapeutic and Diagnostic Applications. *Chem. Rev.* **2017**, 117, 10043−10120.

(24) Ross, M. F.; Kelso, G. F.; Blaikie, F. H.; James, A. M.; Cocheme, H. M.; Filipovska, A.; Da Ros, T.; Hurd, T. R.; Smith, R. A.; Murphy, M. P. Lipophilic triphenylphosphonium cations as tools in mitochondrial bioenergetics and free radical biology. *Biochemistry (Mosc.)* **2005**, 70, 222−230.

(25) Maniatis, T.; Fritch, E. F.; Sambrook, J. Molecular Cloning: A Laboratory Manual; Cold Spring Harbor Laboratory: Cold Spring Harbor, NY, 1982.

(26) Wu, L.; Drinkel, E.; Gaggia, F.; Capolicchio, S.; Linden, A.; Falivene, L.; Cavallo, L.; Dorta, R. Room-temperature synthesis of tetra-ortho-substituted biaryls by NHC-catalyzed Suzuki-Miyaura couplings. *Chem. - Eur. J.* **2011**, 17, 12886−12890.

(27) Richardson, C. C. Phosphorylation of nucleic acid by an enzyme from T4 bacteriophage-infected Escherichia coli. *Proc. Natl Acad. Sci. USA.* **1965**, 54, 158-165.

(28) Novogrodsky, A.; Hurwitz, J. The enzymatic phosphorylation of ribonucleic acid and deoxyribonucleic acid: phosphorylation at 5'-hydroxyl termini. *J. Biol. Chem.* **1966**, 241, 2923-2932.

(29) Novogrodsky, A.; Tal., M.; Traub, A.; Hurwitz, J. The enzymatic phosphorylation of ribonucleic acid and deoxyribonucleic acid: further properties of the 5'-hydroxyl polynucleotide kinase. *J. Biol. Chem.* **1966**, 241, 2933-2943.

(30) Maxam, A. M.; Gilbert, W. A new method for sequencing DNA. *Proc. Natl. Acad. Sci. U.S.A.* **1977**, 74, 560−564.

(31) Maxam, A. M.; Gilbert, W. Sequencing End-labeled DNA with Base-Specific Chemical Cleavages. *In Methods in Enzymology*; Elsevier, 1980; Vol. 65, pp 499−560.

2.5. Appendices A: Gel Electrophoresis

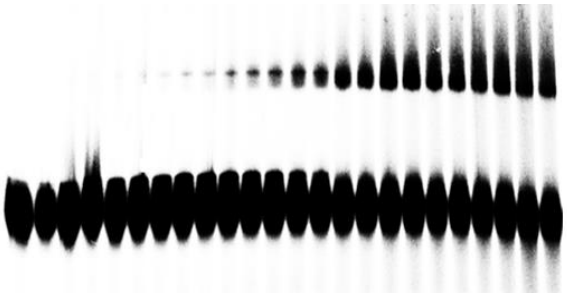

Figure 2-10. Representative gel of time-dependent DNA ICL formation of duplex for **1a** (500 μM) upon 350 nm irradiation at time points 0, 0.17 h, 0.33 h, 0.67 h, 1 h, 1.5 h, 2 h, 3 h, 4 h, 5 h, 6 h, 8 h. Duplicates were done at each time point.

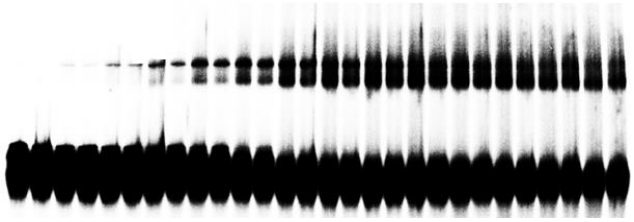

Figure 2-11. Representative gel of time-dependent DNA ICL formation of duplex for **1b** (300 μM) upon 350 nm irradiation at time points 0, 10 min, 20 min, 30 min, 45 min, 60 min, 80 min, 100 min, 120 min, 140 min, 160 min, 180 min, 200 min, 240 min. Duplicates were done at each time point.

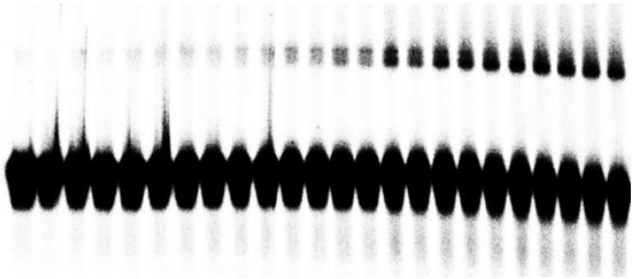

Figure 2-12. Representative gel of time-dependent DNA ICL formation of duplex for **1c** (300 μM) upon 350 nm irradiation at time points 0, 0.17 h, 0.33 h, 0.67 h, 1 h, 1.5 h, 2 h, 3 h, 4 h, 5 h, 6 h, 8 h. Duplicates were done at each time point.

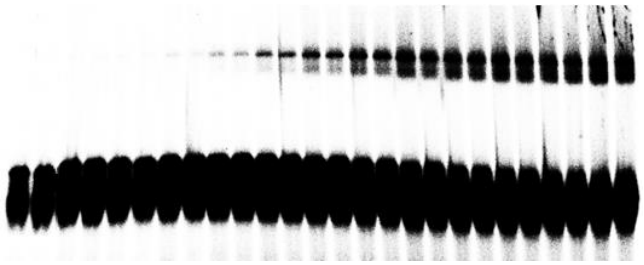

Figure 2-13. Representative gel of time-dependent DNA ICL formation of duplex for **1d** (300 μM) upon 350 nm irradiation at time points 0, 20 min, 30 min, 40 min, 60 min, 80 min, 100 min, 120 min, 140 min, 160 min, 180 min, 200 min, 240 min. Duplicates were done at each time point.

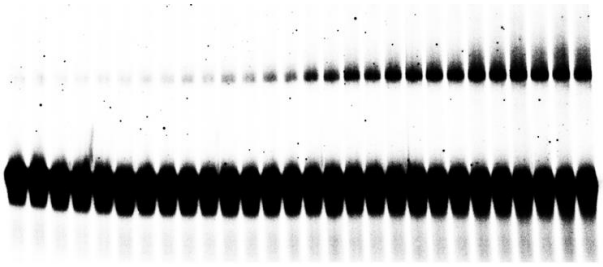

Figure 2-14. Representative gel of time-dependent DNA ICL formation of duplex for **1e** (300 μM) upon 350 nm irradiation at time points 0, 0.17 h, 0.33 h, 0.67 h, 1 h, 1.5 h, 2 h, 3 h, 4 h, 5 h, 6 h, 8 h, 10 h, 12 h. Duplicates were done at each time point.

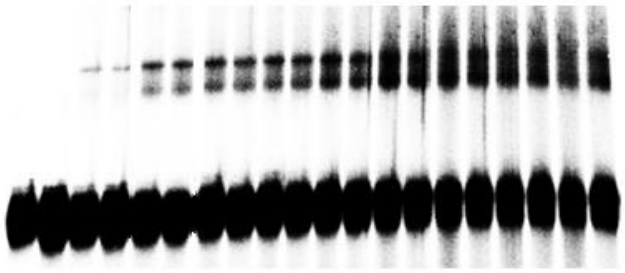

Figure 2-15. The concentration-dependence of ICL formation of duplex for **1a** upon photoirradiation. Phosphor image autoradiogram of 20% denaturing PAGE analysis of **1a** under varying concentration: 0, 0.01 mM, 0.03 mM, 0.05 mM, 0.06 mM, 0.08 mM, 0.1 mM, 0.15 mM, 0.2 mM, 0.3 mM. Reaction mixtures were photo-irradiated at 350 nm for 8 h.

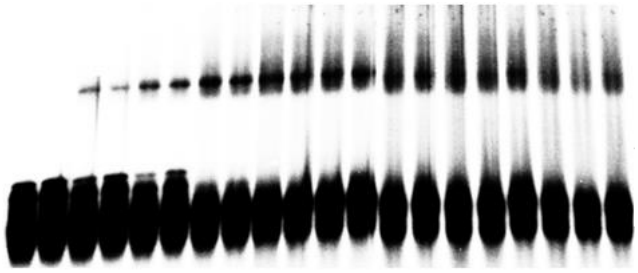

Figure 2-16. The concentration-dependence of ICL formation of duplex for **1b** upon photoirradiation. Phosphor image autoradiogram of 20% denaturing PAGE analysis of **1b** under varying concentration: 0, 0.01 mM, 0.02 mM, 0.05 mM, 0.08 mM, 0.1 mM, 0.2 mM, 0.3 mM, 0.4 mM, 0.5 mM. Reaction mixtures were photo-irradiated at 350 nm for 200 min.

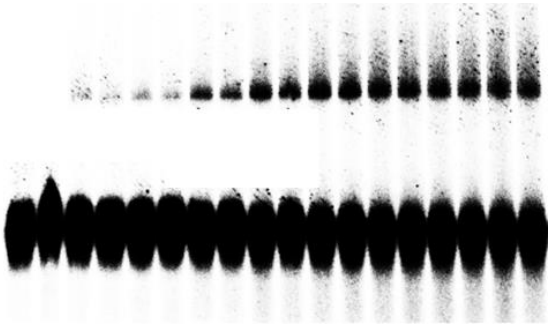

Figure 2-17. The concentration-dependence of ICL formation of duplex for **1c** upon photoirradiation. Phosphor image autoradiogram of 20% denaturing PAGE analysis of **1c** under varying concentration: 0, 0.01 mM, 0.02 mM, 0.05 mM, 0.08 mM, 0.1 mM, 0.2 mM, 0.3 mM, 0.4 mM. Reaction mixtures were photo-irradiated at 350 nm for 8 h.

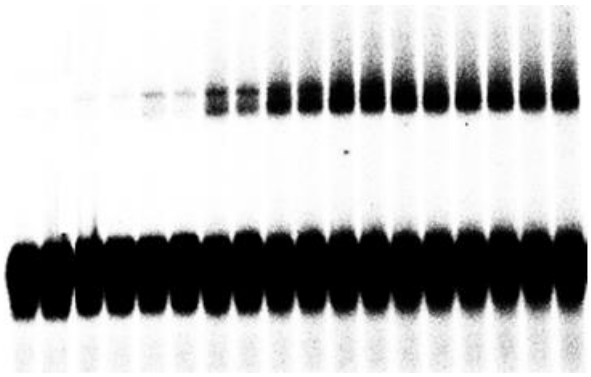

Figure 2-18. The concentration-dependence of ICL formation of duplex for **1d** upon photoirradiation. Phosphor image autoradiogram of 20% denaturing PAGE analysis of **1d** under varying concentration: 0, 0.01 mM, 0.02 mM, 0.05 mM, 0.08 mM, 0.1 mM, 0.15 mM, 0.2 mM, 0.25 mM. Reaction mixtures were photo-irradiated at 350 nm for 4 h.

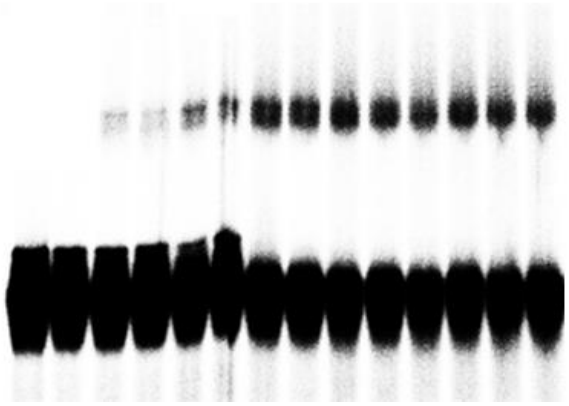

Figure 2-19. The concentration-dependence of ICL formation of duplex for **1e** upon photoirradiation. Phosphor image autoradiogram of 20% denaturing PAGE analysis of **1e** under varying concentration: 0, 0.01 mM, 0.02 mM, 0.08 mM, 0.1 mM, 0.2 mM, 0.3 mM. Reaction mixtures were photo-irradiated at 350 nm for 12 h.

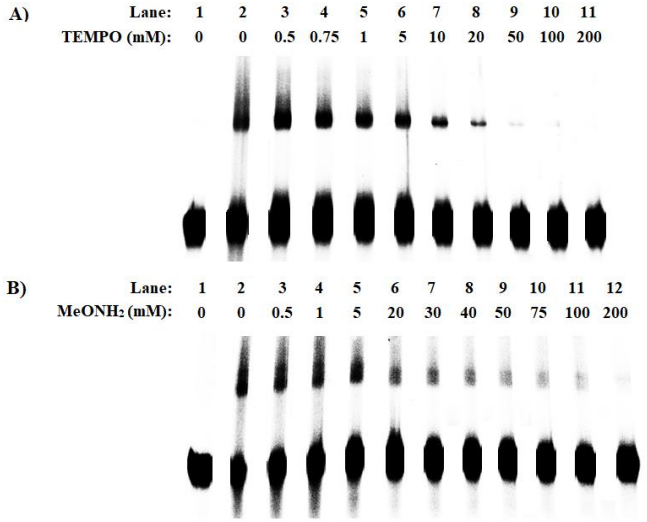

Figure 2-20. The effect of TEMPO and methoxyamine on DNA ICL formation of duplex **5** for **1a.** A mixture of **5** (50 nM) and **1a** (200 μM) in a pH 8 phosphate buffer was irradiated with 350 nm light for 8 h in the presence of varying concentration of $MeONH_2$ (**A**) or TEMPO (**B**).

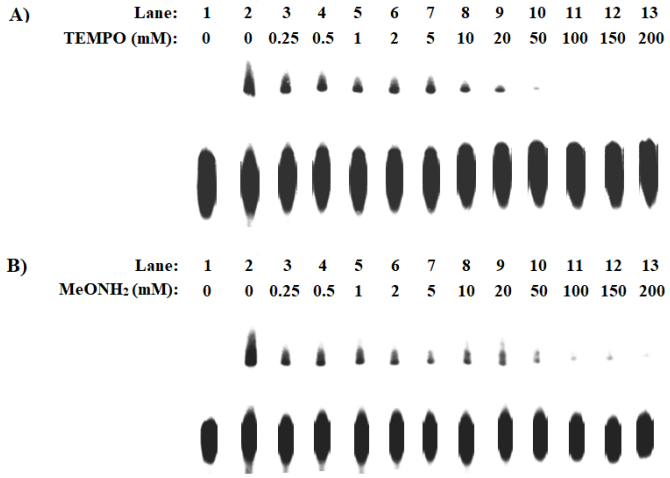

Figure 2-21. The effect of TEMPO and methoxyamine on DNA ICL formation of duplex **5** for **1b.** A mixture of **5** (50 nM) and **1b** (200 μM) in a pH 8 phosphate buffer was irradiated with 350 nm light for 1 h in the presence of varying concentration of $MeONH_2$ (**A**) or TEMPO (**B**).

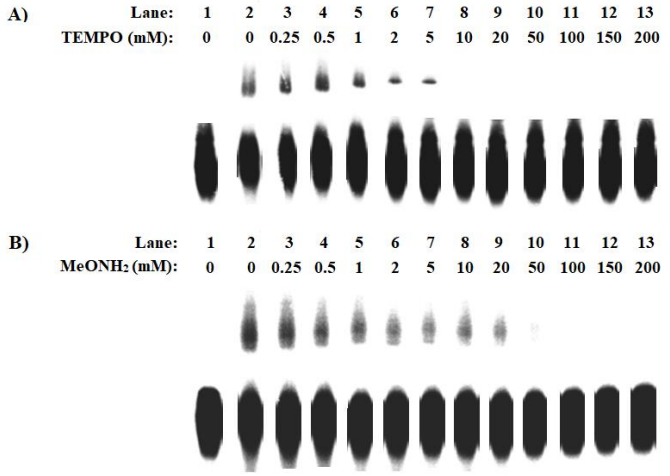

Figure 2-22. The effect of TEMPO and methoxyamine on DNA ICL formation of duplex **5** for **1c.** A mixture of **5** (50 nM) and **1c** (500 μM) in a pH 8 phosphate buffer was irradiated with 350 nm light for 8 h in the presence of varying concentration of $MeONH_2$ (**A**) or TEMPO (**B**).

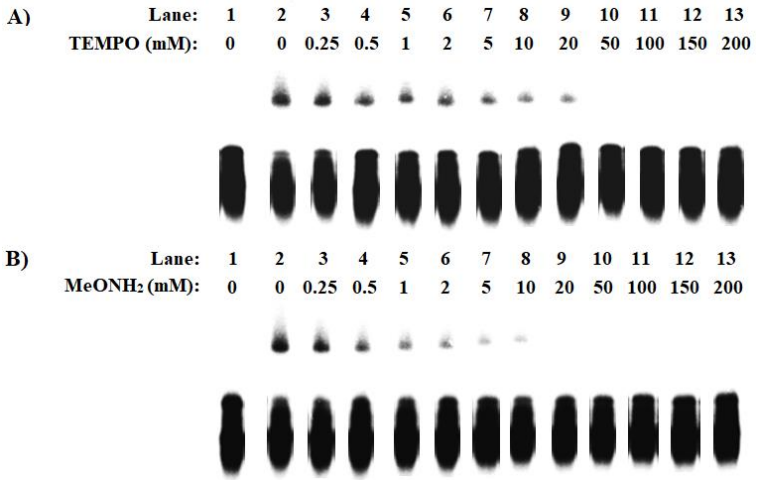

Figure 2-23. The effect of TEMPO and methoxyamine on DNA ICL formation of duplex **5** for **1d.** A mixture of **5** (50 nM) and **1d** (200 µM) in a pH 8 phosphate buffer was irradiated with 350 nm light for 1.3 h in the presence of varying concentration of $MeONH_2$ (**A**) or TEMPO (**B**).

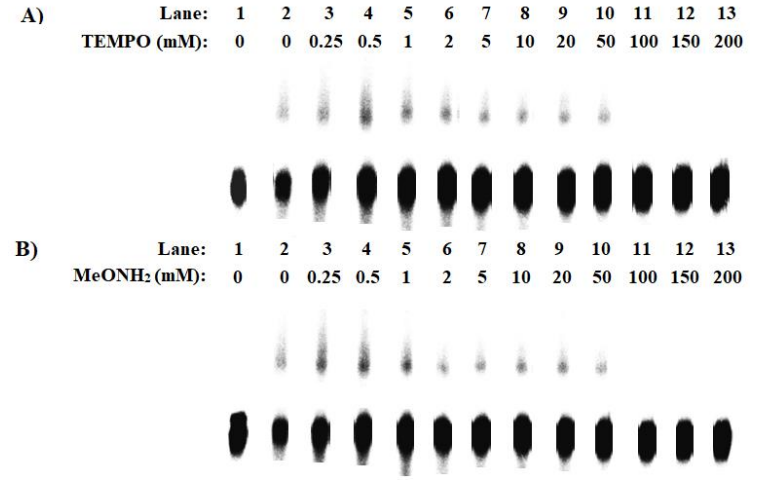

Figure 2-24. The effect of TEMPO and methoxyamine on DNA ICL formation of duplex **5** for **1e.** A mixture of **5** (50 nM) and **1e** (500 µM) in a pH 8 phosphate buffer was irradiated with 350 nm light for 10 h in the presence of varying concentration of $MeONH_2$ (**A**) or TEMPO (**B**).

Chapter 3 Photo-Induced DNA ICL Formation by 4,4'-Dibromo-Substituted Binaphthalene Analogues with Different Leaving Groups

3.1. Introduction

Photoinduced DNA cross-linking is a less toxicity process with high selectivity and biorthogonality, making it has been one popular research area. Photoactivation of DNA-modifying agents has attracted great attention as photoinduction is non-invasive and biorthogonal with high spatio-temporal resolution and control. They have been widely applied in chemical and biology areas, such as being the antitumor and anticancer agents, studying DNA damage and repair, investigating the photomanipulation of DNA and therapeutic gene modulation, and constructing DNA photoswitches.[1] Photocycloaddition and alkylation via quinone methide (QM) formation are first two mechanisms which were figured out in photoinduced DNA cross-linking process and have been studied for a long time. The carbocation formation, however, didn't receive much attention until the last decade when Li and Greenberg research groups found that photo-irradiation of modified thymidines induced DNA interstrand cross-linking via carbocations from free radicals.[2,3] Peng research group later designed and synthesized various bifunctional aromatic compounds and studied their carbocation formation mechanism to produce DNA ICL. These bifunctional aromatic compounds include a series of binaphthalene derivatives,[4,5,6] bisnitroimidazole compounds[7] and benzene analogues.[8,9,10,11] In addition, Peng group has figured out these carbocations formed via either heterolytic cleavage or homolytic cleavage of C-L bond (L: leaving group) and their formation depends on the substrates.[8] Different substituents on the aromatic rings or leaving groups influenced the photoreactivity of these compounds toward DNA.

Naphthalene derivatives, which have π-conjugated ring system, have various pharmacological effects, including anticancer, anti-microbial, antiviral, anti-inflammatory and others. There are many marketed drugs containing naphthalene, such as naphyrone, tolnaftate, duloxetine, lasofoxifene, etc.[12] For DNA interstrand cross-linking, several 2,2'-hydroxyl 1'1-binaphthalene derivatives have been reported to cause DNA ICL formation via Binol-QM formation.[13,14] Our group also developed a series of binaphthalene analogues which are photo-activated to produce naphthalenylmethyl cations via the oxidation of free radicals upon 350 nm irradiation.[4,5,6] It has been concluded that the photoreactivity of benzene analogues were greatly affected by the substituents on the naphthalene ring or leaving groups.[8,10,11] However, there is still not much work about the effect of the leaving groups on the binaphthalene structure. Thus, we were encouraged to develop and characterize more binapthalenes with different leaving groups to figure out the efficiency for inducing DNA ICL. In this work, we synthesized seven new dibromo-substituted binaphthalene compounds with different leaving groups, including acetoxy (**12a**), benzyloxy (**12b**), methylamine (**12c**), dimethylamine (**12d**), morpholine (**12e**), phenylthiol (**12f**) and phenyl selenide (**1g**) (Scheme 3-1). The study emphasizes on studying their photo-irradiation efficiency toward DNA upon 350 nm UV light and investigating the ICL formation mechanism as well as the alkylation sites on DNA strands.

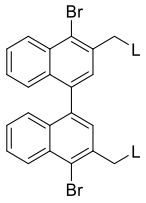

12a: L = OAc;
12b: L = OCH_2Ph;
12c: L = $HNCH_3$;
12d: L = N $(CH_3)_2$;
12e: L = 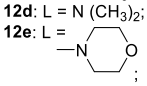

;
12f: L = SPh;
12g: L = SePh.

Scheme 3-5. Dibromo-substituted binapthalene analogues **12a-g**.

3.2. Bromo-Substituted Binaphthalene Analogues as Photo-Inducible DNA Cross-Linking Agents

3.2.1. Synthesis of Compounds 12a-g.

We have designed and synthesized seven 4,4'-dibromo-1,1'-binaphthalene analogues **12a-g** containing different leaving groups (Scheme 3-2). Compounds **12a** and **12c-g** were synthesized via nucleophilic substitution reaction of **2b** that was prepared as previously described.[5] Treatment of **2b** with potassium acetate in the presence of tetrabutylammonium bromide in dimethylformamide (DMF) yielded **12a** containing an acetate as the leaving group. To synthesize the analogues **12c-e** with various amine functional groups, **2b** was treated with methylamine in ethanol (®**12c**), dimethylamine in methanol (®**12d)**, or morpholine (®**12e)** using ethyl acetate as a solvent. Compounds **12a** and **12c-e** were prepared in almost quantitative yields (>92%). By treatment with thiophenol or diphenyl diselenide, **2b** was converted to **12f** (86% yield) or **12g (**83% yield), respectively. Compound **12b** was synthesized from **12a** that underwent hydrolysis (®**13**) followed by ether formation using benzyl chloride and sodium hydride in DMF with 69% yield. All of the new compounds were characterized by NMR and HRMS.

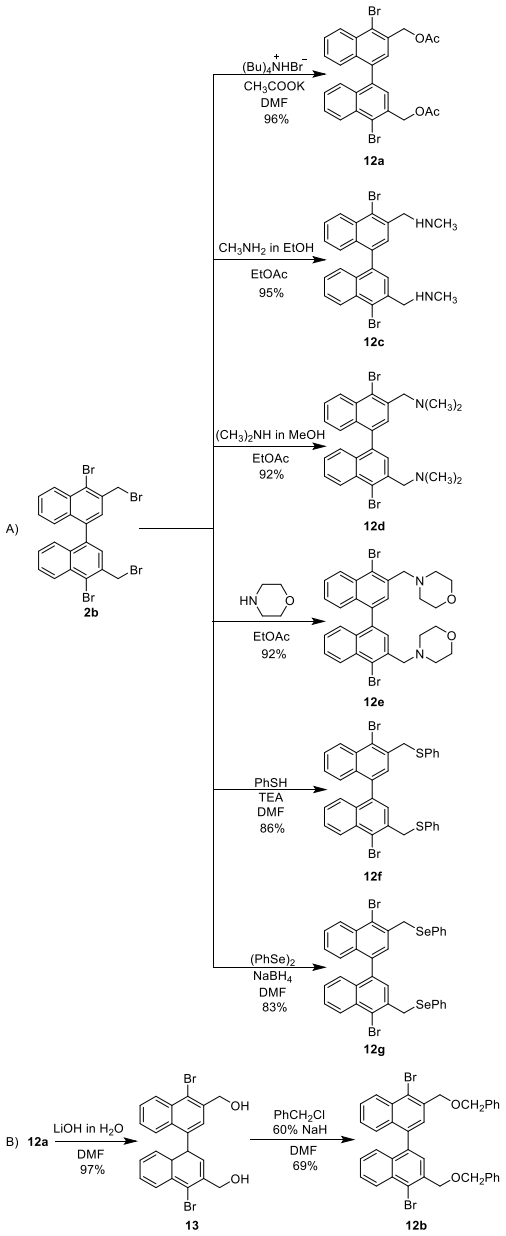

Scheme 3-6. Synthesis of 4,4'-dibromo-1,1'- binaphthalenes **12a-g**.

3.2.2. The reactivity towards DNA of 4,4'-dibromobinaphthalene analogues.

The photochemical reactivity of **12a-g** was investigated by DNA interstrand cross-linking assay using a 49-mer DNA duplex (**5**). The photochemical reactions of **12a-g** with DNA duplex **5** were carried out in a pH 8 phosphate buffer upon 350 nm irradiation in a Model RPR-100 Rayonet© irradiator. The DNA interstrand cross-link (ICL) yields were determined by denaturing polyacrylamide gel electrophoresis (PAGE) with phosphorimager analysis (Image Quant 5.2). Initial study showed that no DNA ICL products were observed with **12a-g** without photo irradiation (Figure 3-1, lanes 1-7) while 350 nm irradiation of **12a-g** led to efficient DNA ICL formation (Figure 3-1, lanes 9-15), which suggested that these compounds are photoactivatable DNA cross-linking agents.

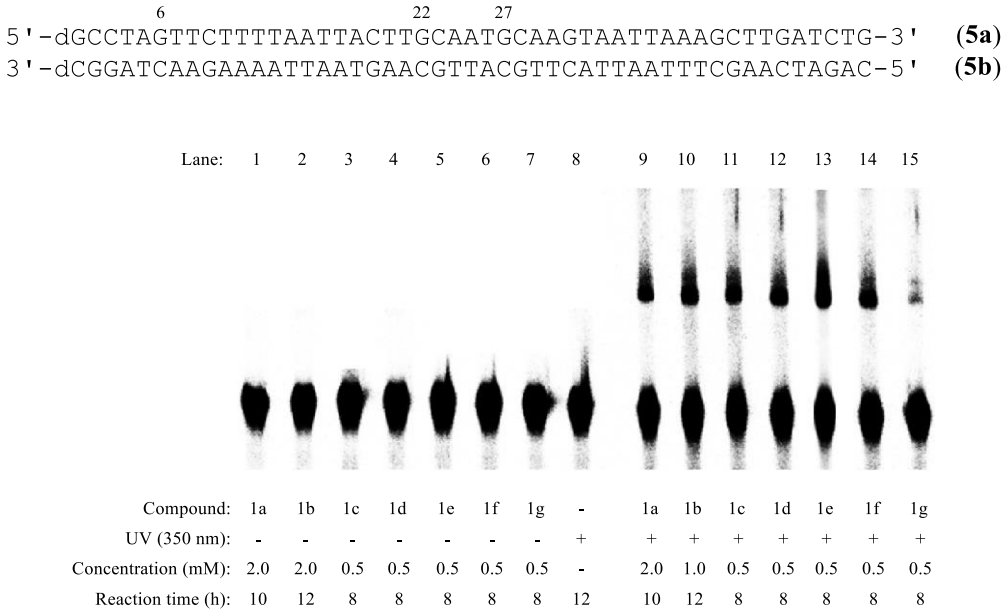

Figure 3-1. Photoinduced DNA interstrand cross-link formation by **12a-g** upon 350 nm irradiation. Lane 1-7: DNA with the drug (optimal concentration) without 350 nm irradiation; lane 8: Only DNA with 350 nm irradiation; lanes 9-15: DNA with **12a-g** upon 350 nm irradiation: lane 9: **12a** (16.9 ± 2.7%); lane 10: **12b** (23.3 ± 1.8%); lane 11: **12c** (26.2 ± 2.9%); lane 12: **12d** (21.5 ± 2.6%); lane 13: **12e** (24.8 ± 1.5 %); lane 14: **12f** (22.1 ± 3.6%); lane 15: **12g** (10.1 ± 2.9%).

After having confirmed that **12a-g** can be activated by photo irradiation to produce ICL formation, we determined their optimal irradiation time for DNA cross-linking reaction with 0.5 mM concentration (Table 3-1, Figure 3-2). The highest ICL yields were observed for **12c-f** after 8 h irradiation and for **12a, 12g** after 10 h irradiation. It took 12 h for **12b** to reach the highest ICL yield. Next, we calculated the reaction rate constant (*k*) for ICL formation induced by these compounds, which was affected not only by the optimal reaction time but also influenced by the DNA ICL yields. Compounds **12c-f** with a shorter reaction time than **12a, 12b** and **12g** showed larger ICL formation rate constants. Among the compounds **12c-f** with similar reaction time, the order of k values is proportional to the order of ICL yields ($k_{12c} > k_{12e} > k_{12f} > k_{12d}$). Similarly, **12g** showed a larger *k* than **12a**. Although **12b** had a longer reaction time than **12a** and **12g**, a larger *k* was observed for **12b** due to its higher ICL yield. Previously, we have shown that photo-induced DNA cross-linking efficiency is correlated with the UV absorption[6,8,10], thus we investigated the effect of UV absorption on DNA ICL formation induced by **12a-g.** The UV absorption of these compounds was measured in $CHCl_3$ with 0.2 mM compound concentration (Figure 3-3). Compound **12g** showed the longest maximum absorption wavelength (>300 nm) with the highest extinction coefficient ($\varepsilon = 18950\ M^{-1}cm^{-1}$). However, the ICL formation induced by **12g** was less efficient than **12b-f** and the reaction rate was slower. The order of the ε values at the maximum absorption was $\varepsilon_{12g} > \varepsilon_{12d} > \varepsilon_{12b} > \varepsilon_{12f} > \varepsilon_{12a} > \varepsilon_{12e} > \varepsilon_{12c}$, which is different from the order of the rate constants ($k_{12c} > k_{12e} > k_{12f} > k_{12d} > k_{12b} > k_{12g} > k_{12a}$). It is noted that **12c** and **12e** showed the largest reaction rate constants ($k > 1.00$) but smallest ε ($< 13000\ M^{-1}cm^{-1}$). Collectively, these data suggested that there is no obvious correlation between the photoreactivity and UV absorbance for these binaphthalene compounds. We propose that the photochemical properties of different leaving

groups play a major role on the ICL reaction induced by these compounds with various leaving groups.

Table 3-1. The ICL yields in optimal irradiation times, reaction rate constants and UV absorption data for 0.5 mM **12a-g**. [a]

Compound	Reaction Time (h)	ICL Yield (%)	k (10^{-5} S^{-1})	λ_{max} (nm)	$\varepsilon_{\lambda max}$ ($M^{-1}cm^{-1}$)
12a (L = OAc)	10	6.9 ± 0.06/14.2 ± 0.66 [b]	0.19	298	14175
12b (L = OCH_2Ph)	12	22.2 ± 0.53/25 ± 0.23 [c]	0.57	299	15425
12c (L = $NHCH_3$)	8	26.1 ± 0.27	1.11	299	12650
12d (L = $N(CH_3)_2$)	8	22.4 ± 0.87	0.87	298	17500
12e (L = $C_5H_{11}NO$)	8	25.0 ± 1.06	1.06	299	12900
12f (L = SPh)	8	24.6 ± 0.55	0.97	296	14800
12g (L = SePh)	10	15.4 ± 0.67	0.45	302	18950

[a] The DNA ICL study was carried out with 0.05 μM DNA duplex in a 10 mM phosphate buffer (pH = 8) upon 350 nm light irradiation. [b] The highest ICL yields obtained with 2.0 mM **12a**. [c] The highest ICL yields obtained with 1.0 mM **12b**. All ICL yield was presented as average ± deviation from duplicate samples in experiments.

With the optimized reaction times of **12a-g**, we performed concentration-dependent study to identify the optimal concentration for these compounds to obtain the highest ICL yields (Figure 3-4). Generally, the ICL yields increased with the increasing concentration of **12a-g** until the highest yields reached. The maximum ICL yield was observed at 2.0 mM for **12a** (14.2%) and at 1.0 mM for **12b** (25%). Only 0.5 mM was required for **12c-g** to reach the optimal ICL yields (15-26%). Furthermore, **12b-f** (>20%) produced much higher optimal ICL yields than **12a** (14.2%) and **12g** (15.4%). The order of ICL efficiency under optimal conditions is consistent with that obtained at 0.5 mM (**1c** ≈ **1e** ≈ **1f** ≈ **1d** > **1b** > **1g** > **1a**) (Table 3-1). We would like to point out that serious DNA damage was observed for **12d**, **12e** and **12g** when the concentration was higher than 0.5 mM, leading to lower DNA cross-linking yields. Collectively, we conclude that among seven functional groups tested, the amine functional groups, such as methylamine (**12c**) or morpholine (**12e**), phenylthiol (**12f**) dimethylamine (**12d**) are superior than others for designing photo-induced DNA interstrand cross-linking agents. Benzyloxy (**12b**) is moderate photo-activatable leaving groups

for the DNA ICL formation because **12b** required higher concentration to obtain the highest cross-linking yield. Acetoxy group (**12a**) or phenyl selenide (**12g**) was poor leaving group for the photo-induced DNA ICL formation.

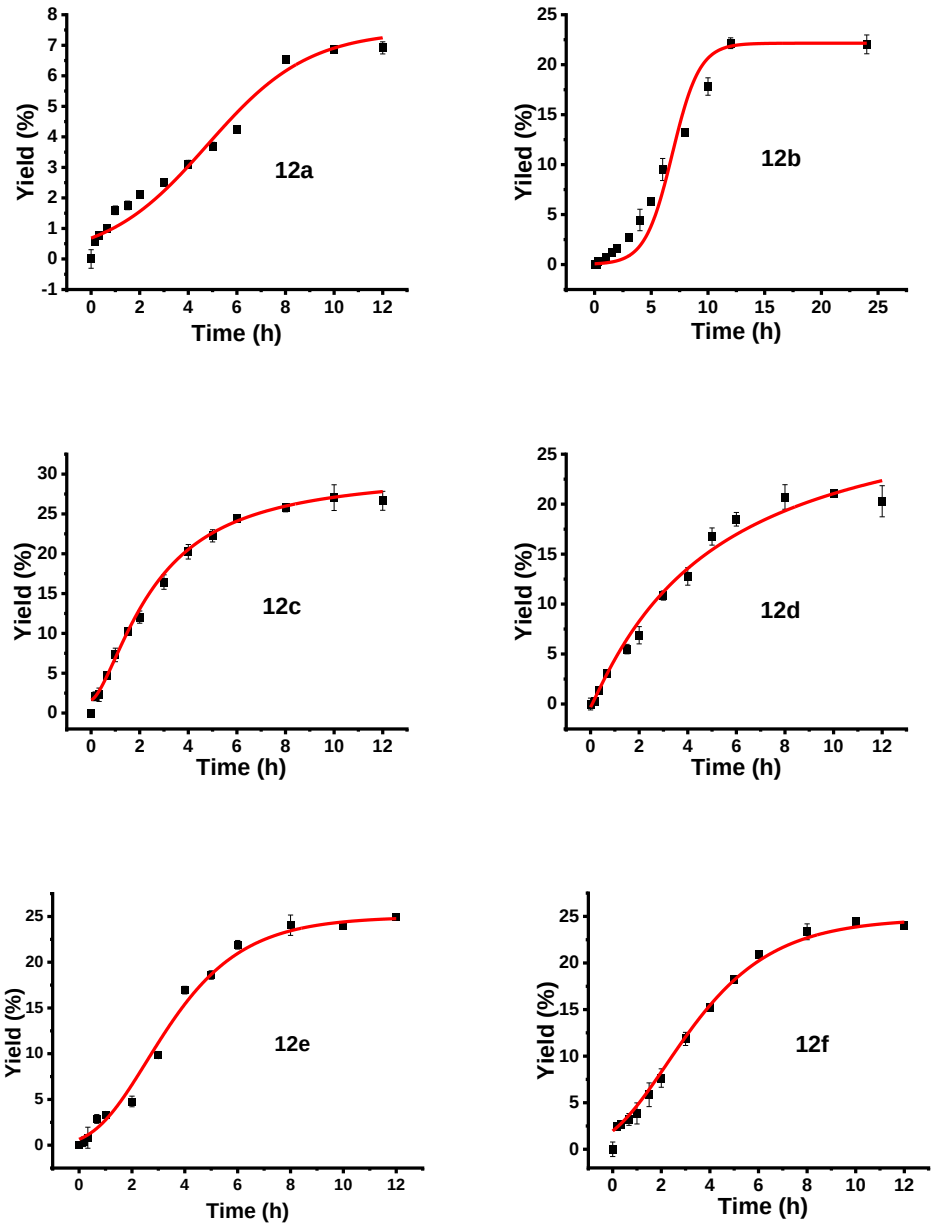

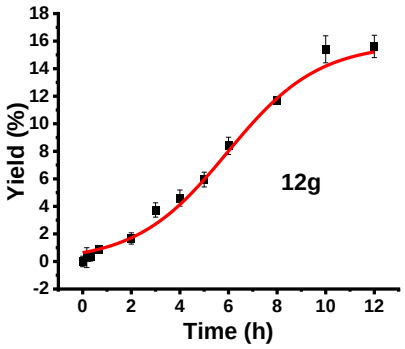

Figure 3-2. Photoinduced DNA interstrand cross-link formation by **12a-g** upon 350 nm irradiation.

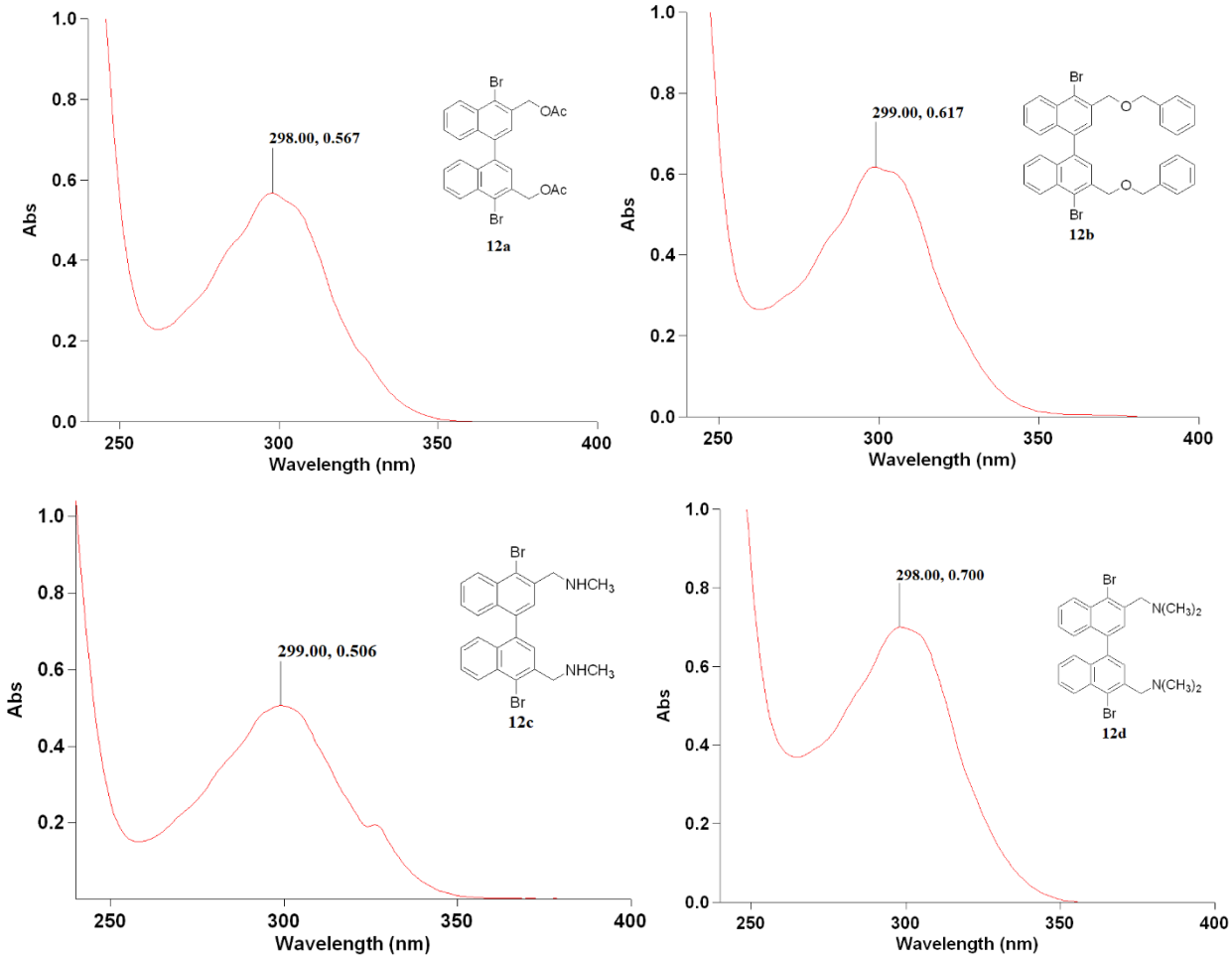

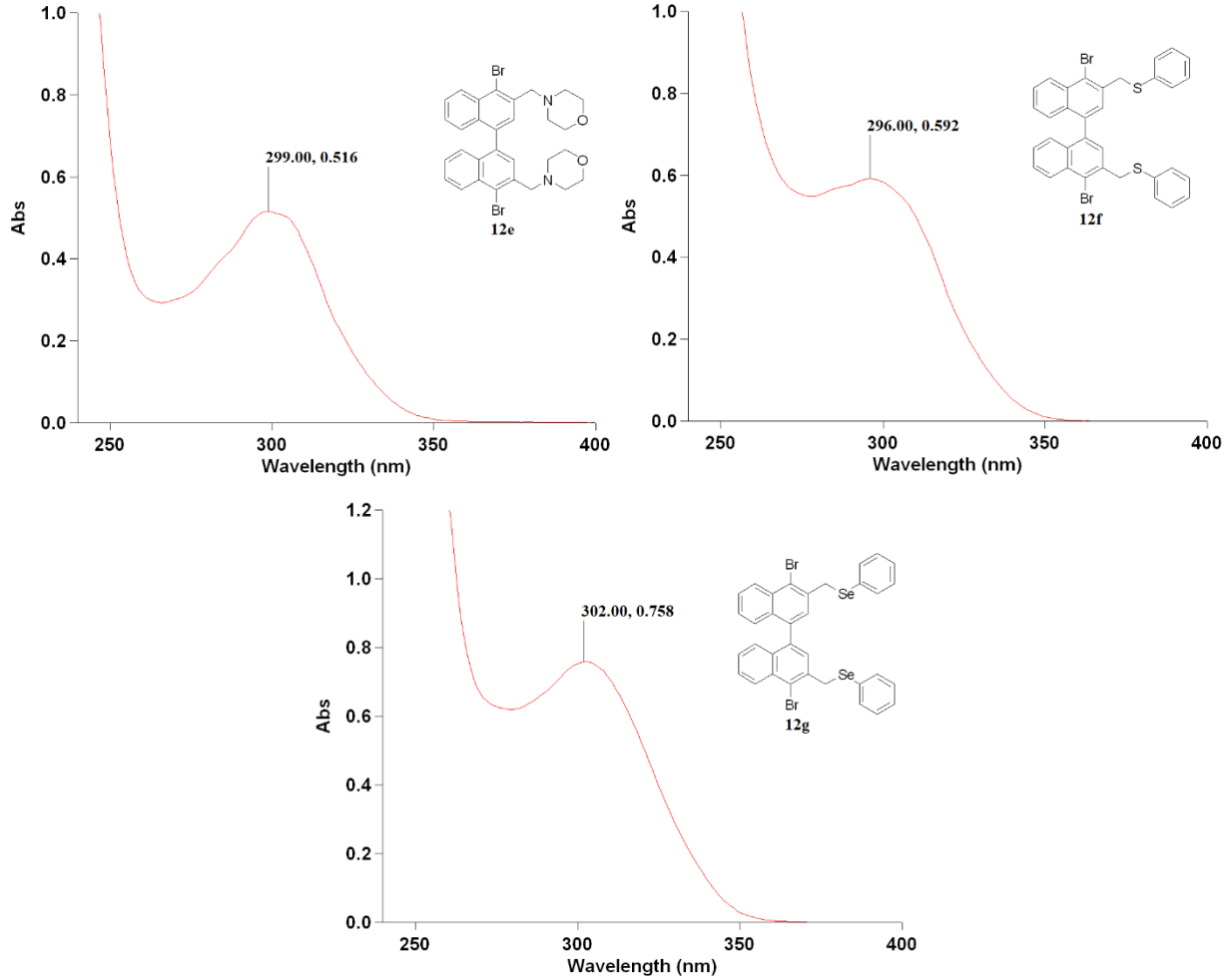

Figure 3-3. UV spectra of **12a-g**.

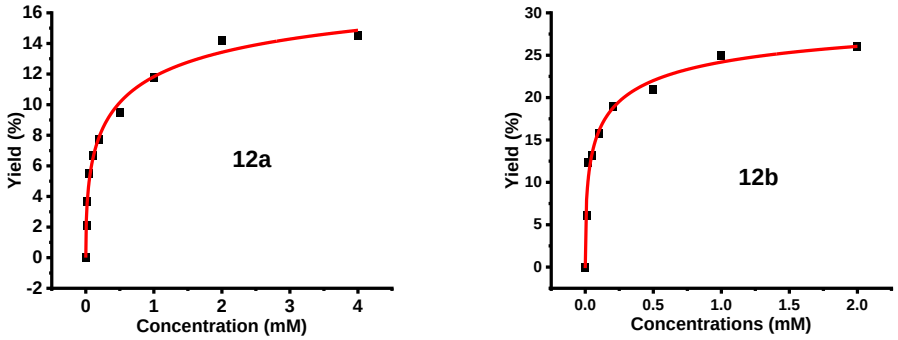

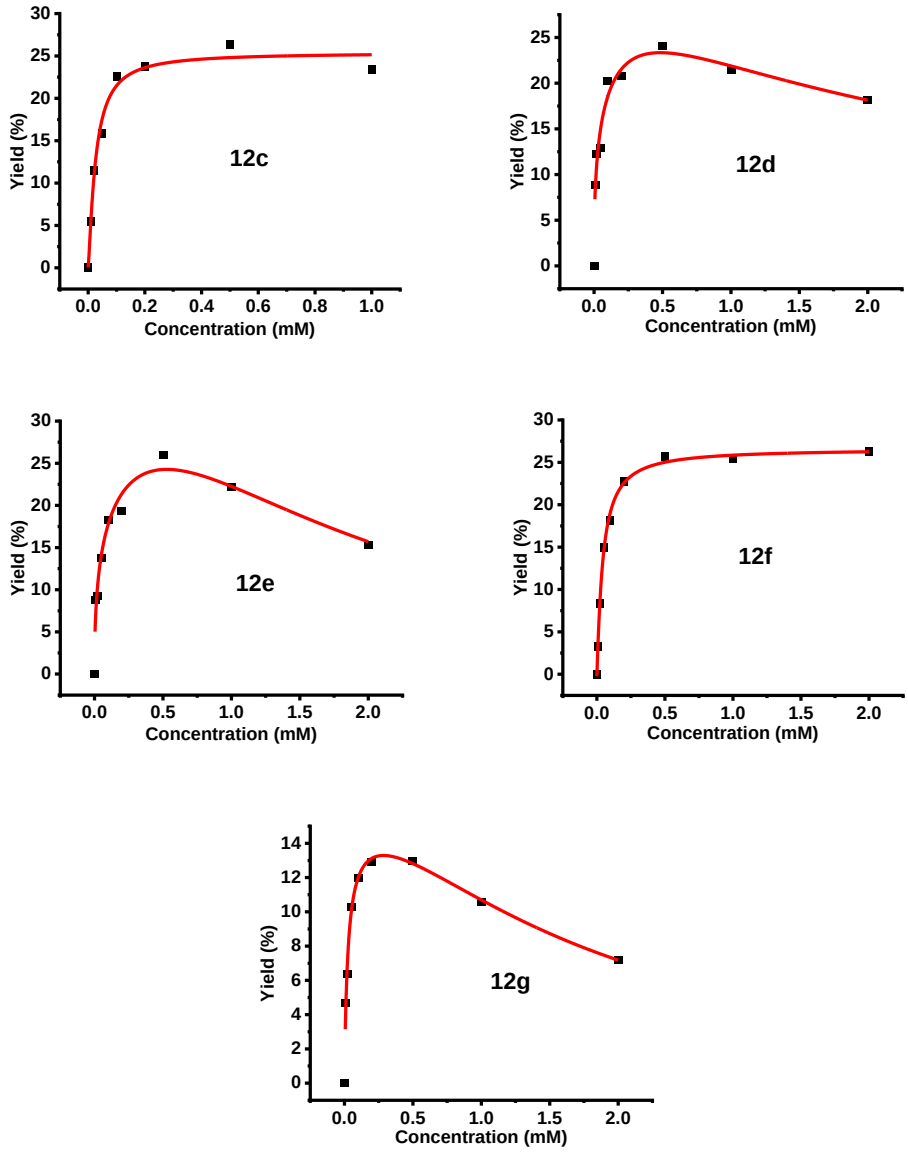

Figure 3-4. Concentration-dependence of DNA ICL formation of duplex **5** for **12a-g** upon photo-irradiation. Phosphor image autoradiogram of 20% denaturing PAGE analysis of **12a-g** under varying concentrations. Reaction mixtures were photo-irradiated under UV (350 nm) for optimal times.

Our previous work indicated that the pH of the phosphate buffer solution affected the efficiency of DNA ICL formation.[5] Therefore, we investigated the effect of pH values on DNA cross-linking induced by **12c-e**. Compounds **12c-e** were chosen for pH-dependent ICL formation study because they contain amine functional groups as the leaving groups that could be protonated under different

pH conditions, which may affect the photoreactivity of these compounds. The pH-dependent ICL formation was carried out with 0.5 mM **12c**, **12d**, or **12e** upon 8 h irradiation. The results showed a large discrepancy on DNA ICL formation among these compounds (Table 3-2, Figure 3-5). In pH = 3 phosphate buffer, DNA damaged seriously and none of the compounds produced DNA ICL (Figure 3-5, Lane 2, 8, and 14). In pH = 5 phosphate buffer, the irradiation produced 17.1% DNA cross-linking with **12e** while caused serious DNA damage with **12c** and **12d** (Figure 3-5, Lane 3, 8, and 15). Although **12c** produced DNA ICL with 32.4% yield in neutral solution (pH = 7), obvious DNA damage was also observed (Figure 3-5, Lane 4). In basic buffer solution, the photoirradiation of these three binaphthalene analogues induced significant DNA interstrand cross-linking. The DNA ICL yields of **12c** were 26.3% and 20.7% in pH = 8 and pH = 9 phosphate buffers, respectively. The irradiation of **12d** caused 22.1% ICL in pH = 8 buffer and 18.3% ICL in pH = 9 buffer. For **12e**, the ICL yields in two basic buffers were similar which were 17.0% (pH = 8) and 17.5% (pH = 9). This DNA ICL formation study indicated that the photoreactivity of binaphthalenes with amine leaving groups is significantly affected by pH values of the phosphor buffer. Among three binaphthalenes, **12e** obtained the efficient cross-links in pH 5-9 phosphor buffer solutions. **12c** with methylamine leaving group could not induce good DNA ICL formation in acidic and neutral solutions (pH $\leq$ 7), and **12d** which has dimethylamine leaving group was not stable under the irradiation in the solution with the pH value lower than 5. The discrepancy of DNA ICL formation in the buffers with different pH values might be correlated with the pKa values of **12c**-**e**. The pKa values of these compounds were calculated and predicted by using Chemicalize®. The pKa values of **12c** and **12d** were 9.19 and 8.48, while the value of **12e** was 7.29. With lower pKa value, **12e** alkylated with DNA strands and produced efficient ICL formation in pH = 5 phosphate buffer. **12d** also formed a few DNA ICL in the pH = 5 buffer although the

serious DNA cleavage damage occurred. However, **12c** which has the largest pKa value could not induce efficient DNA interestrand cross-linking in the acidic buffers with 8-hour irradiation. This might be due to the long-time irradiation which caused serious DNA damage. Thus, we next performed time-dependent studies with **12c** and **12d** in pH = 3 and pH = 5 solutions to investigate the DNA ICL formation in acidic phosphate buffers. The results showed that serious DNA damage occurred immediately in pH = 3 buffer solution when the irradiation started and no efficient DNA ICL produced (not shown in figure), indicating pH = 3 buffer solution is too acidic to form DNA interstrand cross-linking. In pH = 5 solution, **12c** reached the highest ICL yield (12.3%) with only 1 h irradiation (Figure 3-6 (left), Figure 3-26). However, the efficiency of ICL formation was much lower than the formation in pH = 8 buffer solution (12.3% vs 26.3%). For **12d**, the highest ICL yield was obtained with 6-hour irradiation in pH = 5 buffer (Figure 3-6 (right), Figure 3-27). It indicated that the pH = 5 buffer facilitates the ICL reaction, while it might decrease the efficiency of ICL formation. All three compounds **12c**-**e** were protonated in the pH = 5 phosphate buffer and **12c** showed the strongest ability to attract H^+ ions in the solution because of its highest pKa value. Therefore, it has the fastest DNA cross-linking reaction. However, the acidity of solution might suppress DNA ICL formation. The pH study demonstrated that the protonation facilitates the DNA ICL reaction, but the acidity of the solution made the ICL formation less efficient. Overall, the DNA cross-linking study with dibromo-substituted compounds **12a**-**g** indicated that different leaving groups not only affected the reaction rate for DNA cross-linking but also influence the efficiency of ICL formation in phosphate buffer with various pH values.

Table 3-2. DNA ICL yield for **12c**-**e** in phosphor buffers with various pH values. [a]

Compound	Predicted pKa value[b]	pH 3 Buffer	pH 5 Buffer	pH 7 Buffer	pH 8 Buffer	pH 9 Buffer
12c	9.19	n.d.[c]	n.d.	32.4%[c]	26.3%	20.7%
12d	8.48	n.d.	27.1%[d]	25.2%	22.1%	18.3%
12e	7.29	n.d.	17.1%	19.2%	17.0%	17.5%

[a] The DNA ICL study was carried out with 0.05 μM DNA duplex and 0.5 mM **12c-e** in a 10 mM phosphate buffer upon 350 nm light irradiation; [b]; The strongest basic pKa values were predicted by online calculations and predictions platform Chemicalize by Chemaxon Software®; [c] The ICL yield was not determined due to the DNA damage. [d] Obvious DNA damage was observed.

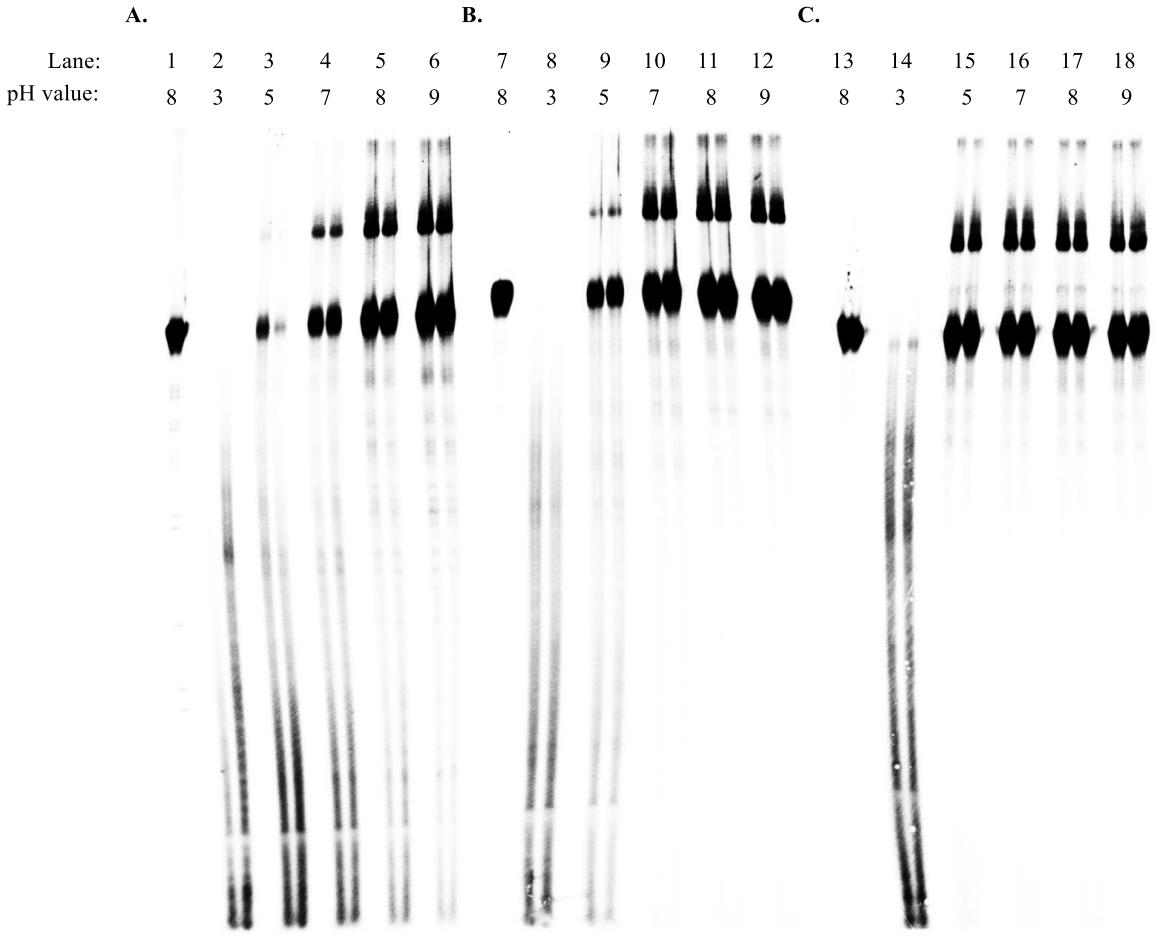

Figure 3-5. Photoinduced DNA interstrand cross-link formation by **12c-e** (optimal concentrations) upon 350 nm irradiation in phosphate buffer with different pH values. A. Lane 1-6: DNA ICL formation by **12c**: lane 1: DNA with **12c** without irradiation; lane 2: DNA with **12c** in pH = 3 buffer (DNA damage); lane 3: DNA with **12c** in pH = 5 buffer (DNA damage); lane 4: DNA with **12c** in pH = 7 buffer (32.4%); lane 5: DNA with **12c** in pH = 8 buffer (26.3 %); lane 6: DNA with **12c** in pH = 9 buffer (20.7%). B. Lane 7-12: DNA ICL formation by **12d**: lane 7: DNA with **12d** without irradiation; lane 8: DNA with **12d** in pH = 3 buffer (DNA damage); lane 9: DNA with **12d** in pH = 5 buffer (27.0%); lane 10: DNA with **12d** in pH = 7 buffer (25.2%); lane 11: DNA with **12d** in pH = 8 buffer (22.1%); lane 12: DNA with **12d** in pH = 9 buffer (18.3%). C. Lane 13-18: DNA ICL formation by **12e**: lane 13: DNA with **12e** without irradiation; lane 14: DNA with **12e** in pH = 3 buffer (DNA damage); lane 15: DNA with **12e** in pH = 5 buffer (17.1%); lane 16: DNA with **12e** in pH = 7 buffer (19.2%); lane 17: DNA with **12e** in pH = 8 buffer (17.0%); lane 18: DNA with **12e** in pH = 9 buffer (17.5%).

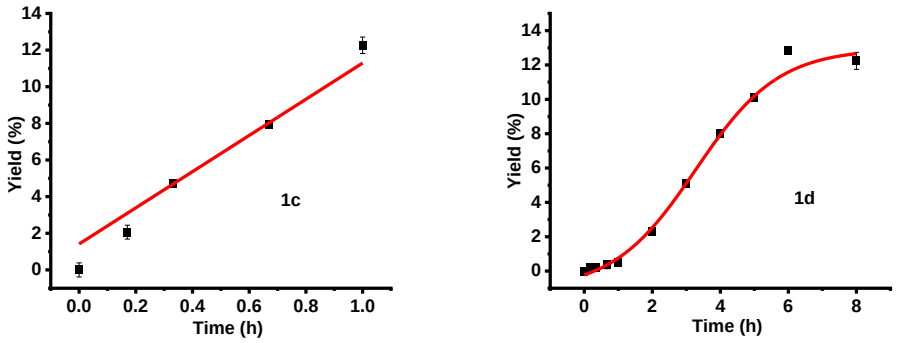

Figure 3-6. Time-dependence of DNA ICL formation of duplex **5** for **12c** (left) and **12d** (right) upon photo-irradiation in pH = 5 phosphor buffer solution.

2.2.3. Mechanism of DNA ICL Formation.

There are two pathways for carbocation formation in photoinduced DNA interstrand cross-linking, including homolysis and direct heterolysis of C-L bond (L = Leaving Groups).[5,8,9,10,11] Previously, we have observed that the carbocation generation depends on the leaving groups of the substrates. The aryl boronates with bromo as leaving group produced benzyl cations via the oxidation of free radicals, while those with trimethyl ammonium salts as leaving groups generated cations via the heterolysis of C-N bond.[9] In another work, it was observed that the carbocations were produced directly in the photoirradiation of phenyl trimethyl ammonium salts containing nitro substituent, while the carbocation formation of the trimethyl ammonium salts with bromo substituent were affected by the various concentrations of 2,2,6,6-tetramethylpiperidin-1-oxyl (TEMPO) which is the free radical trapper in mechanism studies.[8] When the concentration of TEMPO was lower than 2.0 mM, free radicals were involved in the cross-linking process and produced by the homolysis of C-N bond. However, the heterolysis of C-N bond occurred when TEMPO was higher than 2.0 mM and became predominant with 50-100 mM TEMPO. The phenyl compounds with other leaving groups produced DNA ICL via carbocation which was oxidized by free radicals. Therefore,

we investigated the mechanism of DNA ICL formation induced by these binaphthalene analogues that contain different leaving groups. As previously reported, TEMPO and methoxyamine were applied as trapping agents for free radicals and cations, respectively. The trapping effect of TEMPO and $MeONH_2$ on DNA ICL formation induced by **12a**-**g** is shown in Figure 3-7. In general, the DNA ICL yields of **12a**-**g** decreased with the increasing concentration of TEMPO and $MeONH_2$, indicating that both free radicals and carbocations were involved in the DNA ICL formation. When the concentration of TEMPO and methoxyamine increased to 200 mM, the ICL yields of all these compounds was below 5%, demonstrating that the DNA ICL formation was efficiently inhibited by the free radical and cation trappers (Table 3-3). For example, the ICL yield of **12b** dropped from 30% to < 3.0% with the existence of 200 mM TEMPO or $MeONH_2$. Thus, we propose that these binaphthalene compounds produced carbocation via the oxidation of free radicals instead of direct heterolysis of C-L bond.

The different DNA ICL yields with 200 mM TEMPO or $MeONH_2$ indicated that the trapping efficiency was affected by the substrates (Table 3-3). In the presence of 200 mM TEMPO, the highest ICL yield was 3.55 % (**12d**) and the lowest was 0.95% (**12f**). With 200 mM $MeONH_2$, the ICL of **12f** was 4.25% while the ICL of **12a** was only 0.38%. It is worth to note that when the ICL yields decreased to the half of the original yields in carbocation trapping experiments, the discrepancy of the concentrations of $MeONH_2$ was large (Table 3-3). To decrease 50% DNA ICL formation, **12b** and **12f** only needed 0.61 mM and 0.97 mM $MeONH_2$, respectively. For **12a**, **12c**, **12d** and **12e**, less than 4.5 mM $MeONH_2$ were required. However, **12g** required 25 mM $MeONH_2$ to decrease 50% ICL formation, indicating that the cation trapping of **12g** was less efficient than the cation trapping of other compounds. This may explain the low reactivity of the carbocations of **12g** which caused the lowest DNA ICL yield in concentration-dependent study.

Next, we performed monomer trapping reactions with compound **12b** in the presence of TEMPO or methoxyamine. **12b** was chosen as the representative compound in these experiments because of its high efficiency on DNA ICL formation. The thin-layer chromatography was used to monitor the reactions. For TEMPO monomer trapping, it took more than five days until no more **12b** was consumed. With methoxyamine, however, the trapping reaction only spent ~3.5 days to consume all **12b**. It was difficult to purify enough adducts for NMR analysis because of the multiple products in the reaction. Therefore, we did HRMS to analysis the products to figure out the trapping adducts. As shown in Scheme 3-3, the adduct **14** was found and confirmed by HRMS in radical monomer trapping reaction, indicating that radical **14** was produced during the UV irradiation and it formed mono-trapping adduct **15**. We assumed that compound **16** was detected by HRMS instead of **15** due to the leave of the benzyloxy group during the analysis process. When **12b** was irradiated with methoxyamine, carbocation **17** was produced and further transferred to **18** which was also confirmed by HRMS. The analysis of monomer trapping adducts gives the direct evidence of carbocation formation mechanism via the heterolysis of C-L bond. The photoirradiation of Br-substituted binaphthalene analogues produced free radical **19a** which are immediately oxidized to corresponding carbocation **19b** that further alkylates with DNA and cause ICL (Scheme 3-4). The failure of detecting the bisradical or biscation trapping products indicated that the alkylation rate with the second leaving group is much slower and it is the rate-determining step in the cross-linking reaction.

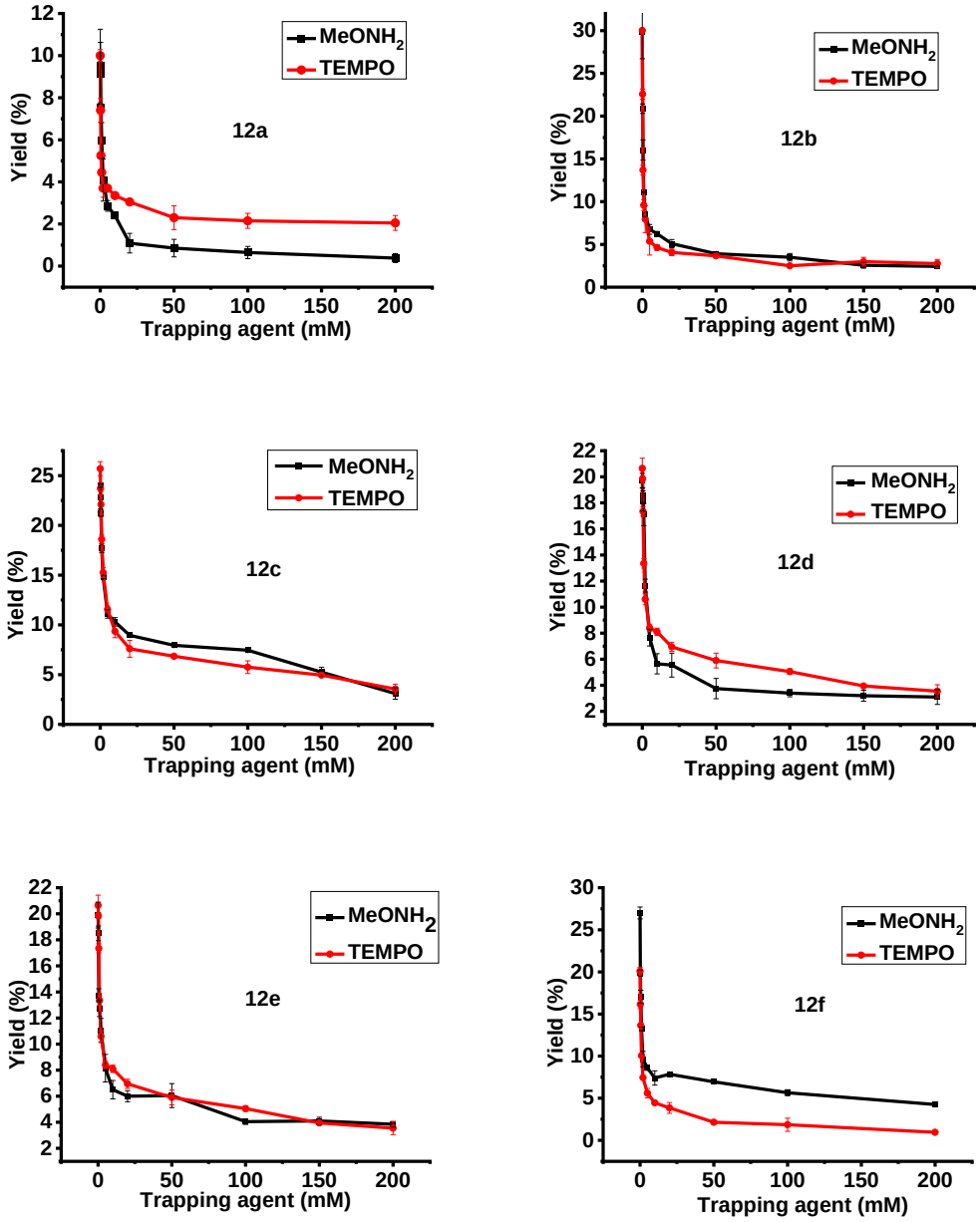

Figure 3-7. The effect of methoxyamine and TEMPO on DNA interstrand cross-linking induced by **12a-g**.

Table 3-3. DNA ICL yields of **12a-g** with 200 mM TEMPO or $MeONH_2$, and the concentrations of $MeONH_2$ to decrease 50% DNA ICL yields of **12a-g**.

Compound	ICL Yield with 200 mM TEMPO (%)	ICL Yield with 200 mM $MeONH_2$ (%)	The concentration of $MeONH_2$ to decrease 50 % DNA ICL yields (mM)
12a (L = OAc)	2.05	0.38	1.64
12b (L = OCH_2Ph)	2.76	2.425	0.61
12c (L = $NHCH_3$)	3.55	3.1	4.27
12d (L = $N(CH_3)_2$)	3.55	3.1	3.31
12e (L = $C_5H_{11}NO$)	3.55	3.85	3.09

12f (L = SPh)	0.95	4.25	0.97
12g (L = SePh)	2.4	3.65	25

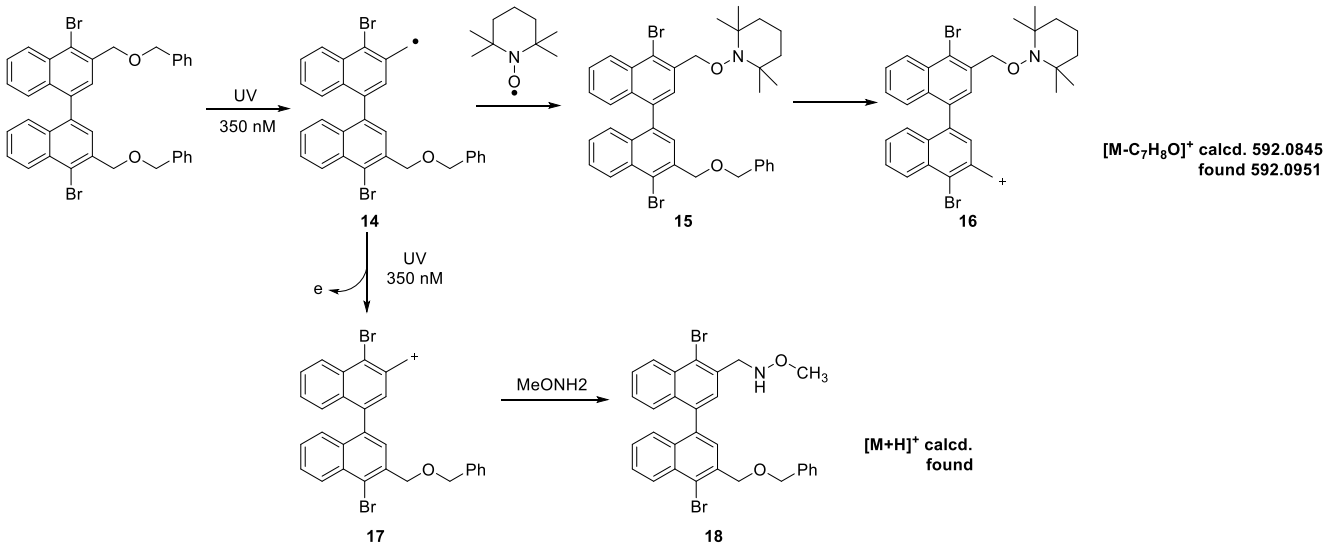

Scheme 3-7. Monomer trapping reactions of **12b**.

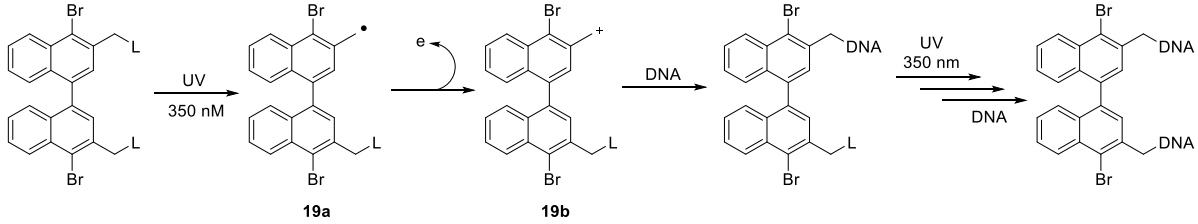

Scheme 3-8. Proposed carbocation formation mechanism under photoirradiation.

3.2.4. The Reaction Sites of Photogenerated Naphthalenyl Methyl Cation in DNA.

Mechanism investigation indicated that both free radicals and carbocations are involved in photo-induced DNA ICL formation by these naphthalene analogues **12a-g**. It is well-known that free radicals may cause alkaline-labile DNA lesions while carbocations can form N7-alkylated purine nucleosides that undergo deglycosylation upon heating under basic conditions leading to the cleavage of DNA strands.[15,16] It has been found that the DNA interstrand cross-linking agents

greatly affect the photoreactivity of naphthalenylmethyl cations toward DNA. [6,8] Thus, we studied the heat stability of DNAs after treatment with **12a-g** upon 350 nm irradiation to determine the possible reaction sites. Initially, DNA ICL products were purified by precipitation after 350 nm irradiation of duplex **5** with **12a-g** under the optimal conditions, then heated in 1.0 M piperidine at 90 ℃ for 30 min. The phosphor-image autoradiogram of 20% denaturing PAGE analysis for the heat stability study of the adducts formed between duplex **5** and **12a-g** is shown in Figure 3-8 and 3-9. The DNA cleavages were observed mainly at dG sites for **12b-f**, such as G22 and G27 (Figure 3-8, lane 7, 11; Figure 3-9, lane 3, 7, 11), indicating that the dGs were the prominent alkylation sites for these compounds. For **12a** and **12g**, cleavage bands were observed not only at dG sites (G22 and G27) but also at dAs (A14, A15, A18, A24 and A25) (Figure 3-8, lane 3; Figure 3-9, lane 15), which suggested that both N7-alkylated dG and dA adducts were formed with **12a** and **12g** upon 350 nm irradiation. These data indicated that the leaving groups influence the reactivity of the photo-generated naphthalenyl methyl cation towards DNA.

The DNA adducts purified by precipitation contain both DNA ICL products and single-stranded ODN **4a**'. After having determined that **1a** and **1g** alkylated DNA at both dG and dA sites, we investigated whether DNA ICL formation took place with both dG and dA. The difference of the alkylation at dAs encouraged us to study whether it took place in the interstrand cross-link reaction, monoalkylation of single-stranded ODN or both. Thus, we isolated DNA ICL products and single-stranded ODN (**5a'**) by denaturing PAGE after treatment of DNA duplex **5** with **12d** or **12g** upon 350 nm irradiation. Next, we performed the heat stability study with the purified ICL products and single-stranded ODN **5a'** formed by **12g**. For the isolated ICL products, the cleavage bands were observed only at dG sites (G22 and G27) but not at dA sites (Figure 3-10, lane 7), suggesting that DNA interstrand cross-linking took place with dGs but not with dAs. However, DNA cleavages

occurred with both dGs and dAs for single-stranded DNA **5a**' (G22, G27, A14, A15, A18, A24 and A25), which indicated that monoalkylation took place with both dG and dA sites (Figure 3-10, lane 9). For comparison, we performed the heat stability study with the isolated ICL products formed with **12d** as well as the single-stranded ODN (**5a**') (Figure 3-10). For both ICL products and single-stranded ODN **5a**', obvious cleavage bands were observed at dG sites not at dA sites, which suggested that **12d** alkylated DNA only at dG sites (Figure 3-10, lanes 5 and 9). These results are consistent with those obtained with the DNA adducts purified by precipitation. Collectively, these data demonstrated that DNA ICL formation mainly occurred at dG sites for all compounds while monoalkylation takes place with dG or dG/dA. The efficiency of the alkylation at dAs in the monoalkylation depends on the substrates which have different leaving groups.

The heat stability study can determine the location of alkaline-labile lesions but could not show the positions of the alkylation products that are stable to heating, including those occurred with pyrimidines. Therefore, we studied the sequence effect on DNA ICL formation. Compounds **12b** and **12g** were chosen as the representatives in this study. Since the above heat stability study showed that **12g** can react with dA by alkylation, we designed a 24-mer self-complementary dAs/dTs duplex **21** to investigate whether alkylation occurs with dTs. No ICL products were observed with the photo-irradiation of **12g** with duplex **12**, which suggested that no alkylation took place at dT sites. As expected, the cleavage bands were observed at dA sites after heating DNA in 1.0 M piperidine possibly due to the formation of N7-alkylated dAs. However, alkaline-labile lesions were observed with dT sites which might be caused by free radicals (Figure 3-11, lane 7)[15,16]. This was not observed with duplex **5**. Similar results were observed with **12b**. These data indicated that 350 nm irradiation of **12b** and **12g** did not produce DNA interstrand cross-links between dAs and dTs, neither between two dAs or two dTs in complementary strands.

Having confirmed that these compounds can alkylate dAs but not dTs upon 350 nm irradiation, we designed DNA duplex **20** that contains dAs/dGs in one strand and dTs/dCs in the complementary strand to investigate whether ICL reaction takes place with dCs. As expected, efficient ICL formation was observed with duplex **20** upon 350 nm irradiation of **12b** (Figure 3-11, lanes 1 and 2) and **12g** (Figure 3-11, lanes 9 and 10). So, we conclude that dG/dCs are the major ICL formation sites. Like duplex **5**, alkaline-labile lesions were not observed at dT sites for duplex **20.** Collectively, these data suggested that the photochemical reactivity of these naphthalene analogues towards DNA are sequence dependent. Overall, for **12a-g**, dGs and dCs are the main alkylation sites in DNA cross-linking, and the alkylation at dAs and dGs were occurred in monoalkylation. The leaving groups of the binaphthalene compounds affect the photoreactivity of cations toward dAs and dGs. Compounds with acetoxy or phenyl selenide leaving groups have a better photoreactivity toward dAs.

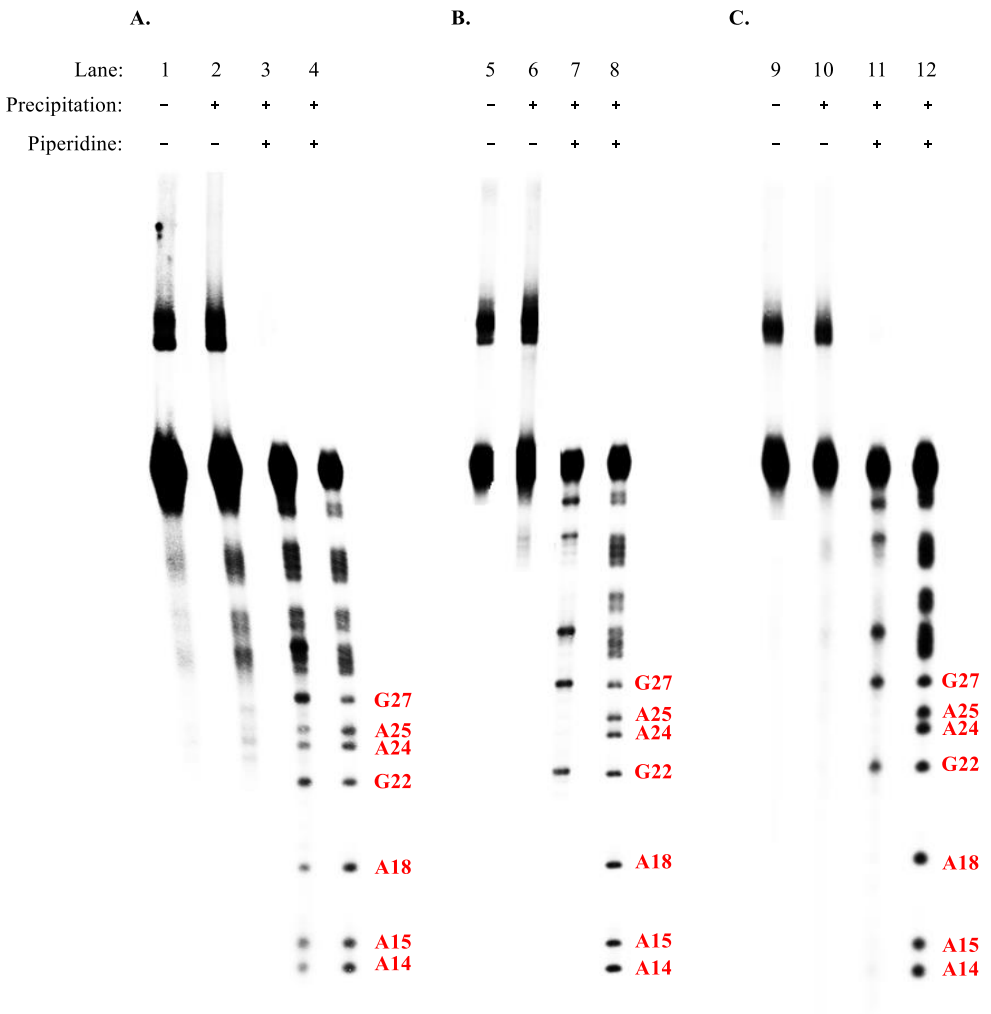

Figure 3-8. Determination of the cross-linking sites of **12a-c** with DNA duplex **5**. Phosphorimage autoradiogram of 20% denaturing PAGE analysis of the DNA ICL products. A. Compound **12a**: lane 1, ICL product formed with **12a** without precipitation; lane 2, ICL product with precipitation (control); lane 3, purified ICL product heated in 1.0 M piperidine at 90 ℃ for 30 min; lane 4, G + A sequencing. B. Compound **12b**: lane 5, ICL product formed with **12b** without precipitation; lane 6, ICL product with precipitation (control); lane 7, purified ICL product heated in 1.0 M piperidine at 90 ℃ for 30 min; lane 8, G + A sequencing. C. Compound **12c**: lane 9, ICL product formed with **12c** without precipitation; lane 10, ICL product with precipitation (control); lane 11, purified ICL product heated in 1.0 M piperidine at 90 ℃ for 30 min; lane 12, G + A sequencing.

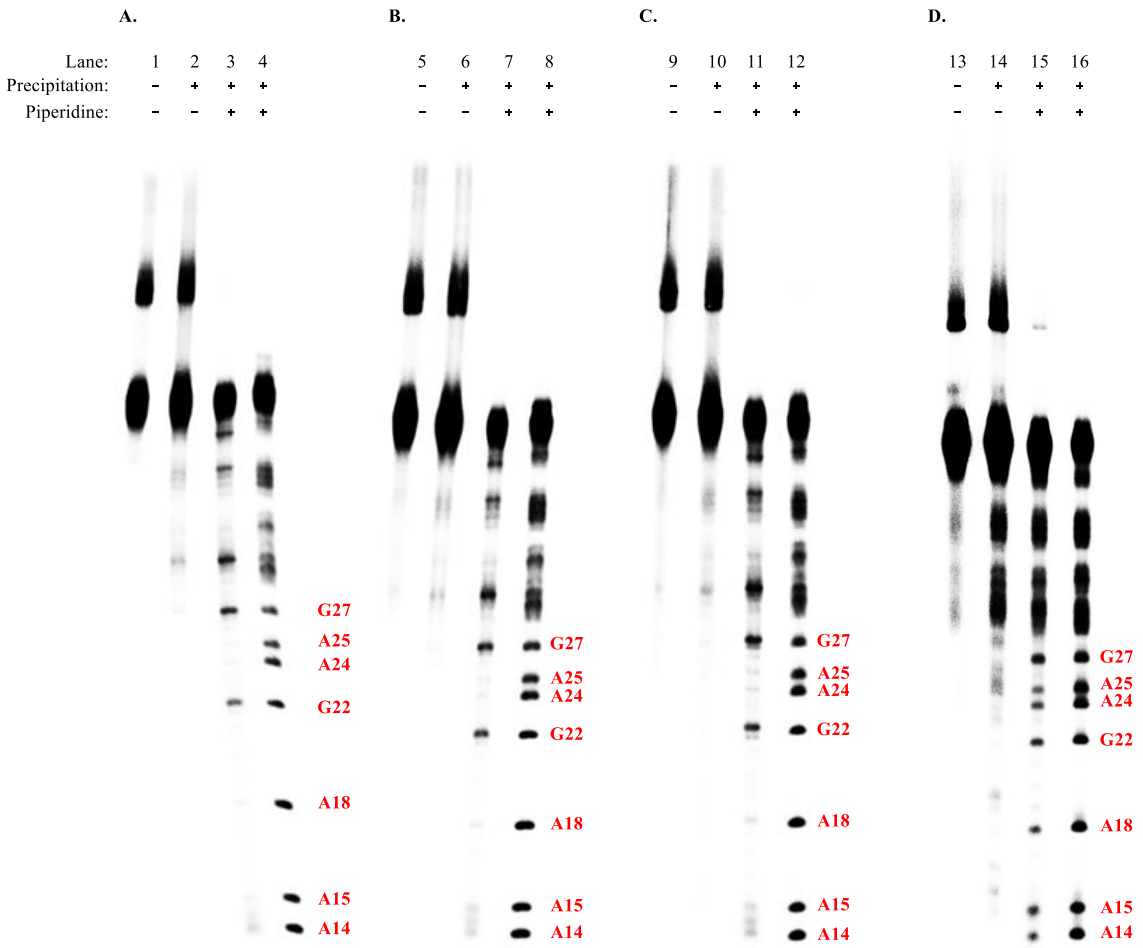

Figure 3-9. Determination of the cross-linking sites of **12d-g** with DNA duplex **5**. Phosphorimage autoradiogram of 20% denaturing PAGE analysis of the DNA ICL products. A. Compound **12d**: lane 1, ICL product formed with **12d** without precipitation; lane 2, ICL product with precipitation (control); lane 3, purified ICL product heated in 1.0 M piperidine at 90 ℃ for 30 min; lane 4, G + A sequencing. B. Compound **12e**: lane 5, ICL product formed with **12e** without precipitation; lane 6, ICL product with precipitation (control); lane 7, purified ICL product heated in 1.0 M piperidine at 90 ℃ for 30 min; lane 8, G + A sequencing. C. Compound **12f**: lane 9, ICL product formed with **12f** without precipitation; lane 10, ICL product with precipitation (control); lane 11, purified ICL product heated in 1.0 M piperidine at 90 ℃ for 30 min; lane 12, G + A sequencing. D. Compound **12g**: lane 13, ICL product formed with **12g** without precipitation; lane 14, ICL product with precipitation (control); lane 15, purified ICL product heated in 1.0 M piperidine at 90 ℃ for 30 min; lane 16, G + A sequencing.

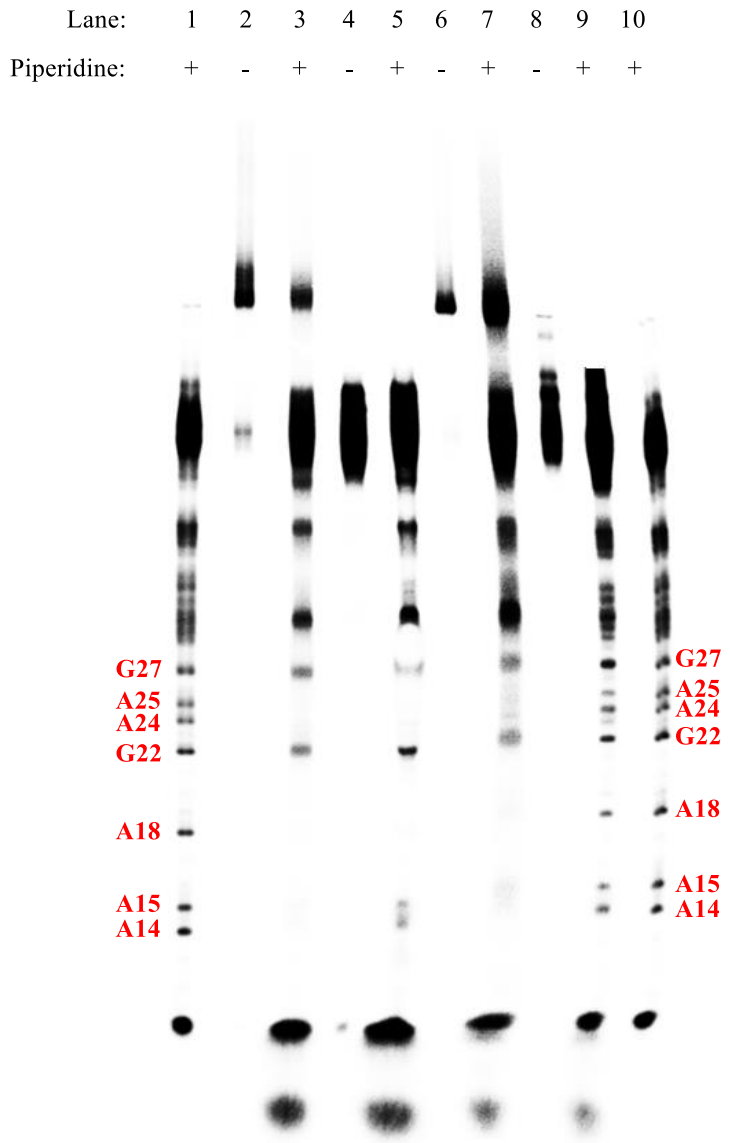

Figure 3-10. Determination of the cross-linking sites of **12d** and **12g** with DNA duplex **5**. Phosphor-image autoradiogram of 20% denaturing PAGE analysis of the DNA interstrand cross-linking products and single-stranded ODN **5a′** isolated from the ICL reaction induced by **12d** and **12g**: lane 1, G + A sequencing; lane 2, DNA interstrand cross-linking products (control) of **12d**; lane 3, DNA interstrand cross-linking products of **12d** heated in 1.0 M piperidine at 90℃ for 30 min; lane 4, single-stranded ODN **5a'** (control) of **12d**; lane 5, single-stranded ODN **5a'** of **12d** heated in 1.0 M piperidine at 90℃ for 30 min; lane 6, DNA interstrand cross-linking products (control) of **12g**; lane 7, DNA interstrand cross-linking products of **12g** heated in 1.0 M piperidine at 90℃ for 30 min; lane 8, single-stranded ODN **5a'** (control) of **12g**; lane 9, single-stranded ODN **5a'** of **12g** heated in 1.0 M piperidine at 90℃ for 30 min; lane 10, G + A sequencing.

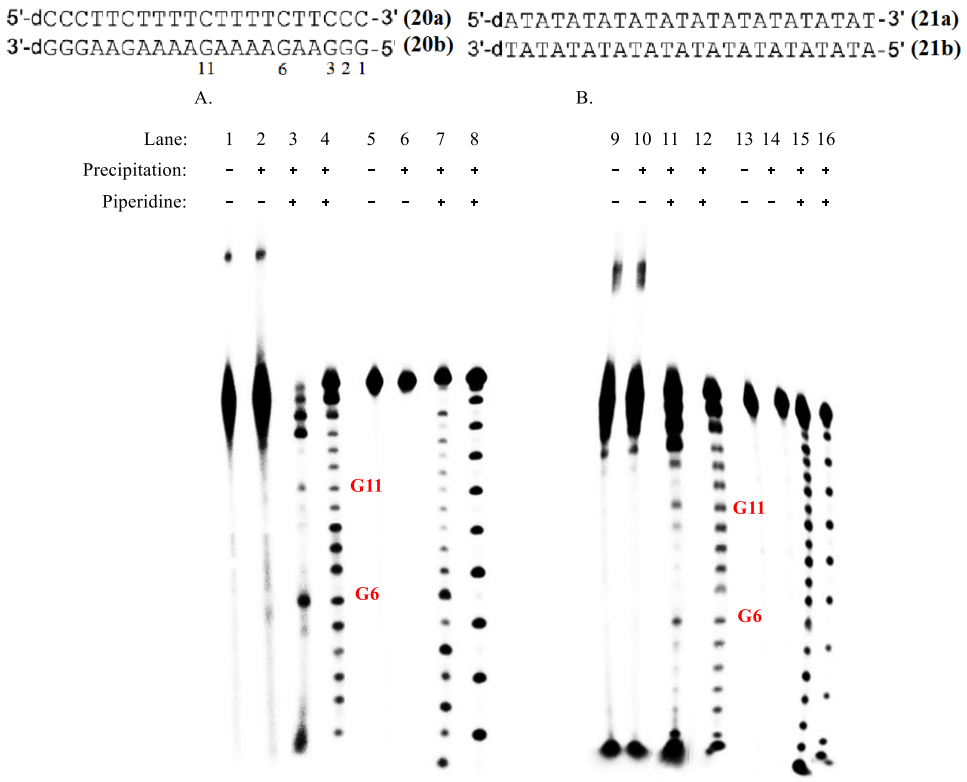

Figure 3-11. DNA sequence effects on ICL reactions induced by **1b** and **1g**. A. The determination of the alkylation sites of **1b** with DNA duplexes **20** and **21**. A mixture of **21** (10 μM) or **21** (10 μM) and **1b** (2.0 mM) in phosphate buffer (pH 8) was irradiated with 350 nm light for 12 h. Lane 1: DNA duplex **20** without treatment; lane 2: DNA duplex **20** with precipitation; lane 3: DNA duplex **20** with precipitation and piperidine treatments; lane 4, G + A sequence of DNA duplex **20**; lane 5, DNA duplex **21** without treatment; lane 6: DNA duplex **21** with precipitation; lane 7: DNA duplex **21** with precipitation and piperidine treatments; lane 8: A sequence of DNA duplex **21**. B: The determination of the alkylation sites of **1g** with DNA duplexes **20** and **21**. A mixture of **20** (10 μM) or **21** (10 μM) and **1g** (0.5 mM) in phosphate buffer (pH 8) was irradiated with 350 nm light for 10 h. Lane 9: DNA duplex **20** without treatment; lane 10: DNA duplex **20** with precipitation; lane 11: DNA duplex **20** with precipitation and piperidine treatments; lane 12, G + A sequence of DNA duplex **20**; lane 13, DNA duplex **21** without treatment; lane 14: DNA duplex **21** with precipitation; lane 15: DNA duplex **21** with precipitation and piperidine treatments; lane 16: A sequence of DNA duplex **21**.

3.2.5. Conclusions

We designed and synthesized seven dibromo-substituted binaphthalene compounds with different leaving groups. The DNA interstrand cross-linking study indicated different leaving groups not only affected the reaction rate but also influence the efficiency of DNA ICL formation. Compounds **12c** and **12e** showed the highest DNA ICL efficiency, indicating that methylamine

and morpholine are good leaving groups to promote the DNA interstrand cross-linking reactions. pH values of the phosphor buffer also have the effect on the DNA ICL formation. The acidic solution (pH = 5) facilitated the cross-linking reaction, but decreased the efficiency of cross-links formation. The photoirradiation in too acidic (pH = 3) solution caused serious DNA cleavage damage. To form DNA interstrand cross-links, these binaphthalene compounds produced carbocations via the oxidation of free radicals, while the reactivity of the carbocations was affected by the leaving groups of the compounds and might influence the ICL formation. The heat stability study of DNA ICL products indicated that the cross-linking reactions mainly occurred at dGs/dCs, and the alkylation at dAs happened in the monoalkylation of the single-stranded DNAs. Different leaving groups on binaphthalenes affected the photoreactivity towards dGs and dAs.

3.3. Experimental Section

General Information

All chemicals and reagents were purchased directly from vendors and used without further purification. For the synthesis and monomer reactions, thin layer chromatography (TLC) was applied to monitor the reactions. The crude synthesis products were purified via column chromatography and confirmed by NMR and HRMS. ^{1}H and ^{13}C NMR spectra were collected on a Bruker DRX 300 or 500 MHz spectrophotometer and HRMS was carried out on a Shimadzu LCMS-IT-TOF mass spectrometer at the University of Wisconsin-Milwaukee Mass Spectrometry Lab. DNA strands (**5**, **10**, **11**) were produced with solid-phase phosphoramidite method and by DNA/RNA ABI synthesizer (Model. 394 from AZCO® BioTech. Inc.) and then deprotected in a mixture of 1: 1 40% aqueous $MeNH_2$ and 28% aqueous NH_3. The DNA strands were further purified by 20% denaturing PAGE and then labeled with [γ-^{32}P] ATP at 5'-ends.

Compound Synthesis and Characterization

(4,4'-dibromo-[1,1'-binaphthalene]-3,3'-diyl)bis(methylene) diacetate (12a). CH_3COOK and $(Bu)_4N^+Br^-$was added in the solution of compound **2b** (0.20 g, 0.34 mmol) in DMF (10 mL) and the solution was heated to 80 ℃ and stirred for 24 h. The reaction was quenched by water (10 mL) and the mixture was extracted with CH_2Cl_2 (20 mL) for 3 times and the organic phase was collected to be washed by brine and dried over Na_2SO_4. Next, the organic phase was concentrated to remove the solvent to obtain compound **12a** as white solid with 96% yield. m.p.℃. ^{1}H NMR (500 MHz, $CDCl_3$): 8.50 (d, *J* = 8.5 Hz, 2H), 7.65 (t, *J* = 7.5 Hz, 2H), 7.55 (s, 2H), 7.41-7.29 (m, 4H), 5.53 (s, 4H), 2.17 (s, 6H). ^{13}C NMR (125 MHz, $CDCl_3$): δ 170.7, 137.4, 133.4, 133.0 132.3, 128.0, 127.8, 127.6, 127.3, 126.8, 123.8, 66.7, 21.0. HRMS (ESI): *m/z* $[M+H]^+$ calcd for $C_{26}H_{21}Br_2O_4^+$: 554.9801, found: 554.9764.

3,3'-bis((benzyloxy)methyl)-4,4'-dibromo-1,1'-binaphthalene (12b). A water solution of LiOH (46 mg, 1.94 mmol) was added dropwise into a solution of compound **12a** (180 mg, 0.32 mmol) in THF (10 mL) and the reaction mixture was stirred at r.t. for 7 hours. The reaction was quenched by water (10 mL) and then filtered by vacuum to obtain white solid **13** which was used directly in the next step. 60% NaH (38 mg, 0.96 mmol was added to a solution of compound **13** in DMF (10 mL) and then $PhCH_2Cl$ (122mg, 0.96 mmol) was added dropwise to the mixed solution at 0 ℃. The reaction mixture was stirred at r.t. for 24 h and then quenched by water (10 mL). The mixture was extracted with EtOAc (20 mL) for three times and the organic phase was collected to be washed by brine and dried over Na_2SO_4. Next, the organic phase was concentrated by vacuum to get crude product which was further purified by column chromatography (Hexane/CH_2Cl_2 = 2/1) over silica gel to obtain compound **12b** as white solid with 69% yield. m.p. ℃ ^{1}H NMR (300 MHz, $CDCl_3$): 8.46 (d, *J* = 8.4 Hz, 4H), 7.70 (s, 2H), 7.62-7.57 (m, 2H), 7.39-7.26 (m, 14H), 4.95 (s,

4H), 3.70 (s, 4H). ^{13}C NMR (75 MHz, $CDCl_3$): δ 137.9, 137.5, 135.5, 133.3, 132.1, 128.4, 128.1, 127.9, 127.7, 127.4, 127.3, 126.9, 126.7, 122.8, 73.0, 72.4.

1,1'-(4,4'-dibromo-[1,1'-binaphthalene]-3,3'-diyl)bis(N-methylmethanamine) (12c). 33 wt % methylamine in ethanol (11.8 mL, 12.6 mmol) was added to a solution of compound **2b** (629 mg, 1.05 mmol) in EtOAc (10 mL) and the reaction mixture was stirred at r.t. over night. The reaction mixture was filtered by vacuum to obtain compound **12c** as white solid with 95% yield. m.p.℃. ^{1}H NMR (300 MHz, CD_3OD): 8.56 (d, *J* = 8.4 Hz, 2H), 7.86 (s, 2H), 7.76 (t, *J* = 7.8 Hz, 2H), 7.52 (t, *J* = 7.5 Hz, 2H), 7.36 (d, *J* = 8.7 Hz, 2H), 4.75 (s, 4H), 2.90 (s, 6H). ^{13}C NMR (75 MHz, CD_3OD): δ 137.6, 133.6, 132.2, 129.5, 128.9, 128.4, 128.2, 127.9, 126.5, 126.0, 52.9, 32.6. HRMS (ESI): *m/z* $[M+2H]^{2+}$ calcd for $C_{24}H_{24}Br_2ON_2^{2+}$: 249.0148, found: 249.0107.

1,1'-(4,4'-dibromo-[1,1'-binaphthalene]-3,3'-diyl)bis(N,N-dimethylmethanamine) (12d). 2.0 M dimetylamine in methanol (6.3 mL, 12.6 mmol) was added to a solution of compound **2b** (629 mg, 1.05 mmol) in EtOAc (10 mL) and the reaction mixture was stirred at r.t. over night. The reaction mixture was filtered by vacuum to obtain compound **12d** as white solid with 92% yield. m.p. ℃. ^{1}H NMR (300 MHz, $CDCl_3$): 8.51-8.46 (m, 2H), 7.65-7.58 (m, 4H), 7.34-7.27 (m, 4H), 3.87 (s, 4H), 2.38 (s, 12H). ^{13}C NMR (75 MHz, $CDCl_3$): δ 137.2, 136.0, 133.2, 132.4, 130.0, 127.7, 127.2, 126.8, 126.5, 124.4, 64.2, 45.7. HRMS (ESI): *m/z* $[M+2H]^{2+}$ calcd for $C_{26}H_{28}Br_2N_2^{2+}$: 263.0304, found: 263.0277.

4,4'-((4,4'-dibromo-[1,1'-binaphthalene]-3,3'-diyl)bis(methylene))dimorpholine (12e).

Morpholine (233 mg, 2.68 mmol) was added to a solution of compound **2b** (400 mg, 0.67 mmol) in EtOAc (10 mL) and the reaction mixture was stirred at r.t. over night. The reaction mixture was filtered by vacuum to obtain compound **12e** as white solid with 92% yield. m.p.℃. ^{1}H NMR (500

MHz, $CDCl_3$): 8.55-8.50 (m, 2H), 7.75-7.70 (m, 2H), 7.63-7.55 (m, 2H), 7.38-7.29 (m, 4H), 3.98 (s, 4H), 3.72 (s, 8H), 2.64 (s, 8H). ^{13}C NMR (125 MHz, $CDCl_3$): δ 133.2, 132.5, 132.5, 132.4, 129.8, 127.8, 127.4, 126.9, 126.8, 126.7, 67.1, 67.0, 63.0, 63.0, 53.7. HRMS (ESI): *m/z* $[M+H]^+$ calcd for $C_{30}H_{31}Br_2N_2O_2^+$: 609.0747, found: 609.0719.

((4,4'-dibromo-[1,1'-binaphthalene]-3,3'-diyl)bis(methylene))bis(phenylsulfane) (12f). PhSH (0.26 mL, 2.51 mmol) and TEA (0.3 mL, 2.16 mmol) was added into a solution of compound **2b** (0.50g, 0.84 mmol) in anhydrous DMF (10 mL) and the reaction mixture was heating to 60 ℃ and stirred for 24 h. The reaction was quenched by water (25 mL) and then extracted with EtOAc (25 mL) for three times. The organic phase was collected to be washed by brine and dried over Na_2SO_4. Next, the organic phase was concentrated by vacuum to get crude product which was further purified by column chromatography (Hexane/CH_2Cl_2 = 10/1) over silica gel to obtain compound **12f** as white solid with 86% yield. m.p.℃ ^1H NMR (500 MHz, $CDCl_3$): 8.51-8.41 (m, 2H), 7.72-7.06 (m, 18H), 4.56-4.46 (m, 4H). ^{13}C NMR (125 MHz, $CDCl_3$): δ 137.5, 137.5, 136.9, 135.8, 135.3, 135.3, 135.2, 134.8, 133.1, 132.9, 132.9, 132.6, 132.5, 131.5, 131.5, 130.5, 129.8, 129.8, 129.0, 129.0, 128.5, 128.0, 127.8, 127.6, 127.2, 127.1, 127.0, 126.8, 126.1, 124.8, 124.7, 124.6, 41.2, 40.8.

((4,4'-dibromo-[1,1'-binaphthalene]-3,3'-diyl)bis(methylene))bis(phenylselane) (12g).

Diphenyl diselenide (0.62 g, 2 mmol) and sodium borohydride (0.15 g, 4 mmol) were dissolved in anhydrous DMF (5 mL) and the mixture was stirred at r.t. for 10 min under nitrogen. A solution of compound **2b** (0.50 g, 1 mmol) in DMF (10 mL) was added dropwise by syringe in the mixture which was further stirred at r.t. over night. The reaction mixture was quenched by water (20 mL) and then extracted with EtOAc (25 mL) for three times. The organic phase was collected to be washed by brine and dried over Na_2SO_4. Next, organic phase was concentrated by vacuum to get

crude product which was further purified by column chromatography (Hexane/CH_2Cl_2 = 20/1) over silica gel to obtain compound **12g** as white solid with 83% yield. m.p. ℃ ^{1}H NMR (500 MHz, $CDCl_3$): 8.46 (d, *J* = 8.5 Hz, 2H), 7.61 (t, *J* = 7.5 Hz, 2H), 7.55 (d, *J* = 7.0 Hz, 4H), 7.32 (t, *J* = 7.0 Hz, 2H), 7.25-7.18 (m, 8H), 7.03 (s, 2H), 4.50 (q, *J* = 11.5 Hz, 4H). ^{13}C NMR (125 MHz, $CDCl_3$): δ 136.8, 136.3, 135.0, 132.6, 132.6, 129.8, 129.4, 129.1, 128.0, 127.7, 127.6, 126.8, 126.6, 124.3, 34.2.

DNA ICL Formation. In a potassium phosphate buffer (pH 8, 100 mM), the ^{32}P-labeled ODN (0.5 μM) was hybridized with the complementary strand (1.5 equiv) by heating at 90 °C for 5 min and cooling to rt naturally. Then, 100 mM potassium phosphate buffer (pH 8, 2 μL), 1 M NaCl (2 μL), and certain concentrations of **12a**−**12g** in CH_3CN (6 μL) were added to the ^{32}P-labeled ODN duplex (2 μL, 0.5 μM). Autoclaved water was added to give a final volume of 20 μL (final concentration range: 0.01−2.0 mM). The reaction mixture was irradiated with 350 nm light, then quenched with an equal volume of 90% formamide loading buffer, and subjected to 20% denaturing PAGE.

Free Radical Trapping Assay of DNA ICL Formation. A solution of TEMPO in CH_3CN (5/2 to 4000/2 mM, 2 μL) was added to a reaction mixture containing 2 μL of ^{32}P-labeled ODN duplex (0.5 μM), 2 μL of NaCl (1 M), 2 μL of pH 8 potassium phosphate (100 mM), 4 μL of **12a**−**12g** in CH_3CN with optimal concentrations, and 8 μL of autoclaved distilled water to give a total volume of 20 μL (final TEMPO concentration: 0.25−200 mM). The reaction mixture was irradiated with 350 nm light for the desired time, quenched with 20 μL of 90% formamide loading buffer, and subjected to 20% denaturing PAGE.

Carbocation Trapping Assay of DNA ICL Formation. A solution of $MeONH_2$·HCl (2 M) was titrated with NaOH (5 M) to pH 7.0, which was diluted to the desired concentration (5/2 to 4000/

2 mM). The resulting $MeONH_2 \cdot HCl$ solution (2 μL) with desired concentration was added to a mixture containing 2 μL of ^{32}P-labeled ODN duplex (0.5 μM), 2 μL of NaCl (1 M), and 2 μL of pH 8 potassium phosphate (100 mM). Then, 6 μL of **12a**−**12g** in CH_3CN with optimal concentrations and 6 μL of autoclaved distilled water were added to give a total volume of 20 μL (final $MeONH_2$ concentration: 0.25−200 mM). After irradiation with 350 nm light for the desired time, the reaction mixture was quenched with 20 μL of 90% formamide loading buffer, then subjected to 20% denaturing PAGE.

Determination of Alkylation Sites by Studying the Heat Stability of DNA ICL Products Formed with 12a−12g. A solution containing 60 μL of ^{32}P-labeled ODN duplex **5** (0.5 μM), 12 μL of NaCl (1 M), 12 μL of pH 8 potassium phosphate (100 mM), and 36 μL of **12a**−**12g** in CH_3CN (optimal concentrations) was irradiated with 350 nm light for optimal times. Then, the reaction mixture (120 μL) was coprecipitated with 40 μL of calf thymus DNA (25 μg/mL) in the presence of 20 μL of NaOAc (3 M) and 540 μL of ethanol at −80 °C for 30 min and centrifuged at 15000 rpm for 5 min by Eppendorf centrifuge. The supernatant was removed. The pellet was dissolved in 60 μL of autoclaved distilled water, precipitated with 10 μL of NaOAc (3 M) and 240 μL of ethanol at −80 °C for 30 min again, and centrifuged for 5 min at 15000 rpm. After removal of the supernatant, the pellet was lyophilized, dissolved in 25 μL of autoclaved distilled water, and aliquoted to two parts. One portion (20 μL) of the precipitated ODN adducts was incubated with 10 M piperidine (10 μL) and autoclaved distilled water (70 μL) at 90 °C for 30 min. The second portion (5 μL) was used as a control sample. Finally, two samples were dissolved in the mixture of 90% formamide loading buffer and H_2O (1:1) and subjected to 20% denaturing PAGE analysis.

Heat Stability Study of the Isolated DNA Cross-Linking Products Formed with 12d and 12g for the Determination of Alkylation Sites. A solution containing 0.5 μM ^{32}P-labeled ODN

duplex **5** (60 μL), 1 M NaCl (12 μL), 100 mM pH 8 potassium phosphate (12 μL), and 5/3 mM **12d** or **12g** in CH_3CN (36 μL) was irradiated at 350 nm for optimal times (**12d**: 8 h, **12g**: 10 h). The alkylated ODNs were purified by 20% denaturing PAGE following standard procedures. The gel band containing cross-linked products or single-stranded ODNs was cut, crushed, extracted with a mixture of NaCl (200 mM) and EDTA (20 mM) (2.0 mL), and further purified on a C18 column (1 cc, 100 mg) eluting with H_2O (3 × 1.0 mL), followed by MeOH/H_2O (3/2, 1.0 mL). The isolated ICL products and single-stranded ODNs were lyophilized by a Centrivap concentrator of LABCONCO. The isolated ICL products were dissolved in 25 μL of autoclaved distilled H_2O and aliquoted into two parts (20, 5 μL). One portion (20 μL) of the isolated ODNs was incubated with 10 M piperidine (10 μL) and autoclaved distilled water (70 μL) at 90 °C for 30 min. The second portion (5 μL) was used as a control sample. Single-stranded ODNs were studied in the same way. Solvent of all samples was removed by vacuum, dissoved in the mixture of 90% formamide loading buffer and H_2O (1:1), and subjected to 20% denaturing PAGE analysis.

3.4. References

(1) Fan, H.; Peng, X. Novel DNA Cross-Linking Reagents. *In Advances in Molecular Toxicology*; Fishbein, J. C.; Heilman, J. M., Eds.; Elsevier, 2016; Vol. *10*, pp 235−292.

(2) Weng, L.; Horvat, S. M.; Schiesser, C. H.; Greenberg, M. M. Deconvoluting the reactivity of two intermediates formed from modified pyrimidines. *Org. Lett.* **2013**, 15, 3618−3621.

(3) Lin, G.; Li, L. Oxidation and reduction of the 5-(2′-deoxyuridinyl)methyl radical. *Angew. Chem., Int. Ed.* **2013**, 52, 5594−5598.

(4) Wang, Y. B.; Lin, Z. C.; Fan, H. L.; Peng, X. H. Photoinduced DNA Interstrand Cross-Link Formation by Naphthalene Boronates via a Carbocation. *Chem. - Eur. J.* **2016**, 22, 10382−10386.

(5) Lin, Z.; Fan, H.; Zhang, Q.; Peng, X. Design, Synthesis, and Characterization of Binaphthalene Precursors as Photoactivated DNA Interstrand Cross-Linkers. *J. Org. Chem.* **2018**, 83, 8815−8826.

(6) Zhang, Q.; Lin, Z.; Peng, X. "Photoreactivity of Binaphthalene Triphenylphosphonium Salts: DNA Interstrand Cross-link Formation and Substiutent Effects". *Chemical Research in Toxicology.* Accepted on March 14th, **2022**.

(7) Han, Y.; Chen, W.; Kuang, Y.; Sun, H.; Wang, Z.; Peng, X. UV-Induced DNA Interstrand Cross-Linking and Direct Strand Breaks from a New Type of Binitroimidazole Analogue. *Chem. Res. Toxicol.* **2015**, 28, 919−926.

(8) Fan, H.; Sun, H.; Peng, X. Substituents Have a Large Effect on Photochemical Generation of Benzyl Cations and DNA Cross-Linking. *Chem. - Eur. J.* **2018**, 24, 7671−7682.

(9) Wang, Y.; Liu, S.; Lin, Z.; Fan, Y.; Wang, Y.; Peng, X. Photochemical Generation of Benzyl Cations That Selectively Cross-Link Guanine and Cytosine in DNA. *Org. Lett.* **2016**, 18, 2544−2547.

(10) Fan, H.; Sun, H.; Zhang, Q.; Peng, X. Photoinduced DNA Interstrand Cross-Linking by 1,1′-Biphenyl Analogues: Substituents and Leaving Groups Combine to Determine the Efficiency of Cross-Linker. *Chem. - Eur. J.* **2021**, 27, 5215−5224.

(11) Fan, H.; Peng, X. Photoinduced DNA Interstrand Cross-Linking by Benzene Derivatives: Leaving Groups Determine the Efficiency of the Cross-Linker. *J. Org. Chem.* **2021**, 86, 493−506.

(12) Makar, S.; Saha, T.; Singh, S.K. Naphthalene, a Versatile Platform in Medicinal Chemistry: Sky-High Perspective. *Eur. J. Med. Chem.* **2019**, 161, 252-276.

(13) Richter, S. N.; Maggi, S.; Mels, S. C.; Palumbo, M.; Freccero, M. Binol quinone methides as bisalkylating and DNA cross-linking agents. *J. Am. Chem. Soc.* **2004**, 126, 13973−13979.

(14) Verga, D.; Nadai, M.; Doria, F.; Percivalle, C.; Di Antonio, M.; Palumbo, M.; Richter, S. N.; Freccero, M. Photogeneration and reactivity of naphthoquinone methides as purine selective DNA alkylating agents. *J. Am. Chem. Soc.* **2010**, 132, 14625−14637.

(15) Dizdaroglu, M.; Jaruga, P.; Birincioglu, M.; Rodriguez, H. Free Radical-Induced Damage to DNA: Mechanisms and Measurement. *Free Radic Bio Med.* **2002**, 32, 1102-1115.

(16) Gates, K. S. An Overview of Chemical Processes that Damage Cellular DNA: Spotaneous Hydrolysis, Alkylation, and Reactions with Radicals. *Chem. Res. Toxicol.* **2009**, 22, 1747-1760.

3.5. Appendices A: Gel Electrophoresis

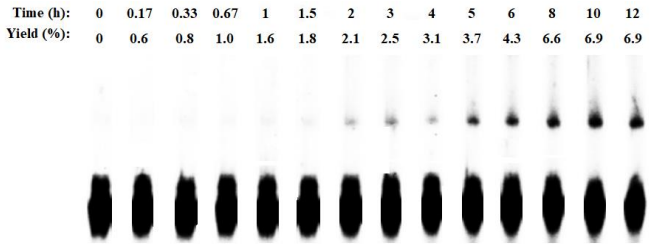

Figure 3-12. Representative gel of time-dependent DNA ICL formation of duplex for **12a** (500 μM) upon 350 nm irradiation at time points.

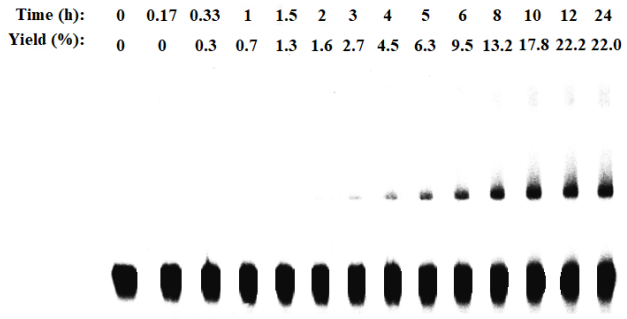

Figure 3-13. Representative gel of time-dependent DNA ICL formation of duplex for **12b** (500 μM) upon 350 nm irradiation at time points.

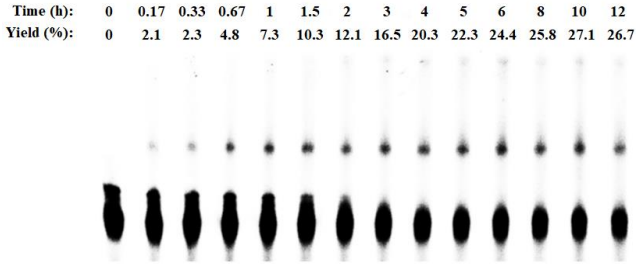

Figure 3-14. Representative gel of time-dependent DNA ICL formation of duplex for **12c** (500 μM) upon 350 nm irradiation at time points.

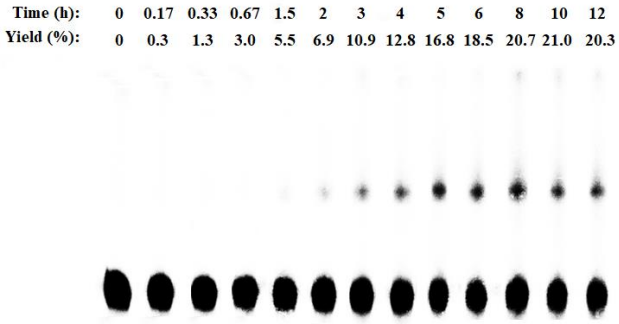

Figure 3-15. Representative gel of time-dependent DNA ICL formation of duplex for **12d** (500 μM) upon 350 nm irradiation at time points.

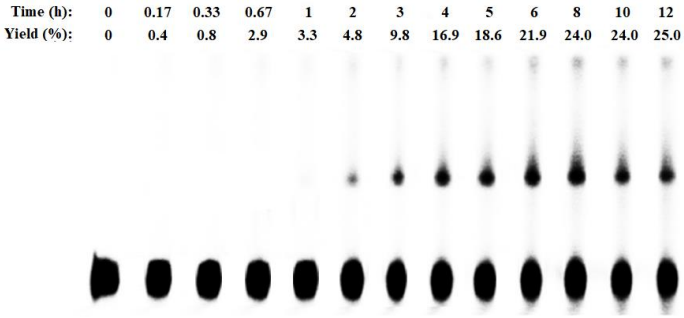

Figure 3-16. Representative gel of time-dependent DNA ICL formation of duplex for **12e** (500 μM) upon 350 nm irradiation at time points.

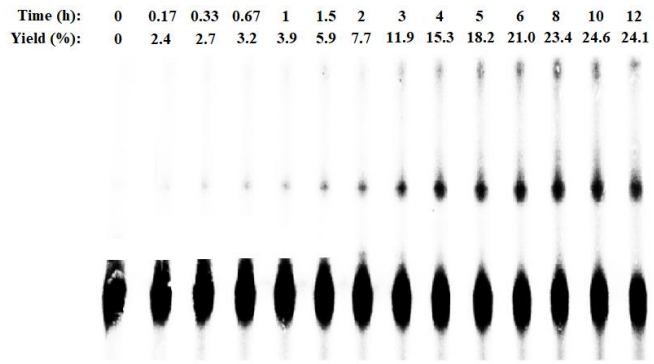

Figure 3-17. Representative gel of time-dependent DNA ICL formation of duplex for **12f** (500 μM) upon 350 nm irradiation at time points.

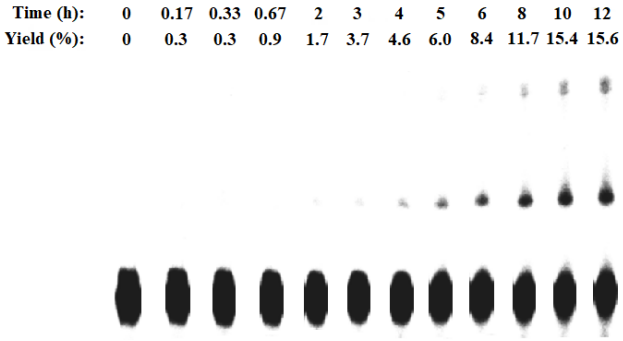

Figure 3-18. Representative gel of time-dependent DNA ICL formation of duplex for **12e** (500 μM) upon 350 nm irradiation at time points.

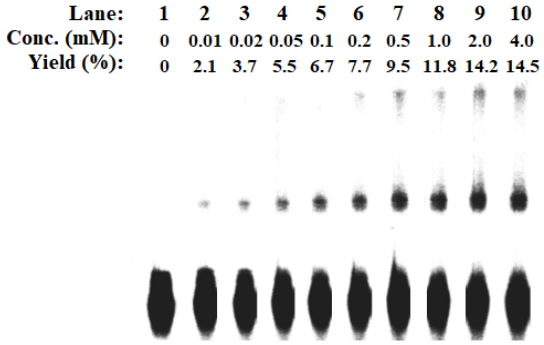

Figure 3-19. The concentration dependence of ICL formation for **12a** upon photoirradiation. Phosphor image autoradiogram of 20% denaturing PAGE analysis of **12a** under varying concentration. Reaction mixtures were photo-irradiated under UV (350 nm) for 10 h.

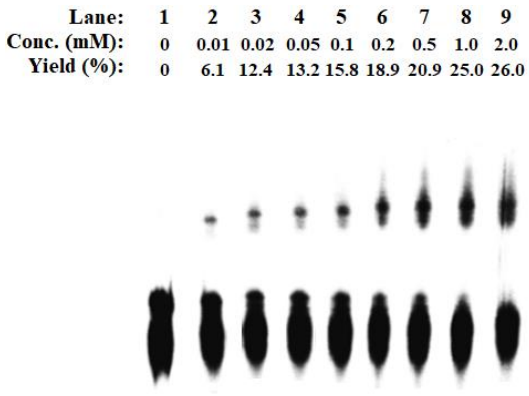

Figure 3-20. The concentration dependence of ICL formation for **12b** upon photoirradiation. Phosphor image autoradiogram of 20% denaturing PAGE analysis of **12b** under varying concentration. Reaction mixtures were photo-irradiated under UV (350 nm) for 12 h.

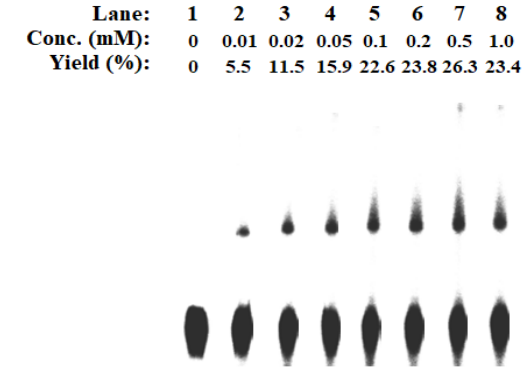

Figure 3-21. The concentration dependence of ICL formation for **12c** upon photoirradiation. Phosphor image autoradiogram of 20% denaturing PAGE analysis of **12c** under varying concentration. Reaction mixtures were photo-irradiated under UV (350 nm) for 8 h.

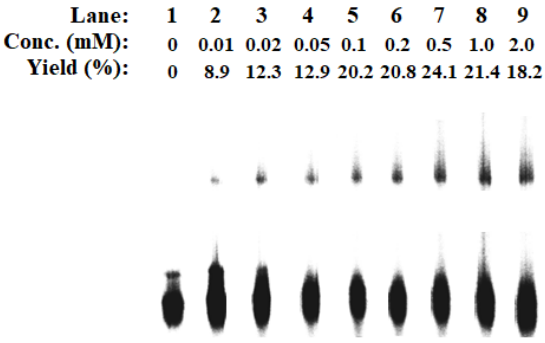

Figure 3-22. The concentration dependence of ICL formation for 12d upon photoirradiation. Phosphor image autoradiogram of 20% denaturing PAGE analysis of 12d under varying concentration. Reaction mixtures were photo-irradiated under UV (350 nm) for 8 h.

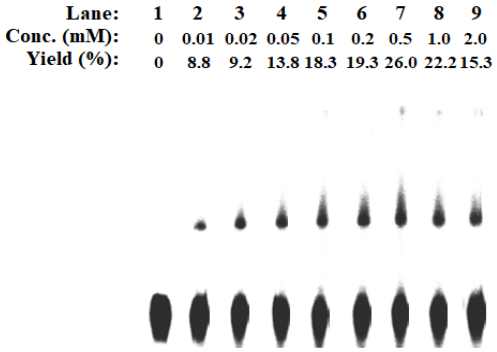

Figure 3-23. The concentration dependence of ICL formation for **12e** upon photoirradiation. Phosphor image autoradiogram of 20% denaturing PAGE analysis of **12e** under varying concentration. Reaction mixtures were photo-irradiated under UV (350 nm) for 8 h.

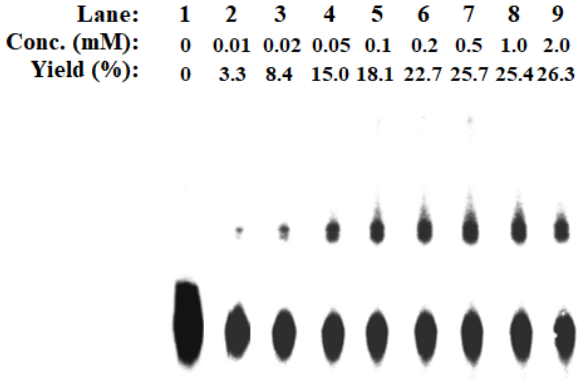

Figure 3-24. The concentration dependence of ICL formation for **12f** upon photoirradiation. Phosphor image autoradiogram of 20% denaturing PAGE analysis of **12f** under varying concentration. Reaction mixtures were photo-irradiated under UV (350 nm) for 8 h.

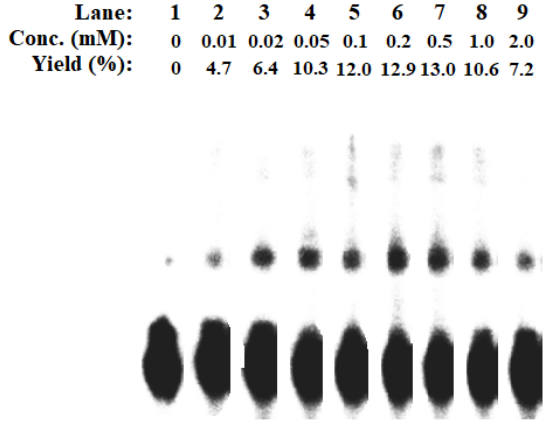

Figure 3-25. The concentration dependence of ICL formation for **12g** upon photoirradiation. Phosphor image autoradiogram of 20% denaturing PAGE analysis of **12g** under varying concentration. Reaction mixtures were photo-irradiated under UV (350 nm) for 10 h.

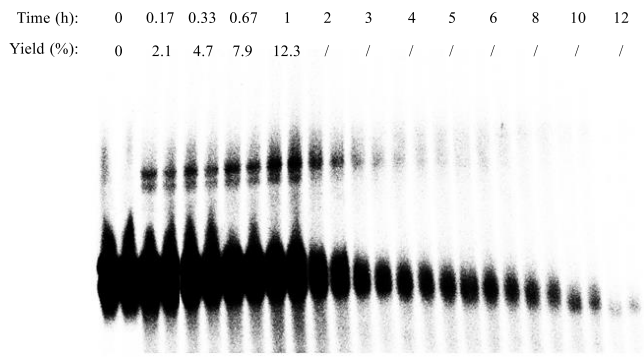

Figure 3-26. Representative gel of time-dependent DNA ICL formation of duplex **5** for **12c** (500 μM) in pH = 5 phosphor buffer upon 350 nm irradiation at time points.

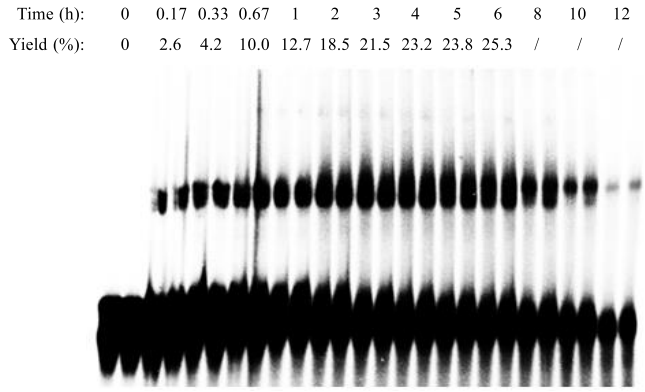

Figure 3-27. Representative gel of time-dependent DNA ICL formation of duplex **5** for **12d** (500 μM) in pH = 5 phosphor buffer upon 350 nm irradiation at time points.

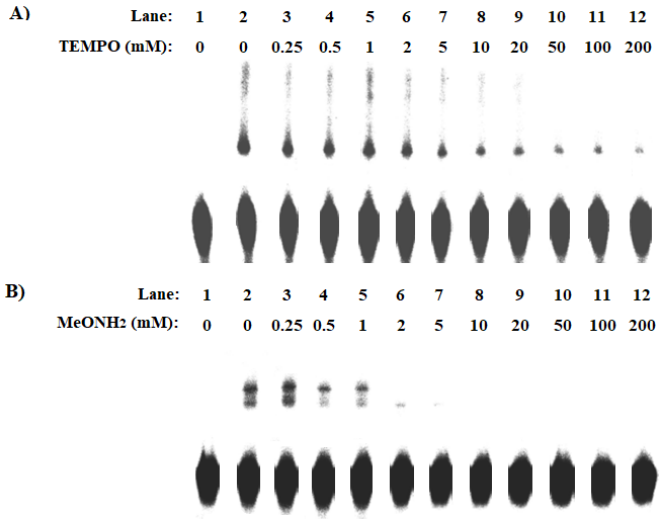

Figure 3-28. The effect of TEMPO and methoxyamine on DNA ICL formation of duplex **5** for **12a**. A mixture of **5** (50 nM) and **12a** (0.5 mM) in a pH 8 phosphate buffer was irradiated with 350 nm light for 10 h in the presence of varying concentration of $MeONH_2$ (**A**) or TEMPO (**B**).

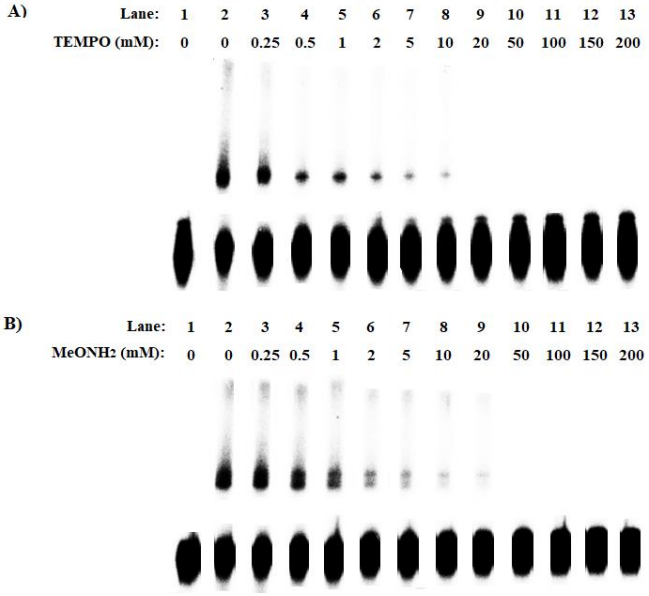

Figure 3-29. The effect of TEMPO and methoxyamine on DNA ICL formation of duplex **5** for **12b.** A mixture of **5** (50 nM) and **12b** (1.0 mM) in a pH 8 phosphate buffer was irradiated with 350 nm light for 12 h in the presence of varying concentration of $MeONH_2$ (**A**) or TEMPO (**B**).

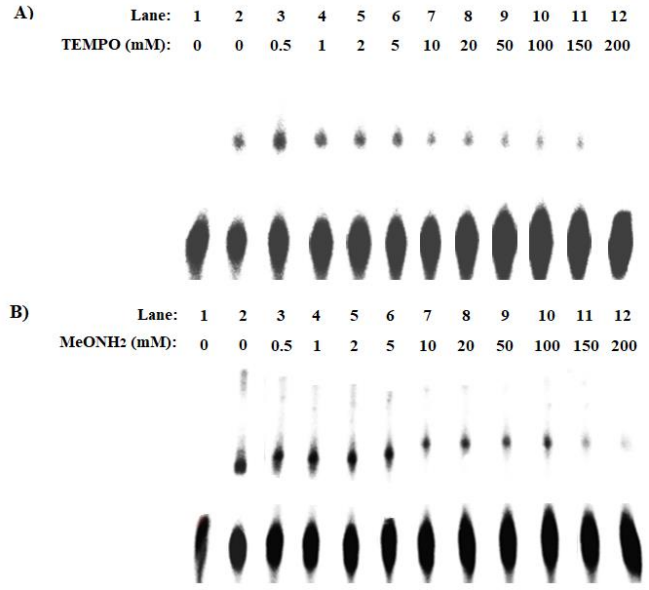

Figure 3-30. The effect of TEMPO and methoxyamine on DNA ICL formation of duplex **5** for **12c.** A mixture of **5** (50 nM) and **12c** (0.5 mM) in a pH 8 phosphate buffer was irradiated with 350 nm light for 8 h in the presence of varying concentration of $MeONH_2$ (**A**) or TEMPO (**B**).

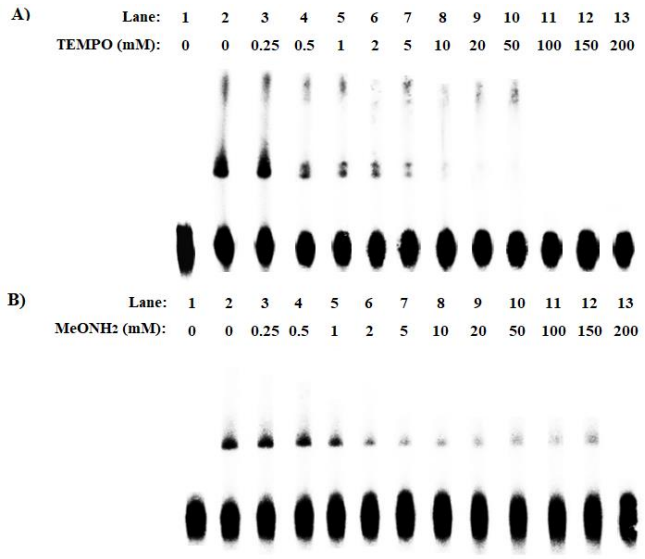

Figure 3-31. The effect of TEMPO and methoxyamine on DNA ICL formation of duplex **5** for **12d**. A mixture of **5** (50 nM) and **12d** (0.5 mM) in a pH 8 phosphate buffer was irradiated with 350 nm light for 8 h in the presence of varying concentration of $MeONH_2$ (**A**) or TEMPO (**B**).

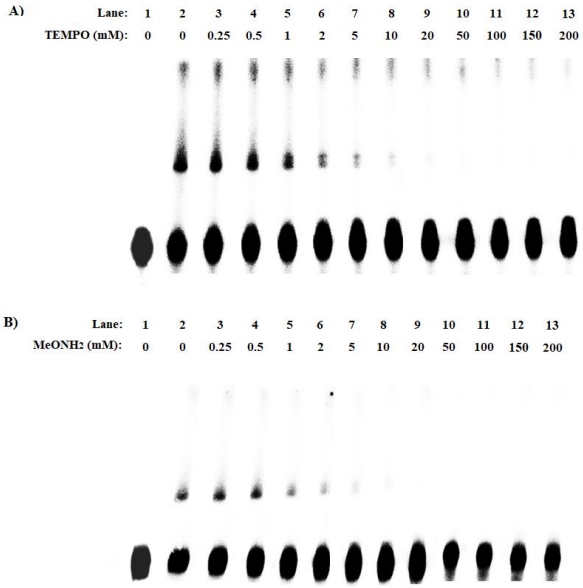

Figure 3-32. The effect of TEMPO and methoxyamine on DNA ICL formation of duplex **5** for **12e**. A mixture of **5** (50 nM) and **12e** (0.5 mM) in a pH 8 phosphate buffer was irradiated with 350 nm light for 8 h in the presence of varying concentration of $MeONH_2$ (**A**) or TEMPO (**B**).

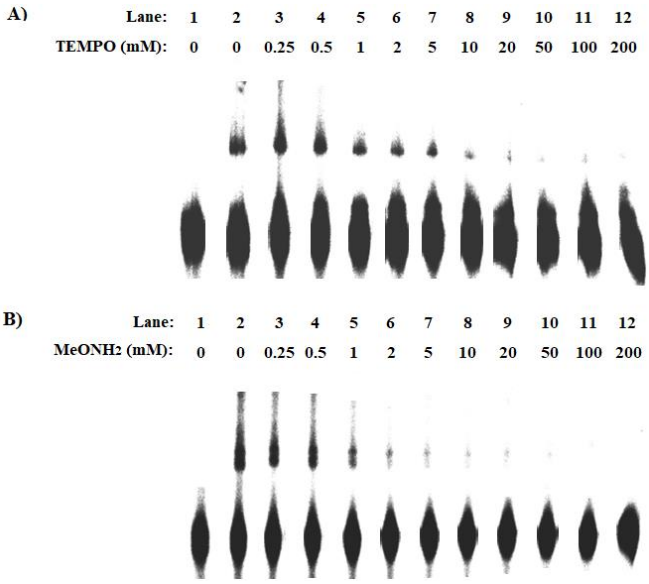

Figure 3-33. The effect of TEMPO and methoxyamine on DNA ICL formation of duplex **5** for **12f**. A mixture of **5** (50 nM) and **12f** (0.5 mM) in a pH 8 phosphate buffer was irradiated with 350 nm light for 8 h in the presence of varying concentration of $MeONH_2$ (**A**) or TEMPO (**B**).

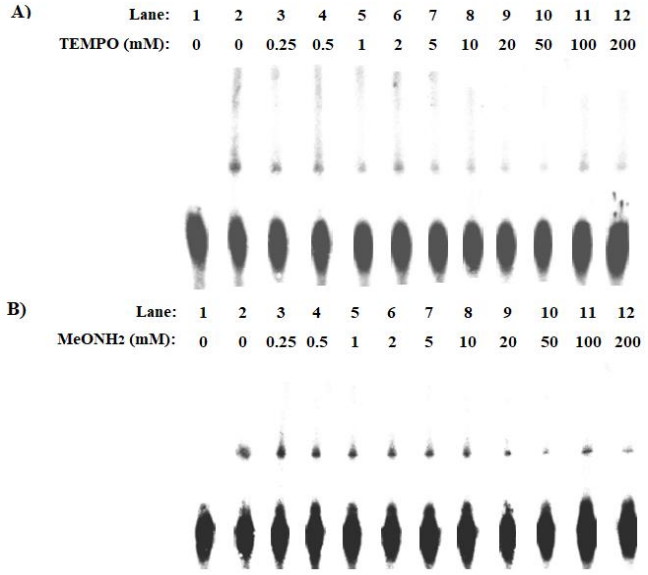

Figure 3-34. The effect of TEMPO and methoxyamine on DNA ICL formation of duplex **5** for **12g**. A mixture of **5** (50 nM) and **12g** (0.5 mM) in a pH 8 phosphate buffer was irradiated with 350 nm light for 10 h in the presence of varying concentration of $MeONH_2$ (**A**) or TEMPO (**B**).

Chapter 4 Substituents and Leaving Groups on Binaphthalene Analogues Combine to Affect the DNA Interstrand Cross-Link Formation

4.1 Introduction

DNA cross-linking is a cytotoxic process of the formation of covalent linkage between two nucleotides, preventing DNA replication and transcription as well as triggering cell death. The formation of covalent bond can be induced by various agents which can be divided into four categories, including inherently reactive agents, oxidatively activated or reductively activated agents and photoactivated cross-linking agents.[1,2] Photoactivated cross-linking agents has attracted a great attention due to its high selectively, high biorthogonal and less toxicity. They have been used in many applications, such as preventing tumor growth and cancer spread, studying DNA damage and repair, photo-manipulating DNA and modulating gene information.[3] Coumarin moieties,[4.5] *p*-stibazole,[6] 3-cy-anovinycarbazole,[7,8,9] BINOL derivatives,[10] phenol, biphenol[11] and many other compounds have been developed and characterized as efficient photoactivated DNA cross-linking agents. These compounds are photoactivated upon lights with various wavelengths and covalently bond to nucleobases through [2+2] cycloaddition, quinone methide (QM) formation or carbocation formation. Coumarin moieties and 3-cy-anovinycarbazole produce cyclobutene structure with dC, dT or dA[4,5,7,8,9] while photocycloaddition reaction can occur between two *p*-stilbazole moieties which have been introduced in base-pairing positions of complementary DNA strands.[6] BINOL derivatives, phenol and biphenol photoinduc DNA interstrand cross-linking via the formation of QM which are strong electrophiles and are highly reactive with nucleobases.[10,11] Carbocation formation was first discovered by Li and Greenberg research groups in 2013 when they studied the interstrand cross-linking mechanism of modified thymidines toward DNA.[12,13] Next, Peng research group developed more compounds which generate carbocations to induce

DNA interstrand cross-link (ICL) formation, including benzene analogues,[14,15,16,17] bisnitroimidazole compounds[18] and binaphthalene analogues.[19,20,21] It was further figured out that the carbocation can be generated via heterolysis of C-L bond (L = leaving group) or homolysis of C-L bond, which depends on the substituents and leaving groups on the substrates. For example, aryl boronate bromides produced benzyl cations via homolysis of C-Br bond while aryl boronate trimethyl ammonium salts generated cations via the heterolysis of C-N bond.[15] In addition, phenyl trimethyl ammonium salts with nitro substituent only involved carbocations in the DNA ICL formation, whereas the pathway of carbocation formation of the salts with bromo substituent might be affected by the various concentrations of TEMPO.[14] In addition, the different substituents and leaving groups on the benzene analogues also affect the DNA ICL formation and photoreactivity towards DNA.[14,16,17,21] This inspires us to develop more binapthalene compounds with various substituents and leaving groups and investigate their effects on photoreactivity, DNA ICL formation as well as the carbocation formation.

4.2 Chloro-, Bromo- and Methoxy-Substituted Binapthalene Precusors with -OR Leaving Groups Efficiently Induce DNA Interstrand Cross-Linking

4.2.1 Synthesis of Compounds.

We have designed and synthesized ten binaphthalene analogues with oxygen-containing leaving groups, including acetoxy (-OAc) (**23a**, **24a**), benzyloxy (-C_7H_7O) (**23b**, **24b**), allyloxy (-C_3H_5O) **(22a, 23c, 24c)** or methoxy (-OCH_3) (**22b**, **23d**, **24d**). These binaphthalene compounds also contain different aromatic substituents at the position-4, such as bromo (-Br) (**22a, b**), chloro (-Cl) (**24a-d)**, or methoxy (-CH_3) (**23a-d)**. Compounds **22a** and **22b** were synthesized starting from 4-

bromo substituted binaphthalene **12a** that was prepared as shown in Chapter 3. Compound **12a** was hydrolyzed to **13** by treatment with lithium hydroxide (LiOH) in THF, followed by Williamson ether synthesis leading to the formation of **22a** with 71% yield and **22b** with 63% yield (Scheme 4.1A). The naphthoic acid **23** served as the starting material for **23a-d.** First, **23** was converted to methyl 1-methoxy-2-naphthoate (**26**) by treatment with $(CH_3)_2SO_4$. Coupling reaction of **26** using lead (IV) acetate as catalyst produced binapthalene compound **27** that was reduced to hydroxyl analogue **28** using $LiAlH_4$. Finally, **28** was converted to **23a-d** by treatment with different halides, including acetyl chloride (→**23a**), benzyl chloride (→**23b**), allyl iodide (→**23c**), and methyl iodide (→**23d**) (Scheme 4.1B). Compounds **24a-d** were synthesized starting with **2a** that was described (Scheme 4.1C)[21]. Compound **2a** was first converted to **24a** with an acetate as leaving group by heating in acetonitrile (CH_3CN) with refluxing in the presence of potassium acetate. In order to synthesize **24b-d**, **24a** was hydrolyzed with LiOH to form **29** that was converted to **24b**, **24c** and **24d** via Williamson ether synthesis by treatment with sodium hydride (NaH) in DMF, followed by different halides, such as benzyl chloride (→**24b**), allyl iodide (→**24c**) or iodomethane (→**24d**). All new compounds were confirmed by NMR and HRMS.

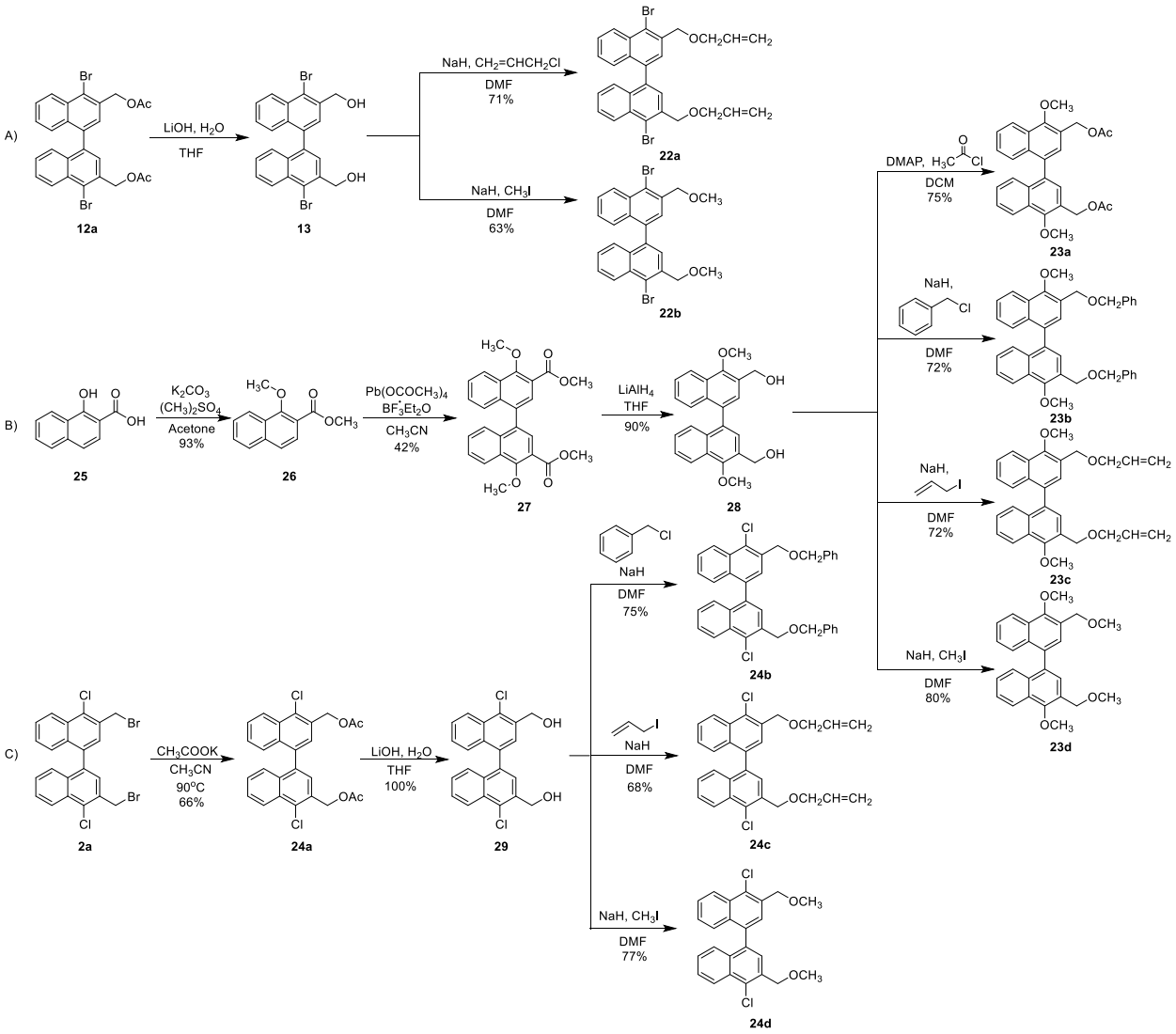

Figure 4-1. Synthesis of Compounds **22a**, **b** (A), **23a-d** (B) and **24a-d** (C).

4.2.2 DNA Cross-Linking Assay

The photoreactivity of **22a**, **b**, **23a-d**, and **23a-d** towards DNA were investigated with DNA duplex **5** in a pH 8 phosphoate buffer upon 350 nm irradiation with Model RPR-100 Rayonet® irradiator. The DNA cross-linking yields were determined by denaturing PAGE with phosphorimager (Image Quant 5.2). The optimal irradiation times of these compounds were first determined by the highest

cross-linking yield with shortest irradiation time. Compounds **22a**, **b** and **24c** were studied with 0.5 mM, **23a**, **b** were investigated with 1.0 mM and **21a**, **b**, **d** were in 0.2 mM (Table 4.1; Figure 4.1). The irradiation time of **22a**, **b** and **23a** to obtain the optimal DNA ICL yields was 8 h and it was 10 h for **23b-d**. However, the reaction required more than 20 h for **24a-d** which have chloro substituent. The photoirradiation of these binaphthalene compounds with DNA followed the first-order kinetics and the rate constant (k) was calculated. For **22a**, **b** and **23a**, the values of k were higher than 0.75 $\times 10^{-5}$ S^{-1} and they were less than 0.6 $\times 10^{-5}$ S^{-1} for **23b-d**. For **24a-d,** the k values were even lower due to the much longer irradiation time. The results showed that compounds with bromo substituent had the faster reactions than most compounds with methoxy or chloro substituent.

Next, the UV absorption of **22a**, **b**, **23a-d** were investigated to figure out if there is any correlation between UV absorption and photo-reactivity (Table 4.1). These compounds were dissolved in $CHCl_3$ and measured with 0.2 mM except **23a** which was 1.0 mM (Figure 4.2). The wavelength of maximum absorption was 299 nm with bromo-substituted compounds (**22a**, **b**). The values of ε_{max} were 297 nm for **23a**, **b** and **d** and the value for **23c** was only 294 nm. Compounds with bromo substituent have shorter irradiation times and showed a maximum UV absorption closer to the irradiation wavelength (350 nm). It indicated that there is a correlation between UV absorption and photo-reactivity. The compounds with the closer wavelength at maximum absorption to 350 nm performed a shorter irradiation time which indicated a higher photo-reactivity. The molar extinction coefficients of these compounds (ε) were also calculated based on Beer-Lambert Law. **22a** has the largest coefficient (21525 $M^{-1}cm^{-1}$) and **23a** has the smallest one which was only 1885 $M^{-1}cm^{-1}$. Compound with electron-withdrawing group (-Br) as substituent showed higher UV absorption and larger coefficients than the compound with electron-donating group ($-OCH_3$) (**22a**

vs. **23c**; **22b** vs. **23d**). It indicated that electron-withdrawing group can promote the UV absorption while the electron-donating group can suppress the UV absorption. The different coefficients of **23a-d** which have different leaving groups indicated the leaving groups also influenced the UV absorption of these compound.

With the optimal irradiation times, the concentration-dependent study was performed to investigate the efficiency of DNA interestrand cross-linking (ICL) formation (Table 4-1; Figure 4-3). Among them, **23d** obtained the highest cross-linking yield which was 39% at 0.25 mM. **22b** and **22a** obtained ~27% yields at 0.5 mM and 0.4 mM, respectively. **22a**, **23c** and **24a** showed more than 20% DNA ICL formation efficiency while **23b** only received 18.4% yield which was the least among these six compounds. There is a huge discrepancy of the minimum concentrations to achieve the highest DNA ICL yield between **22a** and **23c** despite of the same leaving group. Although the ICL yield has only around 3% difference, the minimum concentration of **22a** was 10 times less than **23c** with two-hour less irradiation (0.15 mM vs 1.5 mM), indicating that bromo group is a better substituent than methoxy group to cause DNA ICL formation with higher efficiency. The DNA ICL yield of **23a** with 0.4 mM was 27.4% while it was 22.9% of **24a** with 0.15 mM, indicating that different substituents affected the efficiency of DNA ICL formation. Compared with other compounds, **23b** and **23c** obtained the lowest ICL yields with much higher concentrations. It showed that benzyloxy and allyloxy groups are not good leaving groups for binaphthalene with methoxy as substituent to generate DNA interstrand cross-links. However, the bromo-substituted compound with allyloxy leaving group (**22b**) showed the highest cross-linking yield with less concentration, indicating the substituents and leaving group combine to influence the efficiency of DNA ICL formation. In general, both the photo-reactivity and the efficiency of DNA ICL formation were affected by substituents and leaving groups.

```
                6                      22      27
5'-dGCCTAGTTCTTTTAATTACTTGCAATGCAAGTAATTAAAGCTTGATCTG-3'   (5a)
3'-dCGGATCAAGAAAATTAATGAACGTTACGTTCATTAATTTCGAACTAGAC-5'   (5b)
```

Table 4-1. The optimal cross-linking reaction conditions, ICL yields, and UV absorption data for **22a**, **d**, **23a-d**, and **24a-d**. [a]

Compound	Reaction Time (h)	Conc. (mM) [b]	ICL (%) [c]	λ_{max} (nm)	$\varepsilon_{\lambda max}$ ($M^{-1}cm^{-1}$)	k (10^{-5} S^{-1})
22a (R=Br, L=$OCH_2CH=CH_2$)	8	0.15	23.3 ± 0.5	299	21525	0.80
22b (R=Br, L=OCH_3)	8	0.5	27.6 ± 0.3	299	14975	0.81
23a (R=OCH_3, L=OAc)	8	0.4	27.4 ± 0.9	297	1885	0.78
23b (R=OCH_3, L=OCH_2Ph)	10	3.0	18.4 ± 1.0	294	3400	0.47
23c (R=OCH_3, L=$OCH_2CH=CH_2$)	10	1.5	20.5 ± 0.7	297	5900	0.46
23d (R=OCH_3, L=OCH_3)	10	0.25	39.0 ± 0.4	297	9145	0.55
24a (R=Cl, L= OAc)	20	0.15	22.9 ± 0.5	n.m.[d]	n.m.	0.34
24b (R=Cl, L= OCH_2Ph)	24	0.25	24.4 ± 0.9	n.m.	n.m.	0.36
24c (R=Cl, L= $OCH_2CH=CH_2$)	28	0.5	25.8 ± 1.3	n.m.	n.m.	0.32
24d (R=Cl, L= OCH_3)	32	0.15	25.5 ± 0.3	n.m.	n.m.	0.24

[a] DNA ICL reaction was carried out in a phosphate buffer (pH 8) with DNA duplex **5** upon irradiation of 350 nm light; [b] The minimum compound concentration required to achieve the highest DNA ICL yields; [c] The maximum DNA interstrand cross-linking yields observed for each compound under optimal conditions (the data are presented as average ± standard deviation from two individual experiments). [d] The data was not measured.

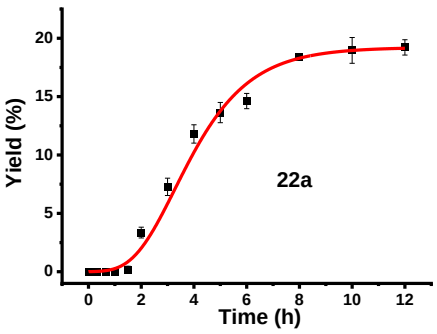

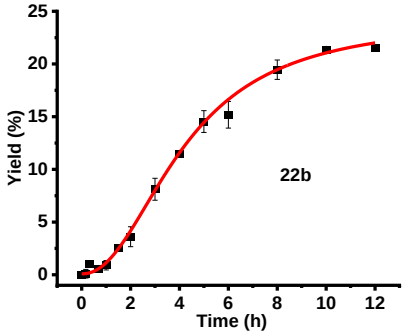

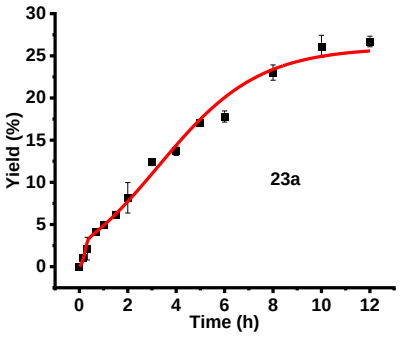
Yield (%)
Time (h)
23a

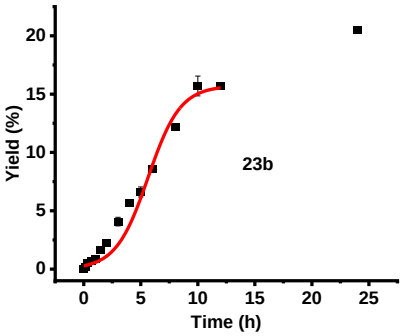
Yield (%)
Time (h)
23b

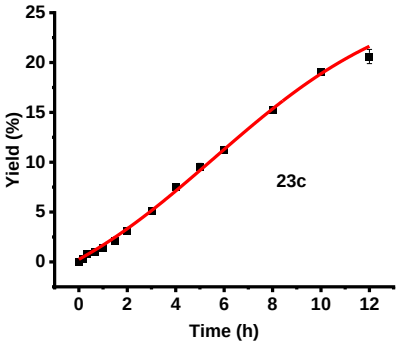
Yield (%)
Time (h)
23c

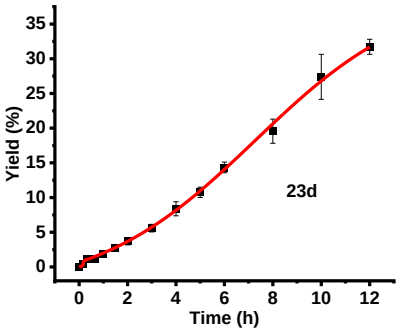
Yield (%)
Time (h)
23d

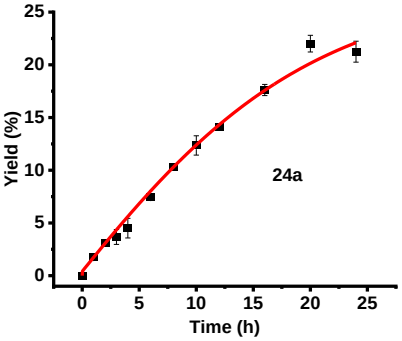
Yield (%)
Time (h)
24a

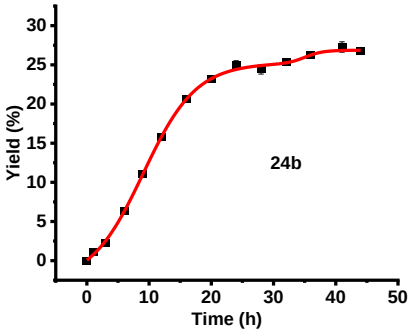
Yield (%)
Time (h)
24b

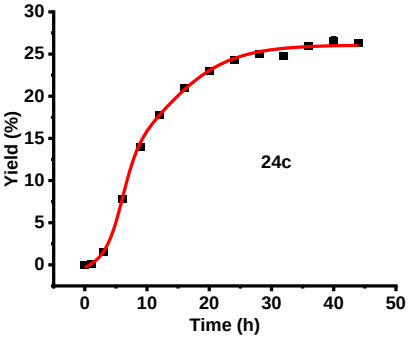
Yield (%)
Time (h)
24c

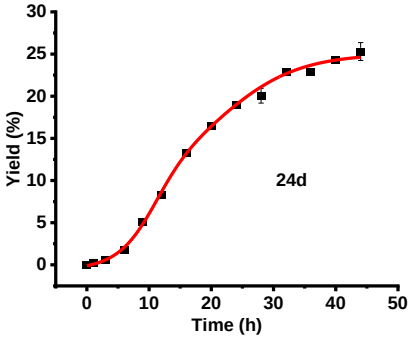
Yield (%)
Time (h)
24d

Figure 4-2. Time-dependence of DNA ICL formation of duplex **5** for **22a**, **b**, **23a-d**, **24a-d** upon photo-irradiation.

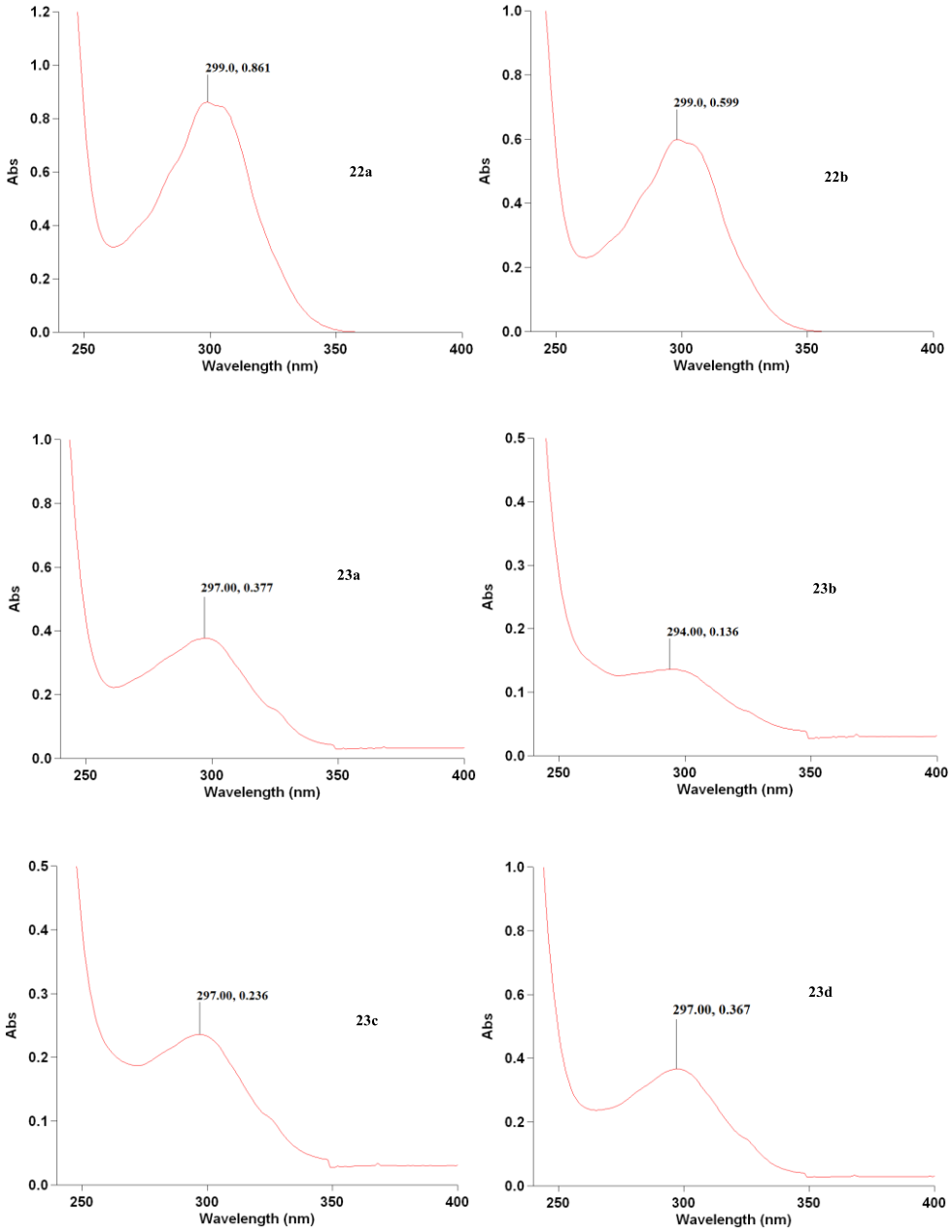

Figure 4-3. UV spectrum of **22a**, **b**, **23a-d** in $CHCl_3$. **23a** was measured with 1.0 mM, others were measured with 0.2 mM.

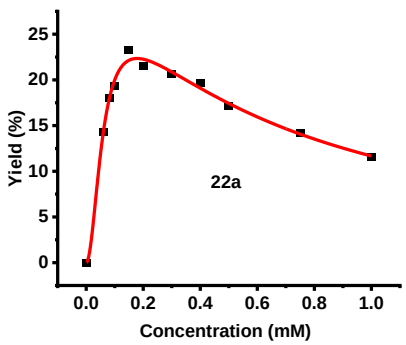
Yield (%)
22a
Concentration (mM)

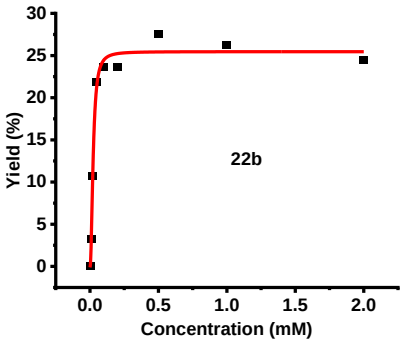
Yield (%)
22b
Concentration (mM)

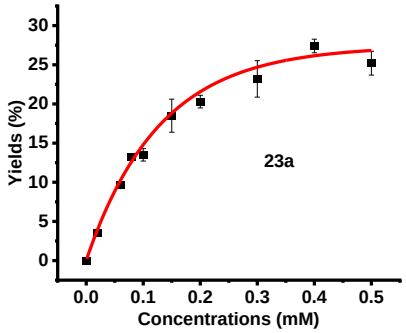
Yields (%)
23a
Concentrations (mM)

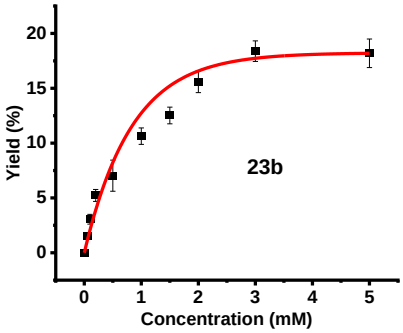
Yield (%)
23b
Concentration (mM)

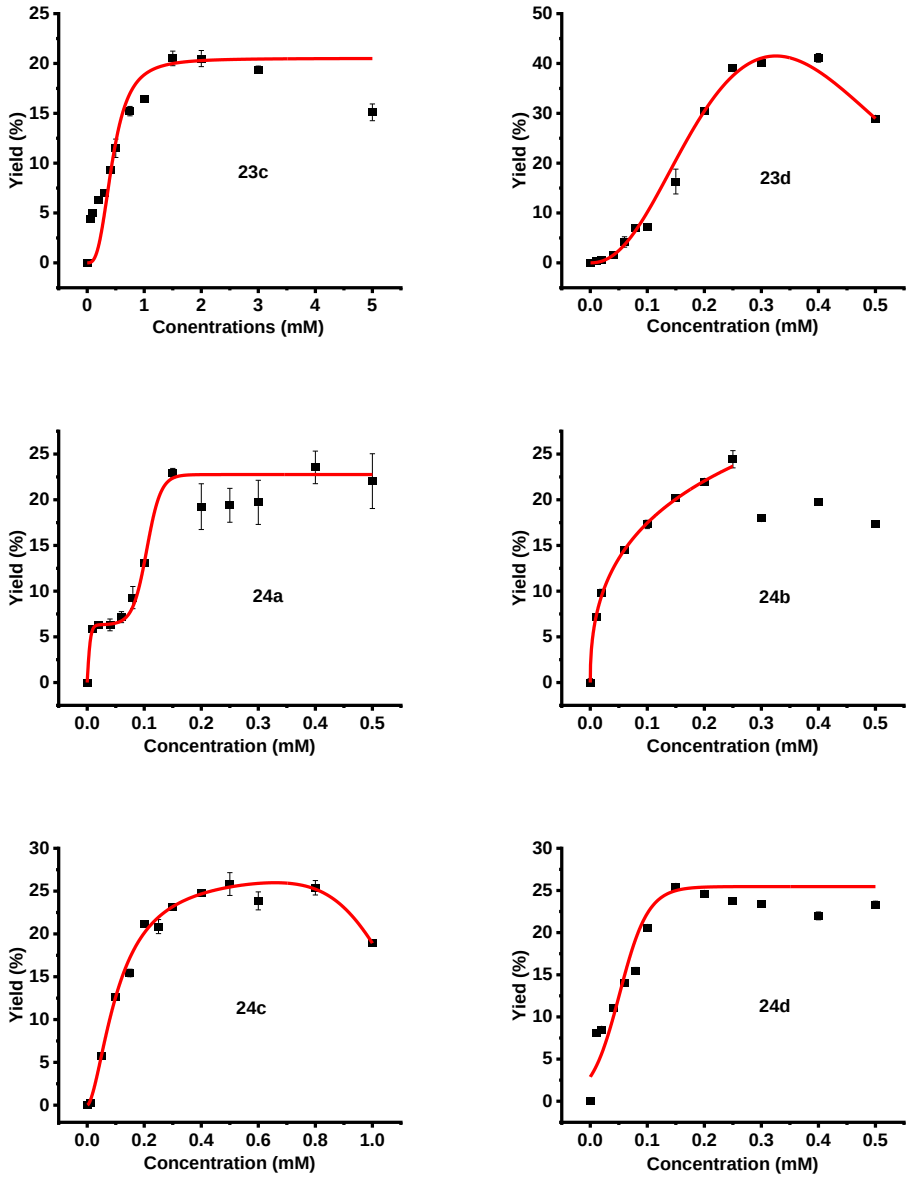

Figure 4-4. Concentration-dependence of DNA ICL formation of duplex **5** for **22a**, **b**, **23a-d**, **24a-d** upon photo-irradiation. Phosphor image autoradiogram of 20% denaturing PAGE analysis of compounds under varying concentrations. Reaction mixtures were photo-irradiated under UV (350 nm) for optimal times.

4.2.3 Mechanism of Photo-induced DNA ICL Formation

Photo-induced DNA interstrand cross-linking can be induced via [2+2] cycloaddition reaction, quinone methide (QM) formation or carbocation formation. Previous study showed that binaphthalene analogues generated DNA interstrand cross-links via carbocation mechanism, including boronate esters, bromides, trimethyl ammonium salts and triphenylphosphonium salts.[19,20,21] Based on the previous study in our group, the photoactive intermediate is generated via two pathways, either by heterolysis of C-L bond (L = leaving group) or homolysis of C-L bond. Different leaving groups or substituents affected the pathway of carbocation formation. Therefore, the mechanism of photo-induced DNA ICL formation with **19a**, **19b** and **20a**-**20b** were investigated by using 4-hydroxy-2,2,6,6-tetramethylpiperidin-1-oxyl (TEMPO) as radical trapper and methoxyamine as carbocation trapper. The study was performed in phosphor buffer with compounds and TEMPO or methoxyamine in different concentrations. Generally, the DNA ICL yield decreased with the increasing concentrations of either TEMPO or methoxyamine. For example, the ICL yield of **19b** decreased from ~21% to ~2.5% with 200 mM TEMPO or methoxyamine. It indicated that both free radicals and carbocations were involved in DNA ICL formation. The final DNA interstrand cross-linking was produced via the carbocation formation via the oxidation of free radicals, which means the homolysis of C-L bond.

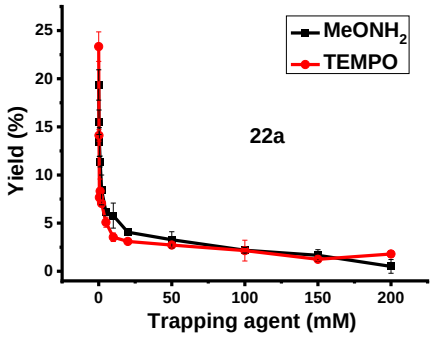
MeONH2
TEMPO
22a
Yield (%)
Trapping agent (mM)

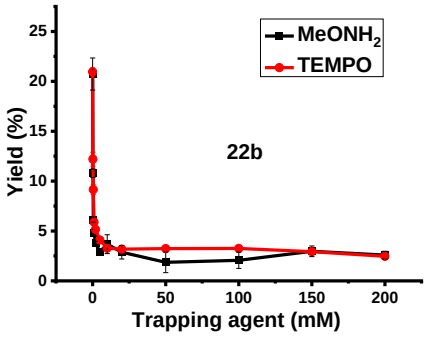
MeONH2
TEMPO
22b
Yield (%)
Trapping agent (mM)

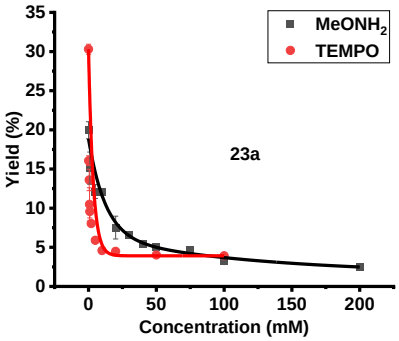
MeONH2
TEMPO
23a
Yield (%)
Concentration (mM)

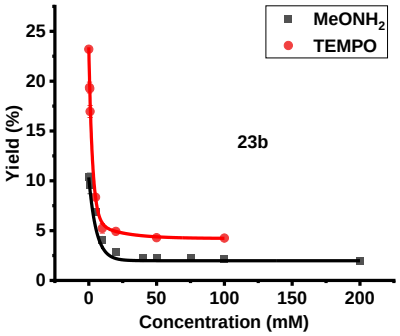
MeONH2
TEMPO
23b
Yield (%)
Concentration (mM)

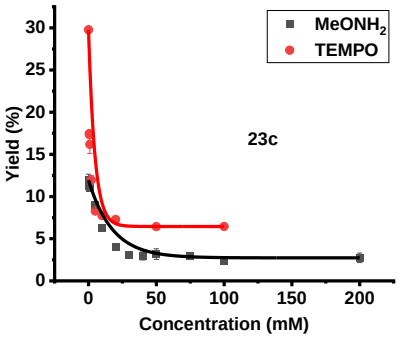
MeONH2
TEMPO
23c
Yield (%)
Concentration (mM)

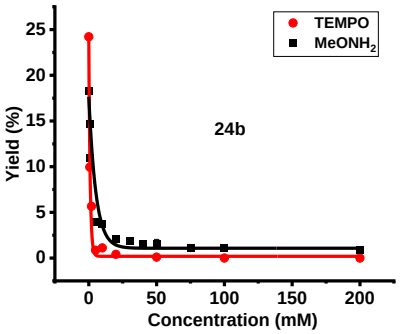
TEMPO
MeONH2
24b
Yield (%)
Concentration (mM)

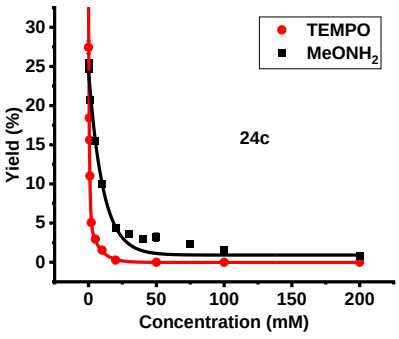
TEMPO
MeONH2
24c
Yield (%)
Concentration (mM)

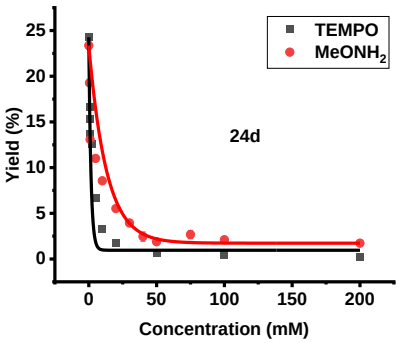
TEMPO
MeONH2
24d
Yield (%)
Concentration (mM)

Figure 4-5. The effect of methoxyamine and TEMPO on DNA interstrand cross-linking induced by **22a**, **b**, **23a-c**, **24b-d**.

4.2.4 Conclusions

In this work, binapthalene compounds with chloro, bromo or methoxy substituent on 4-position of binaphthalene ring were synthesized and their photo-reactivity toward DNA and the efficiency of DNA interstand cross-linking were investigated, as well as the mechanism of DNA ICL formation. These compounds were synthesized with different leaving groups, including acetoxy, benzyloxy, allyloxy or methoxy. The DNA interstrand cross-linking study showed that different substituent and leaving groups influence the photo-reactivity toward DNA and the efficiency of DNA ICL formation. Compounds with bromo substituent had the faster reactions than the compounds with chloro or methoxy substituent. As substituent, the electron-withdrawing group can promote the UV absorption while the electron-donating group can suppress the UV absorption. Benzyloxy and allyloxy groups are not good leaving groups for binaphthalene with methoxy as substituent to generate DNA interstrand cross-links but bromo-substituted compound will allyloxy leaving group had the highest DNA ICL yield, indicating the substituent and leaving group combine to affect the ICL formation efficiency. The trapping experiment in mechanism study indicated that the DNA ICL were generated via carbocation formation from the oxidation of free radicals.

4.3 Experimental Section

General Information

All reagents and chemicals were purchased from the vendors directly and used without further purification. The synthesis reactions were monitored by thin-layer chromatography (TLC) with UV light and the crude products were purified via column chromatography. Oligonucleotides (ODN) were synthesized by DNA/RNA ABI synthesizer from AZCO® BioTech. Inc. (Model. 394) and deprotected by a mixture of 40% aqueous $MeNH_2$ and 28% aqueous NH_3 (1:1) and then purified by 20% denaturing PAGE. The single strand **5a** was [γ-^{32}P] labeled at 5'-end, then hybridized with 5b at 90℃ for 5 min, and cooled to rt as well as stored under -20℃ before use. ^{1}H, ^{13}C NMR spectra were collected on a Bruker DRX 300 or 500 MHz spectrophotometer with TMS as internal stander. High resolution mass spectrometry was carried out on a Shimadzu LCMS-IT-TOF mass spectrometer at the University of Wisconsin-Milwaukee Mass Spectrometry Lab.

Compound Synthesis and Characterization.

3,3'-bis((allyloxy)methyl)-4,4'-dibromo-1,1'-binaphthalene (22a). A solution of LiOH (46 mg, 1.94 mmol) added dropwise into a solution of compound **12a** (180 mg, 0.32 mmol) in THF (10 mL). The reaction was quenched by water (10 mL) after stirring at rt for 7 h. The mixture was filtered by vacuum to get white solid **13**. Next, **13** was dissolved directly in DMF (10 mL) and 60% NaH (38 mg, 0.96 mmol) was added. Then allyl chloride (161 mg, 0.96 mmol) was added dropwise at 0^{o}C into the solution. The reaction mixture was stirred at room temperature for 24 h and quenched by water (10 mL). The mixture was extracted with EtOAc (20 mL) for three times. The organic phase was collected to be washed by brine and dried over Na_2SO_4 and concentrated by vacuum to get the crude product which was purified by chromatography (Hexane/ CH_2Cl_2 = 2/1) over silica gel to get compound **22a** as white solid (0.13 g, 71% yield). mp ℃. ^{1}H NMR (300 MHz, $CDCl_3$): 8.44 (d, *J* = 8.7 Hz, 2H), 7.67 (s, 2H), 7.61-7.56 (m, 2H), 7.33 (brs, 4H), 6.04-5.91 (m,

2H), 5.33 (d, J = 17.1 Hz, 2H), 5.20 (d, J = 10.2 Hz, 2H), 4.90 (s, 4H), 4.17 (d, J = 5.4 Hz, 4H). ^{13}C NMR (75 MHz, $CDCl_3$): δ 137.1, 135.2, 134.0, 132.8, 131.7, 127.5, 127.0, 126.8, 126.5, 126.2, 122.1, 117.1, 71.8, 71.5.

4,4'-dibromo-3,3'-bis(methoxymethyl)-1,1'-binaphthalene (22b). A solution of LiOH (46 mg, 1.94 mmol) was added dropwise into a solution of compound **12a** (180 mg, 0.32 mmol) in THF. The reaction was quenched by water (10 mL) after stirring at rt for 7 hours and filtered by vacuum to get white solid **13**. Next, 13 was dissolved in DMF (10 mL) and 60% NaH (38 mg, 0.96 mmol) was added. Iodomethane (136 mg, 0.96 mmol) was added dropwise at 0^{o}C into the solution. The reaction mixture was stirred at room temperature for 24 h and quenched by water (10 mL). The mixture was extracted with EtOAc (20 mL) for three times. The organic phase was collected be washed by brine and dried over Na_2SO_4 and concentrated by vacuum to get the crude product which was purified by chromatography (Hexane/ CH_2Cl_2 = 2/1) over silica gel to get compound **22b** as white solid (0.10 g, 63% yield). mp ℃. ^{1}H NMR (300 MHz, $CDCl_3$): 8.47 (d, J = 8.4 Hz, 2H), 7.67 (s, 2H), 7.63-7.58 (m, 2H), 7.37-7.34 (m, 4H), 4.86 (s, 4H), 3.53 (s, 6H). ^{13}C NMR (75 MHz, $CDCl_3$): δ 137.5, 135.4, 133.3, 132.1, 127.8, 127.4, 127.3, 126.9, 126.7, 122.5, 74.6, 58.8.

methyl 1-methoxy-2-naphthoate (26) K_2CO_3 (45.5 g, 329 mmol) was added into a solution of 1-hydroxy-2-naphthoic acid **25** (10 g, 53 mmol) in acetone (150 mL) and the solution was stirred at rt for 15 min. Then Me_2SO_4 (7.6 g, 160 mmol) was added dropwise into the solution. The reaction mixture was heated to 55 ℃ and stirred for 12 h. The solvent was evaporated by the vacuum and water (100 mL) was added to the residue. The mixture was extracted with EtOAc (100 mL) for three times and the organic phase was collected to be washed by brine, dried over Na_2SO_4 and concentrated by vacuum to get the crude product which purified by chromatography

(Hexane/EtOAc = 20:1) over silica gel to get compound **26** (11.5 g, 93%) as white solid. The NMR spectra were in agreement with those reported.

3,3'-bis((benzyloxy)methyl)-4,4'-dichloro-1,1'-binaphthalene (27) Boron trifluoride diethyl etherate (16.4 mL, 129.8 mmol) was added dropwise in a solution of compound **26** (9.4 g, 43.3 mmol) and lead tetraacetate (10.6 g, 21.8 mmol) in acetonitrile (100 mL) at 0℃. The reaction mixture was stirred at rt overnight and quenched by water (150 mL). The mixture was extracted with dichloromethane (300 mL) for three times and the organic phase was collected to be washed by brine, dried over Na_2SO_4 and concentrated by vacuum to get the crude product which purified by chromatography (hexane) over silica gel to get compound **27** as white solid. The NMR spectra were in agreement with those reported.

(4,4'-dimethoxy-[1,1'-binaphthalene]-3,3'-diyl)dimethanol (28) $LiAlH_4$ (1.2 g, 31.9 mmol) was added into a solution of compound **27** (4.6 g, 10.62 mmol) in THF (50 mL) at 0℃. The reaction was quenched by water (50 mL) after stirring at rt for 1 h. The mixture was extracted with EtOAc (100 mL) for three times and the organic phase was collected to be washed by brine, dried over Na_2SO_4 and concentrated by vacuum to get the crude product which purified by chromatography (Hexane/Ch2Cl2 = 50:1) over silica gel to get compound **28** (3.58 g, 90%) as white solid. The NMR spectra were in agreement with those reported.

(4,4'-dimethoxy-[1,1'-binaphthalene]-3,3'-diyl)bis(methylene) diacetate (23a) 4-Dimethylaminopyridine (0.49 mL, 4.02 mmol) was added into a solution of compound **28** (500 mg, 1.34 mmol) in dichloromethane (15 mL). Then acetyl chloride (0.38 mL, 5.34 mmol) was added dropwise into the solution at 0℃ and the reaction mixture was stirred at rt for two hours. The reaction was quenched by H_2O (16 mL) and the mixture was extracted with EtOAc (30 mL) for 3 times. The organic phase was collected to be washed by brine, dried over Na_2SO_4 and

concentrated by the vacuum to get the crude product which was purified by chromatography (Hexane/EtOAc = 5:1) over silica gel to get compound **23a** as colorless sticky liquid (0.46g, 75%). HRMS (ESI): m/z $[M+H]^+$ calcd for 399.1567, found: 399.1541.

3,3'-bis((benzyloxy)methyl)-4,4'-dimethoxy-1,1'-binaphthalene (23b) Benzyl chloride (0.51 g, 4.02 mmol) was added into a solution of compound **28** (500 mg, 1.34 mmol) and 60% NaH (0.17 g, 4.02 mmol) in DMF (15 mL) at 0°C. The reaction mixture was stirred at rt for overnight and then quenched by water (15 mL). The mixture was extracted with EtOAc (30 mL) for three times and the organic phase was collected to be washed by brine, dried over Na_2SO_4 and concentrated by the vacuum to get the crude product which was purified by chromatography (Hexane/EtOAc = 10:1) over silica to get compound **23b** as colorless sticky liquid (0.54g, 72%).

3,3'-bis((allyloxy)methyl)-4,4'-dimethoxy-1,1'-binaphthalene (23c) Allyl iodide (0.58 g, 4.02 mmol) was added into a solution of compound **28** (500 mg, 1.34 mmol) and 60 % NaH (0.17 g, 4.02 mmol) in DMF (15 mL) at 0°C. The reaction mixture was stirred at rt for overnight and then quenched by water (15 mL). The mixture was extracted with EtOAc (30 mL) for three times and the organic phase was collected to be washed by brine, dried over Na_2SO_4 and concentrated by the vacuum to get the crude product which was purified by chromatography (Hexane/EtOAc = 10:1) over silica to get compound **23c** as colorless sticky liquid (0.44 g, 72%).

4,4'-dimethoxy-3,3'-bis(methoxymethyl)-1,1'-binaphthalene (23d) Iodomethane (0.57 mL, 4.02 mmol) was added into a solution of compound **28** (500 mg, 1.34 mmol) and 60 % NaH (0.17 g, 4.02 mmol) in DMF (15 mL) at 0°C. The reaction mixture was stirred at rt for overnight and then quenched by water (15 mL). The mixture was extracted with EtOAc (30 mL) for three times and the organic phase was collected to be washed by brine, dried over Na_2SO_4 and concentrated

by the vacuum to get the crude product which was purified by chromatography (Hexane/EtOAc = 10:1) over silica to get compound **23d** as white solid (0.43 g, 80%).

(4,4'-dichloro-[1,1'-binaphthalene]-3,3'-diyl)bis(methylene) diacetate (24a) CH_3COOK (115 mg, 1.18 mmol) was added into a solution of **2a** (100 mg, 0.20 mmol) in CH_3CN (4 mL) and the reaction mixture was refluxed at 82℃ for six hours. The reaction was quenched by water (4 mL) and extracted with EtOAc (10 mL) for three times. The organic phase was collected to be washed by brine, dried over Na_2SO_4 and concentrated by the vacuum to get the crude product which was purified by chromatography (Hexane/EtOAc = 50:1) over silica to get compound **24a** as white solid (60 mg, 66%).

(4,4'-dichloro-[1,1'-binaphthalene]-3,3'-diyl)dimethanol (29) A solution of LiOH (61.8 mg, 2.58 mmol) dissolved in H_2O (5 mL) was added dropwise into a solution of compound **21a** (200 mg, 0.42 mmol) in THF (7 mL). The reaction mixture was stirred at rt for 7 hours and then filtered by vacuum to obtain white solid **29** (165 mg, 100%) which was used directly without purification in the next step.

3,3'-bis((benzyloxy)methyl)-4,4'-dichloro-1,1'-binaphthalene (24b) Benzyl chloride (356 mg, 2.8 mmol) was added into a solution of compound **29** (179.5 mg, 0.47 mmol) and 60% NaH (112 mg, 2.8 mmol) in DMF (10 mL) at 0℃. The reaction mixture was stirred at rt for 24 h and quenched by water (10 mL). Then the mixture was extracted with EtOAc (20 mL) for three times and the organic phase was collected to be washed by brine, dried over Na_2SO_4 and concentrated by the vacuum to get the crude product which was purified by chromatography (Hexane/EtOAc = 90:1) over silica to get compound **24b** as white solid (198 mg, 75%).

3,3'-bis((allyloxy)methyl)-4,4'-dichloro-1,1'-binaphthalene (24c) Allyl iodide (484 mg, 2.88 mmol) was added into a solution of compound **29** (184 mg, 0.48 mmol) and 60 % NaH (115 g, 2.88 mmol) in DMF (10 mL) at 0℃. The reaction mixture was stirred at rt for overnight and then quenched by water (10 mL). The mixture was extracted with EtOAc (20 mL) for three times and the organic phase was collected to be washed by brine, dried over Na_2SO_4 and concentrated by the vacuum to get the crude product which was purified by chromatography (Hexane/EtOAc = 90:1) over silica to get compound **24c** as white solid (142 mg, 68%).

4,4'-dichloro-3,3'-bis(methoxymethyl)-1,1'-binaphthalene (24d) Iodomethane (555 mg, 3.91 mmol) was added into a solution of compound **29** (250 mg, 0.65 mmol) and 60 % NaH (157 mg, 3.91 mmol) in DMF (10 mL) at 0℃. The reaction mixture was stirred at rt for overnight and then quenched by water (10 mL). The mixture was extracted with EtOAc (20 mL) for three times and the organic phase was collected to be washed by brine, dried over Na_2SO_4 and concentrated by the vacuum to get the crude product which was purified by chromatography (Hexane/EtOAc = 10:1) over silica to get compound **24d** as white solid (206 mg, 77%).

DNA ICL Formation. In a potassium phosphate buffer (pH 8, 100 mM), the ^{32}P-labeled ODN (0.5 μM) was hybridized with the complementary strand (1.5 equiv) by heating at 90 °C for 5 min and cooling to rt naturally. Then, 100 mM potassium phosphate buffer (pH 8, 2 μL), 1 M NaCl (2 μL), and certain concentrations of **22a, b, 23a-d, 24a-d** in CH_3CN (6 μL) were added to the ^{32}P-labeled ODN duplex (2 μL, 0.5 μM). Autoclaved water was added to give a final volume of 20 μL (final concentration range: 0.01−2.0 mM). The reaction mixture was irradiated with 350 nm light, then quenched with an equal volume of 90% formamide loading buffer, and subjected to 20% denaturing PAGE.

Free Radical Trapping Assay of DNA ICL Formation. A solution of TEMPO in CH_3CN (5/2 to 4000/2 mM, 2 μL) was added to a reaction mixture containing 2 μL of ^{32}P-labeled ODN duplex (0.5 μM), 2 μL of NaCl (1 M), 2 μL of pH 8 potassium phosphate (100 mM), 4 μL of **22a**, **b**, **23a-c**, **24b-d** in CH_3CN with optimal concentrations, and 8 μL of autoclaved distilled water to give a total volume of 20 μL (final TEMPO concentration: 0.25−200 mM). The reaction mixture was irradiated with 350 nm light for the desired time, quenched with 20 μL of 90% formamide loading buffer, and subjected to 20% denaturing PAGE.

Carbocation Trapping Assay of DNA ICL Formation. A solution of $MeONH_2$·HCl (2 M) was titrated with NaOH (5 M) to pH 7.0, which was diluted to the desired concentration (5/2 to 4000/ 2 mM). The resulting $MeONH_2$·HCl solution (2 μL) with desired concentration was added to a mixture containing 2 μL of ^{32}P-labeled ODN duplex (0.5 μM), 2 μL of NaCl (1 M), and 2 μL of pH 8 potassium phosphate (100 mM). Then, 6 μL of **22a**, **b**, **23a-c**, **24b-d** in CH_3CN with optimal concentrations and 6 μL of autoclaved distilled water were added to give a total volume of 20 μL (final $MeONH_2$ concentration: 0.25−200 mM). After irradiation with 350 nm light for the desired time, the reaction mixture was quenched with 20 μL of 90% formamide loading buffer, then subjected to 20% denaturing PAGE.

4.4 Reference

(1) Rajski, S. R.; Williams, R. M. DNA Cross-Linking Agents as Antitumor Drugs. *Chem. Rev.* **1998**, 98, 2723-2795.

(2) Brulikova, L.; Hlavac, J.; Hradil, P. DNA Interstrand Cross-Linking Agents and their Chemotherapeutic Potential. *Curr. Med. Chem.* **2012**, 19, 364-385.

(3) Fan, H.; Peng, X. Novel DNA Cross-Linking Reagents. *In Advances in Molecular Toxicology*; Fishbein, J. C.; Heilman, J. M., Eds.; Elsevier, 2016; Vol. *10*, pp 235−292.

(4) Sun, H.; Fan, H.; Eom, H.; Peng, X. Coumarin-Induced DNA Ligation, Rearrangement to DNA Interstrand Cross-Links, and Photorelease of Coumarin Moiety. *ChemBioChem*. **2016**, 17, 2046–2053.

(5) Sun, H.; Fan, H.; Peng, X. Quantitative DNA Interstrand Cross-Link Formation by Coumarin and Thymine: Structure Determination, Sequence Effect, and Fluorescence Detection. *J. Org. Chem.* **2014**, 79, 11359–11369.

(6) Kashida, H.; Doi, T.; Sakakibara, T.; Hayashi, T.; Asanuma, H. *p*-Stilbazole Moieties As Artificial Base Pairs for Photo-Cross-Linking of DNA Duplex. *J. Am. Chem. Soc.* **2013**, 135, 7960-7966.

(7) Yoshimura, Y.; Fujimoto, K. Ultrafast Reversible Photo-Cross-Linking Reaction: Toward in Situ DNA Manipulation. *Org. Lett.* **2008**, 10, 3227−3230.

(8) Fujimoto, K.; Konishi-Hiratsuka, K.; Sakamoto, T.; Yoshimura, Y. Site-Specific Cytosine to Uracil Transition by Using Reversible DNA Photo-Crossling. *ChemBioChem*. **2010**, 11, 1661−664.

(9) Fujimoto, K.; Konishi-Hiratsuka, K.; Sakamoto, T.; Yoshimura, Y. Site-Specific Photochemical RNA Editing. *Chem. Commun.* **2010**, 46, 7545-7547.

(10) Richter, S. N.; Maggi, S.; Colloredo-Mels, S.; Palumbo, M.; Freccero, M. Binol Quinone Methides as Bisalkylating and DNA Cross-Linking Agents. *J. Am. Chem. Soc.* **2004**, 126, 13973-13979.

(11) Wang, P.; Liu, R.; Wu, X.; Ma, H.; Cao, X.; Zhou, P.; Zhang, J.; Weng, X.; Zhang, X.; Qi, J.; Zhou, X.; Weng, L. A Potent, Water-Soluble and Photoinducible DNA Cross-Linking Agent. *J. Am. Chem. Soc.* **2003**, 125, 1116-1117.

(12) Lin, G.; Li, L. Oxidation and reduction of the 5-(2′-deoxyuridinyl)methyl radical. *Angew. Chem., Int. Ed.* **2013**, 52, 5594−5598.

(13) Weng, L.; Horvat, S. M.; Schiesser, C. H.; Greenberg, M. M. Deconvoluting the reactivity of two intermediates formed from modified pyrimidines. *Org. Lett.* **2013**, 15, 3618−3621.

(14) Fan, H.; Sun, H.; Peng, X. Substituents Have a Large Effect on Photochemical Generation of Benzyl Cations and DNA Cross-Linking. *Chem. - Eur. J.* **2018**, 24, 7671−7682.

(15) Wang, Y.; Liu, S.; Lin, Z.; Fan, Y.; Wang, Y.; Peng, X. Photochemical Generation of Benzyl Cations That Selectively Cross-Link Guanine and Cytosine in DNA. *Org. Lett.* **2016**, 18, 2544−2547.

(16) Fan, H.; Sun, H.; Zhang, Q.; Peng, X. Photoinduced DNA Interstrand Cross-Linking by 1,1′-Biphenyl Analogues: Substituents and Leaving Groups Combine to Determine the Efficiency of Cross-Linker. *Chem. - Eur. J.* **2021**, 27, 5215−5224.

(17) Fan, H.; Peng, X. Photoinduced DNA Interstrand Cross-Linking by Benzene Derivatives: Leaving Groups Determine the Efficiency of the Cross-Linker. *J. Org. Chem.* **2021**, 86, 493−506.

(18) Han, Y.; Chen, W.; Kuang, Y.; Sun, H.; Wang, Z.; Peng, X. UV-Induced DNA Interstrand Cross-Linking and Direct Strand Breaks from a New Type of Binitroimidazole Analogue. *Chem. Res. Toxicol.* **2015**, 28, 919−926.

(19) Wang, Y.; Lin, Z.; Fan, H.; Peng, X. Photoinduced DNA Interstrand Cross-Link Formation by Naphthalene Boronates via a Carbocation. *Chem. - Eur*. J. **2016**, 22, 10382−10386.

(20) Lin, Z.; Fan, H.; Zhang, Q.; Peng, X. Design, Synthesis, and Characterization of Binaphthalene Precursors as Photoactivated DNA Interstrand Cross-Linkers. *J. Org. Chem.* **2018**, 83, 8815−8826.

(21) Zhang, Q.; Lin, Z.; Peng, X. Photoreactivity of Binaphthalene Triphenylphosphonium Salts: DNA Interstrand Cross-link Formation and Substituent Effects. *Chem. Res. Toxicol.* **2022**, 35, 8, 1334–1343.

4.5 Appendices A: Gel Electrophoresis

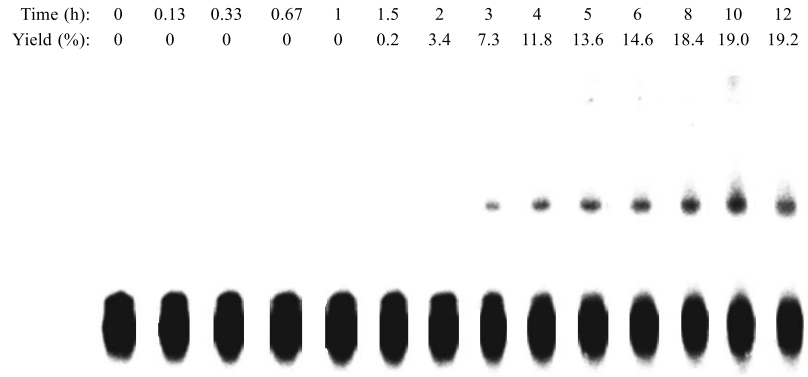

Figure 4-6. Representative gel of time-dependent DNA ICL formation of duplex **5** for **22a** (500 μM) upon 350 nm irradiation at time points.

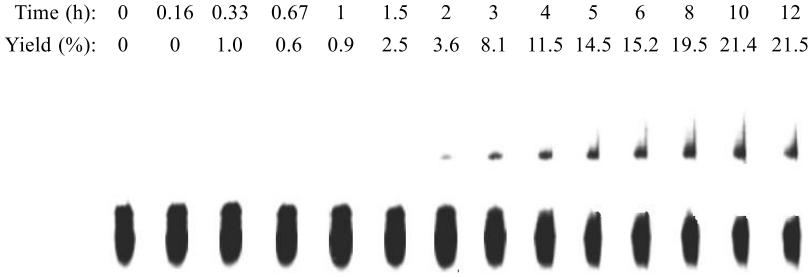

Figure 4-7. Representative gel of time-dependent DNA ICL formation of duplex **5** for **22b** (500 μM) upon 350 nm irradiation at time points.

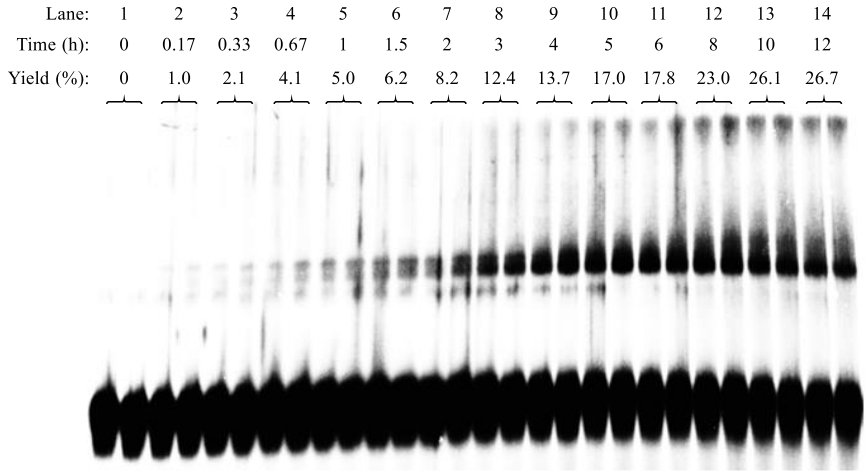

Figure 4-8. Representative gel of time-dependent DNA ICL formation of duplex **5** for **23a** (1.0 mM) upon 350 nm irradiation at time points.

.

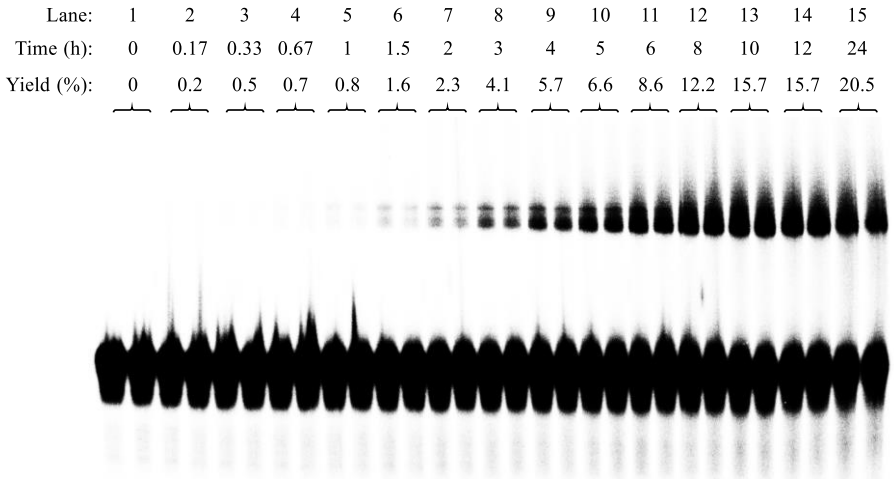

Figure 4-9. Representative gel of time-dependent DNA ICL formation of duplex **5** for **23b** (1.0 mM) upon 350 nm irradiation at time points.

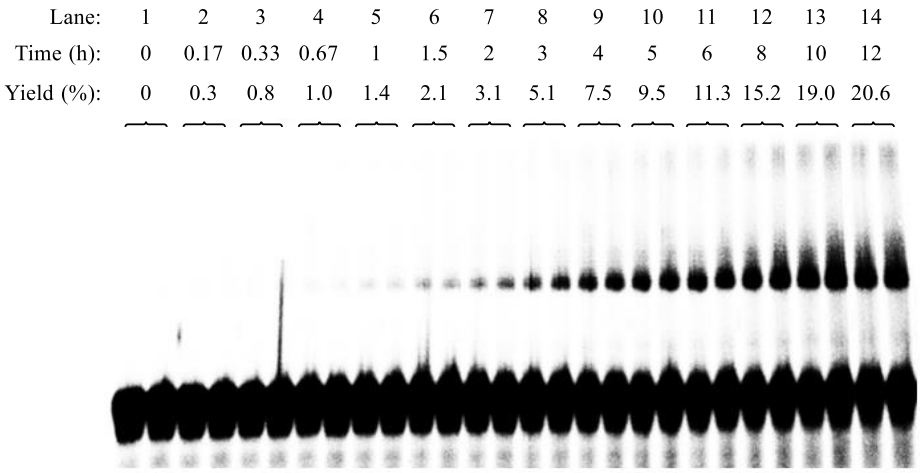

Figure 4-10. Representative gel of time-dependent DNA ICL formation of duplex **5** for **23c** (1.0 mM) upon 350 nm irradiation at time points.

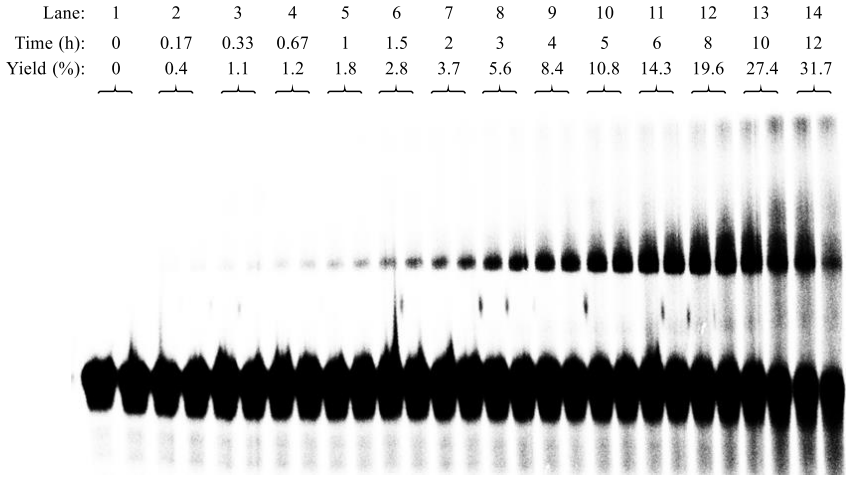

Figure 4-11. Representative gel of time-dependent DNA ICL formation of duplex **5** for **23d** (1.0 mM) upon 350 nm irradiation at time points.

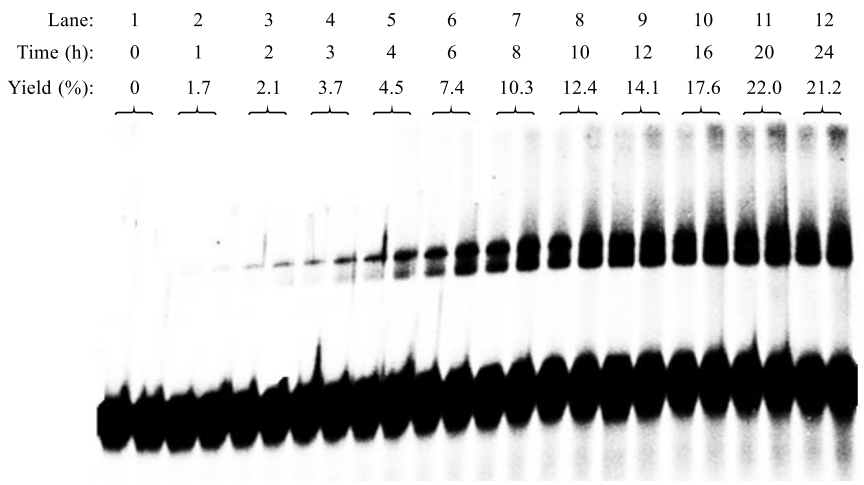

Figure 4-12. Representative gel of time-dependent DNA ICL formation of duplex **5** for **24a** (200 μM) upon 350 nm irradiation at time points.

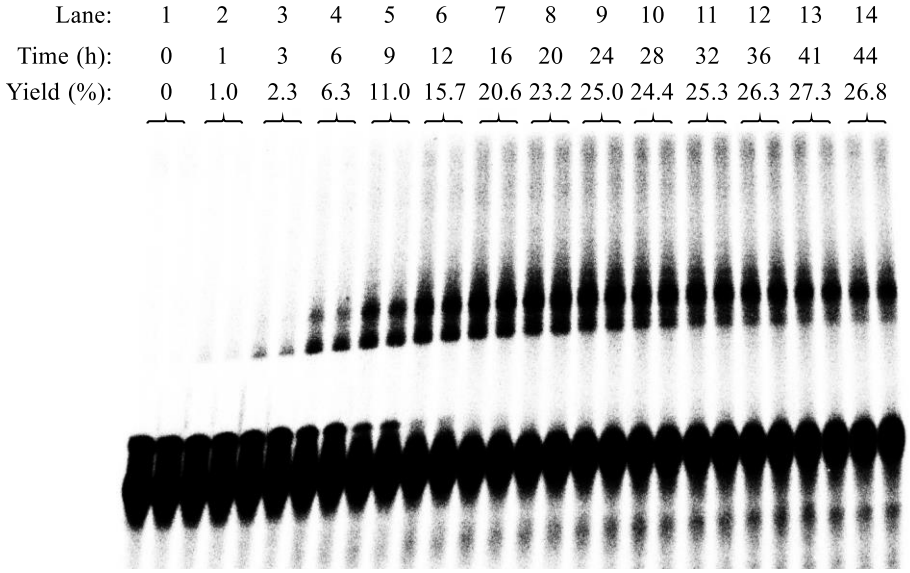

Figure 4-13. Representative gel of time-dependent DNA ICL formation of duplex **5** for **24b** (200 μM) upon 350 nm irradiation at time points.

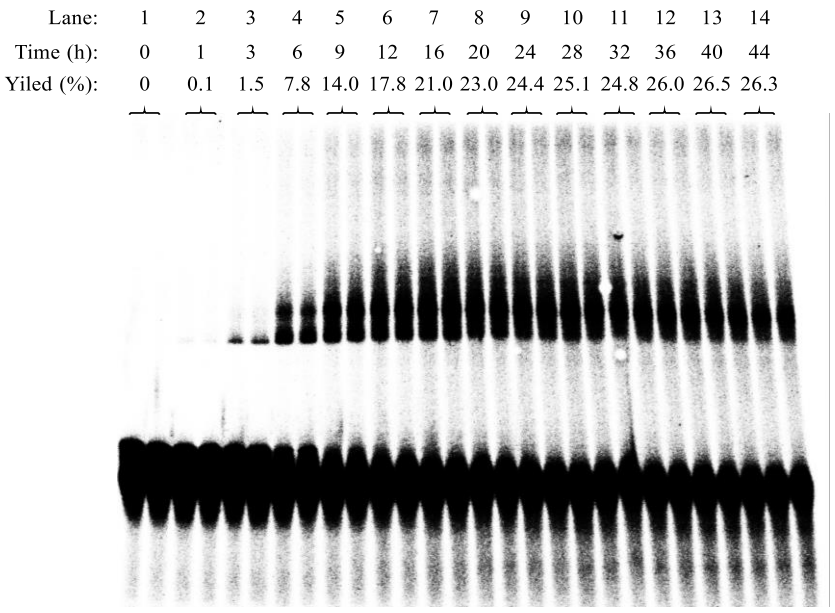

Figure 4-14. Representative gel of time-dependent DNA ICL formation of duplex **5** for **24c** (200 μM) upon 350 nm irradiation at time points.

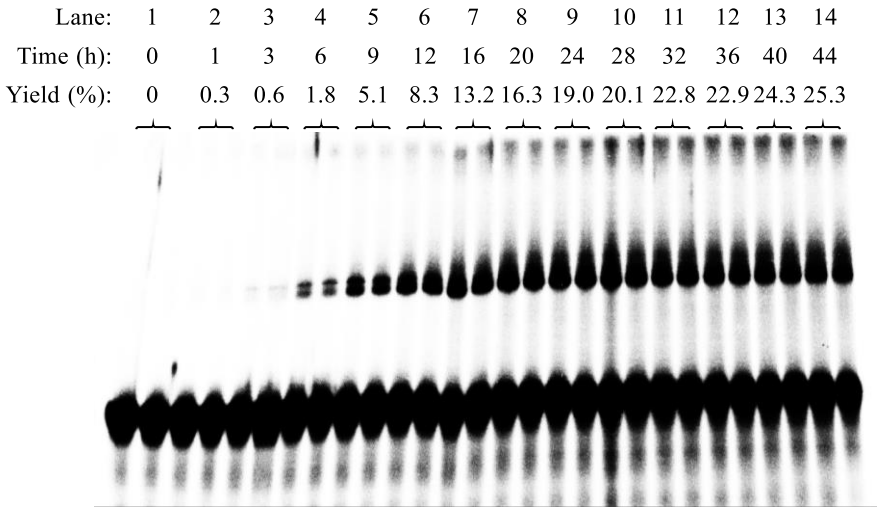

Figure 4-15. Representative gel of time-dependent DNA ICL formation of duplex **5** for **24d** (200 μM) upon 350 nm irradiation at time points.

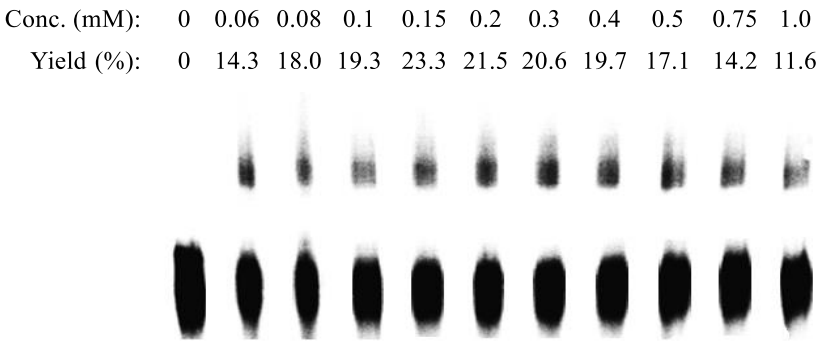

Figure 4-16. The concentration dependence of ICL formation for **22a** upon photoirradiation. Phosphor image autoradiogram of 20% denaturing PAGE analysis of **22a** under varying concentration. Reaction mixtures were photo-irradiated under UV (350 nm) for 8 h.

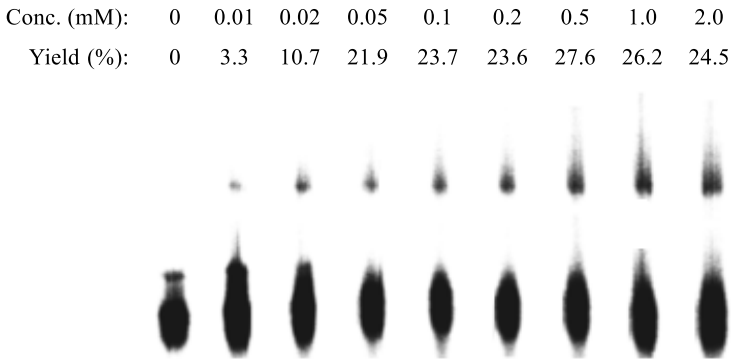

Figure 4-17. The concentration dependence of ICL formation for **22b** upon photoirradiation. Phosphor image autoradiogram of 20% denaturing PAGE analysis of **22b** under varying concentration. Reaction mixtures were photo-irradiated under UV (350 nm) for 8 h.

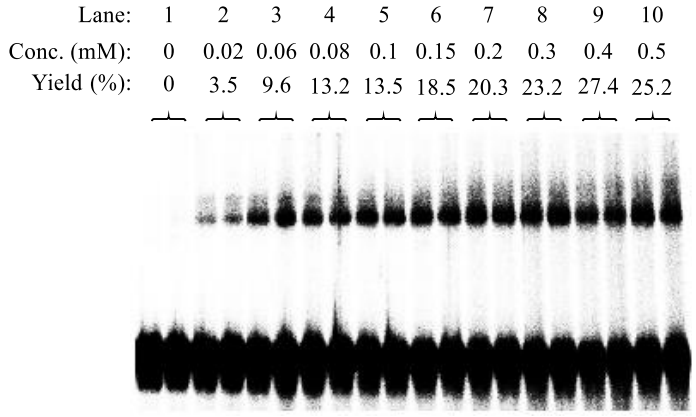

Figure 4-18. The concentration dependence of ICL formation for **23a** upon photoirradiation. Phosphor image autoradiogram of 20% denaturing PAGE analysis of **23a** under varying concentration. Reaction mixtures were photo-irradiated under UV (350 nm) for 8 h.

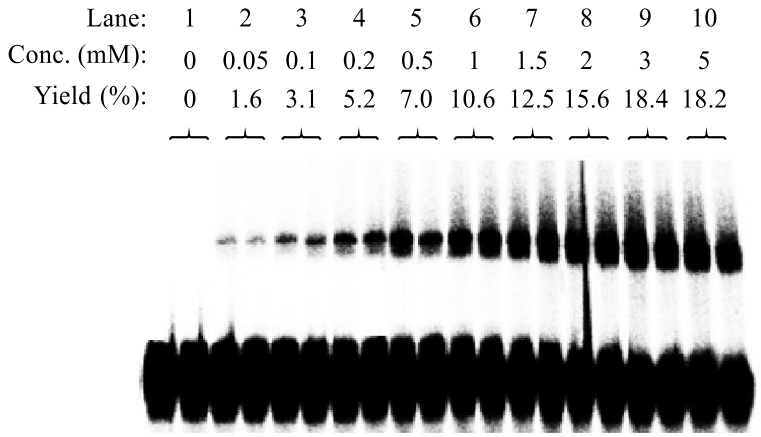

Figure 4-19. The concentration dependence of ICL formation for **23b** upon photoirradiation. Phosphor image autoradiogram of 20% denaturing PAGE analysis of **23b** under varying concentration. Reaction mixtures were photo-irradiated under UV (350 nm) for 10 h.

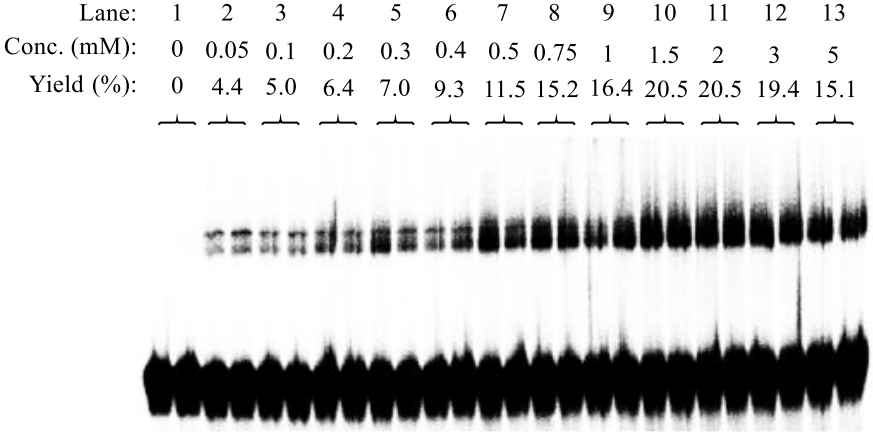

Figure 4-20. The concentration dependence of ICL formation for **23c** upon photoirradiation. Phosphor image autoradiogram of 20% denaturing PAGE analysis of **23c** under varying concentration. Reaction mixtures were photo-irradiated under UV (350 nm) for 10 h.

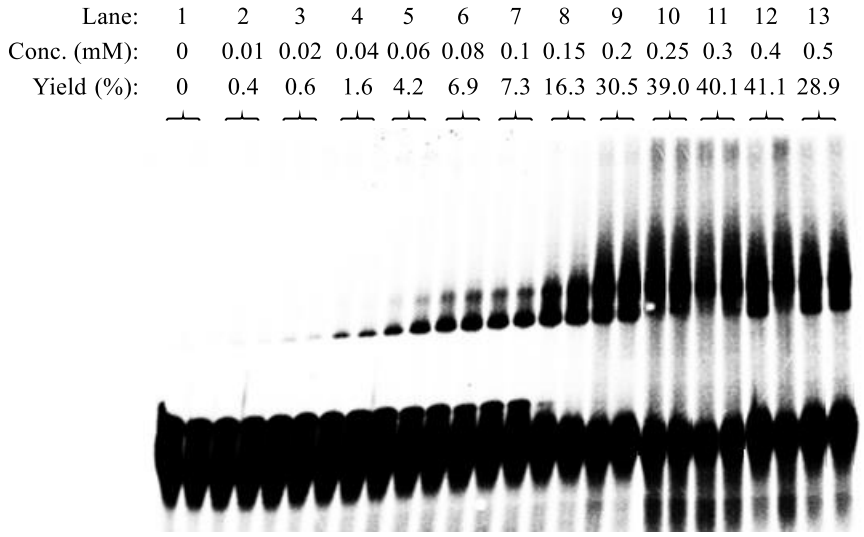

Figure 4-21. The concentration dependence of ICL formation for **23d** upon photoirradiation. Phosphor image autoradiogram of 20% denaturing PAGE analysis of **23d** under varying concentration. Reaction mixtures were photo-irradiated under UV (350 nm) for 10 h.

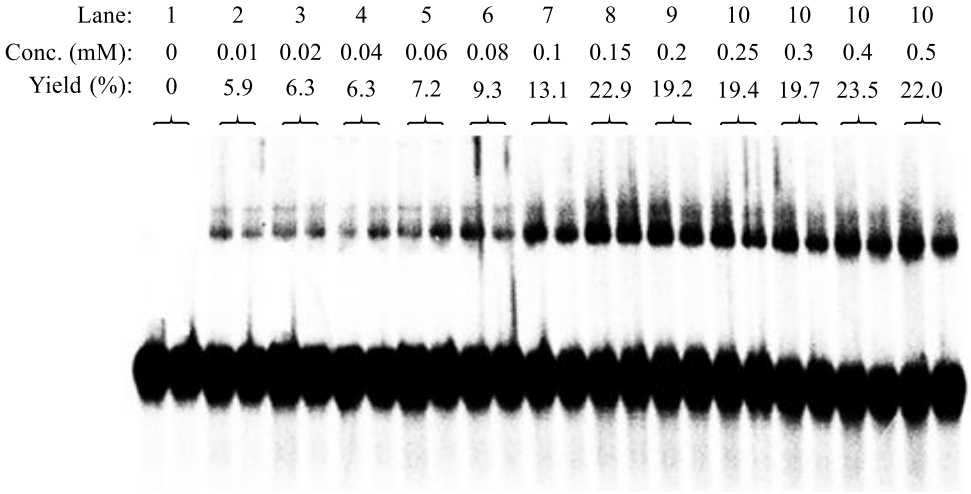

Figure 4-22. The concentration dependence of ICL formation for **24a** upon photoirradiation. Phosphor image autoradiogram of 20% denaturing PAGE analysis of **24a** under varying concentration. Reaction mixtures were photo-irradiated under UV (350 nm) for 20 h.

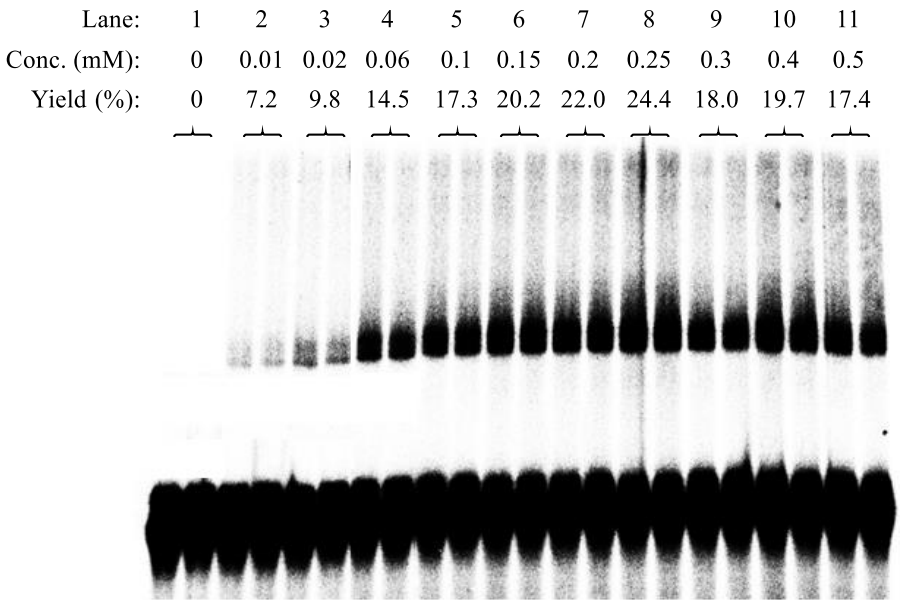

Figure 4-23. The concentration dependence of ICL formation for **24b** upon photoirradiation. Phosphor image autoradiogram of 20% denaturing PAGE analysis of **24b** under varying concentration. Reaction mixtures were photo-irradiated under UV (350 nm) for 24 h.

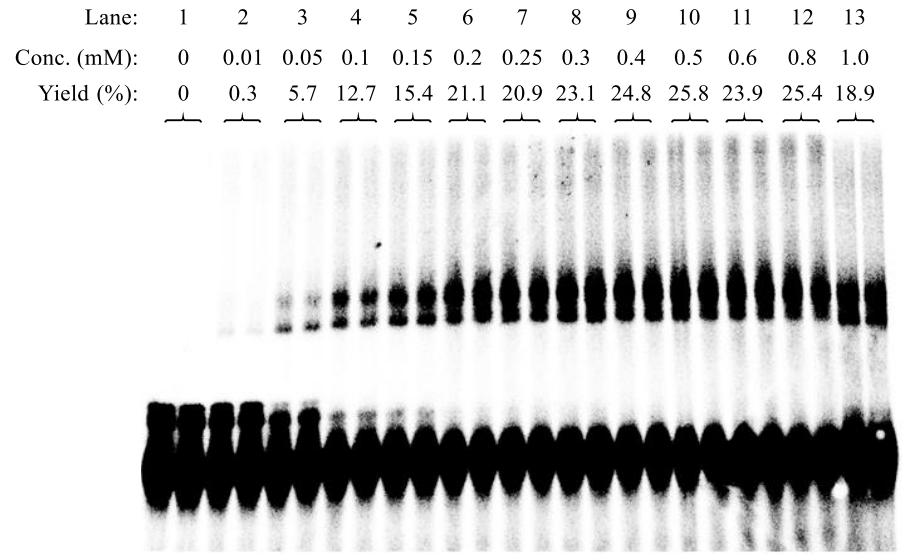

Figure 4-24. The concentration dependence of ICL formation for **24c** upon photoirradiation. Phosphor image autoradiogram of 20% denaturing PAGE analysis of **24c** under varying concentration. Reaction mixtures were photo-irradiated under UV (350 nm) for 28 h.

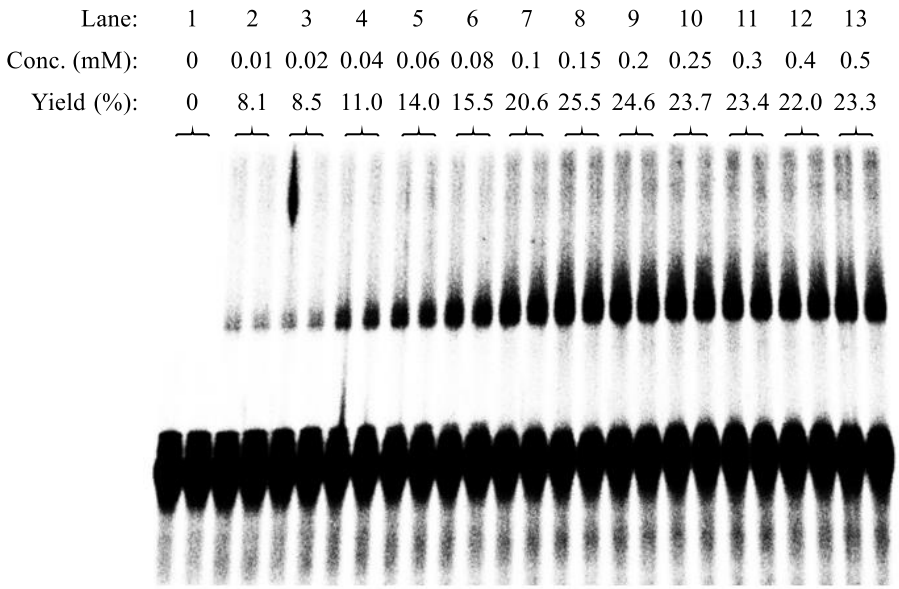

Figure 4-25. The concentration dependence of ICL formation for **24d** upon photoirradiation. Phosphor image autoradiogram of 20% denaturing PAGE analysis of **24d** under varying concentration. Reaction mixtures were photo-irradiated under UV (350 nm) for 32 h.

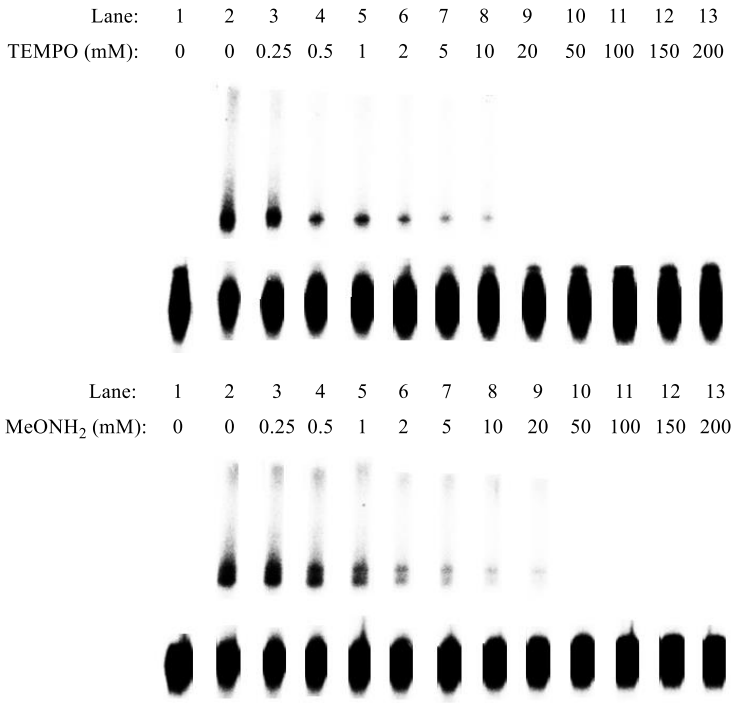

Figure 4-26. The effect of TEMPO and methoxyamine on DNA ICL formation of duplex **5** for **22a**. A mixture of **5** (50 nM) and **22a** (0.5 mM) in a pH 8 phosphate buffer was irradiated with 350 nm light for 8h in the presence of varying concentration of TEMPO (top) or $MeONH_2$ (bottom).

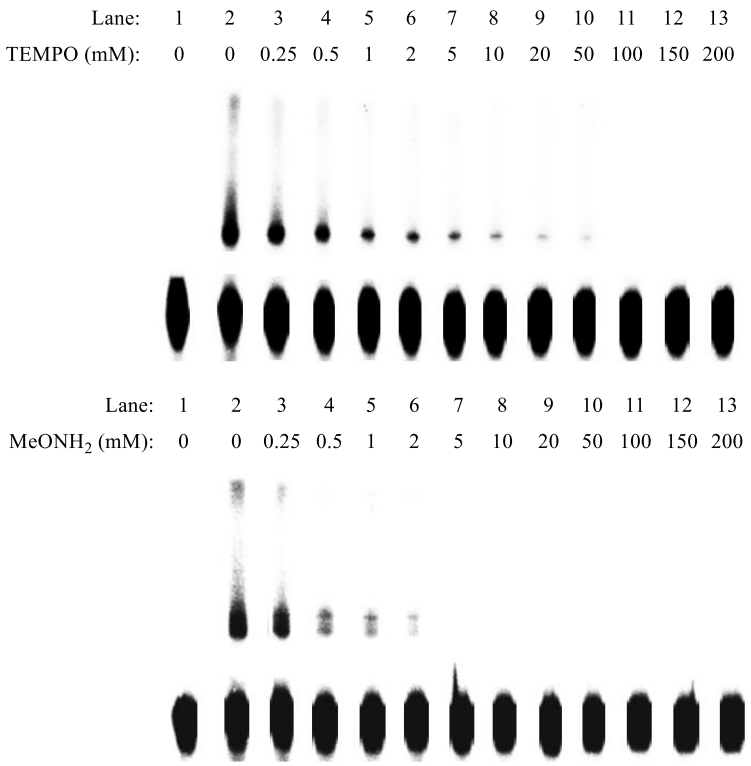

Figure 4-27. The effect of TEMPO and methoxyamine on DNA ICL formation of duplex **5** for **22b**. A mixture of **5** (50 nM) and **22b** (0.5 mM) in a pH 8 phosphate buffer was irradiated with 350 nm light for 8h in the presence of varying concentration of TEMPO (top) or $MeONH_2$ (bottom).

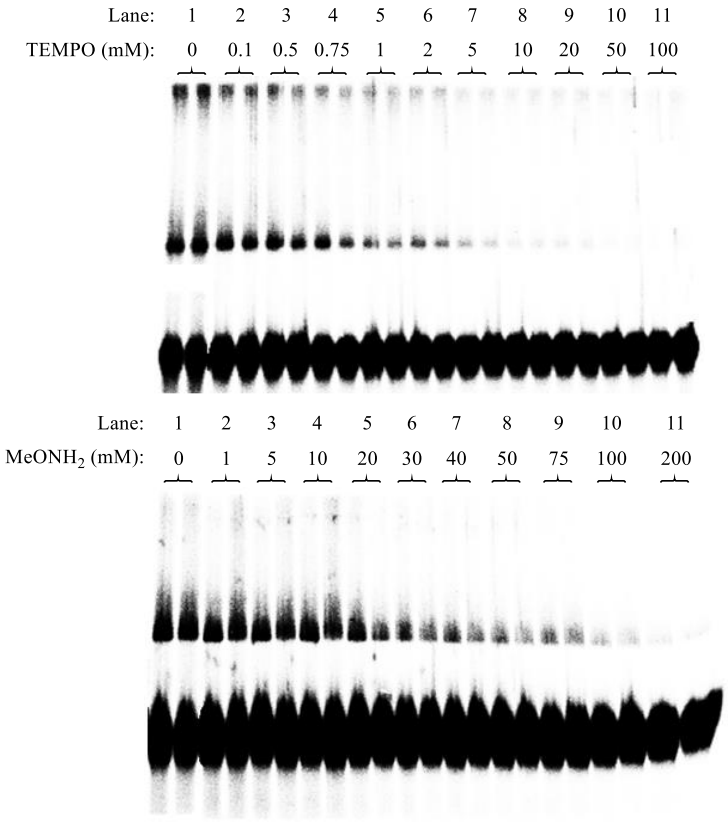

Figure 4-28. The effect of TEMPO and methoxyamine on DNA ICL formation of duplex **5** for **23a**. A mixture of **5** (50 nM) and **23a** (0.4 mM) in a pH 8 phosphate buffer was irradiated with 350 nm light for 8h in the presence of varying concentration of TEMPO (top) or $MeONH_2$ (bottom).

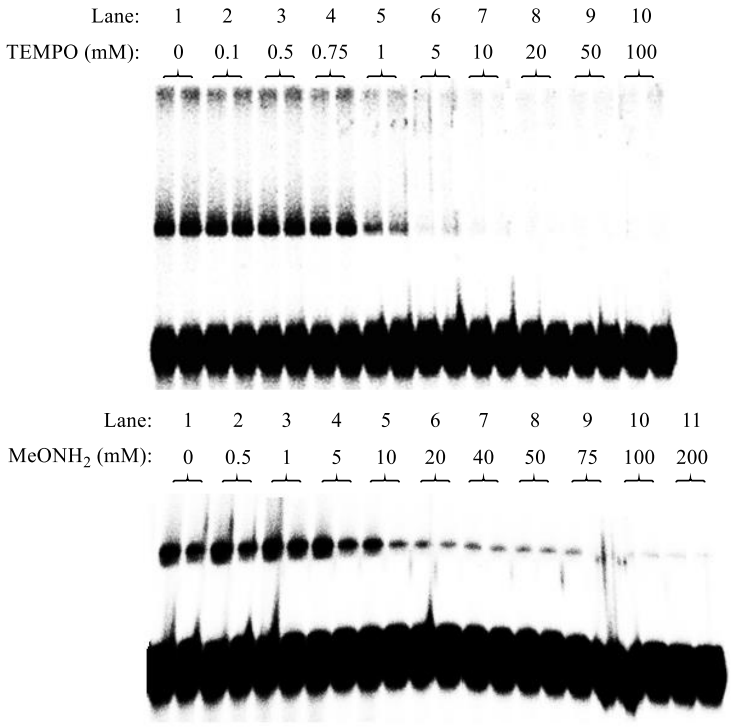

Figure 4-29. The effect of TEMPO and methoxyamine on DNA ICL formation of duplex **5** for **23b**. A mixture of **5** (50 nM) and **23b** (3.0 mM) in a pH 8 phosphate buffer was irradiated with 350 nm light for 10h in the presence of varying concentration of TEMPO (top) or $MeONH_2$ (bottom).

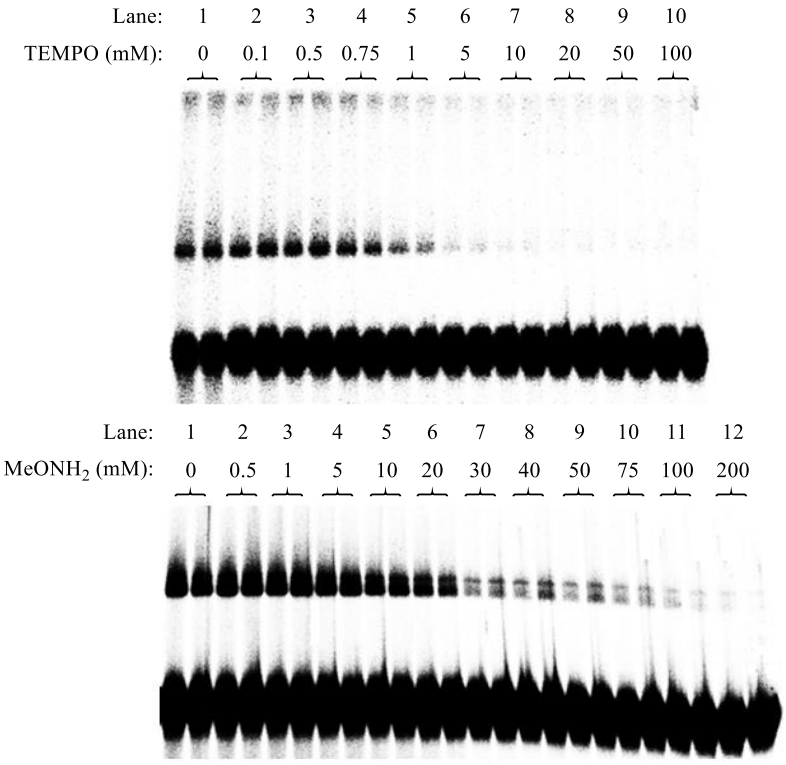

Figure 4-30. The effect of TEMPO and methoxyamine on DNA ICL formation of duplex **5** for **23c**. A mixture of **5** (50 nM) and **23c** (1.5 mM) in a pH 8 phosphate buffer was irradiated with 350 nm light for 10h in the presence of varying concentration of TEMPO (top) or $MeONH_2$ (bottom).

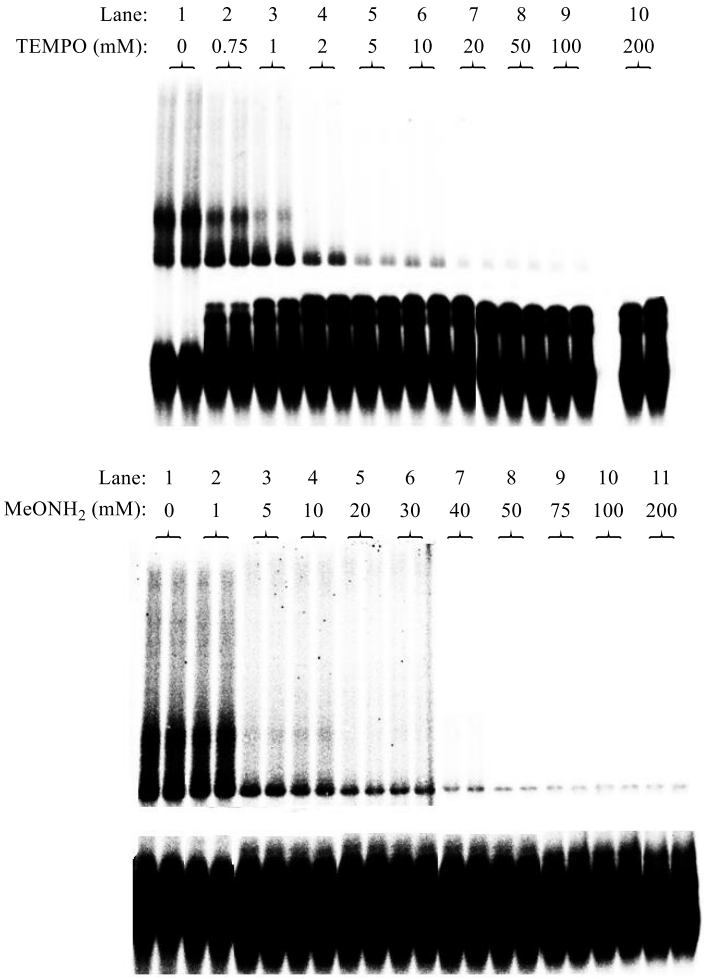

Figure 4-31. The effect of TEMPO and methoxyamine on DNA ICL formation of duplex **5** for **24b**. A mixture of **5** (50 nM) and **24b** (0.25 mM) in a pH 8 phosphate buffer was irradiated with 350 nm light for 24h in the presence of varying concentration of TEMPO (top) or $MeONH_2$ (bottom).

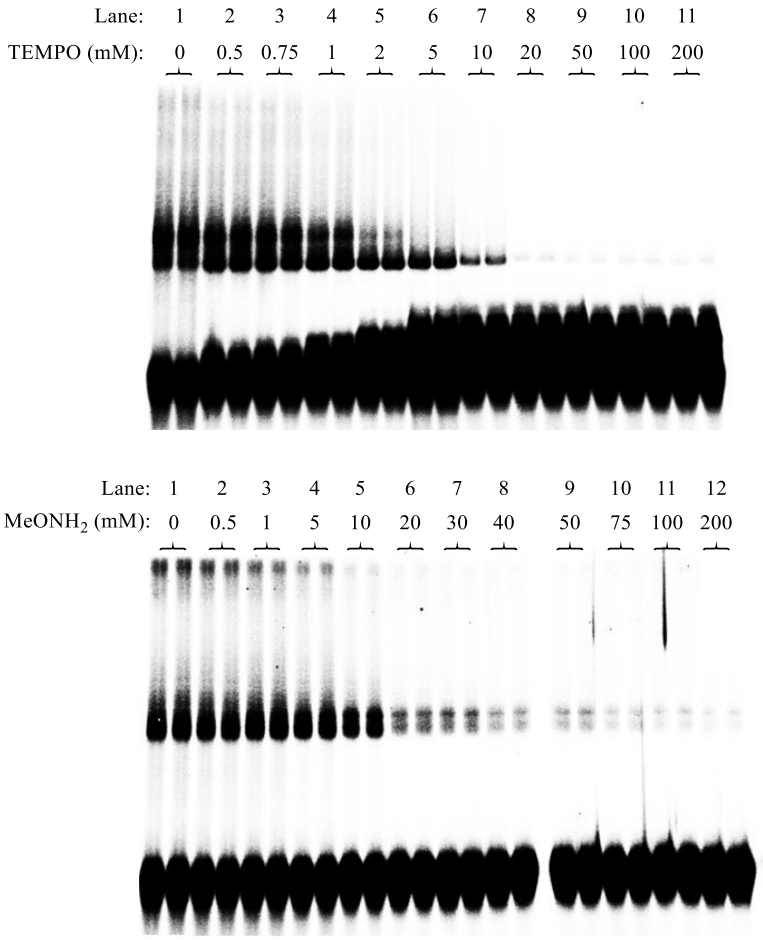

Figure 4-32. The effect of TEMPO and methoxyamine on DNA ICL formation of duplex **5** for **24c**. A mixture of **5** (50 nM) and **24c** (0.5 mM) in a pH 8 phosphate buffer was irradiated with 350 nm light for 28h in the presence of varying concentration of TEMPO (top) or $MeONH_2$ (bottom).

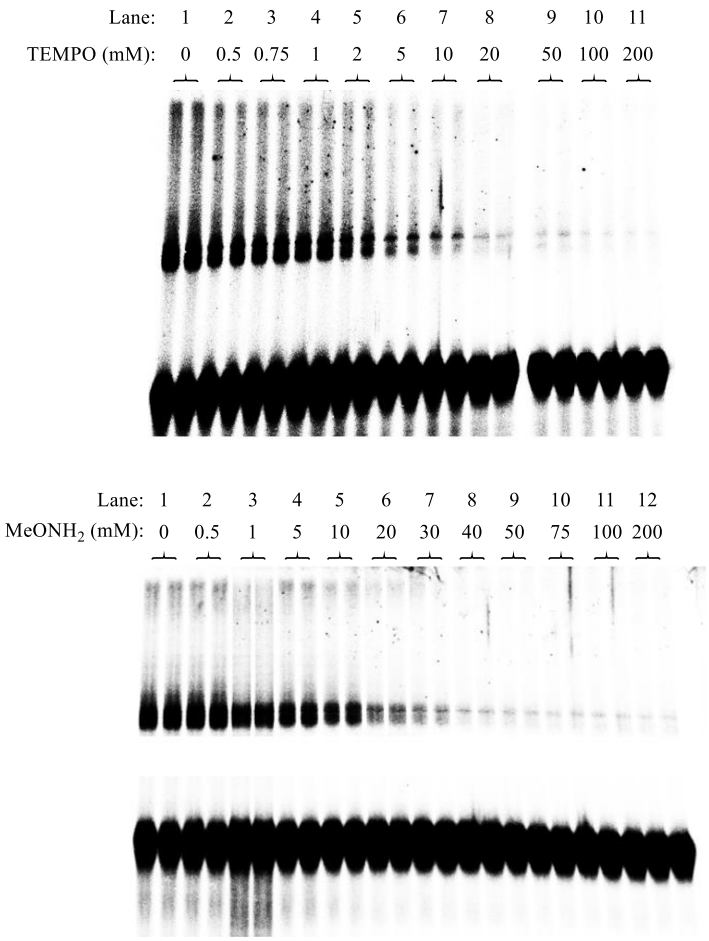

Figure 4-33. The effect of TEMPO and methoxyamine on DNA ICL formation of duplex **5** for **24d**. A mixture of **5** (50 nM) and **24d** (0.15 mM) in a pH 8 phosphate buffer was irradiated with 350 nm light for 32h in the presence of varying concentration of TEMPO (top) or $MeONH_2$ (bottom).

Chapter 5 Binaphthalene Phenyl Selenide Analogues as Photo and Hydrogen Peroxide Dual-Responsive DNA Interstrand Cross-linking Agents

5.1 Introduction

Selenium, a nonmetallic element, was first discovered in 1818 by a Swedish chemist.[1] Since then, it has been attracted a great attention. Selenium is presented in the various oxidation-state species, including selenide (Se^{2-}), selenate (SeO_4^-) or selenite (SeO_3^{2-}) and can be used as the fertilizers.[1] A trace amount of selenium is essential for cellular function in animals as well as humans. Organoselenium compounds, including the selenoproteins and selenium-containing amino acids, play the essential biochemical roles in the living organisms.[2] Among various selenoproteins, glutathione peroxidase is well known as a redox catalyst that participates in electron transfer processes to protect the organisms from oxidative damage.[2] Organic selenium-containing amino acids act as the direct and indirect antioxidants with a great potential use in therapeutics.[3]

Many selenium-based compounds showed great potential as anticancer drugs. They can attack the cancer cells without interfering the normal cells, such as decreasing the angiogenesis that may induce the cancers,[4] activating the tumor suppressor protein P53 and preventing the tumor development.[5] It is well known that selenium can reduce hydrogen peroxide. Many selenide compounds are selected as H_2O_2 acceptors to develop reactive oxygen species (ROS)-responsive prodrugs.[1,6] In the presence of H_2O_2, the selenides undergo oxidation to form selenoxides with a better hydrophilicity. Very recently, Mao group has developed seven ROS-responsive theranostic prodrugs with allyl phenyl selenides as H_2O_2 acceptors (Scheme 5-1).[7] These theranostic prodrugs contain allyl phenyl selenides as H_2O_2-activatable units, a cleavable linker, and camptothecin (CPT) as a topoisomerase inhibitor. The selenides in these prodrugs were oxidized to selenoxides, leading

to Mislow-Evans rearrangement followed by the hydrolysis of hemiacetal and 1,6-elimination reaction of phenoxide (Scheme 5-2). Finally, the active drug CPT was released. Due to much stronger fluorescence of CPT than prodrugs, the activation process can be monitored by fluorescence spectroscopy and the presence of H_2O_2 can be detected. In comparison with conventional boronate ester-based prodrug (Scheme 5-3), these selenide compounds showed better stability in PBS buffer and human plasma, higher efficiency of CPT release and excellent selectivity for tumor cells.

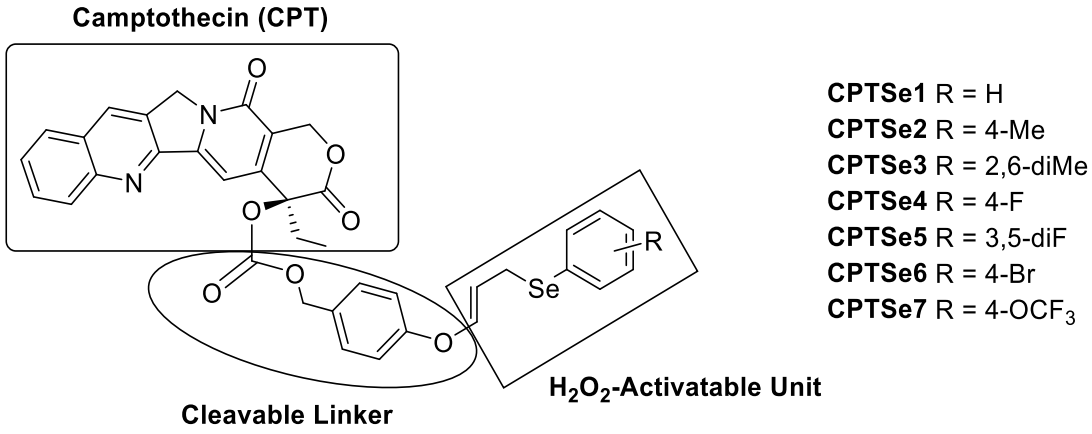

Scheme 5-7. Seven ROS-responsive theranostic prodrugs with allyl phenyl selenides as H_2O_2 acceptors.

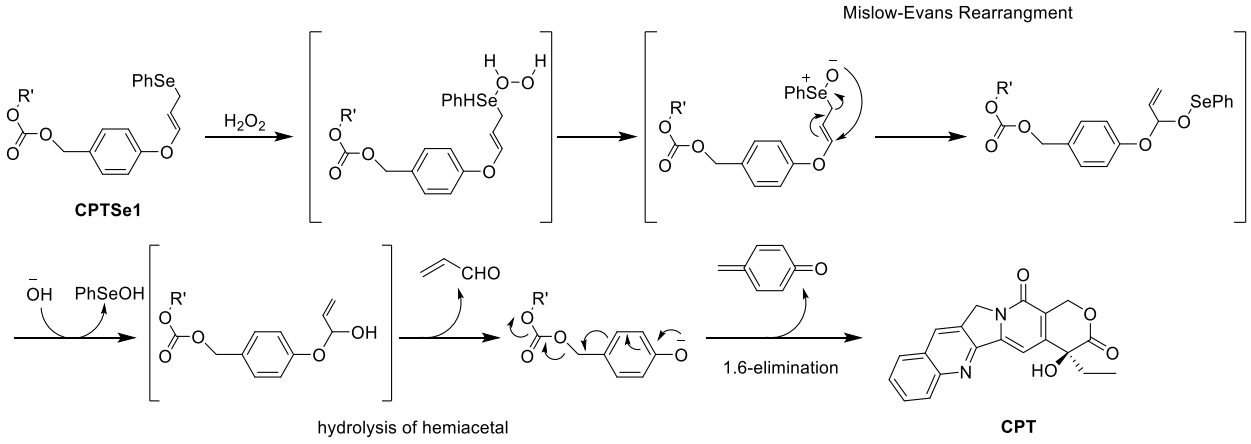

Scheme 5-8. The CPT release mechanism of **CPTSe1**.

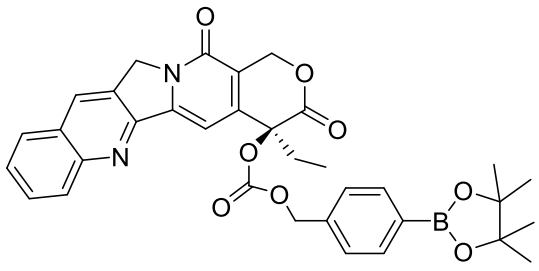

Scheme 5-9. Conventional boronate ester-based prodrug **CPT-B**.

Many antitumor drugs induce DNA ICL formation, which covalently bind two DNA strands, blocking DNA transcription and replication leading to cancer death.[8] Several alkylating agents with selenium have been reported to produce efficient DNA ICL formation upon activation of different oxidants. Greenberg research group showed that the phenyl selenide **V-1** and its derivative 5-methyl-2'-deoxycytidine **V-2** induced DNA ICL formation in the presence of various oxidants, including O_2, $NaIO_4$ and H_2O_2.[9,10] **V-1** and **V-2** can be oxidized to the phenyl selenoxides (**V-3** and **V-4**) by different oxidants to form the quinone methides (QMs, **V-5** and **V-6**) via [2,3]-sigmatropic rearrangement, inducing DNA alkylation with opposing dA or dG bases (Scheme 5-4). Inspired by the work of Greenberg's group, Zhou and his group developed three phenyl selenide compounds **V-7**-**V-9** and investigated their reactivities toward DNA (Scheme 5-5).[11] It was found that these selenide compounds can be activated upon oxidation and caused DNA interstrand cross-linking with oxidant $NaIO_4$ or light. Among them, **V-8** showed the highest ICL yield (80% with only 0.01 mM concentration).

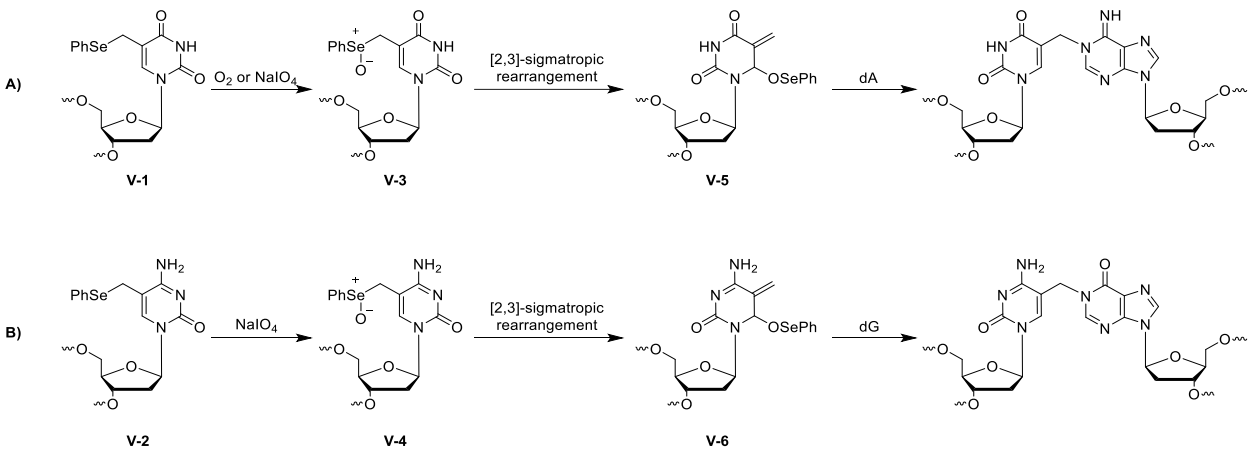

Scheme 5-10. DNA Interstrand Cross-Link Formation with **V-1** (A) and **V-2** (B) under Oxidative Conditions.

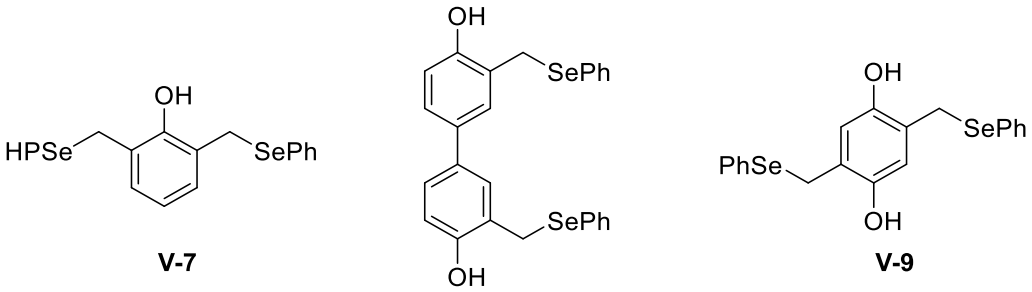

Scheme 5-11. Phenyl selenide compounds **V-7**-**V-9**.

Recently, Sun and his colleagues developed three phenyl selenide-based precursors **V-10**-**V-12** and explored their activities as H_2O_2-inducible DNA ICL agents (Scheme 5-6 (A) right).[12] Similar to the above work, these selenide precursors are oxidized to the selenoxide, releasing benzeneselenenic acid leaving group and promoting the generation of QMs. Compared with the boronate ester-based precursors (Scheme 5-6 (A) left) described in the earlier work, these phenyl selenide precursors are more stable under physiological conditions and showed a good capacity to increase the leaving group properties under specific conditions. In the presence of H_2O_2, the more inert leaving group (-SePh) was converted into a good leaving group, promoting the DNA ICL

formation (Scheme 5-6 (B)). The DNA ICL assay indicated that the introduction of para-substitution on the benzene ring enhanced the DNA ICL efficiency. The electron-withdrawing group (-OMe) showed the higher elevating effect than the electron-withdrawing group (-F) (**V-11** > **V-12** > **V-10**). In addition, these phenyl selenide compounds significantly inhibited on the growth of H1299 lung cancer cells.

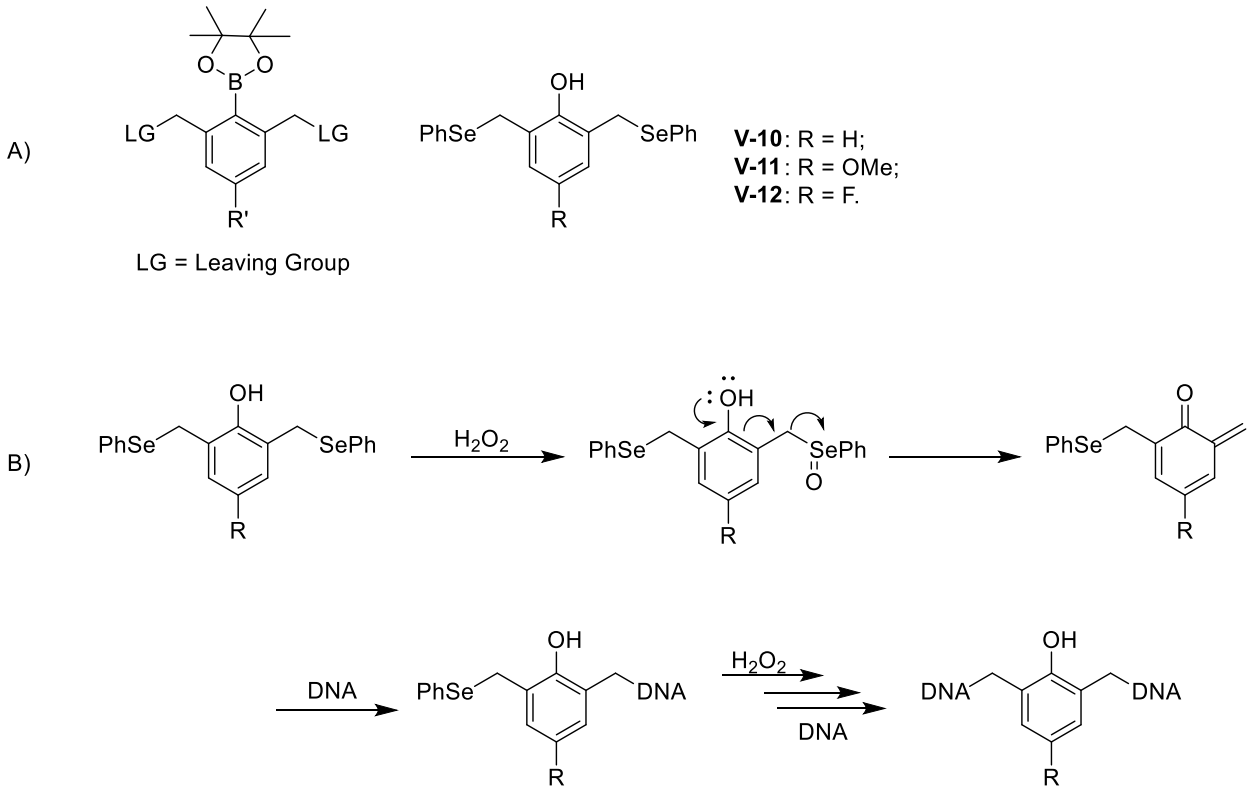

Scheme 5-12. A) Boronate ester-based precursors (left) and phenyl selenide-based precursors **V-10**-**V-12** (right); B) Proposed mechanism of DNA ICL formation with the phenyl selenide-based precursors.

All these previously described work with phenyl selenide-based compounds encouraged us to study the photo reactivity of binaphthalene phenyl selenide compound **12g** in the presence of H_2O_2. We investigated the effect of H_2O_2 on photo-induced ICL formation of **12g,** the optimal ratio of

H_2O_2 to **12g**, irradiation time and concentration of **12g,** and the mechanism of DNA ICL formation induced by **1g**.

5.2. H_2O_2 Enhances the Efficiency of Photo-Induced DNA ICL Formation by Bromo-Substituted Binaphthalene Selenide Compound

5.2.1 Photo-Induced DNA Interstrand Cross-Link Formation of 12g.

Bromo-substituted binaphthalene selenide analogue **12g** was synthesized as shown in Chapter 3.2.1 (Scheme 3-2). In this work, we studied the effect of H_2O_2 on photo-induced DNA ICL formation of **12g** with a 49-mer DNA duplex (**5**) (Chapter 2.2.2). Initially, the DNA ICL reaction was carried out with various concentrations of **12g** upon 8 h 350 nm irradiation with or without H_2O_2 in an Rayonet Model RPR-100 irradiator. The DNA interstrand cross-linking yield was determined by denaturing polyacrylamide gel electrophoresis (PAGE) with phosphorimager analysis (ImageQuant 5.2). Without UV irradiation, **12g** didn't produce DNA ICL products (Figure 5-1, lane 1 and lane 8) in the presence of H_2O_2 (the ratio of H_2O_2 to **12g** was 2:1), suggesting that H_2O_2 alone did not induce ICL formation with **12g**. However, H_2O_2 significantly improved the DNA ICL formation efficiency of **12g** upon 350 nm irradiation. A combination of **12g** (0.5 mM) and H_2O_2 (1.0 mM) produced 16% ICL products upon 350 nm irradiation for 8 h while only 4.8% ICL yield was observed for photo irradiation of **12 g** alone (Figure 5-1. lane 5 and lane 12). Similarly, the ICL yield increased 4 times with 1.0 mM 12g and H_2O_2 (2.0 mM) in comparison with 1.0 mM 12g alone. These data suggested that H_2O_2 greatly improved photo-induced DNA ICL formation of **12g**.

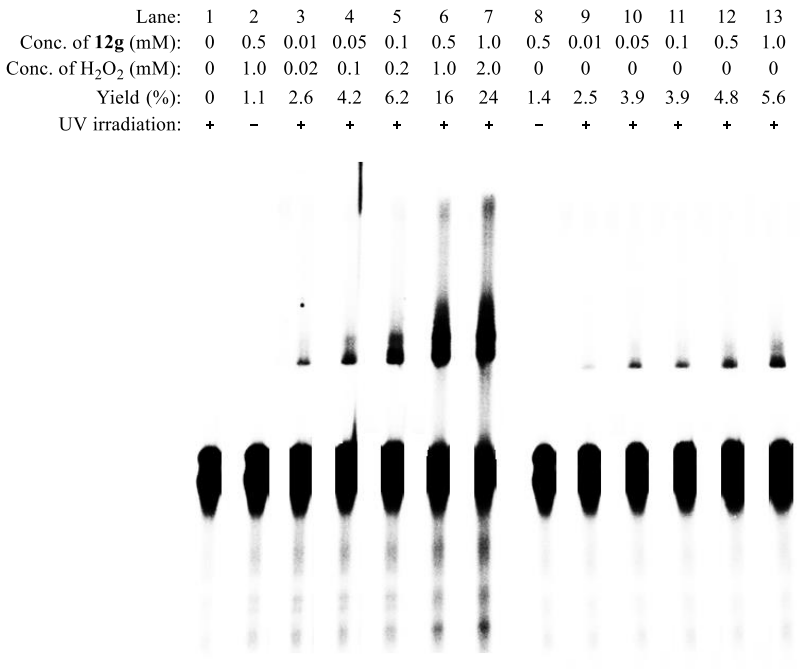

Figure 5-1. Photoinduced DNA interstrand cross-linking formation by **12g** upon 10 h irradiation (350 nm). Lane 1: DNA only; lane 2: DNA with 0.5 mM **12g** in the presence of 1.0 mM H_2O_2 without UV irradiation; lane 3-7: DNA with **12g** in the presence of H_2O_2; lane 8: DNA with 0.5 mM **12g** in the absence of H_2O_2 without UV irradiation; lane 9-13: DNA with **12g** in the absence of H_2O_2.

Further investigation suggested that a few parameters affected the ICL efficiency of **12g**, including solvent, the concentration ratio of H_2O_2 to **12g,** and incubation time before photo irradiation. Due to the poor solubility of **12g** in a phosphate buffer that is typically used for DNA cross-linking study, CH_3CN was added as an auxiliary solvent. Although **12g** can be completely dissolved in CH_3CN, it easily precipitated out when high concentration of **12g** in CH_3CN was mixed with DNA in a phosphate buffer. To avoid the precipitation, we did further study with **12g** at a low concentration (0.1 mM), including optimization of the concentration ratio of H_2O_2 to **12g** and time-dependent study. An optimum ratio of **12g** to H_2O_2 was between 1:3 and 1:4, which yielded the highest ICL yield (Figure 5-2). Thus, the time-dependent study was performed with 0.1 mM **12g**

and 0.4 mM H_2O_2. To ensure **12g** oxidation by H_2O_2, we incubated the ICL reaction mixture of DNA, **12g**, and H_2O_2 at 37℃ before photo irradiation. Different incubation time (ranging from 1 to 5 h) was tested, which slightly affected the subsequent photo-induced DNA cross-linking (Figure 5-3). Under all conditions tested, much higher ICL yields were observed with combination of 0.1 mM **12g** and 0.4 mM H_2O_2 than 0.1 mM **12g** alone, which provide further evidence that H_2O_2 favors photo-induced ICL formation by **12g**. Incubation of ICL reaction mixture at 37℃ before photo irradiation slightly increased the ICL yields by 3%-5%. However, we did not observe significant influence of different incubation time (1-5 h) on the ICL reaction. Although slightly higher ICL yields were observed with the samples that were incubated longer prior to irradiation, the longer incubation time also led to serious DNA damage. For example, the samples with 5 h incubation prior to irradiation produced the highest cross-linking yield of 22.6%, but also caused more DNA damage than those incubated for 1 h, 3 h, or 4 h. Therefore, we chose 1 hour incubation time for further studies. The time-dependent study showed that the optimal irradiation time was 22 h for the DNA sample with 1 h incubation and the cross-linking yield was 18.4% (Figure 5-4). The yield was a little higher with longer irradiation time (i.e. 24 h), but more DNA damage was observed. With the optimized reaction time, we determined the optimal concentrations of **12g** and H_2O_2 (Figure 5-5). The results showed that 0.5 mM **12g** with 2.0 mM H_2O_2 produced the highest cross-linking yield (26.1%) with less DNA damage. Although slightly higher ICL yields were observed with 0.75mM **12g** with 3.0 mM H_2O_2 and 1.0 mM **12g** with 4.0 mM, serious DNA damage was also detected, which can affect the accuracy of ICL yield determination. With the optimal irradiation conditions, we will study the effect of solvent ratio (phosphor buffer: MeCN) on DNA cross-linking efficiency. Collectively, our study demonstrated that **12g** can act as photo and H_2O_2 dual responsive DNA cross-linking agents.

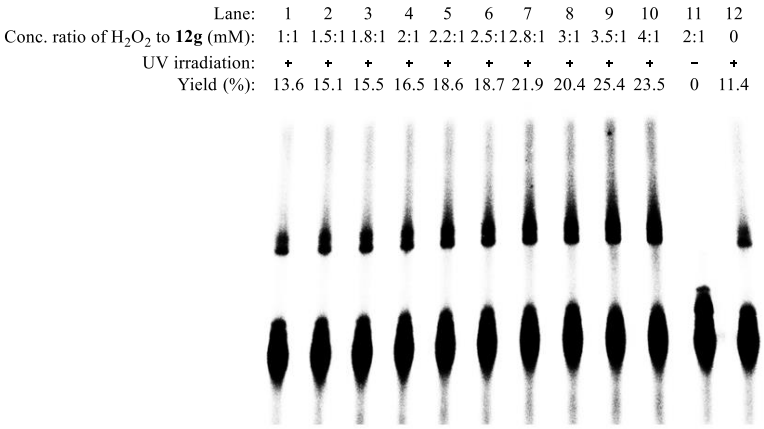

Figure 5-2. DNA ICL formation by 0.1 mM **12g** in the presence of H_2O_2 with different concentrations.

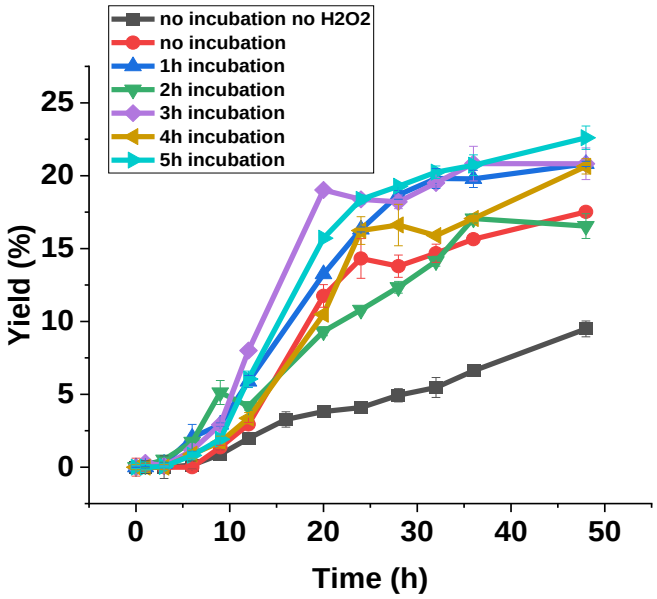

Figure 5-3. Time-dependent cross-linking study of 0.1 mM **12g** in the presence with 0.4 mM H_2O_2. DNA samples were incubated under 37℃ for various hours before the irradiation. The concentration ratio of H_2O_2 to **12g** was 4:1.

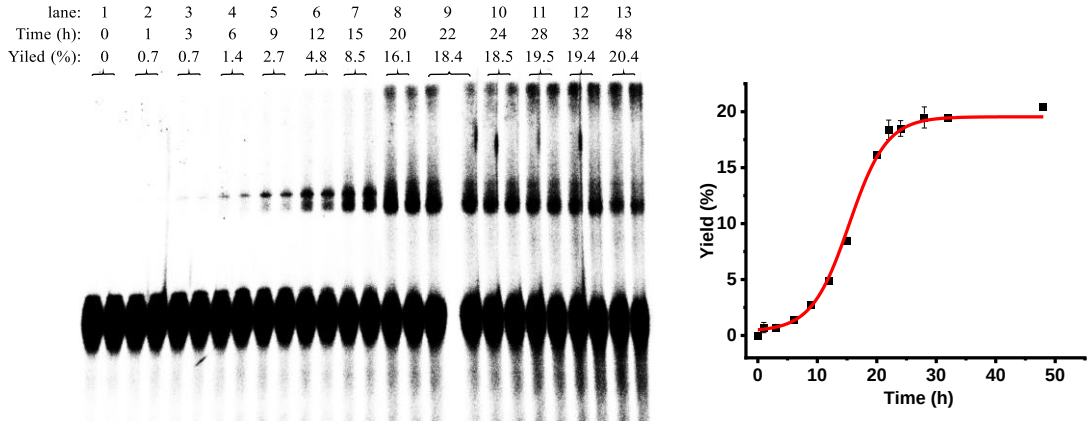

Figure 5-4. Time-dependent cross-linking study of DNA with 0.1 mM **12g** and 0.4 mM H_2O_2. The samples were incubated under 37℃ for 1 hour before the irradiation. The data was presented as average from duplicate samples.

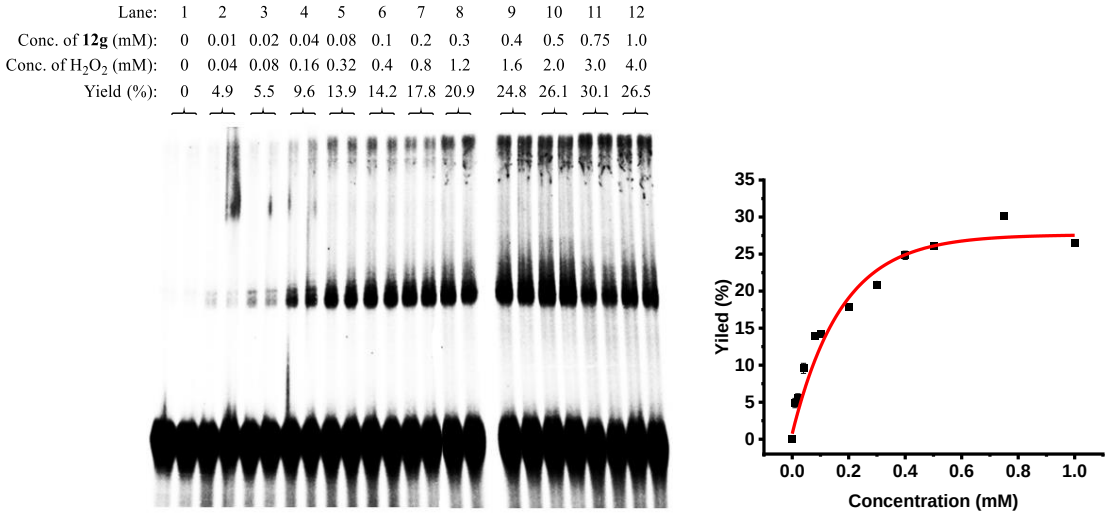

Figure 5-5. Concentration-dependent cross-linking study of DNA with **12g** and H_2O_2. The samples were incubated under 37℃ for 1 hour before the irradiation. The data was presented as average from duplicate samples.

In order to determine whether H_2O_2-enhanced ICL formation is unique to phenyl selenide analogue **12g** or a general property of photo-activatable binaphthalene analogues, we tested the effect of H_2O_2 on photo-induced DNA ICL formation by **12f** containing a phenyl thio group (Figure 5-6). The ICL yields produced by **12f** in the presence of H_2O_2 only slightly increased in comparison with those without H_2O_2, which was observed only with high concentrations of **12f** but not low concentrations. The biggest ICL yield enhancement of **12f** induced by H2O2 was about 4% when

more than 0.5 mM **12f** was employed (Figure 5-6, lane 5 vs. lane 12; lane 6 vs. lane 13). The data suggested that **12f** may not act as a photo- and H_2O_2 dual responsive DNA cross-linker that is a unique property of the binaphthalene phenyl selenide **12g**. We are testing other analogues to provide further evidence on this conclusion.

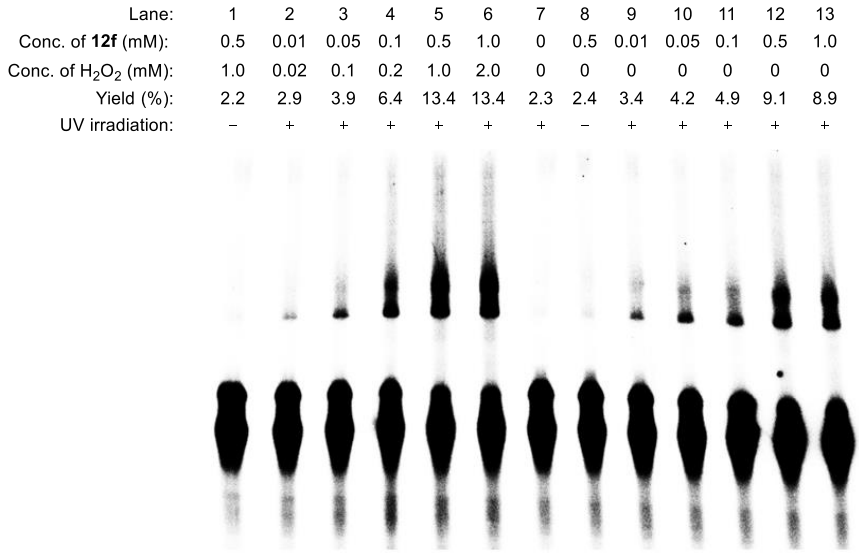

Figure 5-6. Photoinduced DNA interstrand cross-linking formation by **12f** upon 8 h irradiation (350 nm). Lane 1: DNA with 0.5 mM **12f** in the presence of 1.0 mM H_2O_2 without UV irradiation; lane 2-6: DNA with **12f** in the presence of H_2O_2; lane 7: DNA only; lane 8: DNA with 0.5 mM **12f** in the absence of H_2O_2 without UV irradiation; lane 9-13: DNA with **12f** in the absence of H_2O_2.

5.2.2. Mechanism Investigation of Photo-Induced DNA ICL Formation by 12g in the presence of H_2O_2.

Most bifunctional aromatic compounds were reported to induce DNA ICL formation via photogenerated carbocations. Two pathways were proposed for the carbocation generation, either homolysis of C-X bond (X: leaving group) or heterolysis of C-X bond.[13] Previous study showed that homolysis of C-SePh bond occurred with **12g** upon 350 nm irradiation in the absence of H_2O_2

to generate free radical that was spontaneously oxidized to the corresponding cation directly producing DNA ICL products (Chapter 3.2.3). In order to determine whether H_2O_2 affects the mechanism for photo-induced DNA ICL formation by **12g**, we investigated the pathway of carbocation formation induced by **12g** in the presence of H_2O_2. Similar to our previous work, 2,2,6,6-tetramethylpiperidin-1-oxyl (TEMPO) was employed as radical trapper and methoxyamine ($MeONH_2$) as carbocation trapper. Both TEMPO and $MeONH_2$ were tested separately with 0.1 mM **12g** and 0.4 mM H_2O_2. The results are shown in Figure 5-7, which indicates that the cross-linking yield decreased with the increasing concentration of TEMPO or $MeONH_2$. When the concentration of TEMPO or $MeONH_2$ reached 200 mM, the DNA cross-linking yields dropped to ~ 3 %, demonstrating that both free radical and cation were involved in the DNA cross-linking process. We concluded that homolysis of C-SeOPh bond occurred to form the naphthalenylmethyl free radical that was oxidized to the corresponding cation. The proposed mechanism of photo-induced ICL formation by **12g** in the presence of H_2O_2 is shown in Scheme 5-7. The phenyl selenide group in **12g** was oxidized to the phenyl selenoxide in the presence of H_2O_2 to generate **V-13** containing a good leaving group, which produced free radical **V-14** upon 350 nm irradiation. Radical **V-14** was further oxidized to cation **V-15** via one-electron transfer. Monomer trapping reactions with TEMPO and methoxyamine will be performed to obtain direct evidence for the radical and carbocation formation.

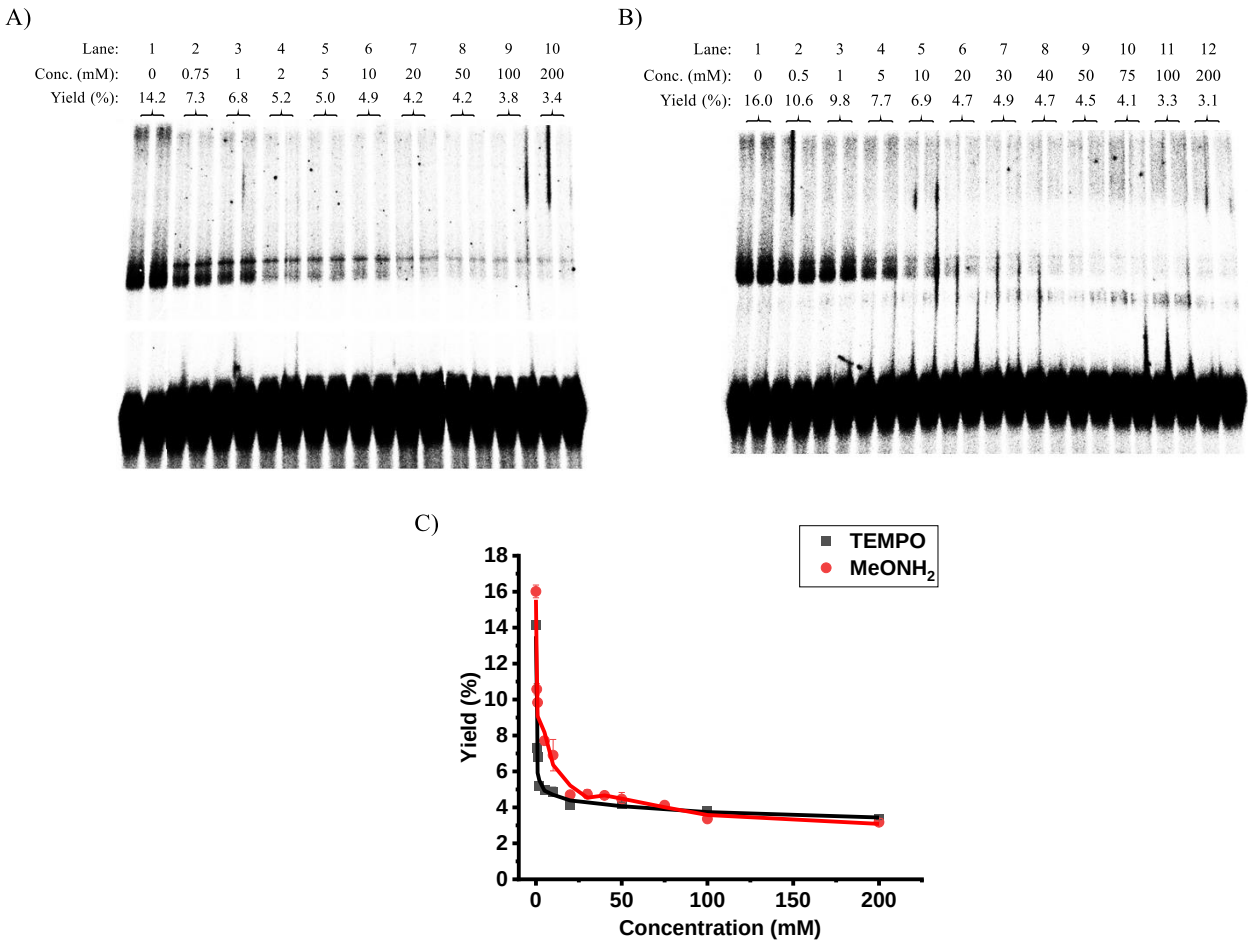

Figure 5-7. The effect of TEMPO and methoxyamine on DNA interstrand cross-linking induced by **12g** in the presence of H_2O_2. A mixture of **5** (50 nM) and **12g** (0.1 mM) with H_2O_2 (4.0 mM) in a pH 8 phosphate buffer was irradiated with 350 nm light for 22 h in the presence of varying concentration of TEMPO (**A**) or $MeONH_2$ (**B**).

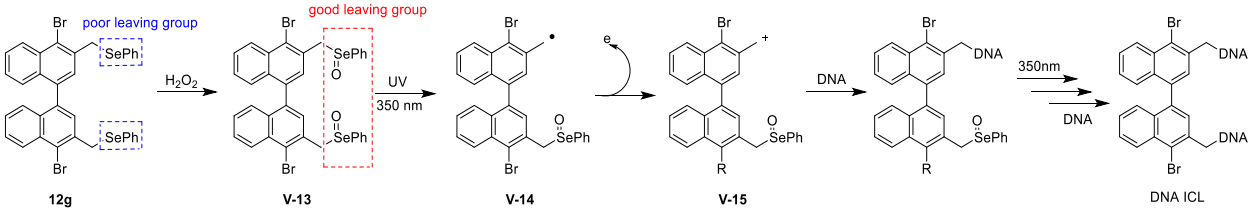

Scheme 5-7. Proposed mechanism of photo-induced DNA ICL formation by **12g** in the presence of H_2O_2.

5.2.3. Conclusions

In this work, we studied the effect of H_2O_2 on photo-induced DNA ICL formation by **12g**. The presence of H_2O_2 significantly increased the efficiency of DNA ICL formation induced by **12g** with 3-4 times increase of ICL yields. We propose that H_2O_2 convert a poor leaving group phenyl selenide to the phenyl selenoxide as a good leaving group, which promoted the homolysis of C-X bond and the subsequent DNA alkylation with nucleosides. Further study showed that both free radical and cation trapper (TEMPO and $MeONH_2$) prevented DNA ICL formation, which provided evidence for that both radicals and carbocations were produced during the photo-induced DNA cross-linking process. The free radicals formed via the homolysis of C-X bond was further oxidized to the carbocation via one-electron transfer. To provide direct evidence for the proposed carbocation mechanism, we will perform the monomer reactions with **12g** and two trapping agents, TEMPO and $MeONH_2$. The effect of the volume ratio of phosphor buffer to organic solvent needed to dissolve **12g** as well as the alkylation sites will be determined. In addition, the cytotoxicity of **12g** in cancer cells will be investigated. Different conditions will be tested, including with and without UV irradiation and/or H_2O_2.

5.3. Experimental Section

General Information. Compound **12g** was synthesized and its structure was confirmed in previous study (Chapter 3). H_2O_2 was purchased from Sigma-Aldrich® and used directly with dilution. The oligonucleotides (ODNs) were synthesized by DNA/RNA ABI synthesizer (Model. 394 from AZCO® BioTech. Inc.), deprotected and further purified as shown in previous studies.

ODNs were labelled with [γ-^{32}P] ATP following standard procedure and hybridized under 90 °C for 5 min and cool to r.t. to form 49-mer DNA duplex **5**.

DNA ICL Formation. Certain amount of **12g** was dissolved in CH_3CN to make the compound solutions with different concentrations (0.1/3 mM-10/3 mM). 30 wt. % H_2O_2 solution (in H_2O) was diluted to the solutions with various concentrations (0.4 mM - 40 mM). 100 mM potassium buffer (pH 8, 2 μL), 1 M NaCl (2 μL), H_2O_2 (2 μL) and **12g** in CH_3CN (6 μL) were added to the ^{32}P-labeled ODN duplex (2 μL, 0.5 μM). Autoclaved water was added to give a final volume of 20 μL (final concentration range of **12g**: 0.01-1.0 mM; final concentration range of H_2O_2: 0.04 mM - 4.0 mM). Then, the reaction mixture was irradiated upon 350 nm UV light, quenched by 20 μL of 90% formamide loading buffer and subjected to 20% denaturing PAGE.

Free-Radical-Trapping Assay of DNA ICL Formation. Certain amount of TEMPO was dissolved in CH_3CN and diluted to the solutions with different concentrations (10/3 mM-4000/3 mM). 100 mM potassium buffer (pH 8, 2 μL), 1 M NaCl (2 μL), H_2O_2 (4 mM, 2 μL), TEMPO (3 μL) and **12g** in CH_3CN (2/3 mM, 3 μL) were added to the ^{32}P-labeled ODN duplex (2 μL, 0.5 μM). 6 μL of autoclaved distilled water was added in the mixture to give a total volume of 20 μL (final TEMPO concentration: 0.5 mM-200 mM; final concentration of **12g**: 0.1 mM; final concentration of H_2O_2: 0.4 mM). The reaction mixture was irradiated with 350 nm light for 22 h, quenched with 20 μL of 90% formamide loading buffer and subjected to 20% denaturing PAGE.

Carbocation Trapping Assay of DNA ICL Formation. A solution of $MeONH_2$·HCl (2 M) was titrated with NaOH (5 M) to pH 7.0, which was diluted to the desired concentration (10/2 to 4000/ 2 mM). 100 mM potassium buffer (pH 8, 2 μL), 1 M NaCl (2 μL), H_2O_2 (4 mM, 2 μL), methoxyamine solution (2 μL) and **12g** in CH_3CN (1/3 mM, 6 μL) were added to the ^{32}P-labeled ODN duplex (2 μL, 0.5 μM). 4 μL of autoclaved distilled water was added in the mixture to give

a total volume of 20 μL (final methoxyamine concentration: 0.5 mM-200 mM; final concentration of **12g**: 0.1 mM; final concentration of H_2O_2: 0.4 mM). The reaction mixture was irradiated with 350 nm light for 22 h, quenched with 20 μL of 90% formamide loading buffer and subjected to 20% denaturing PAGE.

5.4. References

(1) Sortiano-Garcia M. Organoselenium Compounds as Potential Therapeutic and Chemopreventive Agents: A Review. *Current Medicinal Chemistry*. **2004**, 11, 1657-1669.

(2) Stadtman, T.C. New Biologic Functions – Selenium-Dependent Nucleic Acids and Proteins. *Fundamental and Applied Toxicology*. **1983**, 3, 420-423.

(3) Rahmanto, A. S.; Davis, M. J. Selenium-Containing Amino Acids as Direct and Indirect Antioxidants. *IUBMB Life*. **2012**, 64, 863-871.

(4) Collery, P. Strategies for the Development of Selenium-Based Anticancer Drugs. *Journal of Trace Elements in Medicine and Biology*. **2018**, 50, 498-507.

(5) Bjorkhem-Bergman, L.; Torndal, U.; Eken, S.; Nystrom, C.; Capitanio, A.; Larsen, E. H.; Bjornstedt, M.; Eriksson, L. C. Selenium Prevents Tumor Development in A Rat Model for Chemical Carcinogenesis. *Carcinogenesis*. **2015**, 26, 125-131.

(6) Balance, W. C.; Qin, E. C.; Chung, H. J.; Gillette, M. U.; Kong, H. Reactive Oxygen Species-Responsive Drug Delivery Systems for The Treatment of Neurodegenerative Disease. *Biomaterials*. **2019**, 217, 119292-119310.

(7) Yang, X.; Yuan, B.; Xiong, H.; Zhao, Y.; Wang, L.; Zhang, S.; Mao, S. Ally Phenyl Selenides as H_2O_2 Acceptors to Develop ROS-Responsive Theranostic Prodrugs. *Bioorganic Chemistry*. **2022**, 129, 106164-105175.

(8) Fan, H.; Peng, X. Novel DNA Cross-Linking Reagents. *In Advances in Molecular Toxicology*; Fishbein, J. C.; Heilman, J. M., Eds.; Elsevier, 2016; Vol. *10*, pp 235−292.

(9) Hong, I. K.; Ding, H.; Greenberg, M. M. Radiosensitization by a Modified Nucleotide that Produces DNA Interstrand Cross-Links under Hypoxic Conditions. *J. Am. Chem. Soc*. **2006**, 128, 2230-2231.

(10) Peng, X.; Hong, I. S.; Li, H.; Seidman, M. M.; Greenberg, M. M. Interstrand Cross-Link Formation in Duplex and Triplex DNA by Modified Pyrimidines. *J. Am. Chem. Soc*. **2008**, 130, 10299-10306.

(11) Weng, X.; Ren, L.; Weng, L.; Huang, J.; Zhu, S.; Zhou, X.; Weng, L. Synthesis and Biological Studies of Inducible DNA Cross-Linking Agents. *Angew. Chem*. **2007**, 119, 8166-8169.

(12) Yu, D.; Fan, H.; Sun, J.; Xue, L.; Wang, L.; Jia, Y.; Tiuan, J.; Sun, H. Phenyl Selenide-Based Precursors as Hydrogen Peroxide Inducible DNA Interstrand Cross-Linkers. *ChemBioChem*. **2022**, 23, e202200086.

(13) Lin, Z.; Fan, H.; Zhang, Q.; Peng, X. Design, Synthesis, and Characterization of Binaphthalene Precursors as Photoactivated DNA Interstrand Cross-Linkers. *J. Org. Chem.* **2018**, 83, 8815−8826.

Chapter 6 The Effect of Chirality of BINOL Precursors on DNA Interstrand Cross-Link (ICL) Formation

6.1. Introduction

The history for human to utilize natural chiral drugs has been very long, but the chirality was not recognized until the first half of 19th century.[1] In biological system, the enantiomers of a compound can be regarded as different molecular entities due to different behaviors and disparities in pharmacological response.[2] The stereoisomers of a drug can selectively interact with different enzymes, receptors and other binding molecules, undergoing different metabolic pathways and resulting in various types and/or number of metabolites. For example, *S*-Thalidomide can cause birth defects but *R*-Thalidomide is used to treat morning sickness (Scheme 6-1).[3] However, Thalidomide was commercially marketed as a racemate and it was difficult to avoid racemic product due to the considerable racemization during the incubation of pure *R*-thalidomide in buffer solution or serum.[4] Therefore, the different biological properties of the enantiomers were always under debate until Hakoshima, Handa, and their co-workers finally proved the teratogenicity of *S*-thalidomide via structural and biochemical studies of the enantiomers of thalidomide coordinated to cereblon (CRBN) in 2018.[5] Another example is carvone which exists in more than one hundred essential oils.[6] It was found that L-carvone showed higher toxicity than D-carvone toward the insects, such as R. *dominica*, S. *oryzae* and T. *castaneum* (Scheme 6-2). Due to the higher contact toxicity, lower dose was needed to suppress the egg hatching for L-carvone than its D-enantiomer. The L-carvone is a more potent ovicide, larvicide and adulticide.[6]

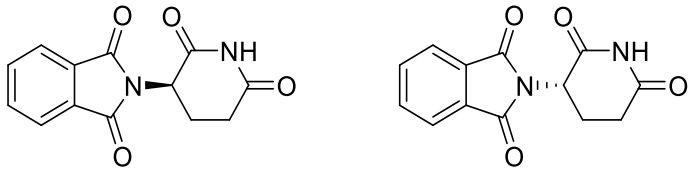

(R)-Thalidomide (S)-Thalidomide

Scheme 6-5. The Stereoisomers of Thalidomide.

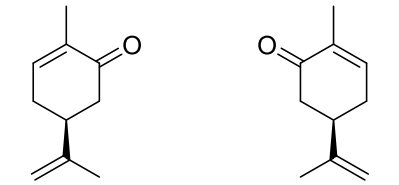

D-Carvone L-Carvone

Scheme 6-6. The Enantiomers of Carvone.

1,1′-Bi-2-naphthol (BINOL) has axial chirality. Different from thalidomide, BINOL has two enantiomers that can be readily separated and are stable toward racemization. Freccero group developed and investigated BINOL quaternary ammonium derivatives as the precursors for inducing DNA interstrand cross-linking via alkylation (Scheme 6-3A).[7] The computational study showed that the DNA cross-linking efficiency was influenced by axial chirality and other features.[7] Freccero group later synthesized a series of BINOL-amino acid derivatives (BINOLAMs) (Scheme 6-3B) and tested their photoreactivity, DNA cross-linking properties and photocytotoxicity.[8] The research showed that diastereoisomer (*R*,*S*,*S*)-**6** is slightly more photoreactive than (*S*,*S*,*S*)-**6**. Photo irradiation of (*R*,*S*,*S*)-**6** generated the monohydrated adduct with a higher conversion yield (56%) than (*S*,*S*,*S*)-**6** (37%). However, later work suggested that no obvious difference in DNA cross-linking capability was observed with these BINOL derivatives.

The chiral properties of these compounds did not confer appreciably different biological activities. The chirality of BINOL-amino acid derivatives had little effect on DNA ICL formation.

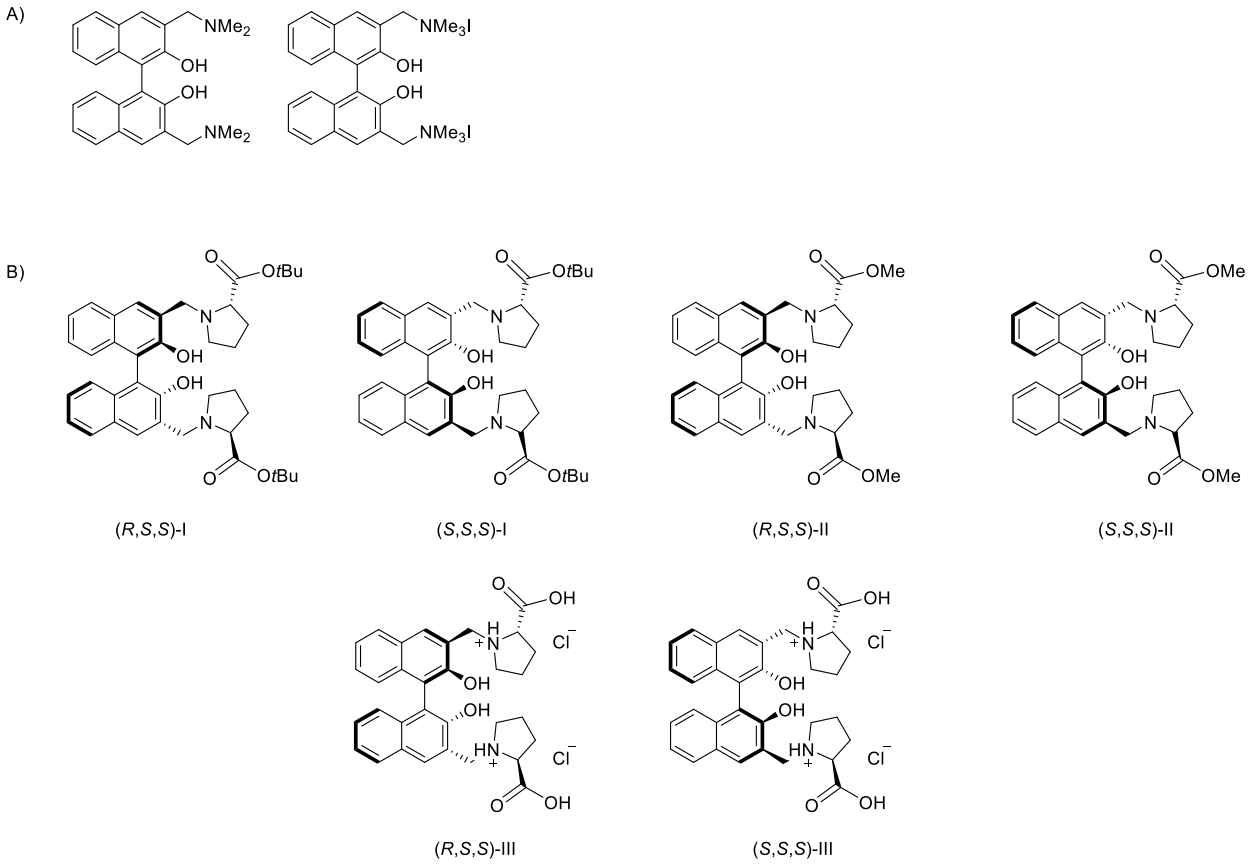

Scheme 6-7. A) BINOL Quaternary Ammonium Derivatives; B) BINOL-Amino Acid Derivatives I-III (BINOLAMs).

It is worthy to note that the BINOL-amino acid derivatives studied by Freccero group produced DNA cross-linking via quinone methide (QM) formation. There is still limited study of the effect of chirality on photoinduced DNA ICL formation via carbocation formation mechanism. Therefore, we design and synthesize several BINOL precursors with different configurations and test their DNA cross-linking efficiency, to figure out the chirality effect on DNA ICL formation.

6.2. The Efficiency of BINOL Precursors on DNA Interstrand Cross-link Formation.

6.2.1. Synthesis

We designed and synthesized three BINOL precursors **34**-**36** and investigated their photo chemical reactivity towards DNA (Scheme 6-4). Compounds **34**-**36** were synthesized starting from [1,1'-binaphthalene]-2,2'-diol (**30a-c**) with different configurations, including racemic (**30a**), rectus *R* (**30b**) or sinister *S* (**30c**). Compounds **30a-c** were converted to the ether analogues **31a-c** by treatment with chloromethyl ethyl ether ($ClCH_2OCH_2CH_3$) and sodium hydride (NaH) in tetrahydrofuran (THF). The aldehyde group was introduced to **31a-c** using N-butyllithium and tetramethylethylenediamine (TMEDA) to form compounds **32a-c** that was further reduced to **33a-c** by reacting with sodium borohydride ($NaBH_4$) in methanol/THF solution at 0 °C. Finally, the BINOL derivatives **34a-c** were obtained by treating **33a-c** with iodomethane and NaH in DMF at rt. Compounds 34a-d underwent acid-catalyzed ether cleavage to generate the BINOL derivatives **35a-c** that was transformed to **36a-c** with phosphorous oxychloride and 1 M hydrochloric acid. All new compounds (BINOL **34**, **35** and **36**) were confirmed by NMR.

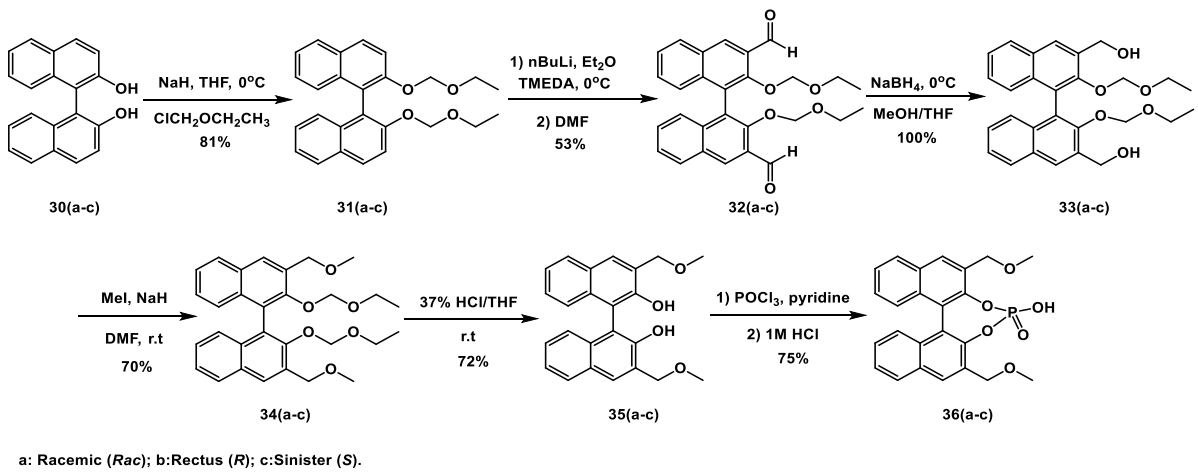

Scheme 6-8. Synthesis of BINOL precursors **34**, **35** and **36**.

6.2.2. DNA Cross-linking Assay.

Organic solvent was used as auxiliary solvent to dissolve compounds in DNA cross-linking study. Different organic solvents influenced the efficiency of DNA ICL formation. We chose three organic solvents, including acetonitrile (CH_3CN), dimethyl sulfoxide (DMSO) and dimethylformamide (DMF), to dissolve the BINOL precursors for DNA cross-linking study. Same to previous studies, a 49-mer DNA duplex (**5**) was used in the photo-irradiation with compounds **34**-**36** upon 350 nm irradiation. The DNA interstrand cross-linking yields were determined by denaturing polyacrylamide gel electrophoresis (PAGE) with phosphorimager analysis (ImageQuant 5.2). DNA with 1.0 mM **34**-**36** were irradiated upon UV irradiation for 48 h. The results showed that different organic solvents affected DNA ICL formation induced by **34**-**36** (Figure 6-1). When DMF was used as an auxiliary solvent for dissolving the precursors **34**-**36**, efficient ICL formation was observed with all compounds tested. The highest ICL yields were observed for **36a-c** while DNA damage was also detected. With DMSO as an organic solvent, only **34** produced stable DNA ICL products, while serious DNA damage was observed with **35** and **36,** which affected ICL formation. When CH_3CN was used, efficient ICL formation was observed with **34** and **35** but not with **36**. Overall, among three organic solvents tested, DMSO is not suitable for photo-induced DNA cross-linking study, MeCN works for **34** and **36**, and DMF can be used for all three compounds. Higher ICL yields were observed with **34** and **36** in MeCN than that in DMF. Compounds with different configurations showed a slight difference on DNA ICL formation (Table 6-1). Most precursors which were racemic obtained higher cross-linking yields with different organic solvents (Figure 6-2). For example, *Rac*-**34** obtained 18% cross-linking yield which was higher than 11% of *R*-**34** and 9% of *S*-**34** with DMF and *Rac*-**35** showed 8% higher than *R*-**35** and 4% higher than *S*-**35**. Dissolved in CH_3CN, both *Rac*-**34** and *Rac*-**35** showed the

highest cross-linking yields than compounds with other configurations (*Rac*-**35** obtained the same yield as *R*-**35**: 38%). Although CH_3CN was not a good solvent for all three precursors on DNA cross-linking formation, it caused the higher cross-linking yields of **6** and **7** than other two solvents. Therefore, CH_3CN was chosen as auxiliary organic solvent for more cross-linking study.

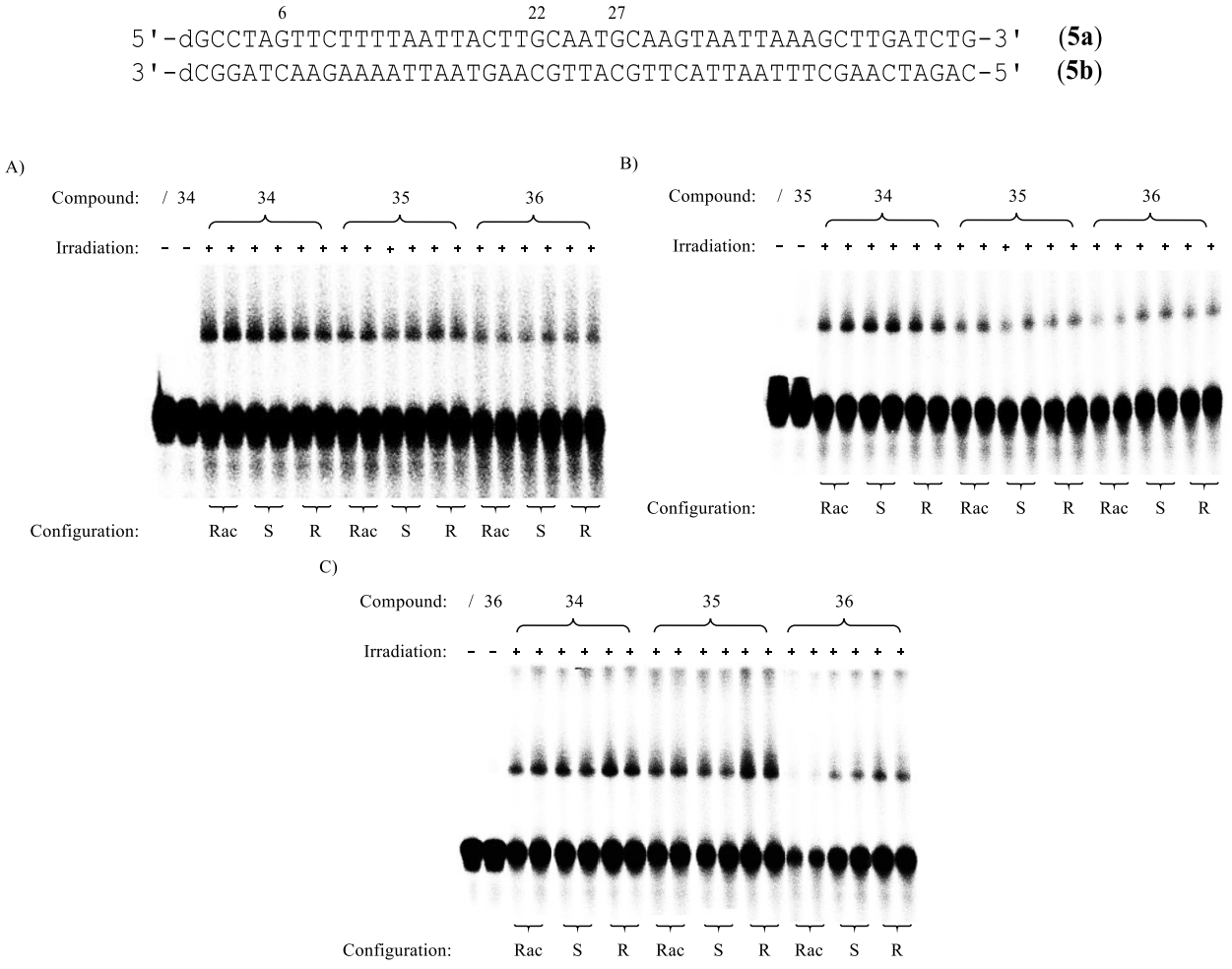

Figure 6-2. Gel images of DNA ICL formation photo-induced by **34-36** dissolved in different organic solvents: (A) dissolved in DMF; (B) dissolved in DMSO; (C) dissolved in CH_3CN.

	BINOL **34**			BINOL **35**			BINOL **36**		
	R	*S*	*Rac*	*R*	*S*	*Rac*	*R*	*S*	*Rac*
DMF	11%	9%	18%	14%	18%	22%	21%	19%	24%
DMSO	21%	17%	20%	n.d. [a]	n.d.	n.d.	n.d.	n.d.	n.d.

CH_3CN	19%	26%	28%	38%	32%	38%	n.d.	n.d.	n.d.

Table 6-1. DNA interstrand cross-linking yields induced by BINOL **34-36** which dissolved in various organic solvents. [a] The ICL yield was not determined due to the DNA damage.

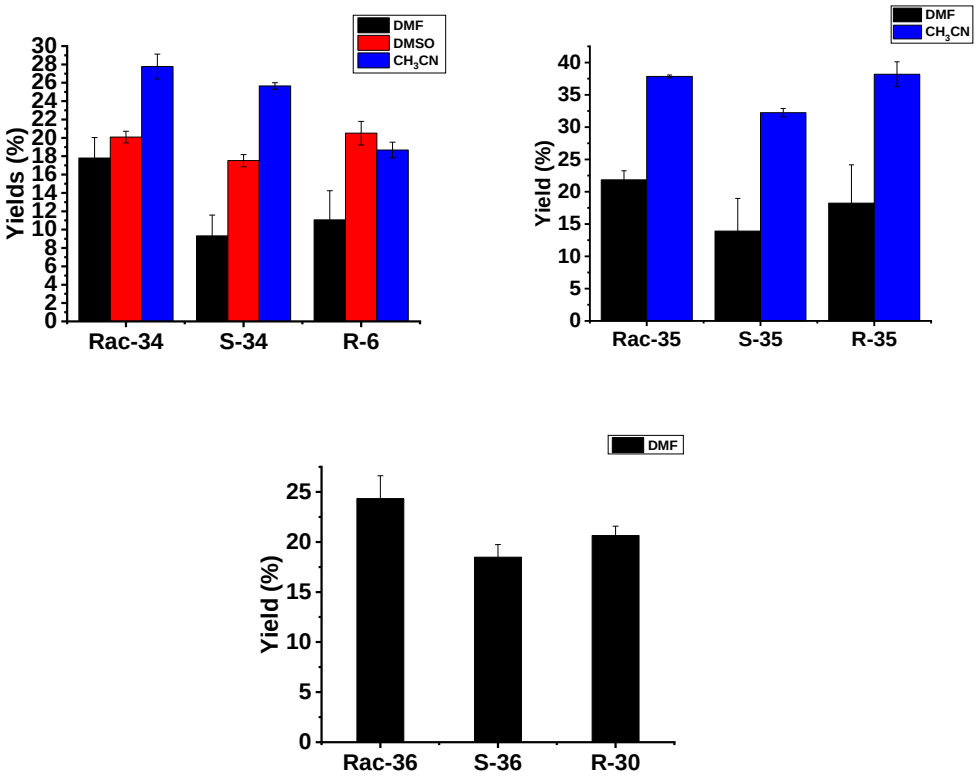

Figure 6-3. DNA cross-linking yields of BINOL **34-36** with different configurations.

Since efficient ICL formation and less DNA damage were observed for **34a-c** upon photo irradiation in different solvent systems, **34a-c** was chosen for further investigation of the effect of chirality on the ICL reaction rate and optimum compound concentration. Thus, we did time- and concentration-dependent study with **34a-c** using MeCN as an auxiliary organic solvent. For time-dependent study, 1 mM of **34a-c** and duplex **5** were irradiated 350 nm light for 36 h. The ICL yields were determined at different time spots (Figure 6-3). The optimal cross-linking yields were

obtained for **34a-c** [24.7% for 34a (*R*), 22.8% for 34b (*S*), and 23.7% for 34c (racemic)] after 28 h irradiation (Figure 6-3A-C). The difference of the optimal DNA ICL yields with different configurations was less than 2% (Figure 6-3. (D)), indicating the chirality of BINOL **34** didn't have a great impact on DNA ICL formation. Then, we did concentration-dependent study for **34a-c** with 28 h 350 nm irradiation (Figure 6-4). All three compounds showed the same optimum concentration of 1.0 mM that produced the highest ICL yields. Furthermore, similar optimum ICL yields were observed for **34a-c** with only 0.6% difference, which are within the experimental errors (*R*-**34a**: 20.2%, *S*-**34b**: 20.8%, *Rac*-**34c:** 20.8%). Both time- and concentration-dependent study didn't show large discrepancy on DNA ICL formation induced by different configurations, suggesting that the chirality didn't influence the efficiency of ICL formation. It is highly likely that due to the small size of **34**, different configurations do not affect its binding interaction with DNA double helixes that have relative much larger size.

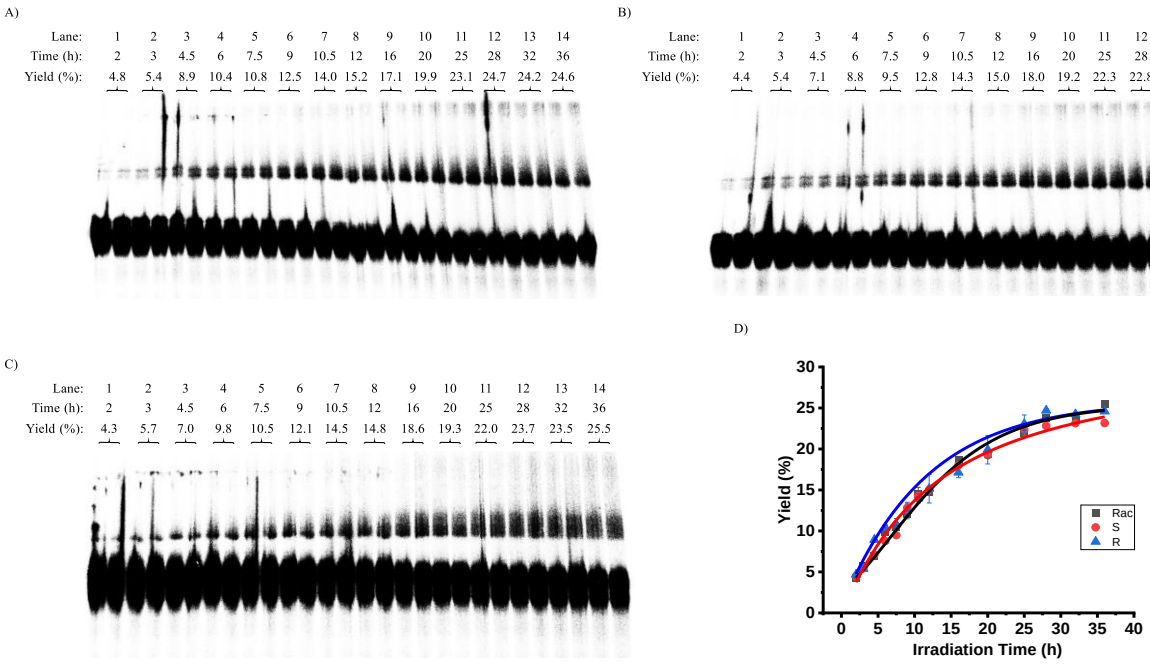

Figure 6-4. Time-dependent study of BINOL **34** with different configurations. (A) Representative gel of *R*-**34**; (B) representative gel of *S*-**34**; (C) representative gel of *Rac*-**34**; (D) ICL yields with increasing irradiation time.

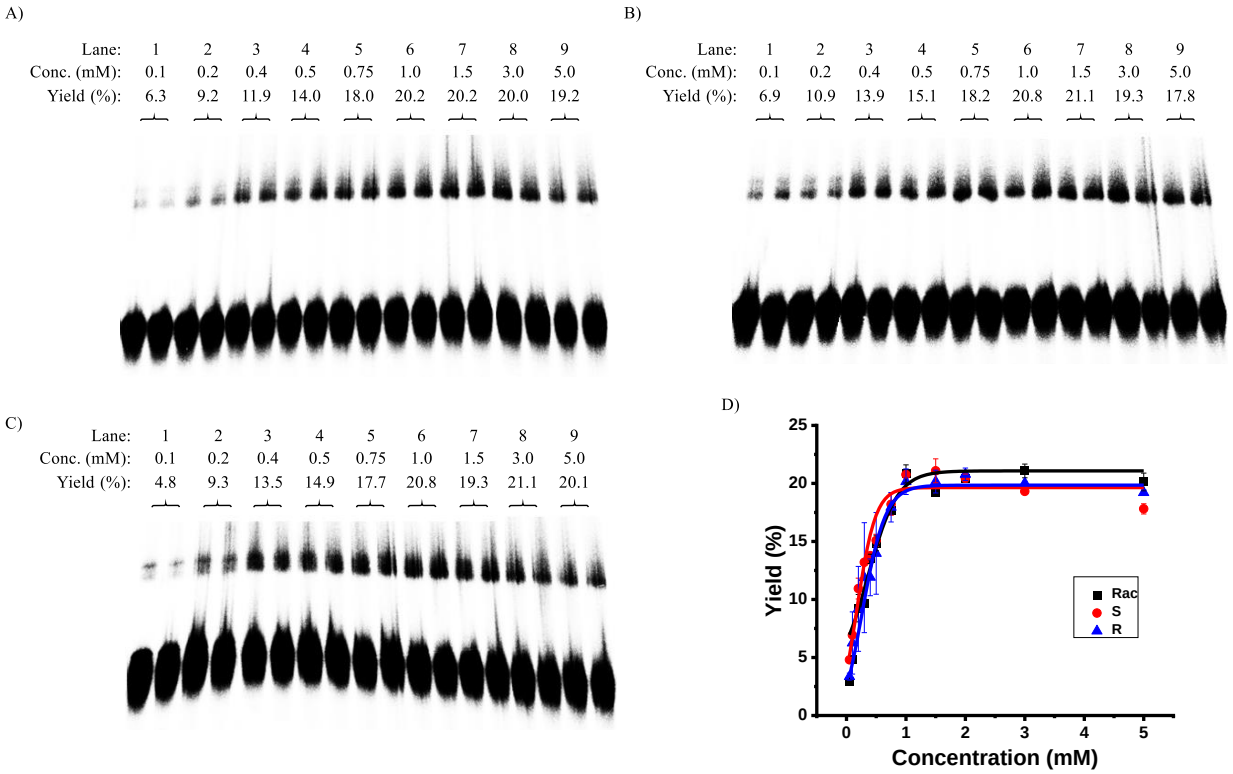

Figure 6-5. Concentration-dependent study of BINOL **34** with different configurations. (A) Representative gel of *R*-**34**; (B) representative gel of *S*-**34**; (C) representative gel of *Rac*-**34**; (D) ICL yields with increasing concentration of **34**.

6.2.3. Conclusions

To figure out the effect of chirality on DNA intertrand cross-linking formation, three BIONL derivatives with different configurations (*R*-, *S*- and *Rac*-) were designed and synthesized. It was found that photo irradiation of compounds dissolved in different organic solvents caused the DNA damage in different degree. Less DNA damage and higher cross-linking formation were observed with BINOL derivatives when CH_3CN was chosen as auxiliary organic solvent. The time- and concentration-dependent study with **34a-c** with different configurations showed that 350 nm irradiation of 1.0 mM substrate for 28 h led to the highest cross-linking efficiency. However, no

great discrepancy for ICL yields was observed with compounds with different configurations, indicating that the chirality didn't affect the DNA interstrand cross-linking formation. It is likely that due to the small size of **34**, different configurations do not affect its binding interaction with DNA double helixes that have relative much larger size.

6.3 Experimental Section

General Information Without additional purification, all chemicals and reagents were used directly after purchased. The organic synthesis was monitored by thin layer chromatography (TLC) and the crude products were purified by column chromatography. Same as the previous study, the DNA cross-linking study used oligonucleonides (ODNs) which were synthesized by Model. 394 DNA/RNA ABI synthesizer from AZCO® BioTech. Inc. with standard sutomated DNA synthesis techniques. The cross-linking yields were determined by a Molecular Dynamics phosphorimager equipped with ImageQuant (version 5.2). ^{1}H and ^{13}C NMR were collected on a Bruker DRX 300 MHz spectrophotometer with TMS as internal stander.

Compound Synthesis and Characterization

2,2'-Bis(ethoxymethoxy)-1,1'-binaphthalene (31) [1,1'-binaphthalene]-2,2'-diol (**30**) (10.0 g, 34.9 mmol) was added in portions in a solution of 60% NaH (9.8 g, 244.3 mmol) in THF at 0 ℃. After the solution was stirred for 10 min, pure chloromethyl ethyl ether (13.2 g, 139.6 mmol) was added in drops and the solution was continually stirred for 1 h at 0 ℃ and then 4 h at r.t. The reaction mixture was poured into water (50 mL) and extracted with CH_2Cl_2 (3 × 50 mL). The organic layers were combined, washed with brine and dried with anhydrous Na_2SO_4, to afford the

crude product that was then purified through column chromatography (Hexane/EtOAc = 20:1 (*Rac*-**31**)), 10/1 (*R*-, *S*-**31**)) to get **31** (*Rac*-**31**; white solid; *R*-, *S*-**31**: light yellow oil).

2,2'-Bis(ethoxymethoxy)-[1,1'-binaphthalene]-3,3'-dicarbaldehyde (32) n-BuLi (44.7 mmol, 2.5 mmol/ml in hexane, 17.9 mL)) was added in drops into a solution of **31** (14.9 mmol, 6.0 g) and TMEDA (59.6 mmol, 9.0 mL) in ether (100 ml) at 0 ºC. The solution was stirred for 1.5 h at the same temperature. Then dry DMF (74.5 mmol, 5.7 mL) was introduced into the solution which was continually stirred for 4 h. The reaction was quenched with 1.0 M HCl and poured into water (50 mL). The mixture was extracted with EtOAc (3 × 50 mL). The organic layers were combined, washed with saturated $NaHCO_3$ and brine, then dried with anhydrous Na_2SO_4, concentrated to afford the crude product which was further purified by column chromatography (Hexane/EtOAc = 20:1 (*Rac*-**32**)), 10/1 (*R*-, *S*-**32**)) to get **32** (*Rac*-**32**; white solid; *R*-, *S*-**32**: light yellow oil).

(2,2'-Bis(ethoxymethoxy)-[1,1'-binaphthalene]-3,3'-diyl)dimethanol (33) $NaBH_4$ (31.4 mmol, 1.19 g) was added in drops into a stirred solution of **32** in MeOH/THF (80 mL, 1:1) at 0°C. The solution was stirred for 3 h at the same temperature. The reaction was quenched by dilute aqueous HCl (~55 mL) after it was completed, and the pH of the solution was tuned to ~7.0 with saturated $NaHCO_3$. After removing the organic solvents under reduced pressure, the aqueous phase was extracted with ethyl acetate (3 × 50 mL). The ethyl acetate layers were combined, washed with brine, dried with anhydrous Na_2SO_4, concentrated to afford product **33** (3.63 g, 100%) as a colorless thick oil residue which was not purified and could be used directly in the next step.

2,2'-Bis(ethoxymethoxy)-3,3'-bis(methoxymethyl)-1,1'-binaphthalene (34) 60% NaH (1.42 g, 35.44 mmol) was added in a solution of the compound **33** (4.10 g, 8.86 mmol) in DMF (54 mL). Then MeI (5.03 g, 2.21 mL, 35.44 mmol) was added in drops in the solution at 0°C. The reaction mixture was stirred at room temperature for 24 h and the reaction was quenched with water (55

mL). The mixture was extracted with EtOAc (3 × 20 mL) and the organic phase was dried over Na_2SO_4, concentrated to afford the crude product which was purified by chromatography (Hexane/ CH_2Cl_2 = 5/1) over silica gel to get compound **34** as light-yellow oil (*Rac*-**34**: 84%; *S*-**34**: 92%; *R*-**34**: 70%). ^{1}H NMR (300 MHz, $CDCl_3$): 8.07 (s, 2H), 7.92 (d, *J* = 8.1 Hz, 2H), 7.42 (t, *J* = 6.9 Hz, 2H), 7.28-7.18 (m, 4H), 4.83 (s, 4H), 4.64 (d, *J* = 5.7 Hz, 2H), 4.52 (d, *J* = 5.7 Hz, 2H), 3.57 (s, 6H), 3.33-3.23 (m, 2H), 2.96-2.86 (m, 2H), 0.83 (t, *J* = 6.9 Hz, 6H). ^{13}C NMR (75 MHz, $CDCl_3$): δ 152.1, 133.6, 132.0, 130.8, 128.4, 128.0, 126.4, 126.0, 125.2, 125.1, 97.9, 70.4, 64.9, 58.6, 14.6.

3,3'-Bis(methoxymethyl)-[1,1'-binaphthalene]-2,2'-diol (35) 37% HCl (10.0 mL) was added slowly to a solution of compound **34** (1.40 g, 2.85 mmol) in 30 mL of THF at 0ºC. The mixture was stirred at r.t. for 3 hours. After the reaction was quenched by adding water (30 mL), THF in the mixture was removed by rotary evaporation. The mixture was extracted with EtOAc (3 × 30 mL) and the organic layers were collected to dried over Na_2SO_4 and concentrated to obtain the crude product which was purified by stirring with Hexane/EtOAc (50 mL, 4/1) for 0.5 h. The mixture was filtered by vacuum to get white solid **35** (*Rac*-**35**: 84%; *S*-**35**: 70%; *R*-**35**:72%). ^{1}H NMR (300 MHz, $CDCl_3$): 7.90 (s, 2H), 7.87 (s, 2H),7.36 (t, *J* = 7.5 Hz, 2H), 7.28 (t, *J* = 8.4 Hz, 2H), 7.16 (d, *J* = 8.4 Hz, 2H), 6.62 (brs, 2H), 4.88 (d, *J* = 3.9 Hz, 4H), 3.56 (s, 6H).

(4S)-4-Hydroxy-2,6-bis(methoxymethyl)dinaphtho[2,1-d:1',2'-f][1,3,2]dioxaphosphepine 4-oxide (36) Phosphorous oxychloride (491.4 mg, 0.3 mL, 3.20 mmol) was added in drops at room temperature in the solution of compound **35** (800 mg, 2.14 mmol) which was dissolved in pyridine (10 mL). The solution was stirred at room temperature for 4 hours and the reaction was quenched by water (0.3 mL) at 0 ºC. After stirring at room temperature for 1 hours, pyridine in the mixture was removed by rotary evaporation. 6 M HCl (17 mL 37% HCl + 17 mL H_2O) was added to the residue at 0 ºC and the reaction mixture was stirred at r.t. for 2 hours. Then the mixture was filtered

by vacuum to get white solid **36** (*Rac*-**36**: 812 mg, 87%; *S*-**36**: 78%; *R*-**36**: 75%) which was further washed with H_2O.^{1}H NMR (300 MHz, $CDCl_3$): 8.01 (s, 2H), 7.86 (d, *J* = 8.1 Hz, 2H), 7.38 (t, *J* = 5.7 Hz, 2H), 7.21-7.14 (m, 4H), 4.88 (d, *J* = 13.5 Hz, 2H), 4.76 (d, *J* = 13.2 Hz, 2H), 3.50 (s, 6H). ^{13}C NMR (75 MHz, $CDCl_3$): δ 149.2, 149.0, 135.7, 135.3, 133.4, 132.9, 132.3, 130.8, 130.3, 129.7, 125.6, 73.6, 62.6.

DNA ICL Formation The procedures in this experiment were the same as previous work (chapter 2-5).

6.4 Reference

(1) Nguyen, L. A.; He, H.; Pham-Huy, C. Chiral Drug: An Overview. *Int. J. Biomed. Sci*. **2006**, 2, 85-100.

(2) Coelho, M. M.; Fernandes, C.; Remiao, F.; Tiritan, M. E. Enantioselectivity in Drug Pharmacokinetics and Toxicity: Pharmacological Relevance and Analytical Methods. *Molecules*, **2021**, 26, 3113-3135.

(3) Francotte, E.; Lindner, W. Chirality in drug research; *Wiley-VCH: Weinheim*, **2006**.

(4) Tokunaga, E., Yamamoto, T., Ito, E.; Shibata, N. Understanding the Thalidomide Chirality in Biological Processes by the Self-disproportionation of Enantiomers. *Sci Rep.* **2018**, 8, 17131-17137.

(5) Mori, T.; Ito, T.; Liu, S.; Ando, H.; Sakamoto, S.; Yamaguchi, Y.; Tokunaga, E.; Shibata, N.; Handa, H.; Hakoshima, T. Structural Basis of Thalidomide Enantiomer Binding to Cereblon. *Sci Rep*. **2018**, 8, 1294-1307.

(6) Tripathi, A. K.; Prajapati, V.; Kumar, S. Bioactivities of l-Carvone, d-Carvone, and Dihydrocarvone Toward Three Stored Product Beetles. *J. Econ. Entomol*. **2003**, 96, 1549-1601.

(7) Richter, S. N.; Maggi, S.; Mels, S. C.; Palumbo, M.; Freccero, M. Binol quinone methides as bisalkylating and DNA cross-linking agents. *J. Am. Chem*. Soc. **2004**, 126, 13973−13979.

(8) Doria, F.; Richter, S. N.; Nadai, M.; Colloredo-Mels, S.; Mella, M.; Palumbo, M.; Freccero, M. BINOL-amino acid conjugates as triggerable carriers of DNA-targeted potent photocytotoxic agents. *J. Med. Chem.* **2007**, 50, 6570−6579.